Heterogeneous Cascade Oxidations Catalyzed by Mesoporous Artificial Enzymes

Manel Boukhallat

THÈSE

Pour obtenir le grade de

DOCTEUR DE L'UNIVERSITÉ GRENOBLE ALPES

École doctorale : CSV- Chimie et Sciences du Vivant
Spécialité : Chimie inorganique et Bio inorganique
Unité de recherche : Laboratoire de Chimie et Biologie des Métaux

Catalyse hétérogène des oxydations en cascade par des enzymes artificielles mésoporeuses

Heterogeneous Cascade Oxidations Catalyzed by Mesoporous Artificial Enzymes

Présentée par :

Manel BOUKHALLAT

Direction de thèse :

Stephane MENAGE — Directeur de thèse
DIRECTEUR DE RECHERCHE, Université Grenoble Alpes

Rapporteurs :

Christelle HUREAU
DIRECTRICE DE RECHERCHE, CNRS délégation Occitanie Ouest
Franck LAUNAY
PROFESSEUR DES UNIVERSITES, Sorbonne Université

Thèse soutenue publiquement le **24 mai 2023**, devant le jury composé de :

Stéphane MENAGE DIRECTEUR DE RECHERCHE, CNRS délégation Alpes	Directeur de thèse
Yasmina MEKMOUCHE CHARGE DE RECHERCHE HDR, CNRS délégation Provence et Corse	Examinatrice
Frédéric AVENIER MAITRE DE CONFERENCES HDR, Université Paris Saclay	Examinateur
Fabrice THOMAS PROFESSEUR DES UNIVERSITES, Université Grenoble Alpes	Président
Christelle HUREAU DIRECTRICE DE RECHERCHE, CNRS délégation Occitanie Ouest	Rapporteure
Franck LAUNAY PROFESSEUR DES UNIVERSITES, Sorbonne Université	Rapporteur

Invités :

Christine Cavazza
Laboratoire Chimie et Biologie des Métaux

Table of contents

Abbreviations

AA	Amino acids
ArM	Artificial metalloenzyme
BFR	Bacterioferritin
BioCE	Bioinspired Chemistry and Environment
Bispicen	N,N'-bis(2-pyridylmethyl)- ethylenediamine
BPMEN	N,N’-bis(2-pyridylmethyl)-1,2-diaminoethane
CC	Cyclic carbonate
CHP	Cumene hydroperoxide
CLEA	Cross linked enzyme aggregate
CLEC	Cross linked enzyme crystal
CP450	Cytochrome P450
CPA	Carboxypeptidase A
cyclam	1,4,8,11-tetraazacyclotetradecane
EDTA	Ethylenediaminetetraacetic acid
EH	Epoxide hydrolase
Et_2O	Diethyl ether
GDH	Glucose dehydrogenase
HEPES	4-(2-hydroxyethyl)-1-piperazineethanesulfonic acid
HRP	Horse radish peroxydase
HSA	Human serum albumin
IBA	Isobutyraldehyde
LCBM	Laboratory of chemistry and biology of metals
MALLS	Multi Laser Light Scattering
MAO	Monoamine oxidase
MeCN	Acetonitrile
MeOH	Methanol
MePicH	Methylpicolinic acid

MOF	Metal organic framework
MOL	Metal organic layers
MP3	MiniPeroxidase 3
MsCl	Methanesulfonyl chloride
O*i*Pr	Isopropyl alcohol
Otf	Triflate anion
PAA	Peracetic acid
PDB	Protein data bank
PicH	Picolinic acid
POM	Polyoxometalate
POP	Prolyl oligopeptidase
PTAT	Phenyltrimethylammonium tribromide
SALEN	N,N′-bis(salicylidene)ethylenediamine
SC	Styrene carbonate
SHC	Cyclase-squalene-hopene
SF	Silk fibroin
SO	Styrene oxide
TBAB	Tertbutylammonium bromide
TBAI	Tertbutylammonium iodide
TBHP	*Tert*-butyl hydroperoxide
TACNAA	1,4,7-(triazacyclononan-1-yl) acetic acid
TPA	Tris(2-pyridylmethyl)amine
TPP	Tetraphenylporphyrin
UAA	Unnatural amino acid
WT	Wild type

General introduction

Throughout the centuries, chemistry has had several breakthroughs significantly influencing the world we live in today. Away from an exhaustive description of the evolution of chemistry, we are going to focus on catalysis. In 1794, Elizabeth Fulhame documented one of the first catalytic assays. When attempting to produce metal tainted cloths, she discovered the experimental reduction of metallic salts, mainly silver, with the influence of light. This has unravelled the principle of catalytic photo-reduction.[1] The definition of catalysis has evolved to reach current consensus under which a catalyst is a recyclable substance that accelerates a reaction's rate.[2]

Currently, catalysis represents a corner stone of sustainable chemistry as it crosses out as one of the twelve green chemistry principles as defined by Paul Anastas and John Warner in 1998.[3] The attractiveness of the design of novel catalysis approaches stands out of both environmental and financial profit.[4] Indeed, catalysts are designed to enhance the selectivity, and the efficiency of the chemical reaction, in addition to cutting costs on solvents and chemical utilizations.[5–7]

The current need of the development of novel catalytic routes is related to the urging requirements of a greener and sustainable industry. Fundamental research takes a great part in pathing the routes for the development of these novel strategies. For instance, inspired by the outstanding efficiency of enzyme catalysis, chemists and biologists have been demonstrating a great interest in mimicking the activity of these biological entities. An example of this dynamic is the growing interest in synthetic biology, with the goal of replacing chemical process. Nevertheless, applications of such systems in the catalysis of abiotic reactions remain scarce. The natural evolution of enzymes leads them to be very efficient but in a strictly defined environment. Their stability and efficiency depend greatly on their native optimum conditions and can range from standard and ambient conditions for temperature and acidity to very acidic and harsh conditions for extremophiles. Nevertheless, the optimum range of activity of native enzymes remains narrow.

Then, native enzymes tend to have a narrow scope of activity standing and a low substrate tolerance. Recent advances have addressed the issue of stability and substrate availability, two aspects which will be introduced in this thesis. Many suppliers offer immobilized enzymes for selective chemical transformations. For instance, Novozyme © has a panel of commercial lipases and esterases for small molecule functionalization. Replacement

of the chemical transformation steps is also very interesting in the field of pharmaceuticals as growing regulations narrow the range of accessible synthetic pathways. In addition, the replacement of some of the synthetic steps by biocatalyzed transformations can be less expensive.

In an attempt to tackle efficiency, selectivity and step economy, this phD project was built around the concepts of artificial metalloenzymes, cascade transformations and heterogeneous catalysis. In an ambitious fashion, efforts have been put toward the creation of a series of stable enzymes to fill the gap in the enzymatically catalyzed abiotic transformations.

This thesis will be divided into four chapters, the first one will be dedicated to the bibliographic introduction focused on the definition of artificial metalloenzymes, their preparation and stabilization methodology, and cascade transformations. The second chapter will concern the preparation and characterization of metal complexes and novel protein scaffolds. Anchoring assays implying both actors will be discussed in the third chapter. Finally, the catalytic activity of the produced artificial metalloenzymes will be discussed in the fourth chapter.

Chapter I Bibliographic introduction

1. Artificial Metalloenzymes (ArMs)

ArMs are engineered metalloenzymes designed to exhibit the desired catalytic properties. They result from the association of a biological entity (peptide, protein, DNA, RNA…) with a an artificially modified metal cofactor (a metal complex or metal ion).[8] Investigations on ArMs date back to the 60s with the work of S. Akabori *et al.* on asymmetric synthesis of amines and amino acids.[9] At that time, it was already common knowledge that chirality can be induced from the use of chiral catalysts. The novelty of their work comes from associating a chemical compound, palladium chloride, with a biological entity, silk fibroins (SF). At the time, no structural description of SF was available. Current interests on SF in materials science allowed a better understanding of SF secondary structure, ***figure 1.*** The chiral and achiral arrangements of SF β-sheets depend greatly on the environment of the protein and factors like solvents, concentration and temperature.[10–12]

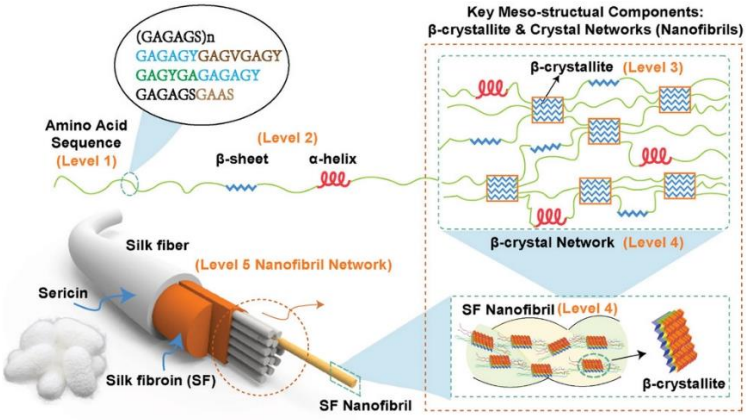

Figure 1*: SF structure description: i) Primary structure (level 1): amino acid sequence; ii) Secondary structure (Level 2): α-helices and β-sheets; iii) Tertiary structure (Level 3): β-crystallites; iv) Quaternary structure (Level 4), β-crystal networks, in which β-crystallites are connected to one another by amorphous chains (α-helices and/or random coils); v) Quinary structure (Level 5): Nanofibrils' bundle/network.*
Figure from Ronghui Wu et al. Adv Sci. 2022;9(4):2103981[12]

The newly designed chiral hydrogenation catalyst was obtained through the adsorption of palladium chloride on SF followed by the reduction of the catalyst under hydrogen. The chirality brought by the biological entity allowed the preparation of optically active glutamic acid, phenylalanine and diphenylethylenediamine by enantioselective hydrogenation.

Although quite impressive at the time, these results did not shake a lot of interest in ArMs. In fact, it has been slowly gaining enthusiastic interest until becoming trendier in the recent years. The recent advances in robotic technologies for parallel measurements and the burst of the entire "omics" techniques have opened a wider spectrum for structure-activity

studies. The enhanced description and understanding of the structure-activity relationship of complex entities is one of the factors behind the current burst in ArM development.

In the following paragraphs, will be unveiled the diverse modes to which the jigsaw puzzle pieces of the protein scaffold and metal cofactors can be associated, with examples on their applications. As to widen the description of ArMs, some examples will lean on molecular decoys in which case the non-natural cofactor is, in fact, not a metal cofactor.[13–15]

Although this manuscript will lean towards advances on ArMs design in the field of catalysis, it is worth noting that their applications extend to include biosensors, fluorescent probes and cancer treatments.[16–19]

1.1.Artificial metalloenzymes conception and applications

1.1.1. The Trojan horse strategy

1.1.1.1. The Biotin-avidin couple

The most popular example of a key-like or Trojan horse interaction is the avidin – biotin couple. Avidin is a protein composed of four subunits. Each subunit binds a biotin moiety, the natural substrate of avidin. The supramolecular network formed therein is one of the strongest interactions known with a determined K_d at 10^{-15} M. The remarkable stability of the Avidin-biotin couple is the main reason for which it has been extensively studied in ArMs development. The first ArM based on the avidin scaffold was reported by Whiteside and Wilson in 1978.[20] They successfully prepared an enantioselective hydrogenation catalyst by associating the avidin scaffold with a biotinylated rhodium diphosphine complex, $RhNBD^{+}Tf^{-}$, seen in ***figure 2***.

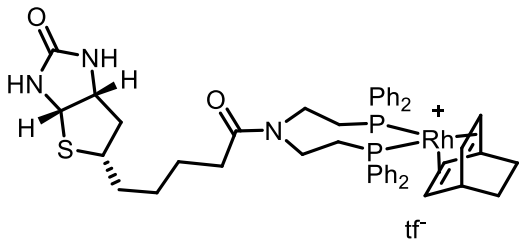

Figure 2: *structure of the RhNBD+Tf- complex adapted from ref 20.*

The catalytic activity of the complex alongside the tertiary structure of the protein's binding pocket, was expected to affect the overall enantioselectivity of the reaction. When

tested under homogeneous conditions, the ArM displayed enhanced overall catalytic efficiency on the reduction of α-actemidoacrylic acid to N-acetylalanine, ***scheme 1***.

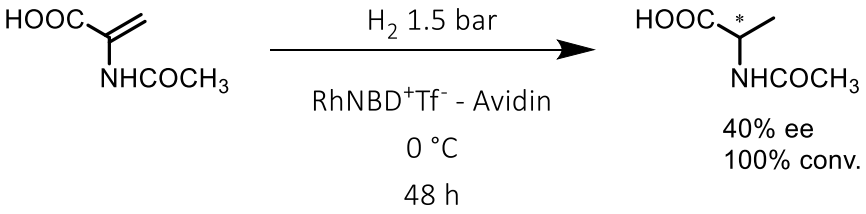

Scheme 1: *the reduction of α-actemidoacrylic acid by an avidin-based artificial enzyme Adapted from Wilson et al. J. Am. Chem. Soc. 1978, 100 (1), 306–3071978*

Compared to the free catalyst, which displayed 475 TON (Tunover number: number of moles of converted substrate per mole of catalyst) and no enantioselectivity, the designed ArM reached 500 TON with 40% of enantiomeric excess (ee). In order to confirm these results, the authors performed a control test on which they pre-incubated *apo*-avidin with an excess of biotin prior to the catalyst incubation, thus saturating all of the biotin anchoring sites on the protein. Results have shown no ee, proving that the catalytic transformation does occur inside the binding pocket.

This research work has first proven that it is possible to successfully associate a complex with a protein under homogenous conditions producing a catalytically active hybrid. This was also the first significant evidence of the possibility of exploiting a protein's chirality to enhance the enantioselectivity of a catalytic transformation. The rationale of the chiral control is named the 2nd sphere coordination based on supramolecular interactions between the biotin motif and the avidin scaffold. Later, Livnah *et al.* provided a description of the crystal structure of the avidin-biotin complex. This study has unveiled that the presence of a complex network of polar and hydrophobic interactions englobing an array of polar and aromatic residues, some of which form "hydrophobic patches" that are occupied by the biotin cofactor.[21]

In 2003, Collot *et al.* took on the development of a panel of ArMs employing the same biotinylated rhodium complex with avidin-like proteins, in an effort to highlight the immediate effect of the protein on the ee. For this purpose, a comparative study was carried out on avidin, streptavidin and neutravidin based ArMs in. The three scaffolds bind Biotin with high and comparable affinities. Avidin is extracted from eggs of oviparous vertebrate, neutravidin is its deglycosylated analogue, and streptavidin is derived from the bacterium *Streptomyces avidinii* and is characterized with having a deeper binding pocket as compared to Avidin, ***figure 3***.[22–25]

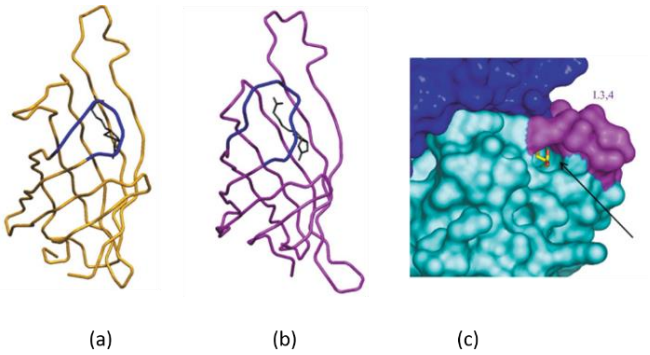

***Figure 3**: stick representations of the monomeric structure of (a) avidin, (b) streptavidin. (c) Surface presentation of the biotin-binding pocket*
Adapted from Eisenberg-Domovich et al. Acta Cryst. (2005). D61, 528–538, 2005 [22]

To further highlight the effect of the geometry of the cavity, they investigated the effect on the "depth" of the metal center within the binding pocket by the introduction of several amino acid chain spacers of different lengths. They were able to reach 37% ee using avidin as the host protein against 10% using Neutravidin. Surprisingly, the streptavidin-based ArM yielded 90% ee. This outstanding enantioselectivity was attributed to the biotin binding cavity located deeper within the protein matrix that provides an enhanced confinement effect on the metal complex.[26,27]

Later, Ward *et al*. have intended to enlarge the application scope for the biotin-avidin based ArM library previously established. They investigated the asymmetric allylic alkylation (AAA) of 1,3-diphenylallyliacetate, ***scheme 2***, by screening the library of biotinylated ligands (with and without spacers) and proteins (avidin, streptavidin) associated to the $[Pd(Ph_2allyl)Cl]_2$.

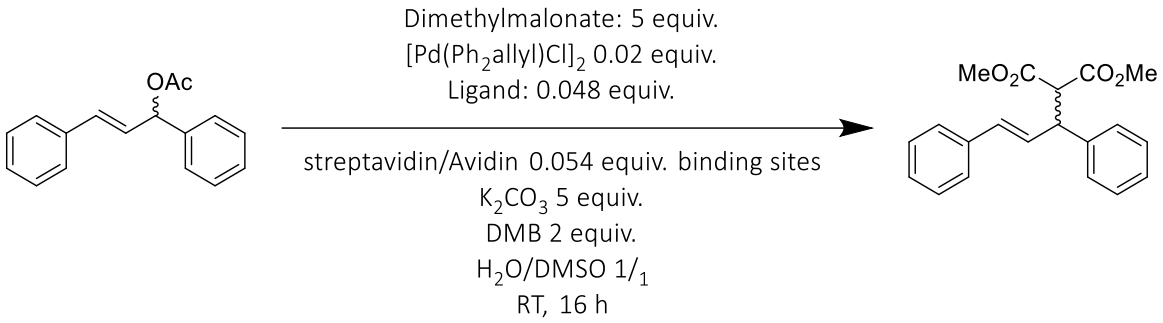

***Scheme 2:** asymmetric allylic alkylation of of 1,3-diphenylallyliacetate, adapted from ref 28.*

Although in most cases, they obtained the hydrolysis product, the combination of constrained biotinylated ligands and spacers have yielded interesting results. Up to 95% conversion and 90% ee were reached with the ability of generating either the S or the R product depending on the ligand—protein couple employed. These constrained systems tend to place the metal center in more confined areas of the protein favoring the nucleophilic attack on the

metal center as opposed to hydrolysis. These results are particularly interesting as no similar activity is found in the enzymatic field, proving that ArM design can provide a better access to abiotic reactions.[28]

1.1.1.2. ArMs from Human Serum Albumin (HSA)

HSA is an attractive protein for ArM developers. It is cheap, abundant, and has been subjected to many characterization studies, which constitutes a good starting base for ArM design. It is a water-soluble monomeric protein that englobes three domains: each domain has two subdomains A and B where A represents two long loops and B represents a third shorter loop.[29] It is a known transporter for drugs, fatty acids and hormones and thus has many binding sites.[29,30] The main drug binding domains are the Sudlow binding sites **II** and **I** located in the protein subdomains **IIA** and **IIIA** respectively, as illustrated in ***figure 4***.[31]

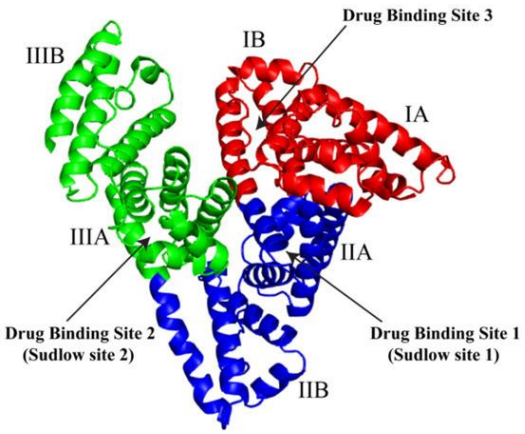

Figure 4: *domain organization of human serum albumin. Domain I (red), domain II (blue), and domain III (green) Adapted from Mishra et al. Int. J. Mol. Sci. 2021, 22(16), 8411*

Based on these known binding characteristics of **HSA**, Rondot *et al.* were able to design a new HSA-based ArM for sulfide oxidation. Following a Trojan horse strategy, an iron N,N'-bis(2-pyridylmethyl)-1,2-diaminoethane (BPMEN) derivative ligand with an ibuprofen motif (**FeL_{ibu}**) was designed to target specifically the binding site located in **IIA**, known to have a good affinity for ibuprofen.[29,30,32,33]

The activity of the designed ArM was tested for the catalytic oxidation of thioanisole by sodium hypochlorite (NaOCl). 62% yield of sulfoxide with up to 69% selectivity were observed with the newly designed ArM whereas the complex alone formed the sulfone product exclusively.[32] The hybrid catalyst remained stable after 4 runs with little to no change in activity. Moreover, the changes in the activity observed during competition experiments where the

hybrid FeL_{ibu} bound HSA was formed in the presence of ibuprofen or thyroxin, confirmed that they target the same binding spot thus proving the success of the Trojan horse approach.

1.1.1.3. Antibody based artificial metalloenzymes

Mahy and *coll.* leaned on ArM development using antibodies based on the antigen-antibody recognition. Through a Trojan horse strategy approach, they successfully designed a number of ArM hybrids for selective oxidations.[34–38] For instance in 2008, they reported an estradiol–iron metalloporphyrin conjugate associated to the anti-estradiol 7A3 for thioanisole sulfoxidation with hydrogen peroxide. The monoclonal antibody, anti-estradiol 7A3 was produced by mice immunization with the estradiol antigen. Then, they functionalized the porphyrin ligand with and estradiol motif, ***figure 5***.

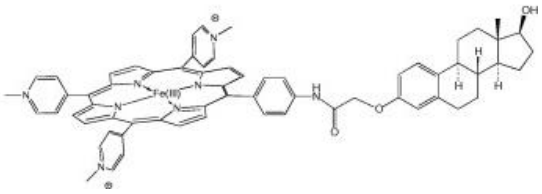

Figure 5: *metal porphyrin-estradiol complex adapted frrom ref 34*

The K_d of this antibody-antigen couple is as high as 10^{-10} M whereas the newly produced hybrid was able to bind two metal cofactors with a K_d estimated at 10^{-8} M.[36] The high stability of the designed hybrid made it promising for catalytic investigations. A comparative study between the antibody bound metalloporphyrin catalysts and the sole catalyst was carried out. Results, seen in ***figure 6***, show that the ArM kinetics are 1.5 times faster reaching a 2 folds higher yield as compared to the catalyst alone. Nevertheless, the overall activity remained low, 15% yield with a low enantiomeric excess of 8% observed with the hybrid only, which confirmed that the stereoselectivity was induced by the protein scaffold. Later, they investigated the peroxidase activity of the newly engineered hybrid. This activity was monitored using 2,2′-azino-bis(3-ethylbenzothiazoline-6-sulfonate) ABTS as a substrate. Based on their results, they concluded that despite no direct coordination of the side chain to the metal center- UV profile of the complex remained unchanged-, the 7A3 antigen has an accelerating effect on the reaction. Indeed, the initial transformation rate remained two folds higher with the hybrid compared to the free catalyst. [38]

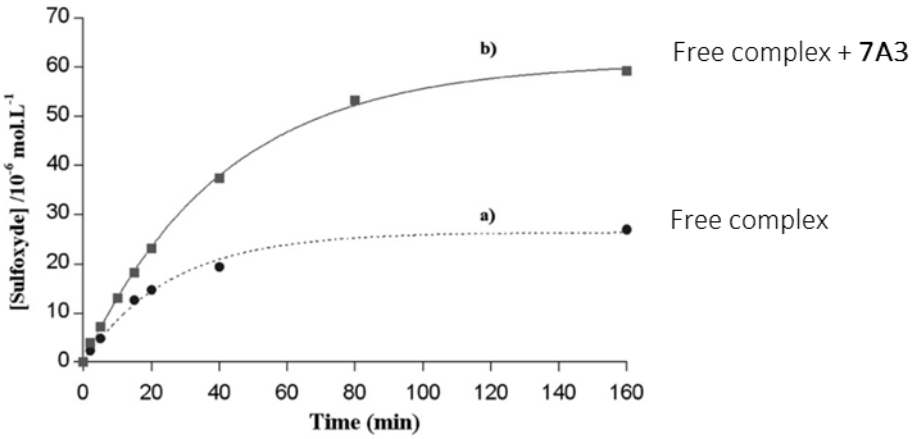

Figure 6: *sulfoxidation of 0.5 mM of thioanisole by 0.25 mM H_2O_2; (a) in the presence of 5 µM of the free complex; (b) in the presence of 5 µM of the free complex and 12.5 µM of the 7A3 protein.*

In 2014, following the same strategy, they designed a new hybrid based on the Neocarzinostatin and testosterone interaction. Neocarzinostatin is a widely studied chromoprotein that appears to be quite versatile. Heyd *et al.* and Drevelle *et al.* have been investigating the introduction of new binding sites on this chromoprotein by *in vitro* evolution.[39,40] It is able to bind testosterone with a Kd of 13 $.10^{-6}$ M and surprisingly, the newly designed hybrid displayed an even stronger affinity with a Kd at 1.6 $.10^{-6}$ M. When tested on thioanisole sulfoxidation, both the free catalyst and the hybrid afforded the same yield for the sulfoxide formation. While the free catalyst afforded the racemic product, the hybrid displayed 8% of ee in favor of the S enantiomer.[41]

These examples illustrate the very vivid and accessible ArM collections thanks to the Trojan horse approach by ingeniously taking advantage of highly stable native protein-ligand interactions.[8]

1.1.2. Metal ion exchange

Another strategy to design ArMs is the substitution of the naturally present metal ion in the metalloenzymes with a different metal center in order to influence the enzymatic activity.[42] One of the oldest evidence on the influence of metals on enzymatic activities resides in the work of Cuatrecasa *et al.* on the DNAase and ARNase activities of micrococcal nuclease. The micrococcal nuclease enzyme was known to have a phosphodiesterase activity. They found out that Ca^{2+} ions had activation properties towards DNase and RNase activities. Interestingly, when Ca^{2+} was replaced by a Sr^{2+} ion, only DNAase activity could be observed while substitution by other heavy metals resulted in complete inactivation of both activities.[43]

From the point of view of ArM developers, the ability of tuning an enzymatic activity by metal substitution is attractive. Many research interests investigating the effect of metal ion substitution have emerged. For instance, in 1976, Kaiser and Yamamura *et al.* developed an ArM for ascorbic acid oxidation by repurposing the Zinc based carboxypeptidase A (**CPA**). The active site of native CPA consists of two histidines coordinating a Zn^{2+} metal ion and exhibits both esterase and peptidase activities. Strikingly, replacement of the Zn^{2+} metal ion with a Cu^{2+} ion results in a copper-based CPA that exhibits oxidase activity only.

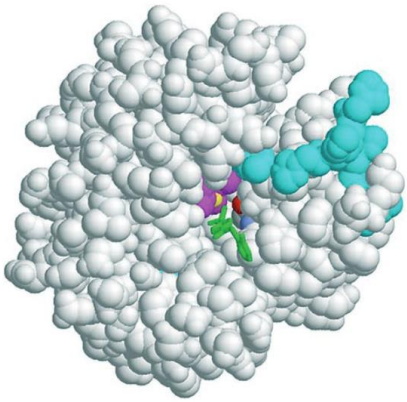

Figure 7: *structure of carbonic anhydrase (coordinates from 1G1D in the Protein Data Bank) featuring a bound benzenesulfonamide inhibitor (highlighted in green), the three histidines (magenta) coordinating the metallic ion (yellow), Thr199 (side-chain oxygen in red) and the peripheral histidines (cyan) from Fernandez-Gacio et al.* ChemBioChem. 2006;7(7):1013-1016.

More recently, Fernández-Gacio *et al.* were inspired by manganese-based catalysts for styrene epoxidation that were reported to be active in buffered solutions, ***figure 7***.[44] The N_2O_2 coordination mode of the Zn^{2+} in the carbonic anhydrase is similar to the N_2O_2 coordination of manganese centers in epoxidation catalysts such as the famous Jacobsen Mn(salen) complex. Therefore, the Mn metal center was expected to exhibit a similar activity in the enzyme. The metal substitution was performed in a buffer though preincubation of bovine and recombinant human carbonic anhydrases with Mn (II) followed by a slow addition of the substrate, then bicarbonate activated hydrogen peroxide, affording an enantioselective epoxidation catalysis. Surprisingly, they have discovered that phosphate buffers inhibited the non-catalyzed reaction improving the overall ee which ranged from 18 to 52% for yields ranging from 9-57% depending on the substrate and equivalents of oxidant used.

Other examples stand out of the work of Hartwig *and coll.* who designed an ArM from a hemoprotein by metal substitution.[45] Their work leaned on investigations such as carbene and nitrenes insertions into C–H Bonds and cyclopropanation. One of their interests was the

design of new **P450** containing noble metals by metal ion substitution. They worked with **CYP119**, a **P450** enzyme from the theromphilic bacterium *Sulfolobus solfataricus*. Because of its origin, **CYP119** was expected to have a good thermal stability therefore allowing assays to be performed at elevated temperatures. Several ArMs based on **CYP119** (***figure 8)*** were produced by replacing the native hemin active site with other **M-PIX** complexes.

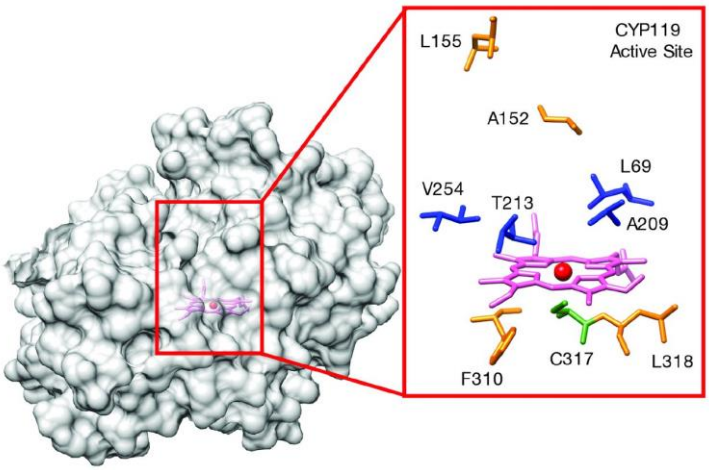

***Figure 8**: Structure of WT Fe-CYP119[45], adapted from Dydio et al. Science. 2016;354(6308):102-106.*

Beside the metal substitution, in order to induce higher ee, relying on directed evolution, they generated a library of mutants in the inner, middle and outer sphere of the binding the site by directed evolution. The results showed that the iridium based enzyme mutants exhibit interesting catalytic activities on carbene intramolecular and intermolecular insertion into C-H bonds, with ee as high as 98%, ***scheme 3***.[46] Good catalytic performances were also reported on cyclopropanation of terminal and internal olefins using the different **CYP119-Ir(Me)-PIX** ArMs and on Nitrenes insertion into C-H bonds as well. [47,48]

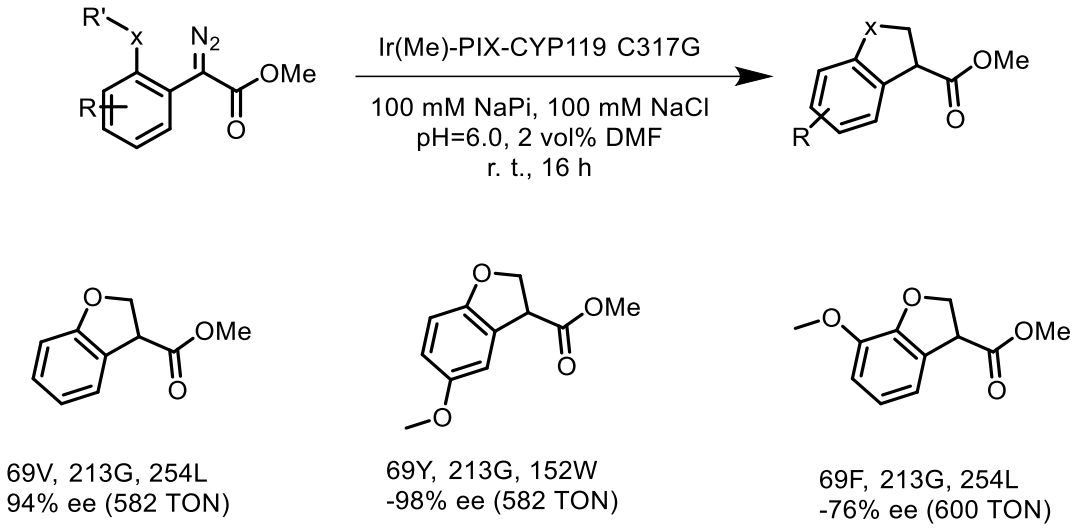

Scheme 3 : dihydrobenzofuran synthesis by carbene insertion into C-H bond by Ir(Me)PIX CYP119[48]

Following the same design strategy, Fujieda *et al.* reported a new artificial osmium-based peroxygenase. The mononuclear osmium ArM was produced using the ***TM1459*** gene from *Thermotoga maritima* encoding a homodimeric Mn-binding protein. As illustrated in ***figure 9a***, the cleft type active site of manganese (the native metal) or osmium, constituted of four histidines, is very reminiscent of the tris(2-pyridylmethyl)amine (TPA) metal complexes. Crystallographic data and biochemical assays on osmium-based TM1459 showed that the structure is similar to the native Mn based active site and exhibits high thermal and chemical stability as well. The activity of the ArM was tested on the dihydroxylation of 2-methoxy-6-vinylnaphtalene. Under acidic conditions (pH 2.0), the ArM afforded 92% of the dihydroxylated product after two hours at 70°C. After further optimizations, they were able to reach 9100 TON after 12 h similar, if not higher than the Os-TPA model, ***figure 9c***, with a reported TON range of 2500-5500.[49]

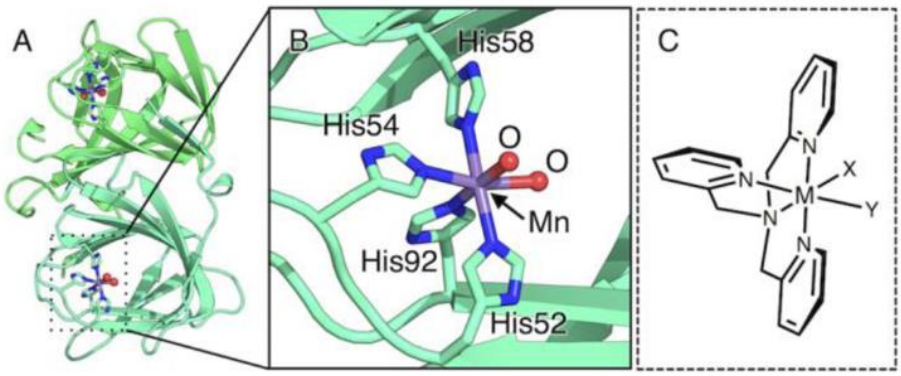

Figure 9: (*A) Overall structure and (B) Mn center of TM1459 protein (PDB code: 1VJ2). (C) Schematic representation of TPA-metal complex.*

These non exhaustive examples on ArM design via metal substitution highlight the tunable properties of many natural enzymes. This simple yet elegant approach can be easily coupled with other techniques such as site-directed mutagenesis and introduction of unnatural amino acids to further enlarge the scope of accessible reactivities and selectivity.[42]

1.1.3. Covalent binding

Covalent modification towards ArM development can range from the covalent anchoring of a metal cofactor to amino acid sequence modifications.[50] Metal complexes can be covalently anchored to an enzyme bearing reactive amino acids such as cysteine and lysine residues, or by click chemistry with the introduction of unnatural amino acids (UAA).[51–53] The different strategies evolve from the bioconjugation methodology developed by Bertozzi and collaborators, acknowledged by a Nobel prize in 2022.[54] This strategy has the great advantage to control perfectly the localization of the inorganic complex as the artificial active site and has gained interests with the original use of UAA. Conversely, it is a less generalized methodology as a consequence of the narrow catalogue of UAA in addition to the need of particular AA. The following paragraphs will include some ArM developed through covalent anchoring, their strategy and applications and the current state of the art of click chemistry in ArM development.

1.1.3.1. Covalent anchoring on cysteine residues

Thiol groups provided by cysteine residues are a great starting point for functionalization for both synthetic chemists and ArM developers. Strategies for selective thiol –*cysteine*- functionalization include -*but are not limited to*- the disulfide bridge formation (the bond stability might be found unsatisfactory for abiotic catalysis), SN_2 reaction with α-halocarbonyl moieties and the thiol-ene reaction that can proceed either through a free-radical reaction of through a Michael addition pathway.

For instance, Lu *and coll.* designed two ArMs by introducing one or two cysteine in *apo*-myoglobin scaffold near the active site of the enzyme, selected by computational calculations as illustrated. After removal of the prosthetic group, the cysteine residues were intended to covalently link a manganese salen complex functionalized by reactive methane thiosulfonate motifs on both aromatic rings, ***figure 10***.

Investigations on enantioselective thioanisole sulfoxidation with the newly designed ArMs, revealed that the double mutated ArM - on which the complex is bound from both of the aromatic rings - proceeds with an 8 folds higher rate and an ee of 51% compared to 12% for the mono mutated one, highlighting the influence of geometrical constrains on the ee.[55]

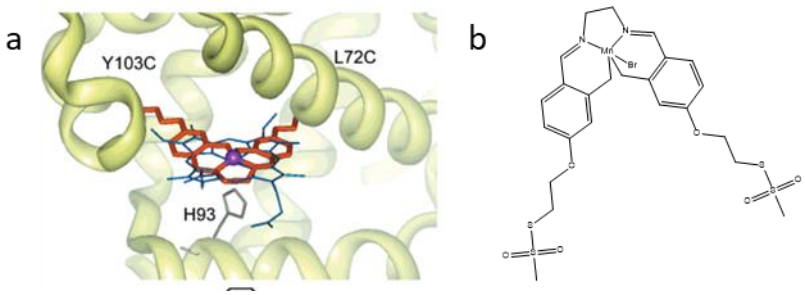

***Figure 10**: (A) Computer model of Mb(L72C/Y103C) with A covalently attached overlayed with heme. (B) Complex A adapted from Caret et al. J Am Chem Soc. 2004;126, 10812-10813*

Salmain and coworkers investigated the catalytic activity of papain-based ArM with (η6-Arene) ruthenium (II) complexes on a Diels Alder transformation between cyclopentadiene and acrolein. For the covalent modification of papain, the complex was functionalized with an α-halocarbonyl group, the covalent anchoring will then proceed by the nucleophilic substitution of the halogen by the thiol group of the cysteine. The newly designed ArM exhibited 88% yield with a ratio endo/exo of 92/2 and a TOF of 220 h^{-1} as opposed to 62% yield and a roughly 10 folds lower TOF for the free complex.[56]

Roelfes and *coll.* reported a number of ArMs based on the multidrug resistance regulator from *Lactococcus lactis* (LmrR) represented in ***figure 11***.[57] LmrR is known to adopt a dimeric form resulting in a quite large and accessible hydrophobic cavity to accommodate organic precursors and metal complexes.[58] In addition, it is a quite interesting scaffold for selective covalent modifications as it does not contain any cysteine residue. By taking advantage of this cavity, Bos *et al.* reported an ArM in which a copper (II) phenantroline complex was covalently bound to LmrR following the strategy described in ***figure 11***. The covalent modification was achieved by first localizing the anchoring position for the introduction of cysteine residues via site directed mutagenesis. In this case, it was the positions 19 and 89 for being localized at the far end of the cavity thus avoiding any interference between the two copper complexes. On the other hand, the phenantroline and the bipyridine ligands were functionalized with a bromoacetamide arm, allowing the covalent bond formation through an SN_2 pathway by the thiol group on the cysteine residue. Catalytic assays were

performed by adding a copper (II) salt to the previously modified LmrR in a MOPS buffer solution. The activity of the ArM was tested on asymmetric Diels Alder transformation as depicted in *scheme 4*.

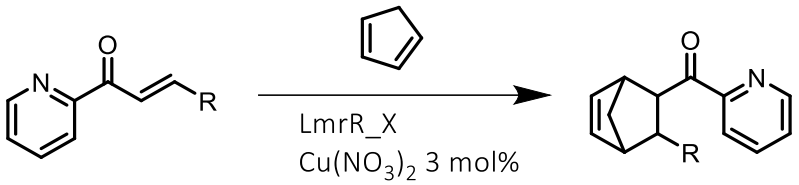

R= Ph, m-MeOPh, Me
X=M89C, N19C

Scheme 4

Differences between the tested ArMs were highlighted through the catalytic assays. Indeed, the position on the complex inside the pore had a great influence on the ee of the transformation. Interestingly, on the phenyl substituted substrate, the bipyridine ligand gave the opposite enantiomer as compared to the phenanthroline ligand when both coupled to the M89C LmrR mutant with ee of 66% and 95% respectively. Moreover, when comparing the influence of the mutation position, with the phenanthroline copper complex, the M89C mutant gave much more interesting results with conversion at 95% and 95% of ee compared to 25% of conversion and 53% ee for the N19C mutant. These results underline the great influence that can be exerted from the protein environment as a second coordination sphere to the catalyst. It offers the possibility of tuning this influence by the introduction of different amino acids around the active site in order to change locally the structure of the protein and the constraints, with hopes of enhancing the catalytically activity as well.

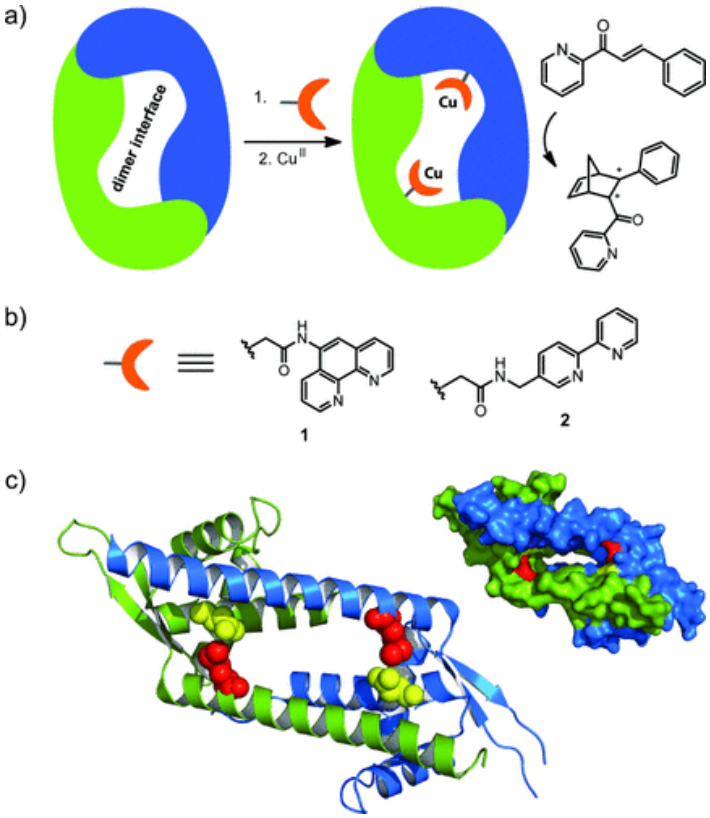

***Figure 11**: a) Schematic representation of the proposed artificial metalloenzyme in which a Cu^{II} complex is grafted on the dimer interface of a protein. b) Ligands used for grafting on the dimer interface. c) Pymol representations of dimeric LmrR in a ribbon and a space-filling model (protein data bank (pdb) code: 3F8B). Either position 89 (red) or 19 (yellow) were used for the covalent binding of ligand 1 or 2. From Bos et al. Angew. Chem. Int. Ed.2012,51, 7472 –7475.*

1.1.1.1. Click chemistry on protein scaffolds:

Nobel Prize winners Barry Sharpless and Morten Meldal have both laid the basis of click chemistry in the early 2000. The principle of click chemistry refers to the Huisgen alkyne-azide [3+2] cycloaddition (AAC), ***scheme 5***.[59,60] It is also a misnomer that englobes a certain range of reactions that afford new molecules by joining two smaller molecules with relative ease in water or bio-fluids. It is a useful tool to construct complex molecular structures as well as enzyme modification. Historically, the reaction was run at high temperature for long reaction times. However, it can be catalyzed by Cu(I) salts where the Cu(I) catalytically active species is obtained *in situ* through the reduction of $CuSO_4$ by sodium ascorbate. Other investigated metal salts and complexes such as the half sandwich $Cp^*RuCl(PPh_3)_2$ catalysts, can allow the formation of one or the other [3+2] product preferentially.[61,62]

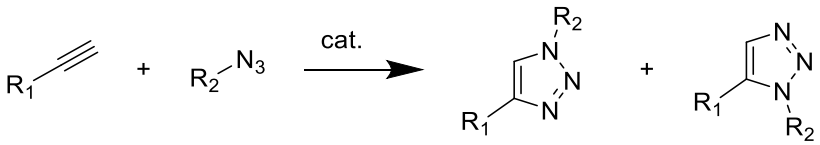

***Scheme 5** : the Huisgen cycloaddition [60]*

Other cycloadditions close to the click reaction approach include the Diels-Alder reaction, the Staudinger ligation and the thiol-ene reaction.[63] The fact that these reaction types can be processed at room temperature and provide little to no side products has been quite appealing for synthetic biologists and chemists. One of the most common applications has been in the design of fluorescent labeling and probes. Semisynthetic enzymes can be engineered by the incorporation of clickable unnatural amino acids (UAA).[64] Nevertheless other examples of click chemistry are reported in the literature: Lewis *and coll.* reported an ArM for olefin cyclopropation following the introduction of a clickable UAA.[65] Their bioconjugation approach was carried on a prolyl oligopeptidase (POP). In addition to a good thermal stability, POP are interesting for ArM design due to their cylindrical structure and their large internal cavity that can be suitable for ligand enclosure. The scaffold choice was based on extensive research on the crystal structures available in the protein data bank (PDB) in order to identify proteins with interesting three-dimensional arrangements. Selected WT-POP enzymes have an amide hydrolase activity, they share Ser-Asp-His triad located in the active site. For the ArM design, the serine residue was replaced for an azido containing UAA.

This mutation allows to abolish the native activity of the protein and to locate the non-native metal cofactor in the native cavity. Following the strategy illustrated in ***figure 12a***, they produced a POP based ArM through covalent anchoring of the dirhodium complex shown in ***figure 12b*** by click chemistry of the azide moiety from the UAA, on the alkyne moiety of the complex. However, another crucial parameter was the accessibility of the active site for bioconjugation. Indeed, to allow access of the complex to the mutated active site, mutations were introduced on AA located in the channel, believed to grant access to active site.

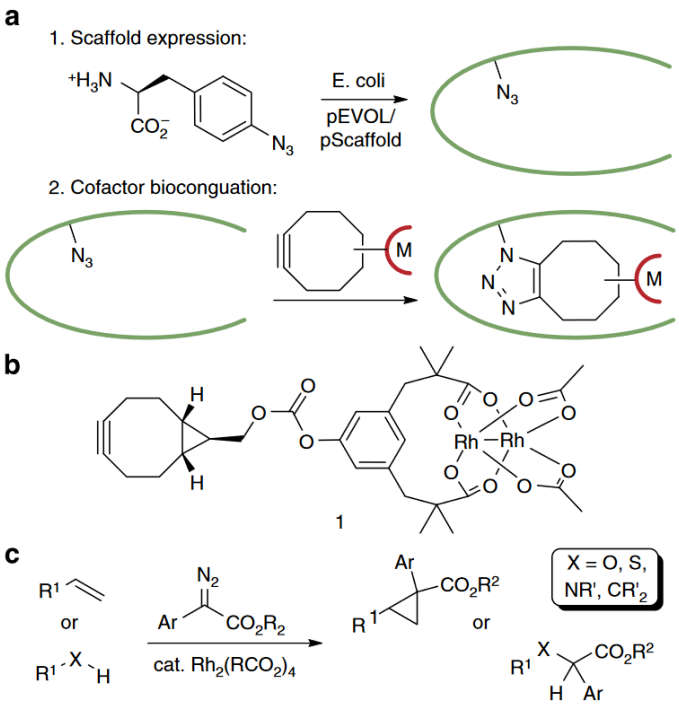

Figure 12 *ArM formation and reactivity. (a) ArM formation using the SPAAC reaction. (b) Structure of the dirhodium cofactor. (c) Representative reactions catalyzed by dirhodium complexes.* [65]

Surprisingly, the produced ArM **POP-ZA$_4$** in which the four AA were mutated to alanine residues underwent rapid bioconjugation, which confirms that the mutated AA were blocking access to the active site. In addition, other genetic optimization was carried out by introducing greater constraints on the attached complex for stereocontrol of the reaction. Catalytic assays on enantioselective cyclopropanation of aromatic olefins, showed that the ArM **POP-ZA$_4$-HFF-1** (where HFF are the induced mutations and **1** is the dirhodium complex) exhibits promising enantioselectivity on a scope of substrate with yields as high as 74% and 92% of ee, ***scheme 6***.

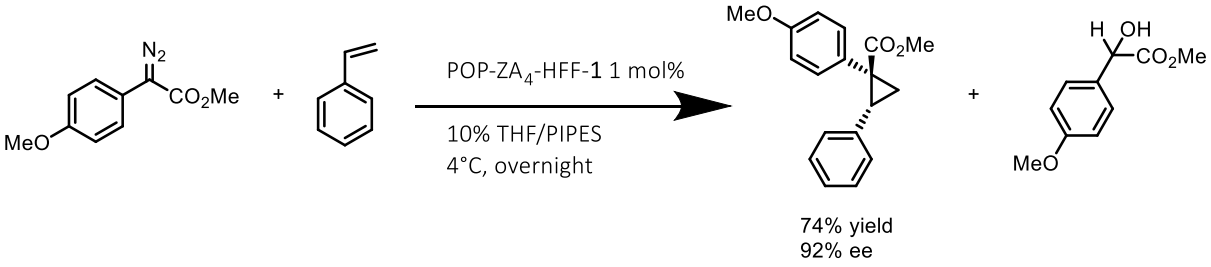

Scheme 6 *:cyclopropanation catalysis by Prolyl peptidase based ArM.*[65]

In the work of Salmain *et coll.,* half-sandwich cationic [(ŋ6-arene)Ru(dpa)Cl]$^+$ complexes where arene is either a benzyl or a *p*-cumene synhtesized as metal cofactors for ArM design, ***figure 13***. [66]

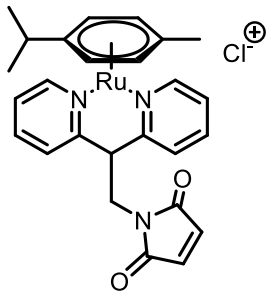

Figure 13: *structure of the [(η6-arene)Ru(dpa)Cl]+ complex reported by Haquette et al.* [66]

The 2, 2'-dipyridylamine (dpa) derivative containing the maleimide motif was intended for the covalent anchoring of the complex to the papain protein from *papaya latex*, a cysteine protease from the peptidase C1 family. The half sandwich Ru (II) complexes with known inhibitory activity towards papain activity, were proven much more efficient when covalently bound to the protein.

In 2018, Doble *et al.* reported an ArM for lignin oxidative degradation. They associated a modified iron TPA complex on which one of the pyridines was functionalized with a maleimide arm, with SCP-2L mutants, a steroid binder.[67] The modified TPA ligand was covalently anchored on the protein via Michael's addition, then ArM was formed *in situ* by adding the metal co-factors during catalytic assays. The resulting ArM was investigated on lignin degradation with prior assessment of solvent and co-solvent tolerance and investigations on benzylic oxidation using hydrogen peroxide. The oxidative degradation of lignin proceeds in either benzylic oxidation or a β-O-4 cleavage as indicate in ***scheme 7***. Under investigated conditions, the iron TPA analog provided lower conversion 45% with no control of the reaction products. On the other hand, the designed ArM provided the benzylic oxidation product only, with yields as high as 85% in MES buffer.

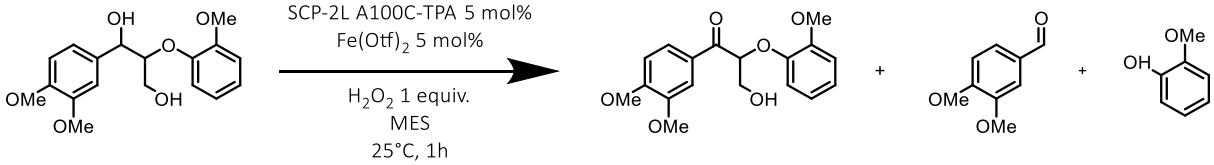

Scheme 7: *lignin model degradation catalyzed by a SCP-2L-Fe(TPA) ArM*[67]

Laureanti *et al.* have designed an ArM for carbon dioxide hydrogenation. The ArM was designed by covalently anchoring a rhodium bis-diphosphine complex to the LmrR protein. As illustrated in ***scheme 8***, the reported dirhodium complex is likely to bound to either one or two proteins engaging either one or both of its maleimide arms. Interestingly, only the ArM exhibits catalytic activity towards carbon dioxide hydrogenation. The structure of the complex bearing

two Michael's acceptors offers the possibility of a 1:1 or 1:2 coupling (***scheme 5***, 2). Mass analysis of the formed ArM showed that the majority of the ArM formed are in a 1:1 ratio with yields of 96% regardless of the number of equivalents of the rhodium complex. Catalytic assays showed that neither the free complex nor the combination of the **LmrR** protein and the complex without the maleimide (no covalent anchoring), exhibit any catalytic activity. On the other hand, the **LmrR** based ArM performed catalytic CO_2 hydrogenation at room temperature at a rate of 0.38 ± 0.03 h^{-1} after 16 h at room temperature. This is an example of the design approach towards the creation on a new catalytic activity by associating two entities that are otherwise ineffective.

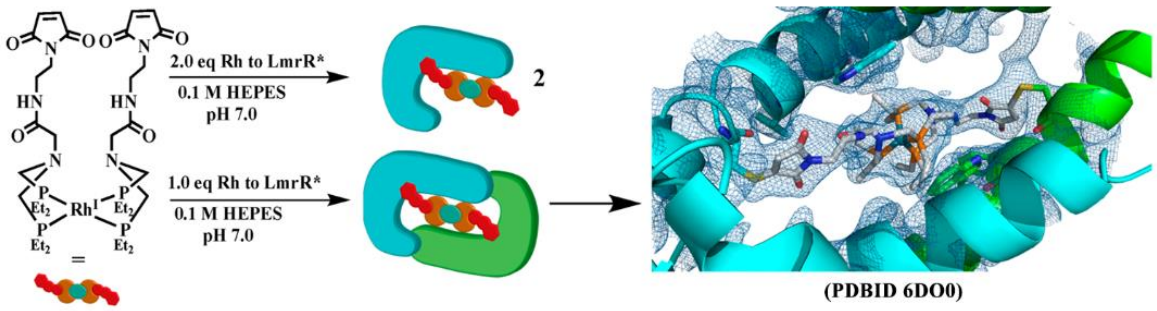

Scheme 8 *: ArM construction using LmR protein with dual covalent anchoring* [58]

1.1.4. *De novo* conception strategy

ArMs can be constructed from scratch based on the knowledge of polypeptides association and self-assembly. Some interesting examples can be issued from the work of DeGrado *et al.*and Faiella M. *et al*. For instance, in 2012 Faiella *et al.* reported the *de novo* design of a hemoprotein, MiniPeroxidase 3 (**MP3**) inspired from the bacterioferritin (BFR). In an attempt to downsize the BFR structure, the **MP3** was constructed out of four helix bundle protein scaffolds, two of which were covalently linked to the deuteroporphyrin cofactor. The resulting loop–helix/heme/helix–loop–helix sandwich ArM shown in ***figure 14***, exhibited horse raddish peroxidase (**HRP**)-like activity with H_2O_2/ABTS. Although the activity of the de novo designed ArM was much lower than natural peroxidases, it is still a great proof of concept of *de novo* designed ArM.[68]

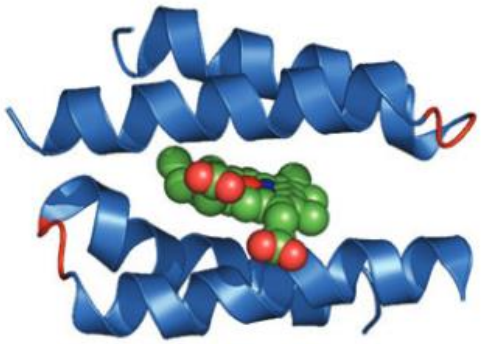

Figure 14: *cartoon representation of heme facing helices from bacterioferittin used for the design of* ***MP3****, adapted from Faiella et al.* [68]

Other research groups have demonstrated interests in *de novo* designed peptides either for imaging like in the work of Anna peacock and colleagues, where they designed several lanthanide-containing coiled coils for applications as contrast agents.[69–71] The engineering of this new ArM family was focused around the synthesis and assembly of peptide chains with an enhanced control of the size of the hinge region and the "twist" of the coils. Moreover, the intrinsic design of new AA chains for these applications allow the creation of coordination sites for metal centers.[72] Coiled coils ArM can also be applied to catalysis, the intrinsic control of the metal centers coordination providing a fine control of their reactivity. For instance, Pecoraro *and coll.* designed a three stranded coiled coil with a copper coordination site (three histidine residues, one per strand) with nitrite reductase activity.[73] The generated Cu(I) and Cu(II) ArMs exhibited activity in excess of nitrite and ascorbate with at least 5 TON.

Lately, Leone *et al.* reported a new ArM based on manganese and iron porphyrin catalysts embedded between two small peptide chains.[74] The bulky mini enzyme exhibited great catalytic properties on thioanisole sulfoxidation and indole oxidation.

1.1.5. Supramolecular interaction

ArM production can also be based on supramolecular interactions between the protein and the nonnative cofactor. Many proteins have been reported to have exclusive supramolecular interactions with their native ligands. Those interactions are, most of the time, the combination of several types of interaction including salt bridges, π-π stacking and hydrogen bonds. The LmrR protein, described earlier in this manuscript, is known to engage and stabilize protein-ligand bonds by π-π stacking thanks to the tryptophan residues present in its cavity. In addition to the examples cited above, Roelfes *and coll.* reported an LmrR ArM

based on π-π stacking interaction between the protein and a Cu (II) phenantroline complex.[75] The designed ArM exhibited excellent results on catalytic Friedel–Crafts alkylation of indoles with α,β-unsaturated 2-acylimidazoles with ee up to 94% at full conversion. Another heme-based ArM was reported as well, associating the **LmrR** scaffold with hemin for catalytic cylopropanation reactions.[57,76]

Other proteins like serum protein which have several characterized binding sites are good candidates for ArM development on the basis of supramolecular binding. For instance, Rousselot-Pailley *et al.* reported a thioanisole sulfoxidation ArM based on **HSA**-Mn(salen) hybrid. The localization of the binding site was proven tricky due to the numerous possibilities provided by the protein. Competitive binding with known HSA ligands like ibuprofen and thyroxine as well as circular dichroism experiments led to assume that the salen complex targets the cleft location of the protein near the subdomain **IIA** shown earlier in ***figure 4***.[77]

A seminal work was illustrated by Watanabe *and coll*. in which they demonstrated through crystal structure of metal Schiff base complexes in the cavity of apo-myoglobin that the metal complex mimics the same supramolecular interactions as those of the heme, including the N-histidine –metal bond.[78] The same principle applies to ArMs developed from serum proteins and NikA.[79–82] Other groups have also selected this native site reconstitution strategy mainly using myoglobin, by exchanging its prosthetic groups with other porphyrin analogs.[83]

The Bioinspired Chemistry and Environment (BioCE) group in the laboratory LCBM has selected this strategy to develop new ArMs for oxidation reactions based on the periplasmic nickel transporter NikA from *Escherichia coli* as the host, and different complexes as active sites for oxidation reactions. Follows the description of the host protein and the current state of the art of NikA based ArMs.

1. 1. 5. 1 The protein NikA

Wild type (WT) **NikA** is a transport protein that belongs to a family of periplasmic proteins encoded by the *nikABCDE* operon in *E. coli*. It has a crucial role in the regulation of nickel homeostasis within the cytoplasm.[84–86]

It was determined in the 90s that **NikA** was able to bind Ni^{2+} with high affinity and a dissociation constant at 10^{-7} M as well as other metal ions such as iron, copper and cobalt but with a ten folds lower affinity.[87] Structural studies on **NikA** started with a genuine interest in the

determination of the nickel transport mode. As many transport proteins, the structure is constituted of two lobes connected by a hinge region adopting two conformations, the open *apo*- form, which upon ligand binding switches to a closed form bearing the ligand-anchoring site in the protein cavity, ***figure 15***.[86,88]

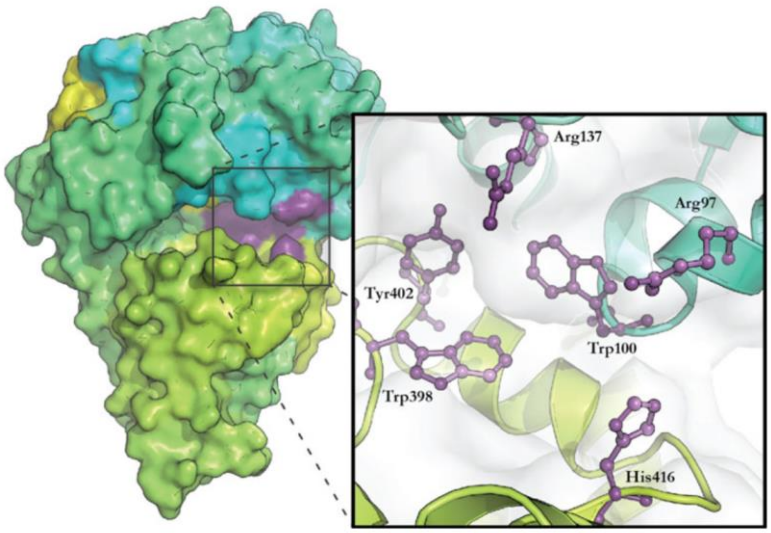

Figure 15: *three-dimensionalrepresentation of NikA in a closed conformation highlighting the main residues present in the binding pocket. Figure from Cherrier et al. J Biol Inorg Chem (2012) 17:817–829*

The first structural description of the Nickel binding site in **NikA** was provided by Heddle *et al.* in 2003. They were able to obtain **NikA** crystals using the hanging drop technique in which they used an excess of nickel chloride in both the precipitating and the cryoprotectant buffer.[86] Under these conditions, the nickel-bound **NikA** provided orthorhombic crystals in the $P2_12_12_1$ space group. Analysis of the crystallographic data has shown that the two lobes do not enclose the nickel fully, forming a relatively large cavity accessible to water molecules and ligands. Indeed, the electron density retrieved from crystallographic data shows that the Ni^{2+} ion residing in the cavity is surrounded by a ligand. The electronic density was first attributed to water molecules complexing the metal ion, one of which forming a salt bridge with the residue **Arg137**. The residues **Arg97** and **Glu221** point towards the nickel as well although it was unclear if they were involved in a salt bridge. Nevertheless, no direct coordination to the nickel was observed. Later in 2005, Cherrier *et al.* were able to demonstrate that the electron density surrounding the Ni^{2+} corresponds in fact to an EDTA ligand instead of water molecules. When attempting to elucidate the structure of the apo form of **NikA**, surprisingly, they obtained orthorhombic NikA-FeEDTA crystals. Out of their experimental results, they have concluded that when EDTA is used either in the periplasmic extraction step, during the purification

procedure or in the crystallization solution, orthorhombic NikA-Metal EDTA complex crystals are obtained.

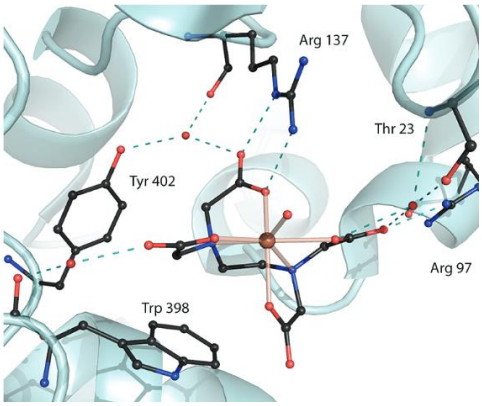

Figure 16: *crystallographic snapshot of the cavity of Fe(EDTA)-NikA ArM highlighting the different supramolecular interactions adapted from Cherrier et al. Biochemistry, Vol. 47, No. 38, 2008*

They corroborated their results with a crystallographic analysis of the NikA-FeEDTA crystals where they confirmed that both of the residues Arg137 and Arg97 are involved in a salt bridge with a carboxylate moiety from the EDTA ligand, ***figure 16***. This suggested that the "metal stabilization" results from an accumulation of small electrostatic interactions involving a metallophore called nickelophore, with a only direct interaction between the nickel and the residue His416 of the protein (ref 2008). In addition, they summarized the different protein-ligand interactions present concluding that the main interactions are the salt bridges involving Arg137 and Arg97 and CH\π hydrogen interactions with surrounding Trp residues.[88,89] These results reinforce the assumption that the natural nickelophore bears structural similarities with EDTA. Later, Lebrette *et al.* determined the crystal structure of NikA in complex with a $Ni(His)_2$ complex, ***figure 17***.[90]

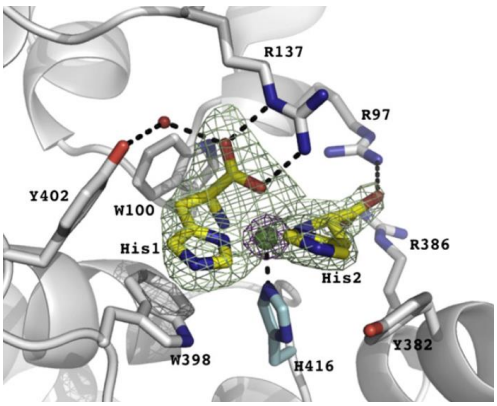

Figure 17*: Structure of* ***NikA*** *active site with its supposed natural ligand $(His)_2$ showing the coordination of His416. Figure from Lebrette et al. Journal of Inorganic Biochemistry 121 (2013) 16–18*

$Ni(His)_2$ is most likely the native form under which nickel is transported by NikA. It as it has been proven by crystallographic data and reinforced by biochemical studies, where Chivers *et al.* showed that *in vivo* the nickel uptake increases according to the histidine supply.[91,92]

1. 1. 5. 2 NikA-based artificial metalloenzymes

A good description of native ligand-protein interactions provides valuable tools for ArM developers. ArM development very often relies strongly on mimicking and reproducing these interactions using engineered ligands. The BioCE team has expertise in ArM design from NikA applied to catalysis. Early investigations on **NikA** ArMs was carried using **NikA** –complex hybrids, in solution, in crystals and cross-linked crystals. For instance, in 2017, Lopez et al. have published their work on new **NikA**-ruthenium complex catalysts for oxychlorination. The catalysis was performed using NikA incubated with a ruthenium complex in a buffer solution. In order to depict the binding mode of the complex, NikA crystals were also analyzed by X-ray diffraction after soaking with the complex solution. The X-ray structures showed the successful replacement of the iron EDTA present in the binding pocket. With a metal protein ratio of 1 to 1, they achieved a TON of 180 of α-hydroxy-β-chloro chlorohydrins from corresponding alkenes.[93]

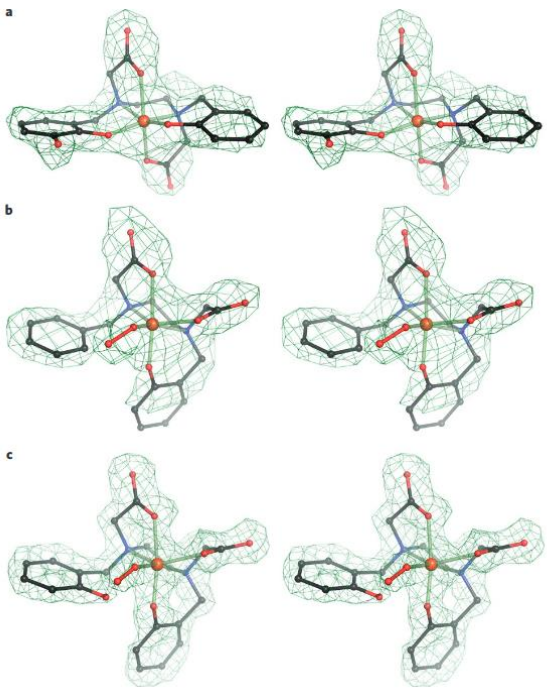

Figure 18: *stereopairs corresponding to omit Fourier electron density maps contoured at 3s of NikA-bound complex FeL0 at different aromatic hydroxylation stages. a, Structure of the doubly hydroxylated complex species. b, Structure of the diatomic oxo intermediate prior to hydroxylation. c, Structure of the (hydro)peroxo intermediate where the phenyl ligand is ortho-hydroxylated. Figure from Cavazza et al. Nature Chemistry 2010, 2, 1069–1076.*

Working on enzyme crystals in a heterogeneous catalysis setup, allows monitoring the transformations that undergoes the active site using time resolved X-ray crystallography. In the work of Cavazza *et al.,* the degradation of the active site of the **NikA** ArM was followed, revealing the dihydroxylation of the phenyl group of the iron complex, the inorganic active site, via reductive O_2 activation. Results revealed that the catalysts **FeL0** undergoes irreversible oxidative degradation leading to the deactivation of the catalyst after one cycle as seen in ***figure 18***.[94] This led to the development of several complexes inspired by **FeL0** as illustrated in ***figure 19***, where the degradation was avoided through the functionalization of the phenyl ring with a methyl sulfide moiety.

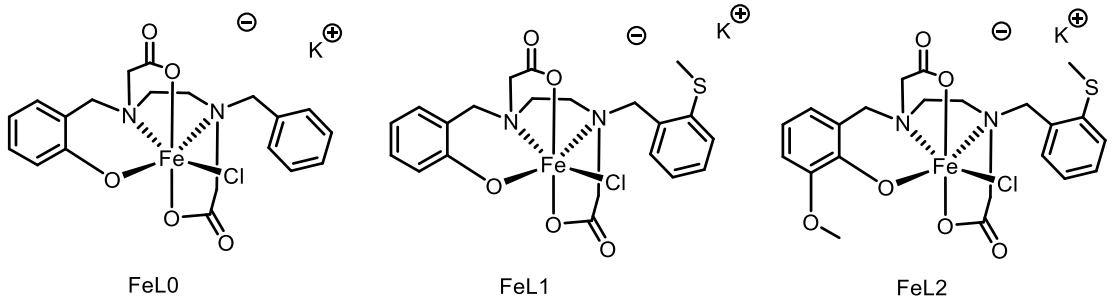

***Figure 19**: some of the investigated complexes for ArM development using **NikA**[95,96,97]*

The new generation of complexes was subjected to catalytic investigations, Lopez *et al.* leaned on oxidative cleavage and oxychlorination of alkenes and sulfide oxidation.[95,96]

Finally, there are also other ways to activate artificial active sites, triggered by the binding of a substrate or a small protein, evoking the mimic of the allosteric effect of natural ligands. Two examples illustrate this strategy: First, decoy molecules have been used to fill the regular substrate-binding site of CP450 that allowed the oxidation of small substrates such as methane.[97–99] A version of this process in whole cells has been also recently published reporting the *in vivo* transformation of benzene into phenol by *E coli* expressing recombinant **P450-BM3**. The transformation is facilitated by engineered outer membrane proteins, which aid the transport of the substrate and the decoy molecule into the cell.[100] The second example is based on the design of a trigger-able artificial hemoperoxidase formed by covalently binding a manganese(III)-teraphenylporphyrin to artificial bidomain repeat proteins from the αRep family.[101] The **αRep bA3-2** protein is known to induce the opening of the (**A3A3'**) interdomain region resulting in the catalytic 2 electrons-oxidation of *ortho*-phenylenediamine into 2,3-diaminophenazine by H_2O_2.

1.2. Enzyme stabilization

In general, enzymes have relatively narrow conditions in which they remain stable. They are prone to degradation or denaturation in response to external stresses such as pH changes, temperature variations and the use of chemicals. To circumvent these phenomena, enzymes can be stabilized using a carrier like an organic polymer, MOFs, silica gels etc… either by encapsulation,[102,103] or by covalent linking on functionalized supports.[102,104–106] Enzyme immobilization allows the combination of heterogeneous and enzyme catalysis. It improves the stability and reusability of the biocatalysts. [102–104,107] Silica sol-gels are one of the earliest supports used for enzyme stabilization. One of the first reports on enzyme immobilization on silicates derivatives dates back to 1998 in the work of Iqbal Gill and Antonio Ballesteros. One of the first challenges they encountered was the biocompatibility of the sol-gel substrates. For a successful immobilization, the substrates used ought to be water soluble and compatible with the condition range in which enzymes are stable. They successfully encapsulated several famous enzymes such as Horseradish peroxidase (HRP), superoxide dismutase and even yeast cells in matrixes of silica sol-gel, metallosilicate sol-gel or alkylsiloxane sol-gels with satisfying encapsulation yields and improved stability.[108] Metal organic frameworks (MOF) are another example of a carrier type: Farha *et al.* demonstrated that the encapsulation of organophosphorus acid hydrolase by a water stable zirconium based MOF resulted in a high thermal stability and reactivity improvements at higher temperatures compared to the free enzymes.[109,110] Although it improves the enzyme's stability, the use of a carrier raises several questions concerning the enzyme loading. Indeed, a typical 0.1-10% w/w activity loading resulting from the mass addition (the carrier) and eventual leaching are to be considered as well as the the ratio of the enzymes loading. [111]

Enzyme stabilization can also be performed in a carrier-free manner using polyhydric alcohols and salts[112] and bi-functional bridging agents. The latter is commonly called stabilization by cross-linking and has been around since the late 1960s. Early reports on enzyme cross-linking arose from the work of D. Thomas *and coll.* with the design of cellophane-glucose oxidase membranes using glutaraldehyde.[113] Enzyme cross-linking has since been developed to include several bridging agents and often the procedure is combined with other stabilizing treatments such as aggregation and crystallization. Moreover, it is a generalized method that can be applied on dissolved, aggregated and crystallized enzymes.

1.2.1. Cross-linked dissolved enzymes

Cross-linked dissolved enzymes are one of the first developed cross-linked enzymes. It consists on the stabilization of dissolved enzymes by bridging agents. Erarslan, Ertan and Kazan *et al*. reported a thermally stable penicillin G acrylase (PGA) that was obtained using bisimidoesters as cross-linking agents.[114,115] Despite the enhanced thermostability, this method provides low activity and poor reproducibility.[104,113] Moreover, the poor control on the cross-linking step often leads to uncontrolled cross-linking resulting in gelatinous hybrids with poor mechanical stability.[104]

1.2.2. Cross-linked enzyme crystals (CLEC)

CLEC are obtained by treating enzymes crystals with a cross-linker, which will react with amines, carbohydrates or thiol groups forming inter and intramolecular covalent bounds preserving the overall 3D structure of the crystallized enzymes. Once the enzyme crystallization is optimized, a panel of bridging agents can be used depending on the functional groups offered by the amino acid sequence. For instance, di-aldehyde coupling requires the presence of lysine residues (terminal amine/ ammonium functions).[111] One of the most widely used di-aldehyde is glutaraldehyde, which has been in use since the late sixties. One of the first documented CLECs stands out of the work of Quiocho and Richards on carboxypeptidase A (CPA).[116,117] In 1964, they concluded that treatment of CPA with 1% of glutaraldehyde for one hour yielded irreversibly modified crystals, able to withstand pH change and treatments with urea and semicarbazide.[117]

Other options are possible like cross-linking of the carbohydrate moieties in glycoproteins. Very stable carbohydrate CLEC can be obtained first by the oxidative cleavage the *cis*-diol functions of carbohydrates yielding di-aldehydes followed by treatment with diamines and a subsequent reduction of the formed imines bonds .[118,119]

Stabilized enzymes thus obtained exhibit a high stability in different media as well as a broad pH range stability and enhanced thermal stability as compared to free enzymes. This allows the access to more drastic reaction conditions.[95,102,120,121] These properties are valuable when applied in heterogeneous catalysis using artificial enzymes as reported by Lopez *et al.*[95] Working on NiKA CLEC opened a wider range of accessible transformations, interesting in the stream of oxidation catalysis where the conditions used are quite harsh, and often do not

comply with buffered media (strong oxidant, extreme pH values and temperature changes). In addition to the stability concerns of the system, another interesting aspect of working with CLEC ls is the ability of working in organic media. In most cases this enhanced stability leads to high reusability yields.

Ueno et al. reported another application example of this stabilization method in 2014.[122] The insertion of [Ru(benzene)Cl_2] complex into hen egg white lysozyme crystals led to enantioselective reduction of acetophenone with sodium formate as the reductant. Although the recorded TON were low (up to 5 only) a large conversion up to 50% and an interesting ee of 31% were reached. Moreover, comparative studies on various crystal morphologies (orthorhombic or tetragonal) highlighted the effect of crystal packing as different enantiomers were obtained according to the crystal geometry.

1.2.3. Cross-linked enzyme aggregates (CLEA)

Sheldon *and coll*. developed CLEA as an ersatz between cross linked dissolved enzymes and CLEC, intending to develop a more efficient stabilization than Cross linked Enzymes by concomitantly avoiding the hassle of enzyme crystallization.[102,104,104,123]

The aggregation of enzymes using a precipitant (such as ammonium sulfate), followed by a cross-linking step using a bridging agent, allows the formation of CLEA. Sheldon *et al.* reported stable PGA CLEA that catalyzed the synthesis of ampicillin in a broad range of organic solvents with better stability, activity retention, and immobilization yields compared to cross linked dissolved enzymes.[124]

CLEA conformations depend on the precipitating agent used in the process. This suggests that it is likely possible to access different enzymes arrangements within the aggregates to produce CLEA that might exhibit interesting reactivity differences.[123–125] A very interesting example of these observations are hyperactive lipase CLEA. The use of precipitants such as $(NH_4)_2SO_4$/sodium dodecyl sulfate provides CLEA that exhibit activity enhancement up to twelve folds higher than the free enzyme in organic solvent.[126] Finally, up to now, there is no CLEA of ArM.

2. Enzymatic and chemo-enzymatic cascade transformations

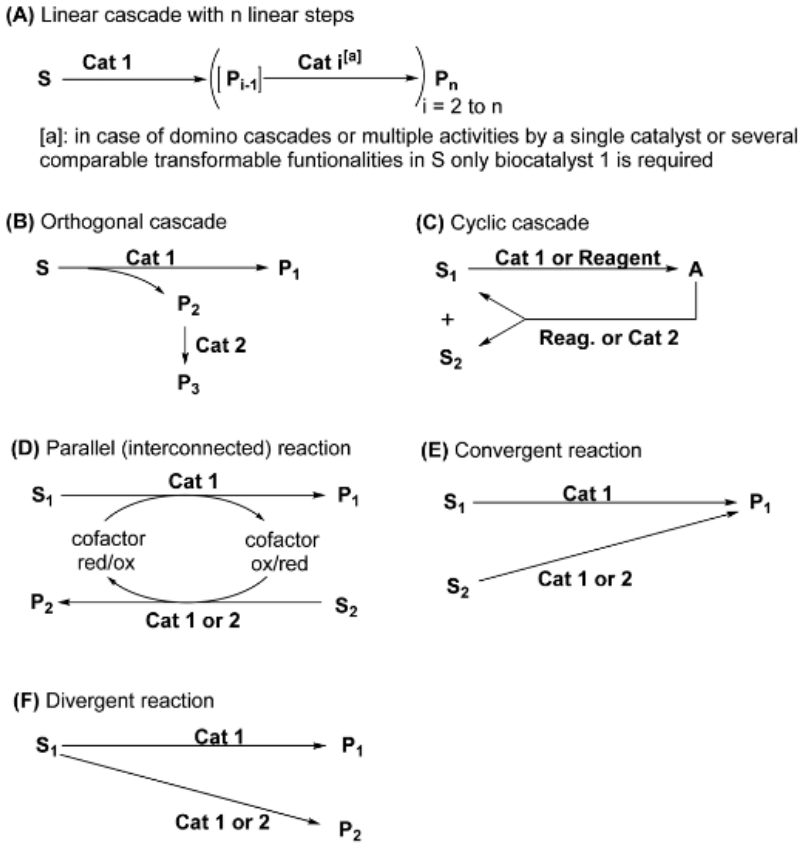

Scheme 9: different cascade reactions schemes form Kroutil et al. Chem. Rev. 2018, 118 (1), 270–348.

A cascade transformation, as defined by Kroutil and collaborators, is the combination of two or more chemical steps with no isolation of the reaction intermediates.[127] The symbiosis of living organisms offers mesmerizing examples of cascade transformations. If we consider natural metabolism networks, involving intricate multi-steps reactions, they represent the grail for synthetic chemists and biologists. Currently, multistep one-pot reactions are accessible and represent an attractive concept both economically and practically. Indeed, the decrease of reaction steps resulting in the subsequent economy of purification and separation steps affords a significant gain of time and costs. Moreover, designing a transformation in a tandem fashion offers the possibility of generating unstable reaction intermediates that can be directly formed *in situ* and engaged in the following reaction.

Cascades can be performed with either one or more chemical catalysts, a combination of enzymes or an association of catalysts and enzymes, the latter commonly categorized as chemo-enzymatic cascades. They can be classified according to parameters like the number of

steps and catalysts involved and according to the dynamic of the reaction as well. The main types include orthogonal, cyclic, convergent, divergent, and parallel transformations, depicted in *scheme 9*.

With the concern of limiting this introduction to the stream of our interest, this section will focus only linear cascades, the method subjected to investigations throughout this thesis. In a linear cascade, a substrate S would, upon the activity of catalyst C1, yield the product P1. This transformation can be repeated n+1 times depending on the number of the intrinsic transformations involved. Linear cascades include domino transformations during which, after the first catalytic transformation, the product P1 goes through spontaneous transformations yielding the last product Pn (*Scheme 9A*).

2.1.Single enzyme triggered cascades

Some enzymes can trigger a domino cascade reaction only by intervening in the first step of the transformation. In this case, the generated intermediates, often unstable, will undergo a spontaneous cyclisation. The transformation can be a nucleophilic C-O bond formation or an electrophilic C-C bond formation and are commonly known as enzymatic cascade cyclization. Epoxide hydrolases (EH) are one of the most popular examples.

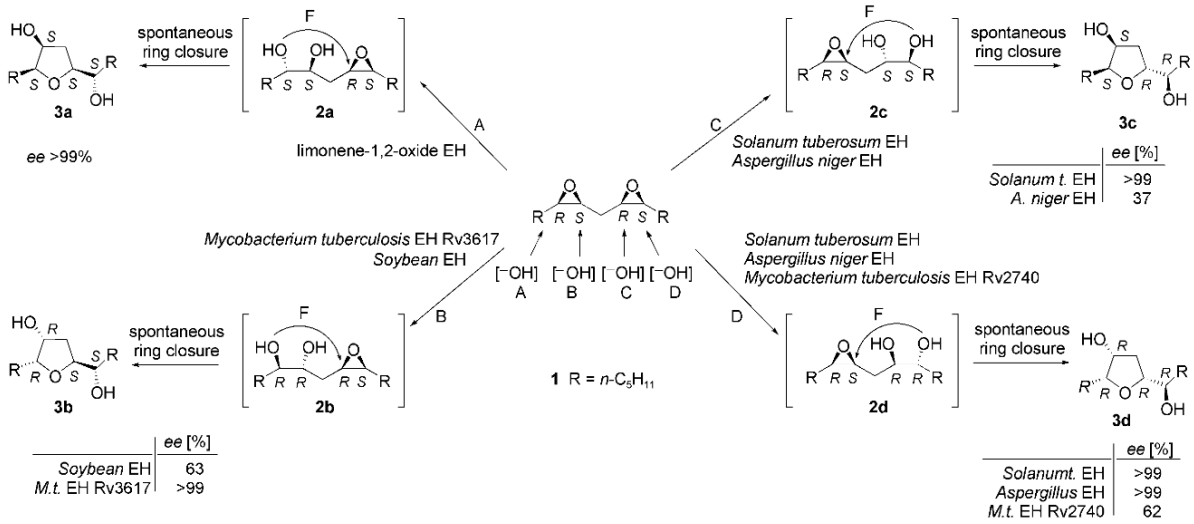

Scheme 10: *an example of enzyme-triggered cascades*[128]

Initially, EH are known to convert epoxide-containing molecules to their diol derivatives. Often unstable, the formed diols undergo cyclization process forming tetrahydrofuran or epoxide motifs. It can be fairly expected that the cyclization might result from a cyclase activity. Ueberbacher *et al.* have investigated this phenomena that occurs spontaneously upon the

hydrolysis of epoxide moieties.[128] Technically, epoxide hydrolase are used directly from lyophilized bacterial cells with no prior purification of the enzymes. According to Ueberbacher *et al.,* the whole cell catalyzed the biotransformation of meso-bis-epoxides **A** shown in ***scheme 10*** to THF containing molecule **3** with outstanding ee (from 37% to 99%). Moreover, they demonstrated that the stereoselectivity of such transformations varies according to the bacterial strains.

Another example concerning a C-C bond formation, involves the triterpene cyclase. Their activity relies on the formation of a carbocation (through the action of a Brϕnsted acid) that will engage in a series of cyclizations through C-C bonds formation. Although highly selective and interesting, triterpene cyclases are not yet widespread in synthetic biology due to their low yields. For instance, cyclase-squalene-hopene (**SHC**), one of the most studied cyclases, exhibits high substrate tolerance but very low yields. Nevertheless, their high substrate tolerance has encouraged investigations on the biotransformation of non-natural substrates using **SHC** from several bacteria like *Alicyclobacillus acidocaldarius*. Introducing mutations and double mutations has led to the development of a new range of SHC variants able to yield up top 54% on squalene analogues compared to basal to no activity with WT-SHC, ***scheme 11***.[129]

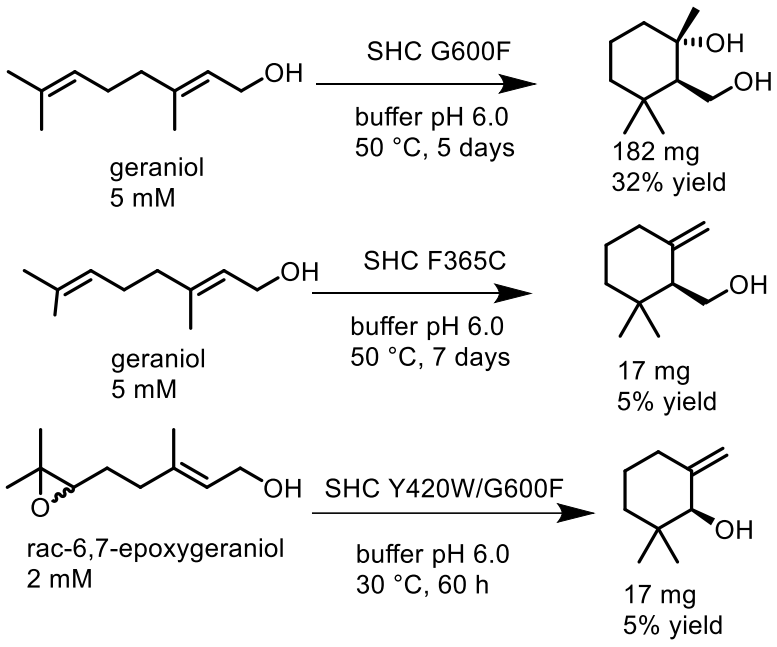

Scheme 11: *mutations on squalene hopene cyclase affords high yields of cyclization* [129]

Other enzymes have been noticed to trigger chain transformations such as laccases known for the dimerization and polymerization of phenolic compounds through the generation

of radical intermediates.[130–132] For instance, alcohol dehydrogenases can trigger lactone formation through the asymmetrical reduction of δ and ϒ keto-ester derivatives. [133]

2.2.Linear cascades

In some cases, linear cascades result from the reaction of a single catalyst on the substrate then the intermediates leading to the final product. The subsequent oxidation of hexane-1,6-diol by an alcohol dehydrogenase from *thermoanaerobacter ethanolicus* leading to ε-caprolactone is a relevant example. The same product can be obtained from cyclohexanol through a cascade process during which the starting substrate is oxidized by alcohol dehydrogenase to cyclohexanone followed by the Baeyer-Villiger monooxygenase oxidation yielding the desired product with 93% of yield, ***scheme 12***.[134]

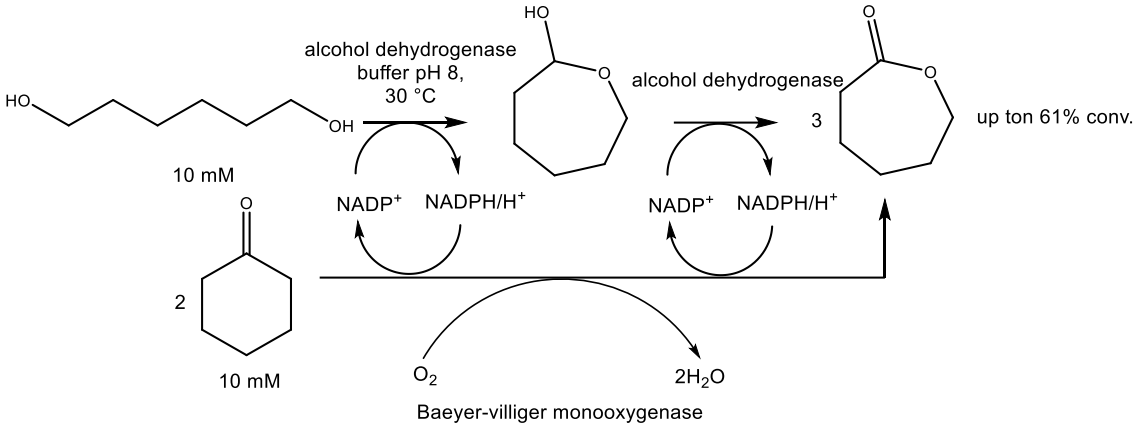

Scheme 12: *linear cascade biotransformation of 1,6 hexanediol into cyclohexanone*[134]

Besides the high activity and selectivity of the alcohol dehydrogenase, maintaining its enantioselectivity is the challenge when designing the cascade reaction. In fact, many *in vitro* cascades are designed towards the isomerization and kinetic resolution of interesting building blocks. It is the case with enzymatic redox isomerization of α,β- unsaturated aldehydes through consecutive reduction activity by ene-reductase followed by the oxidation activity of aldehyde dehydrogenase with yields and ee as high as 99%.[135] Kinetic resolution of secondary alcohols can also be achieved with comparable yields through an oxidation\reduction pattern of their corresponding racemate by associating stereocomplementary alcohol dehydrogenases.[136] The same scheme can be applied to the deracemization of secondary amines combining monoamine oxidase with transaminase as well as in the preparation of D-amino acids from their L analogues or their racemate, with the action of L-amino acid deaminase coupled to transaminase.[137]

Linear enzyme cascades can also be designed toward the production of small molecules with high industrial values. For instance, styrene oxide (as well as a range of aliphatic oxiranes) can be obtained from α-chloroketone derivatives with 99% ee and 84% yield using alcohol dehydrogenase and halohydrin dehydrogenase.[138] Using the same system, β-azidoalcohols and their cyano derivatives can be obtained by introducing a nucleophile (N_3^- or CN^-) in the oxidation step with halohydrin dehalogenase.[139,140] Lactams, known for their antibacterial properties, can be obtained from tetrahydroquinolines using monoamine oxidase and xanthine dehydrogenase.[141,142]

Apart from oxidation/reduction patterns, other cascades toward enantioselective C-C bonds formation are accessible. For example, α-hydroxyketones can be obtained from aliphatic alcohols through the formation of the corresponding aldehydes by the action of alcohol oxidase followed by C-C bond formation by benzaldehyde lyase.[143]

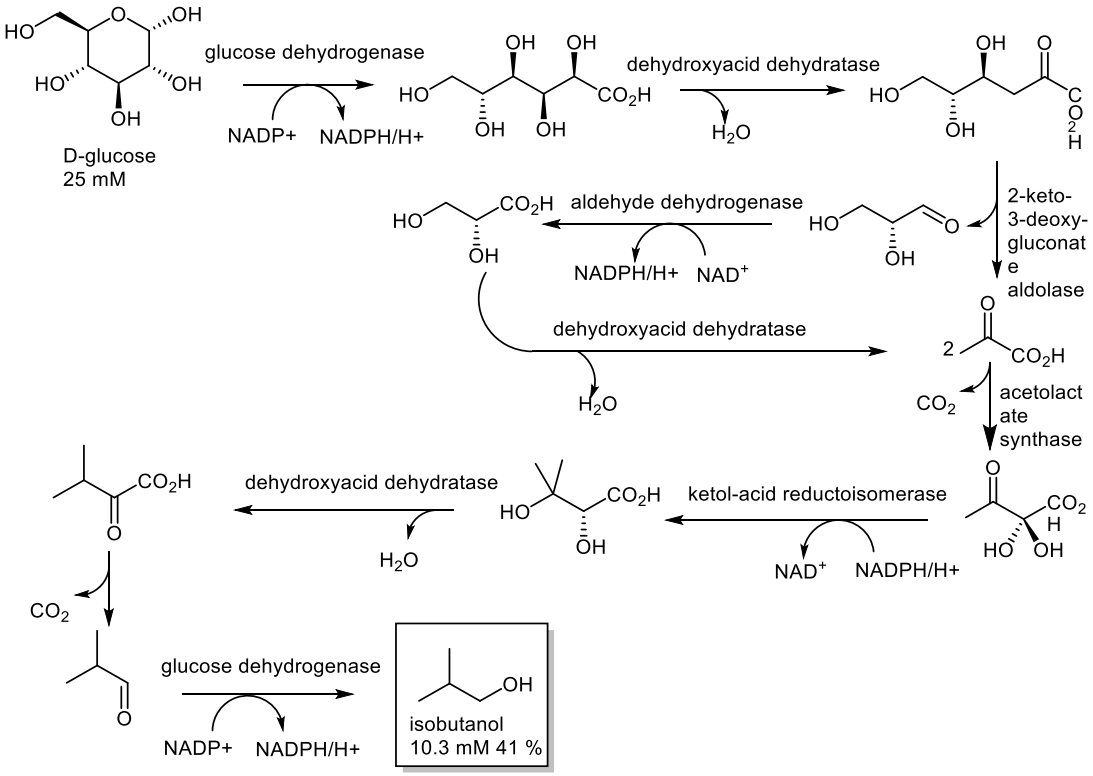

Scheme 13: *glucose tranformation into isobutanol via 8 successives biotranformations (conditions: pH 7.0, 50 °C, 23 h)* [144]

Other cascades can be designed without involving a redox transformation. For instance, amylose can be obtained from sucrose through the cleavage and phosphorylation of the latter by sucrose phosphorylase followed by the oligomerization with α-glycan phosphorylase.[145] Other examples including four or more steps are described in the exhaustive review of Kroutil

and coll. with examples involivng up to 8 enzymes per cascade for the elegant formation of isobutanol from D-glucose with 41% global yield after 10 steps, ***scheme 13***.[144]

2.2.1. Sequential linear cascades

Often, the choice of a sequential mode in a linear cascade is determined by the stability of the enzymes or the drastically different conditions in which the intrinsic transformations are optimal. In addition, it is the appropriate approach when interferences or antagonist activity of the enzymes towards each other might be noticed. Indeed, designing sequential cascades as opposed to linear cascades allows to circumvent this issue. For example, the synthesis of piperidines and pyrrolidines can be achieved by the regioselective amination of diketones or ketoaldehydes by transaminases forming the corresponding cyclic imines. The latter product can then be reduced stereoselectively reduced by (R) or (S)-imine reductase.[146] The whole cell containing the imine reductases was observed to inhibit the first step of the transformation. Adding the second catalyst after 24h hours allows the total conversion of the starting material by the transaminase leading to an optimized cascade that exhibit astonishing activities (98% yields, de and ee).

A comparative study on different approaches for a three steps cascade for the synthesis of (1S,2S)-2-hydroxycyclopentanecarboxylic acid was provided by Agudo and Reetz, ***scheme 14***.[147]

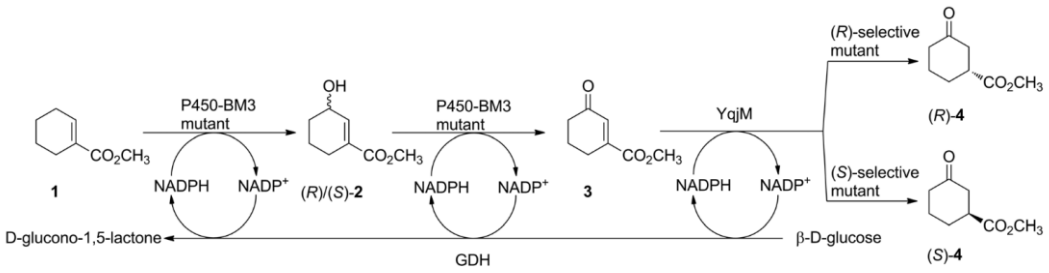

***Scheme 14**: biosynthesis of (1S,2S)-2-hydroxycyclopentanecarboxylic acid via cascade reactions*

Starting form 1-cyclohexene carboxylic acid methyl ester, two successive, regioselective, P450-catalyzed oxidations followed by stereoselective olefin reduction catalyzed by (R)- or (S)-selective mutants of an ene-reductase yielded the product of interest. The first approach consisted in the use of two designed *E. coli* cells, in a one pot process, one hosting the ***P450-BM3*** gene and the second containing the ***yqjM*** gene for the enoate reductase expression, allowing a better control on the ratio of both cells. In the second approach, they associated two different plasmids that encode for P450-BM3 and YqjM mutants in the same

cell. Finally, as a third approach, they engineered *E. coli* strains with the ***yqjM*** gene inserted into the genome and the ***P450-BM3*** remaining in a plasmid. Under optimized conditions, the first approach gave significantly interesting results, with 99% ee for the S or the R enantiomer (depending on the mutant) and 85% yield compared to 48% yield for comparable ee recorded for the second approach. Surprisingly, the third approach, which offers lesser control on the reaction parameters, afforded interesting results as well with yields up to 55% and 99% ee.

2.3.Chemo-enzymatic cascades

Cascades can be engineered towards the combination of enzymes or metalloproteins with non-native catalysts, mixing whole cells or isolated enzyme with chemical reagents, organocatalyts or metal catalysts. Chemo-enzymatic cascades is a promising methodology for cascade reactions, with the aim of associating the best of both worlds, *i.e.* substrate range for chemical catalysts and the outstanding enantioselective activity of enzyme catalysis. Tenbrick *et al.* reported promising results using a Grubbs type ruthenium catalyst for the metathesis step associated with an NADPH-dependent enzyme. [148] The reported cascade was efficient both on aliphatic and aromatic alkene although more efficient in the case of the latter with ee% up to 99% for 40% of conversion. A cascade towards THF derivatives formation was designed by Wang *et al.* using esterase or lipase for the hydrolysis of the substrate forming the corresponding alcohol followed by the cyclization step by an encapsulated gold catalyst.[149] Many other examples can be found in a sequential fashion due to relevant incompatibilities between the cascade's actors. 2,5-disubstitued pyrrolidine can be accessed from 1,4-diketones using transaminase to form the secondary amine that can spontaneously form the cyclic corresponding imine. The second stage of the transformation consists of the reduction and deracemization of the cyclic imine by the synergetic effect of ammonia borane and monoamine oxidase. The formed pyrrolidine derivatives were optically pure and isolated with 82% yield.[150]

2.4.Cascade transformations involving ArMs

Some linear cascades including ArM have been reported by Ward *and coll.*[151,152] First, they designed an NADPH-dependent artificial transfer hydrogenase ATHase by associating a biotinylated Cp*Ir complex possessing a 4,7-dihydroxy-1,10-phenanthroline ligand with streptavidin.

For the cascade transformation, they associated the ATHase for the imine reduction, glucose dehydrogenase (GDH) for NADPH regeneration, catalase and monoamine oxidase (MAO) to yield enantiopure through the pattern illustrated in ***figure 20***.

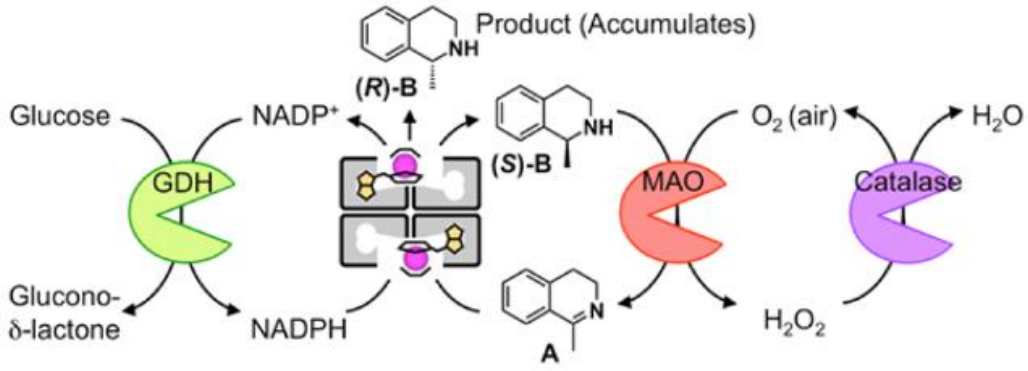

***Figure 20**: illustration of the cascade transformation for the deracemization of α-chiral amines*[151]

The cascade transformation was designed towards the deracemization of α-chiral amines. Genetic optimizations were carried out on the streptavidin isoform as to enhance the first step of the transformation. At optimized conditions, the cascade afforded the desired product with quantitative yield and ee.[151]

3. Cascade transformation towards cyclic carbonates

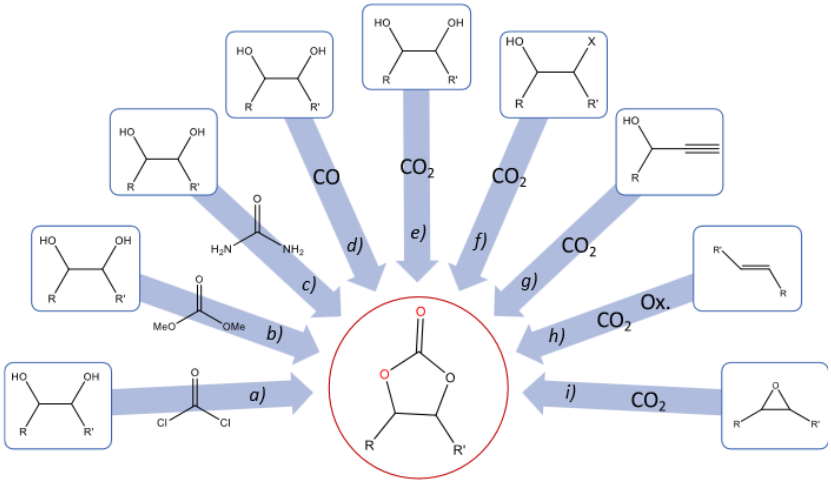

***Scheme 15 :** organocatalytic methods for cyclocarbonate synthesis.adapted from*[153]

Cyclic carbonates are quite economically attractive small molecules. They are good candidates for phosgene and isocyanates replacement in the production of polyurethanes and as a source of quaternary carbon. [154–156] Applications of cyclic carbonates diverge from the production of biocompatible polymers, as solvents and in lithium batteries to other less common applications in medicinal chemistry. There are various routes for cyclic carbonates

formation; ***scheme 15*** highlights some of the existing organocatalytic methods. Other routes designed towards the reactivity of metal centers include the use of metal complexes, ionic liquids, POM, MOF … etc.

For instance, Deng et al. developed a synergetic Zinc-based ionic liquid for the production of cyclic carbonates from urea and diols. They recorded yields as high as 96% for ethylene carbonate formation with a suspected regeneration of the starting material.[157,158]

Currently, there is a growing interest in process development for cyclic carbonates production, particularly through cascade transformation of alkenes. The most common cascade scheme is through the epoxidation of the alkene followed by a CO_2 cycloaddition into the epoxide ring. The overall process gives a great opportunity for investigations on more efficient synthetic routes. Indeed, until recent years, cyclic carbonates formation required high CO_2 pressure and elevated temperatures. The greater challenge here, in terms of optimization, is to obtain the desired carbonates from epoxide under ambient pressure and temperature conditions. Launay *and coll.* have summarized the current state of the art of cascade transformations for cyclic carbonates formation in a review published in 2021.[156] In this part, will be included a succinct overview of metal catalysts applied for both steps of the transformation.

3.1.Alkene epoxidation

Epoxide chemistry is a very vast subject spanning from small-scale epoxidation oxidants used in organic synthesis to homogeneous and heterogeneous patented processes. Epoxidation reactions have been the subject of tremendous achievements in catalysis as this organic function is a valuable building block for organic synthesis and affords the creation of chiral centers optionally. Several reviews have dealt with this field in homogenous conditions involving manmade catalysts with metal centered systems or enzymatic systems.[159–164] The former were mainly based on redox metals such as Cu, Fe, Mn or Ru and Os, while monooxygenases and epoxide hydrolases for kinetic resolution were selected.[165] Several predominant oxidation pathways have been used for enantioselective epoxidation that include direct oxygen transfer on the double bond, nucleophilic substitution on halohydrins or kinetic resolution methods from diols and epoxides. Biotechnological processes concern the use of porcine pancreatic lipase for racemate resolution via hydrolysis of epoxy esters.[166] Epoxide

hydroxylases have been also employed in order to generate chiral indene oxide in a patented Merck process,[167] while (S) *p*-nitrostyrene oxide was isolated through a Janssen process.[168]

The chemical counterpart concerns the Sharpless and Jacobsen processes that implicate the stoichiometric use of a Ti(O*i*Pr)$_4$ a pure dialkyltartrate and *tert*-butyl hydroperoxide (**TBHP**) as the oxygen donor which gave source to several processes used by Arco chemicals.[169,170] Then, Jacobsen used the famous Mn(salen) complex as a precatalyst with hypochlorite salts leading to a ChiRex process at multitone scale. Alternatives concerned a two-step process in which dihydroxylation of alkene is followed by conversion into epoxides. The use of OsO_4 for the epoxidation step and the use of $K_3[Fe(CN)_6]$ preclude its use nowadays. Conversely, hydrolytic kinetic resolution designed by Jacobsen *et al.* with the design of a Co(salen) catalysts was developed by Rhodia Chirex.[171,172]

As observed in the examples mentioned above, the different synthetic solutions are rather stoichiometric or with a high loading of catalyst, which justified the continued efforts in this field. Prior to chiral solutions, new ligands have been developed that include pyridine and amino based ligands, porphyrin or porphyrinoid molecules.[173,174] The initial effort was put towards the stabilization of the metal-oxo species guaranteeing the selectivity of the reaction. This has been successful with the major contribution of Que Jr *et al*. and Costas *et al,* by defining mono and binuclear Mn and Fe complexes containing TPA , Bispicen or cyclam ligands, illustrated in ***figure 21***.[175,176]

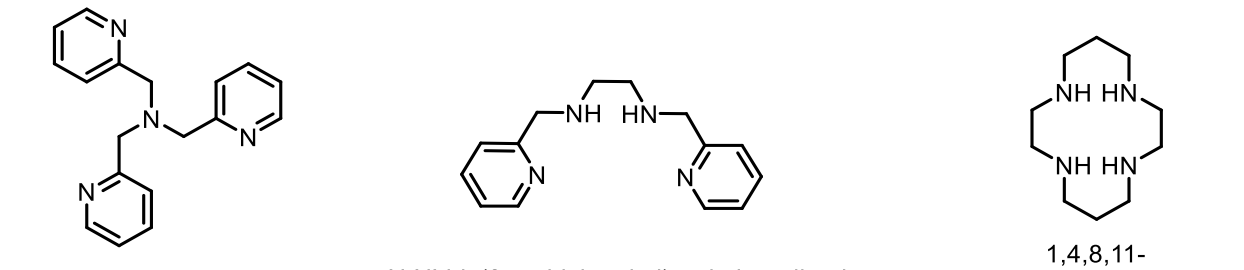

tris(pyridin-2-ylmethyl)amine **TPA**

N,N'-bis(2-pyridylmethyl)- ethylenediamine **Bispicen**

1,4,8,11-tetraazacyclotetradecane **cyclam**

***Figure 21**: structures of TPA , Bispicen and cyclam ligands*

The oxygen transfer mechanism has been deciphered, and has put to light the importance of high valent Mn or Fe- oxo species.[177,178] Nam *et al.* have also added examples that involved other 3d-block metals.[179–182] Some of the most efficient non heme iron systems reached over 1000 TONS at -30 °C using peracetic acid as the oxidant[183] or with tetradentate

iron-NHC complexes with incredible TOF of over 410000 h^{-1}.[184] Another highly efficient catalyst is the porphyrinic Mn(**TPP**), that reaches over 7. 10^6 TON.[185] At LCBM, our group had designed a μ-oxo diferric complex containing bipyridine ligands capable of efficient and rapid enantioselective epoxidation with up to 62% of recorded ee.[186]

Another example for efficient alkene epoxidation involves iron picolinates complexes inspired by the Goagg system. Remarkably, picolinate and 6-Methylpicolinate ligands stabilized iron(III) species forming Fe(pic)(6-Mepic)$_2$, the supposed catalytic form, *in situ*. The catalytic solution containing the metal precursor and the ligands oxidizes with high efficiency the transformation of alkenes with hydrogen peroxide as the oxidant. It has to be noted that such catalytic systems require a high concentration of metal and catalyst loading.[187,188]

Finally, a greener and more attractive strategy involves the use of dioxygen as the oxidant to perform the enantioselective catalysis.[163] The seminal work by Mukaiyama comprises a Mn(salen) complex, with a high catalytic loading (2 to 5%), the use of dioxygen in sus of an aldehyde (isobutyraldehyde (IBA) or pivalic aldehyde) to transform conjugated olefins.[189] Drawbacks were the high loading, the limitations to cyclic conjugated olefins and the low specificity. High TON were reported with a manganese complex with a bisdiamide ligand.[190] However, the uncatalyzed reaction yield was quite high and the reaction requires moderate temperatures.[191] E. Jacobsen *et al*. developed a process in which they circumvent the use of a reductant as the solvent is oxidized into an oxidative specie. Iron systems were also reported in which a sacrificial co-substrate, here a α-ketoester, was playing the role of the metal ligand during a selective epoxidation of stilbenes.[192] Tetra-amido macrocyclic ligand (TAML) iron (II) species was found to oxidize at 50°C and up to 80 TON in 20 hours through the formation of high valent oxidizing diiron species.[193] Ruthenium porphyrin and ruthenium or nickel Schiff base complexes have been reported to be active as well.[194,195]

The enantiospecificity is reached by their enzyme counterpart, using iron or flavin-dependent monooxygenases as in the work of Mutti and coworkers[196] and references therein; Li et al. [197] or peroxygenases[198] with the emphasis that the oxidant is either O_2 or H_2O_2 but needs the presence of a FAD reductase enzyme to promote epoxidation reactions.

Finally, the transfer of porphyrin-based catalysts from homogeneous to heterogeneous media has led to a tremendous enhancement of stability, via their grafting to solid phase Fe_3O_4

nanoparticle for better separation,[199] on graphene oxide,[200] and on silica.[201] Their non heme counterpart such as Mn(salen) are available as well. A recent review on immobilization of enzymes devoted to cascade reactions illustrate the latest achievements combining microfluidic advances and modes on entrapments that can be valuable for the heterogenization of in lab catalytic process such as epoxidation amongst others.[202]

3.2.Metal catalyzed CO_2 cycloaddition with epoxides

CO_2, a stable and abundant molecule, is a great source of carbon. The high economical value of cyclic carbonates and polycarbonates in general resulted in the merging of several interesting routes for CO_2 utilization. Here, we are interested in cyclic carbonates (CC) production. The synthesis of CC from epoxide and CO_2 englobes some commercially available processes.[203–205]

Beside the general attractiveness of cascade transformations, producing cyclic carbonates from alkene derivatives rather than their epoxide analogues is even more appealing, as the latter tends to be more costly and less stable. Following general cascade classification, CC one pot process can be either sequential or simultaneous. Moreover, within the one pot transformation scheme, depending on the number of catalysts employed (considering a catalyst able to perform both transformations), these transformations can be categorized as shown in ***scheme 16*** with regards to the classification terminology employed by Launay and coworkers.[156]

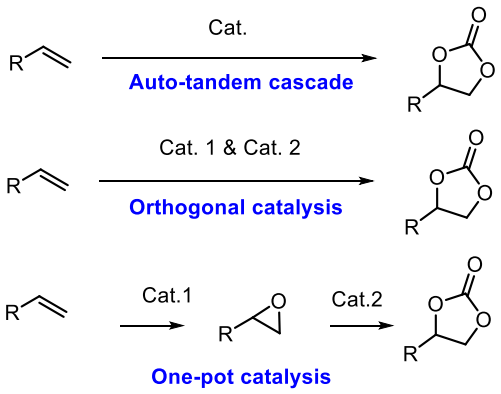

***Scheme 16**: classification of cascade transformations*[156]

Auto-tandem catalysts are very attractive catalytic entities with functionalities that confer the ability to catalyze both alkene epoxidation and CO_2 cycloadditions. A notable example of engineered auto-tandem catalysts is Metal Organic Frameworks (MOF). The overall

structure of MOF provide great tuning possibilities in terms of motifs, metal centers, size and distances between each catalytic site.[206]

The cycloaddition of CO_2 into epoxide rings can be initiated by the activation of either or both substrates. There are two proposed mechanisms for this transformation. In the first one, CO_2 is activated by a nucleophilic attack forming an intermediate that will then promote the ring opening of the epoxide assisted with a Lewis acid. Then, the last cyclization step results in the formation of the desired product and the regeneration of the nucleophile.

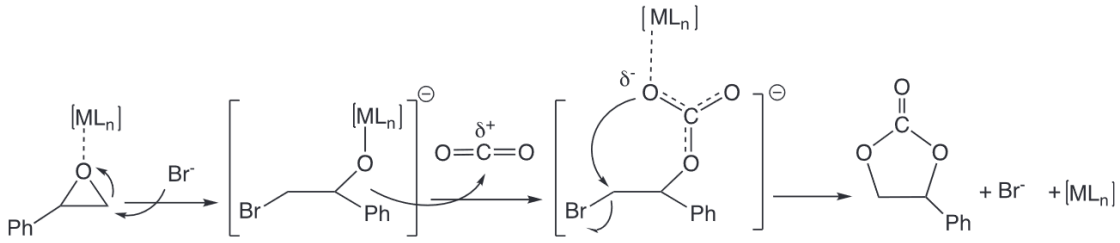

Scheme 17 *two steps mechanism of cycloaddition of epoxides by CO_2*[156]

A second mechanism suggests a two steps process: i) the first step of the transformation is the activation of the epoxide by a nucleophilic attack causing the epoxide ring opening promoted by a Lewis acid.; ii) subsequent insertion of the CO_2 molecule into the oxygen-Lewis acid bond followed cyclization step resulting in the formation of the desired product and regeneration of the nucleophile, ***scheme 17***.

Whether both or either mechanisms are considered, the information that stands out is that this transformation requires both a nucleophile and a Lewis acid. The reaction can be catalyzed under homogeneous conditions using organometallic compounds, metal salts and organocatalyts or under heterogeneous conditions using metal organic framework or supported catalysts.

There are several strategies for the cycloaddition of CO_2 to epoxides, with a recent effort to perform this reaction under ambient conditions following greener pathways.[207] Remarkably, cycloaddition is a process that can be carried out under these conditions because it is thermodynamically favored, and its driving force depends on the release of energy from the ring chain contained in the epoxide substrate.

The synthesis of cyclic carbonates from CO_2 is already used in industry. Two major processes have been reported: The Shell omega process, in which intermediate ethylene carbonate is

hydrolyzed to ethylene glycol[208] and the Asahi Kasei Process for the production of bisphenol A polycarbonate.[209]

Salen and analog complexes are prominent candidates for homogeneous catalysis of CO_2 cycloaddition, particularly attractive for the easiness to tune their structure and the accessibility to their asymmetrical form. The seminal work brought by Nguyen *et al.* demonstrates the ability of a Cr^{III}(salen) complex to catalyze the reaction at room temperature, in the presence of a pyridine-based nucleophile. While energetically interesting, the process still required 7 bar of CO_2 pressure.[210] It has been followed by Al^{III}, Mn^{III}, Co^{III} analogues either in their monometallic or bimetallic form.[211] A chiral version allowed the kinetic resolution of epoxides by cycloaddition of CO_2.[212]

The performance of these systems (TON above 100 and TOF 4 h^{-1}) were exceeded by the use of Zn(TPP) porphyrin systems, substituted with a tetraalkylammonium chain with TOF up to 34 h^{-1} and TONs over 1500, justified by a cooperative mechanism between the pendant alkyl chain of the ligand and the metal center. These performances are also accessible with bismuth complexes bearing a sulfur bridged bisphenolato ligand.

Heterogeneous catalysis has also been undertaken, considering immobilization of the Lewis acid with a large amount of the nucleophile. Under these conditions, bimetallic Al(salen) complexes anchored to Merrifield resin or silica afforded a large improvement of the activity compared to the non-grafted analog complexes.[213] Microporous organic polymers were found the more efficient heterogenous catalysts. First, Al or Mn salen conjugated polymers,[214]formed by a Sonogashira coupling between a preformed salen and a polytopic ligand afforded an excellent TON and reusability.[214] Again, the insertion of **TPP** into wall of 3D Porous organic polymers had a great impact on its catalytic properties. The radical polymerization of vinyl functionalized **TPP** led to enhanced properties compared to their homogeneous analogues. The best system reported so far consists in the **TPP-**based hyper cross-linked polymers containing Al center, reaching TOF up to 103 h^{-1} and 3101 TON under ambient conditions.[215] Increasing nucleophile concentration, here **TBAB**, led to a drop of the TON but a higher frequency.[216] The excellent capacities of the **TPP** based POP results probably from the contribution of the intrinsic catalytic activity of the metalated **TPP** coupled to the microporous environment, the latter helping to concentrate the CO_2 near the catalytic centers.

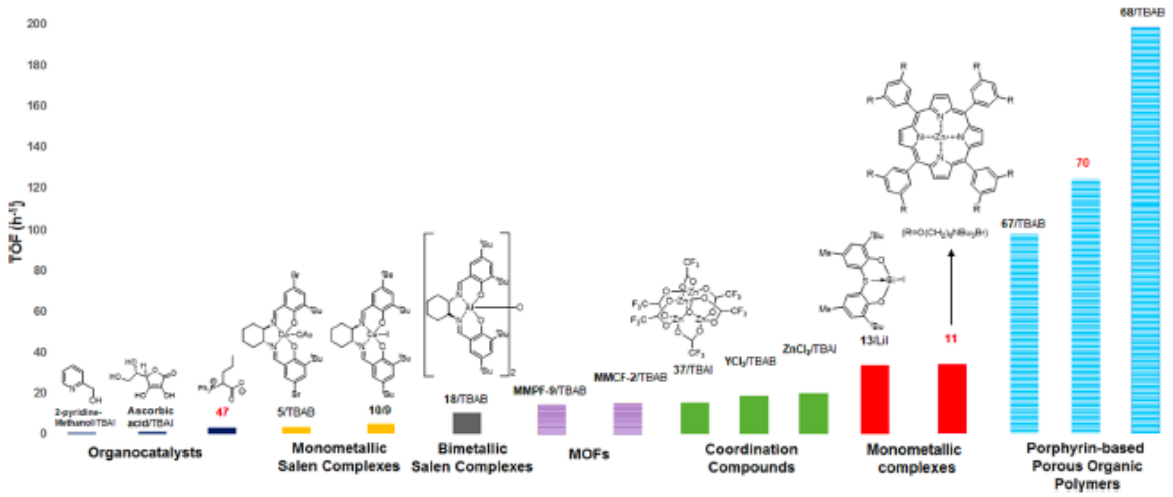

***Figure 22**: prominent examples of catalytic systems for CO_2 cycloaddition and their relative activity*[217]

3.3.Cascades using O_2 and CO_2

When comparing several catalytic systems for CO_2 cycloaddition, the interesting parameters include substrate to catalyst ratio, CO_2 pressure, temperature, and reaction time. In 1987, Aresta *and coll.* reported a cascade in which they used Rhodium (I) complexes as sole catalysts for the transformation. With 1% catalyst loading, 0.5 bar of CO_2 and O_2 partial pressure, at 40 °C degrees in THF, they achieved a complete conversion of styrene with 25% of styrene carbonate (SC) formation yield.[218] The lower SC yield is partially due to the poor selectivity of the epoxidation step. In fact, this transformation is in competition with the oxidative cleavage of the styrene thus, resulting with the formation of benzaldehyde. The overall selectivity of the transformation was strongly influenced by solvents, temperature, and pressure. For instance, the optimum selectivity for styrene oxide was reached at lower dioxygen pressure. This example is one of the first tandem reactions reported that combined O_2 and CO_2 for SC formation. Such examples in the literature remained scarce until the latest years.

In 2010, Bai *et al.* reported a new catalytic process that consisted of a cascade scheme in which they associated a dioxo(tetraphenylporphyrinato)ruthenium(VI) complex with quaternary ammonium salts for SC formation from styrene. 89% of SC after 60h with 4% of catalyst loading, 2 equivalent of tetrabutylammonium iodide (TBAI) under 16 bar of gas pressure (CO_2/O_2: 1,1/ 0,5) were obtained under optimized conditions. The reported catalytic process was also applicable to aliphatic olefins, where the recorded yields were lower as compared to styrene, which is to be expected for non-activated olefins. The influence of the ammonium salt on the reaction with aliphatic olefins was also highlighted. For instance, the

case of 1-octene, using **TBAI** afforded less than 1% of the corresponding carbonate whereas using phenyltrimethylammonium tribromide (**PTAT**) afforded 78% yield. Interestingly, this trend was reversed in the case of 3-Chloropropylene where **TBAB** allowed 56.7% of yield compared to 4,6% with **PTAT**. The same trend was observed for styrene, highlighting the importance of choosing the right co-catalyst for the right substrate.[219]

Other notable examples using O_2 and CO_2 under homogeneous conditions stand out of the work of Launay *and coll.* that were inspired by the mukayiama epoxidation involving O_2 and an aldehyde as the electron donor coupled with a Mn(salen) catalyst. They combined the Jacobsen catalyst with Choline at 0,1 mol% and 1.6 mol% respectively adding IBA for O_2 activation and TBAB for CO_2 activation. Preliminary investigations on both of the intrinsic transformation has shown that the epoxidation step is optimum when carried out in a flask under 80ml/min oxygen flow as opposed to the pressure reactor under 5 bar of oxygen with recorded yields at 60% and 35% respectively. Moreover, for this, the optimum temperature determined was of 80°C for the first step and 120 °C for the second one. As it can be expected, combining the optimum reaction conditions for both steps resulted in poor SC yield, 1% at 120°C and no SC formation at 80°C in a pressurized reactor. To circumvent this incompatibility, they adopted a two temperatures pathway in which the catalytic mixture containing all of the actors for the cascade, in the pressurized reactor, under 5 bars of O_2 and 15 bar of CO_2 was put under 80°C for 3 h then 120°C for 20 h. Unfortunately, the cascade transformation remained unsuccessful. This example remains relevant as it highlights the typical difficulties encountered when designing a cascades transformation. The authors were able to attribute this to the presence of IBA in the mixture that hinders the formation of SC out of several blank assays.[220] In a later publication, they reported a novel one-pot approach for SC formation, using a chromium Salophen catalyst alongside IBA and TBAB. SC was formed at 34% yield in an orthogonal setup where the reaction actors were mixed in the pressurized reactor under 11 bar of CO_2 and 3.5 Bar of O_2 at 80°C for 23h.[221]

3.4.Cascades using peroxides and CO_2

Cascades using hydrogen peroxides and alkyl hydroperoxides have been reported since the early 2000. In this part will be differentiated one-pot cascades (where the second catalyst, for the second transformation, is added at a later stage) with possible condition variations from

orthogonal cascades (where the initial catalytic mixtures contain all the cascade constituents and condition optimized for the overall transformation). [156] A widely used alkyl hydroperoxide is terbuylhydroperoxide (**TBHP**) and in some cases cumene hydroperoxide (**CHP**) as well. In some reported cascades, the epoxidation step was non-catalyzed. Thus, **TBHP** was directly associated with the cycloaddition catalyst. Girard *et al.* investigated several immidazolium salts as ionic liquid catalysts for CO_2 cycloaddition. They determined N-butyl-N'-methylimidazolium bromide, **BMImBr**, as the most efficient catalyst out of the tested series; at a CO_2 pressure of 5 bar, with 10% of catalyst loading, they afforded 70% of SC at 100 °C and 90% at 150 °C with a stability up to three runs. In an orthogonal scheme, they associated this catalyst with 1.5 eq of **TBHP** for the direct synthesis of SC from styrene. 90 % conversion of styrene was observed with 40% of SC selectivity after 6 h at 150 °C.[222] Many examples of cascades were designed using heterogeneous conditions with catalysts embedded in silica, CNT, metal oxides and MOF/MOL (Metal Organic Layers). Sun *et al.* reported a process in which they associated a Au/SiO_2 catalyst as the epoxidation catalysts alongside either **TBHP** or **CHP** with **$ZnBr_2$/TBAB** for the cycloaddition. They were able to afford 42% of SC under typical conditions, 4 h at 80°C under 10 bars of CO_2. Surprisingly, higher CO_2 pressure did not result in higher SC yields.[223]

Han *et al.* designed a POM-based MOF using pyrrolidine motifs as organocatalyts and POM as oxidation catalysts. The complex and intricate design of the MOF as described in ***figure 23*** displayed astonishing catalytic results. The catalytic performances of the MOF reached yields as high as 92% for SC production and ee of 79% after 96 h of reaction time at 50 °C.[206]

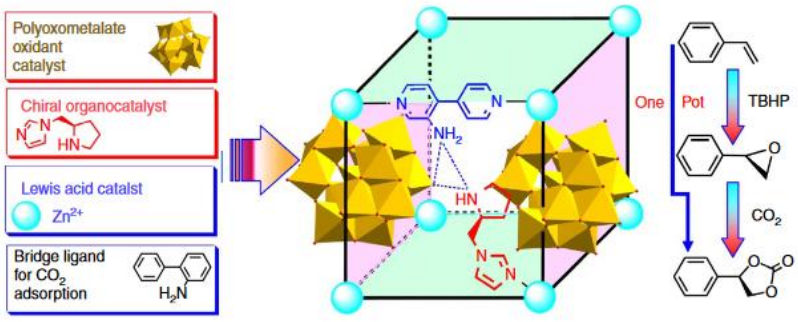

***s 23**: illustration of the MOF catalyst designed by Han et al.*[206]

4. Conclusion and project description

This non exhaustive bibliographical introduction lays the foundations around which this thesis project was constructed. Indeed, the aim of the project is to design a CLEC dual-site ArMs for the synthesis of cyclic carbonates from alkene derivatives. To tackle the project, the transformation was divided into an epoxidation-CO_2 cycloaddition pathway, ***scheme 18.***

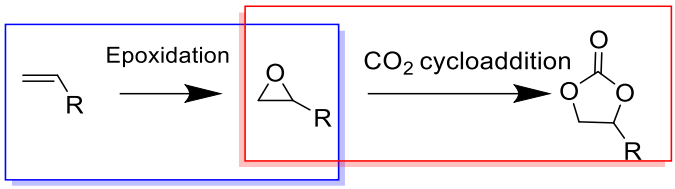

***Scheme 18** : targeted reaction pathway for carbonate synthesis*

The project revolves around three major tasks: i)- The design of the protein scaffold and the preparation of the metal catalysts (artificial active sites), ii)- Protein complex anchoring assays and the characterization of the designed ArM, iii)- ArM stabilization and catalytic investigations on the cascade transformation.

First, the scaffold of choice for this project is the protein NikA. Up to now, we have been exploiting its natural cavity to anchor the catalyst via supramolecular interactions. In order to create a second active site, we have chosen to covalently bind a second catalyst to the protein. Generally, covalent modification of proteins is performed via the modification of either lysine or cysteine residues.[224,225] Since lysine residues present in NikA are to be engaged in the cross-linking step with glutaraldehyde, mutants containing one cysteine were produced via site-directed mutagenesis. WT NikA is cysteine free, and this particularity gives total control of the location of the second complex by choosing the mutation position.

The intracrystalline mesoporosity of NikA crystals affords two interesting areas for the introduction of a second active site, the protein cavity or the solvent channels, ***figure 24.*** Introducing the second site near the protein cavity, would allow the two active sites to be in close proximity and therefore it might improve the substrate availability during the catalytic cascade reaction. The second target area are the solvent channels. They correspond to the outer surface area of protein units meaning that the cysteine would be exposed and accessible in solution and *in cristallo,* either by the metal complex for the anchoring step or the reaction substrate during catalysis.

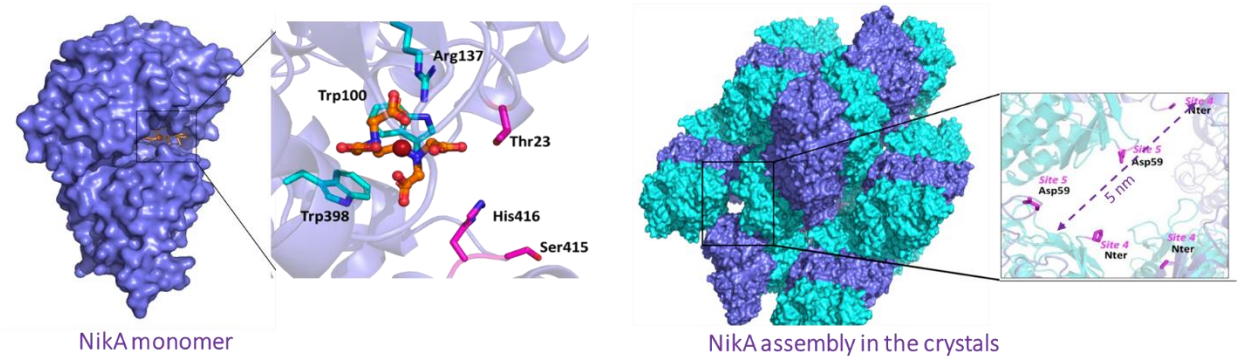

***Figure 24**: selected mutation positions shown in pink in the cavity (left) and solvent channels (right)*

As described earlier in this chapter, there are many ways to covalently modify cysteine residues. Our initial choice was the Michael addition, commonly used in protein modification and reported to be highly selective for the cysteine.[224,226]

The catalyst choice is influenced by the anchoring mode intended for the complex, and by extension its size and its localization within the protein scaffold. For alkene epoxidation, in order to exploit the cavity of the protein, we have preselected reported epoxidation catalysts that can either be easily functionalized or readily contain a carboxylate moiety for the successful displacement of FeEDTA in NikA , ***figure 25***. [96,187,188,227] In addition to the presence of the crucial carboxylate function, the geometry and size of these candidates were deemed suitable for NikA's cavity based on previously investigated complexes.[95,96]

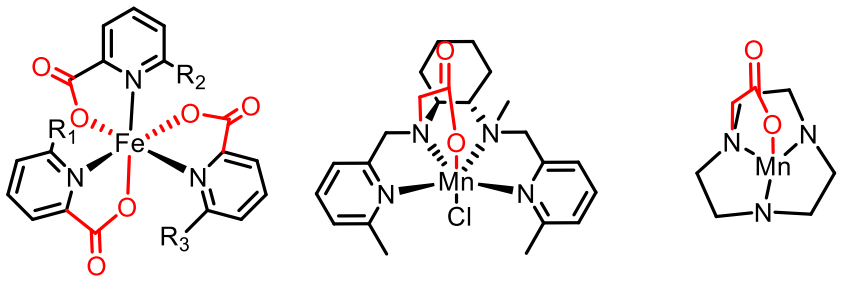

***Figure 25:** epoxidation complexes intended for supramolecular protein-complex interaction*

Covalent anchoring adds more liberty to the complex choice as it allows the exploration of other areas within NikA, besides its native cavity. Indeed, the relatively large diameter of the solvent channels (5 nm) can bear more constraints structures, for instance, metal (salen) complexes. Interests in salen ligands stems out their versatility for both epoxidation and CO_2 cycloaddition. Therefore, we aimed at the design of versatile ligands that can be applied to alkene epoxidation (Mn or Fe metal centers) or CO_2 cycloaddition (Co metal center), ***figure 26***.

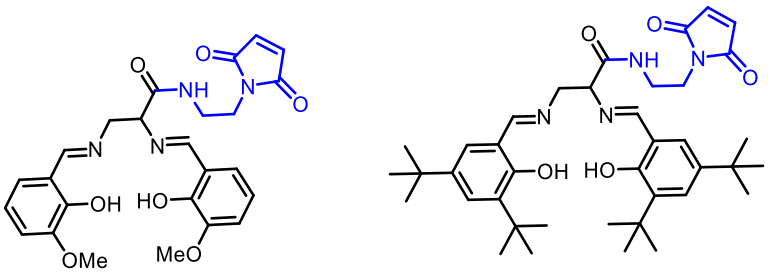

Figure 26: *versatile salen ligands for covalent anchoring*

Secondly, efforts were put towards the preparation of the dual-site ArM by the optimization of the crystallization of NikA mutants and the protein-complex anchoring assays as well. The main challenge throughout this study is to be able to localize the complex and formally identify the C-S bond formation. Lastly, the designed mono-site and dual-site ArM were investigated on alkene epoxidation, CO_2 cycloaddition and the cascade transformation.

In the upcoming chapters, will be discussed the strategy and the results obtained throughout these investigations. The first chapter will be dedicated to the synthesis and characterization of the ArM building blocks: the complexes and the NikA mutants. Next, a chapter will be dedicated to the protein-complex anchoring assays and characterizations of the mono- and dual-site ArM prepared. Finally, catalytic investigations on the prepared heterogeneous ArM will be discussed with the highlight on the influence of the ArM preparation methodology and the oxidant choice on the efficiency of the catalytic process.

Chapter II Catalysts and enzymes preparation

To tackle the project one building block at a time, the first step is the preparation and characterization of the main jigsaw puzzles, the proteins and the complexes. Our first interest is the creation of artificial ArM for a cascade transformation. Second, we are interested in the investigation and promotion of stereoselectivity through the process, brought either by a chiral complex, by the protein environment or by the combination of both. The design and production of dual-active site ArM from NikA starts with the creation of a new active site, additional to the native binding pocket, the latter transformed to an active site by supramolecular anchoring of an active metal complex.

For the second active site, we opted for a covalent anchoring mode, orthogonal to the first mode. The first step for the introduction of this site starts with the choice of the AA to be covalently modified. We opted for a cysteine residue to be introduced via site-directed mutagenesis, as no cysteine is present in the native NikA sequence. This particularity gave the opportunity to choose freely the position of the mutation site. Nevertheless, this choice is restricted by three factors: the accessibility of the cysteine residues, the space available for the complex introduction and the integrity of the protein crystals. For the first and second factors, the evident areas of choice are the solvent channels, that confer the mesoporous aspect to the protein crystals and the native cavity (***figure 24***) as it has already been investigated and validated as a great host for catalytically active complexes.[93,96,228,229] The third factor eliminates evident crucial positions for successful protein crystallization, the Arg137 residue responsible for the salt-bridge and the nearby Arg97, Tyr398 and Tyr402 residues involed in complex stabilization. On the other hand, as stated previously, the targeted complexes were selected based on their ability to provide efficient epoxidation and carbonation catalysis in organic solvents and the presence of a function ensuring their insertion into the protein.

In this chapter, will be discussed the preparation and characterization methods for both the catalysts and the protein mutants. For clarity purposes, the cavity of the protein will be referred to as the ***first site*** and the added cysteine as the ***second site***. Moreover, complexes intended for each site will be sorted accordingly.

1. Preparation and characterization of the metal complexes

1.1.Complexes for anchoring to the *first site*

For the first active site, we have selected a series of oxidation catalysts that include a carboxylate moiety. It was postulated that this readily present function would engage in a salt bridge with the **Arg137** residue ensuring the formation of a stable ArM. Following are the preparation and characterization efforts for the selected complex candidates.

1.1.1. Iron picolinates derivatives

At first glance, iron picolinate derivatives illustrated in ***figure 27***, appear suitable for the NikA system. The picolinic acid derived ligands are commercially available and they readily contain carboxylate moieties that could target the first anchoring site on the protein.

The reported catalytic species $Fe^{III}(Pic)(MePic)_2$ **A**, known to catalyze epoxidation with hydrogen peroxide was described as being more efficient compared to its homo-ligand analogs.[230] It is supposedly formed *in situ* by mixing equimolar quantities of 6-methylpicolinic acid (MePicH) and 2-picolinic acid (PicH), with $Fe(OAc)_2$. The reported X-ray structure of $Fe^{III}(Pic)(MePic)_2$ **A**, was obtained through crystallization of the acetonitrile (MeCN) catalytic solution.[230]

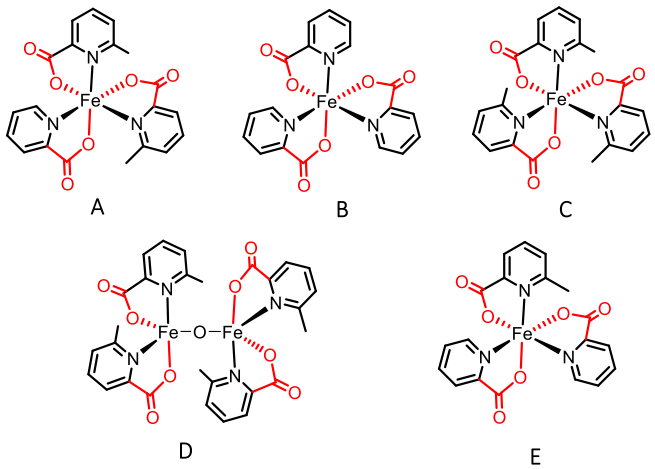

***Figure** 27: iron picolinates species used in this study*

The $Fe^{III}(Pic)(MePic)_2$ complex was prepared according to the reference[230] : after 30 min at 40°C in acetonitrile (MeCN), the solution was left at room temperature overnight and no crystals were formed. Unfortunately, in our case, several crystallization attempts remained

unfruitful. Instead, we noticed the formation of a light-yellow precipitate. The recovered precipitate had very low solubility in organic solvent at room temperature including in MeCN.

ESI-MS analysis in MeCN suggests the presence of several iron species including the expected form as seen in ***figure 28***. Alongside the expected species at 473 m/z corresponding to the species $(Pic)(MePic)_2\ Fe^{III}$ + Na^+ and at 489 m/z corresponding to $(Pic)(MePic)_2\ Fe^{III}$ + K^+ several fragments correspond to other recognizable iron picolinates species. For instance, $(Pic)_3\ Fe^{III}$+ Na^+ at 445 m/z and $(MePic)(Pic)_2\ Fe^{III}$+ Na^+ at 459 m/z.

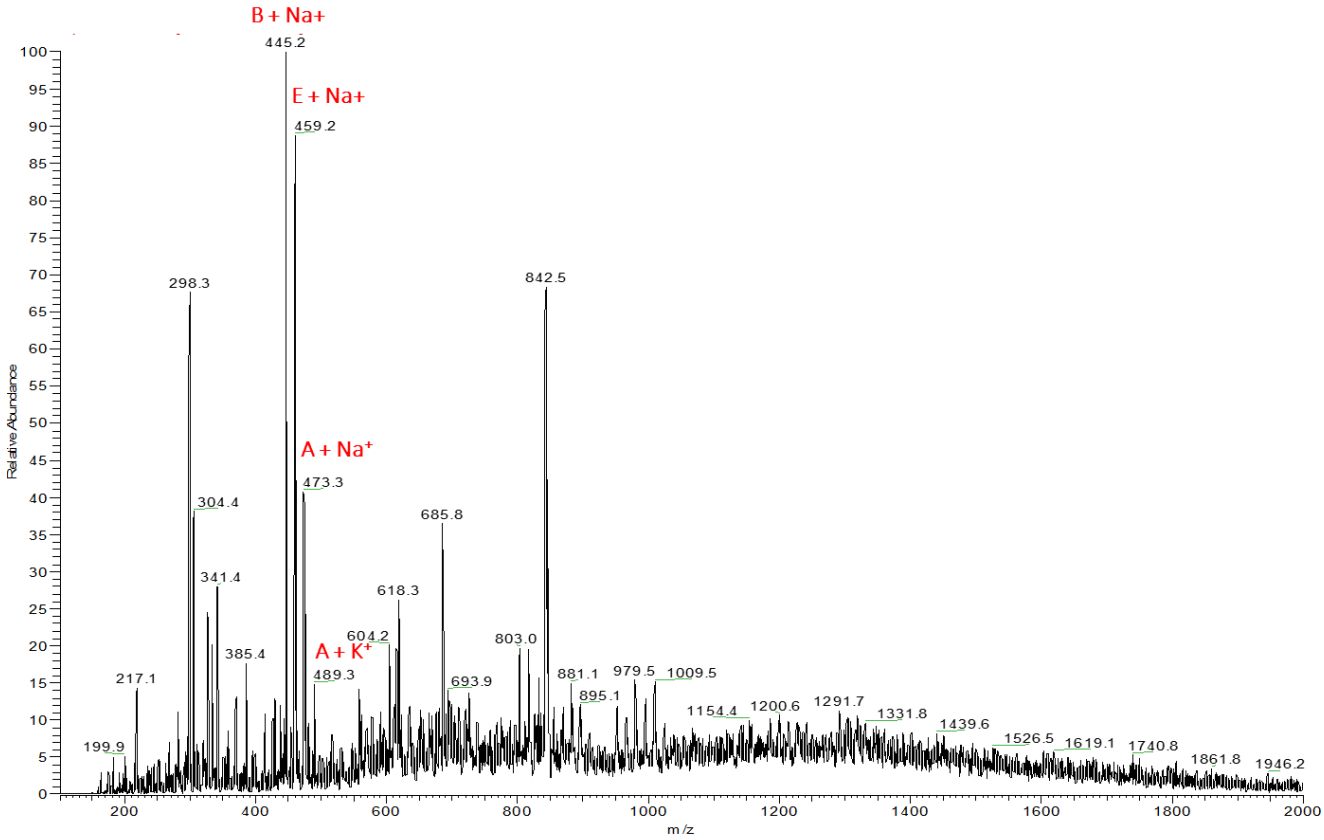

Figure 28 *: positive mode ESI-Ms spectrum of Fe(Pic)(MePic)² sample in MeCN showing the presence of species* ***A, B*** *and* ***E***

At first, we assumed that the mixture of species resulted from the competition between the two different ligands with no direct explanation that would favor the formation of one specie out of the others. In order to avoid the hassle of sorting out the active form out of many, we have decided to work with one ligand at a time.

Following an identical preparation method, we prepared the catalyst solutions of both of $Fe^{III}(Pic)_3$ **B** and $Fe^{III}(MePic)_3$ **C**. Attempted crystallization by slow evaporation of acetonitrile overnight yielded light green crystals corresponding to both catalysts.

As seen in ***figure 31***, mass analysis of $Fe^{III}(pic)_3$ **B** sample highlights the presence of a peak at 445 m/z corresponding to the $(Pic)_3Fe^{III} + Na^+$ species alongside with a dimer structure at 867 m/z for $2(Pic)_3\ Fe^{III} + Na^+$ and 882.8 m/z $2(Pic)_3\ Fe^{III} + K^+$. Trimers fragments at 1288.6 and 1304.4 m/z ($3(Pic)_3\ Fe^{III} + Na^+$ and $3(Pic)_3\ Fe^{III} + K^+$ respectively) and tetramers at 1710 and 1870 ($4(Pic)_3\ Fe^{III} + Na^+$ and $4(Pic)_3\ Fe^{III} + K^+$ respectively) were detected as well. Although it is unclear if these species are association oligomers resulting from the electrospray ionization or fom bridging carboxylate moieties, it is worthy to note that crystals from **B** correspond to the expected monomer and afforded comparable ESI-Ms once dissolved in MeCN.

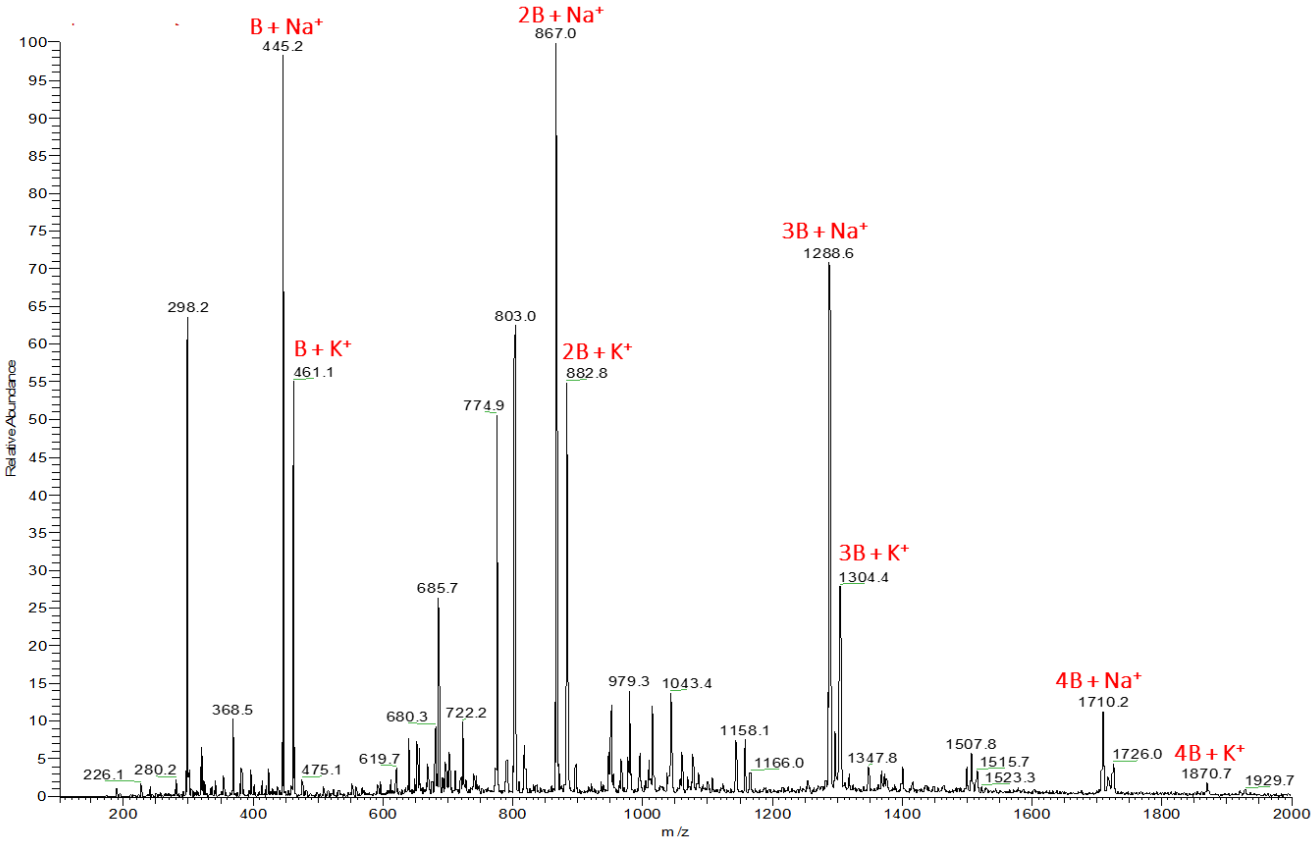

Figure 29 *: ESI-MS spectrum of solubilized crystals of Fe(pic)$_3$ in MeCN*

Surprisingly, mass analysis of $Fe^{III}(MePic)_3$ **C**, seen in ***figure 30***, displayed the formation of the µ-oxo binuclear complex **D** at **711** m/z alongside the monomer **C (see *figure 27*)**. Control by crystallography confirms that in fact under these conditions, the crystallized form is the µ-oxo dimer **D**, identical to previous studies.[188] Solubilization of the crystals afforded the starting mass spectra showing **C** and **D** whereas adding two equivalents of MePicH to the solution afforded the spectrum shown in ***figure 31*** in which only the monomer **C** is observed.

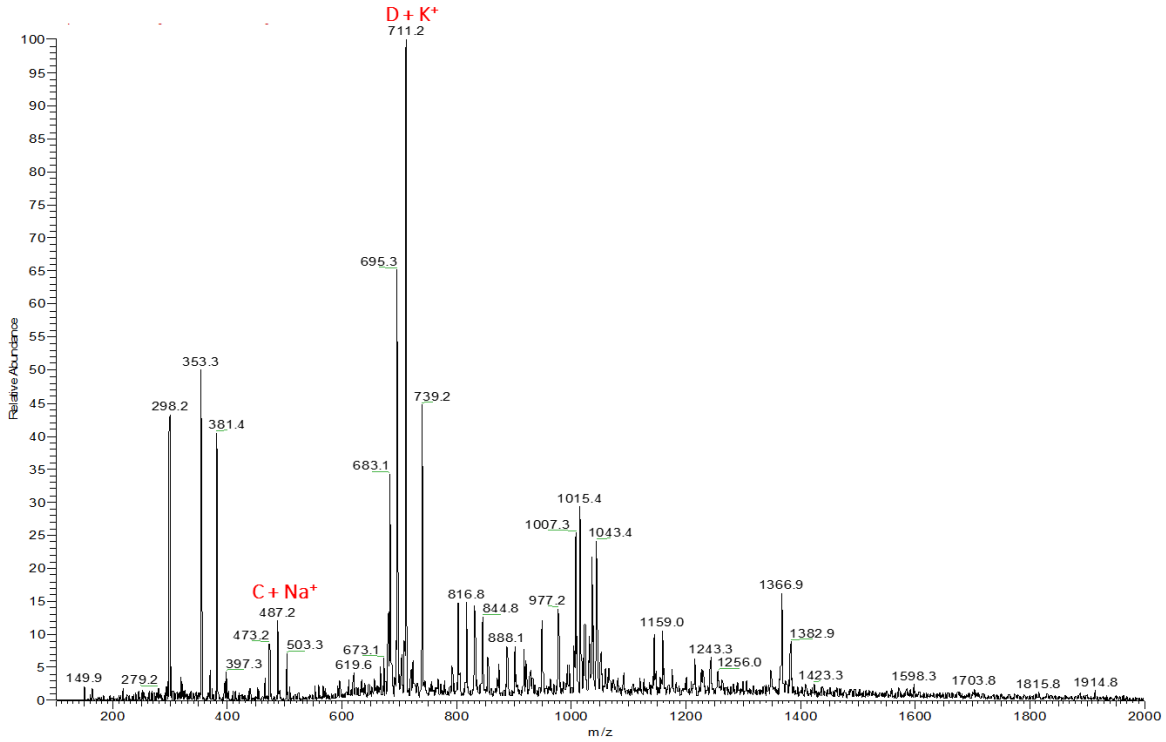

Figure 30: *ESI-Ms spectrum of* ***C*** *Fe(Mepic)$_3$ in MeCN*

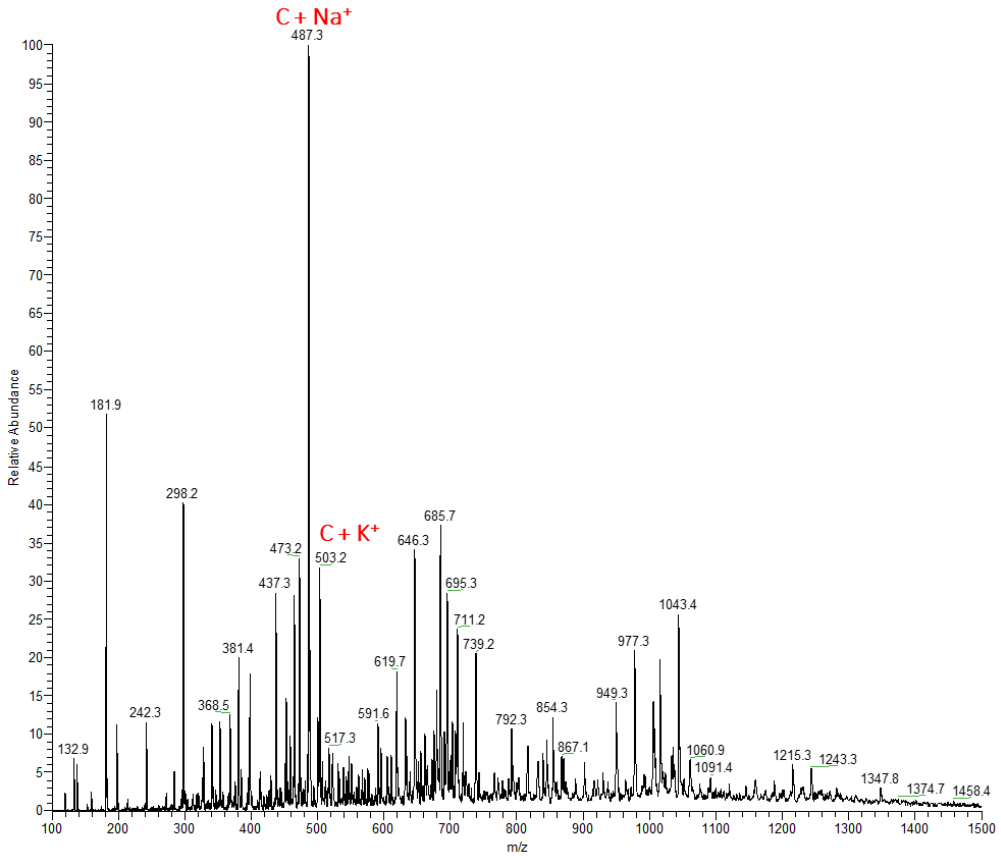

Figure 31: *ESI-Ms spectrum of sample* ***D*** *with 2 equivalents of MepicH in MeCN*

As the room available in the NikA cavity might be insufficient to accommodate the dimeric form, we have prepared a catalyst solution of $Fe^{III}(MePic)_3$ **C** using six equivalents of ligand MePic in order to favor the formation of the monomer. This solution was let to sit overnight at room temperture. $Fe^{III}(MePic)_3$ **C** was recovered as green crystals with a 60% yield. Unfortunately, solubilization of theses crystals in MeCN resulted in the complete degradation of the complex as seen in ***figure 32***.

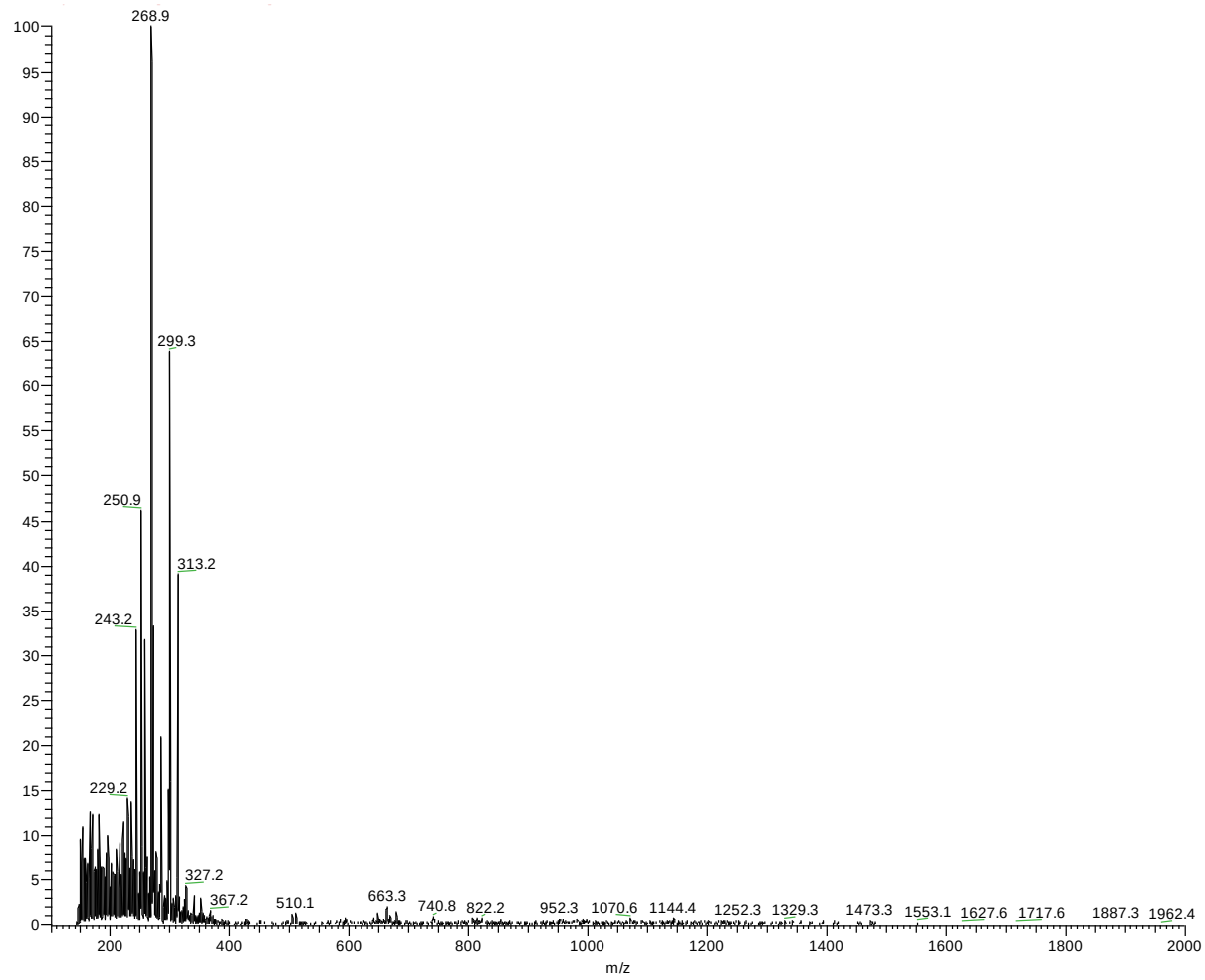

Figure 32: *ESI-MS data of solubilized $Fe^{III}(Mepic)_3$ **C** crystals in MeCN*

Out of these characterization efforts, we have confirmed that these catalysts are prone to the formation of several species. Questioning on the catalytic active form remains unanswered. Nevertheless, we did pursue catalytic investigations in solution in order to rule out the obvious inactive species. In addition, we assumed that the protein cavity might display a "sorting" effect by selectively binding the form to which it has the highest selectivity. These investigations aspects will be discussed in chapter IV.

1.1.2. MnL_{III} complex inspired by iron bpmcn

The idea to work with $Mn^{II}L_{III}$ was inspired by their $Fe^{II}L_{III}$ analog reported by the team, [$L_{III}H$ = *2-{[(1S,2S)-2-{methyl[(6-methylpyridin-2-yl)methyl]amino}cyclohexyl][(6-methylpyridin-2-yl)methyl]amino}acetic acid*], for its sulfoxidase activity when associated with NikA.[96] Knowing that the overall geometry of the complex was compatible with NikA's cavity did in fact make the ligand choice appealing. Nevertheless, the iron analog tends to oxidize from Fe^{II} to Fe^{III} which might not affect its catalytic activity in solution but may lower NikA's affinity towards the most charged form (Fe^{III}), due to the presence of positively charged residues inside NikA cavity (**Arg97** and **Arg137**).

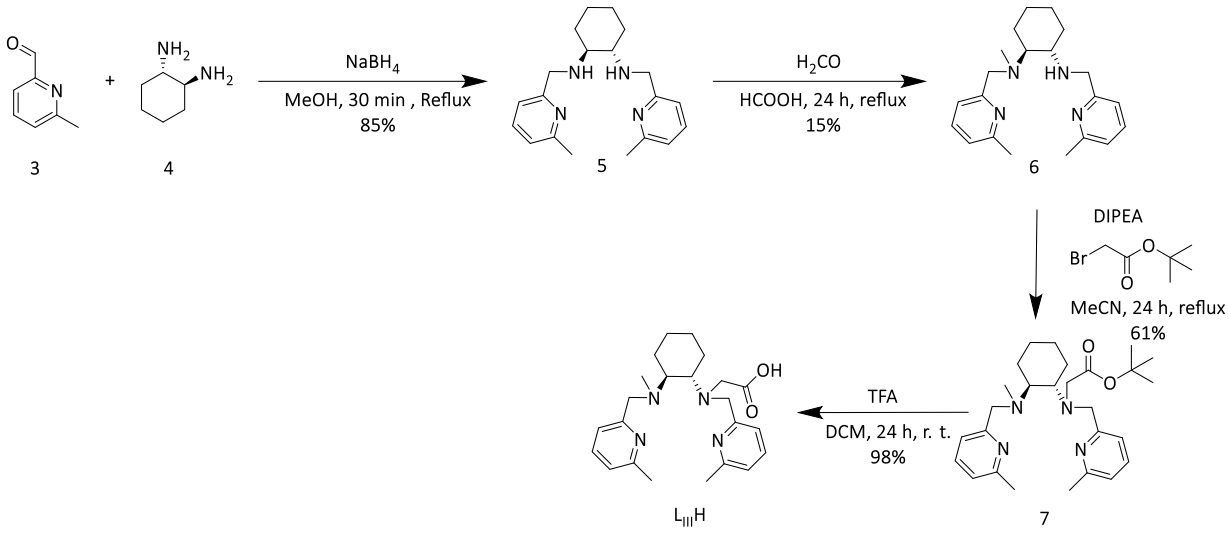

Scheme 19 : *synthetic pathway of $L_{III}H$*

The solution that has been previously adopted was to perform anchoring assays in the glovebox under inert conditions. Furthermore, preliminary investigations on FeL_{III} have shown no conclusive results on epoxidation of alkenes. For all the above reasons we have decided to prepare the manganese analogue, as manganese complexes are often suitable for epoxidation catalysis.[231] The synthetic pathway was adapted from the previously reported methods.[96] As described in ***scheme 19***, product **5** was obtained in 85% yield from the condensation of **4** with 2 equiv. of **3** followed by the reduction *in situ* of the obtained diamine with sodium borohydride. The obtained product was mono-methylated through Eschweiler–Clarke methylation process with para formaldehyde and formic acid allowing the formation of **6** in 15% yields mainly due to the formation on the dimethylated product. The protected carboxylate moiety was then introduced through nucleophilic substitution of 2-bromo-*tert*-butyl acetate by the remaining secondary amine forming the product **7** in 61% yield. Finally, the ligand L_{III} was obtained in 98%

yield after the deprotection of **7** using 20 equiv. of TFA in dichloromethane overnight. All the different species were identified by ^{1}H and ^{13}C NMR (see material and methods section).

The ligand $L_{III}H$ was then engaged in a complexation step at room temperature for two hours with either $MnCl_2$ or $MnOtf_2$ as the metal source in MeCN, ***scheme 20***. In both cases, the complex was recovered as a white solid after precipitation using diethyl ether Et_2O. ESI-MS analysis of the obtained powders confirmed the presence of $L_{III}Mn$ at 451 m/z attributed to $[L_{III}Mn]^+$ ion with both metal salts, suggesting that the counter ions are non-coordinated. No further investigations were pursued regarding the effect of the counter ion, as in most cases, once introduced into NikA, labile ligands and counter ions are replaced with water molecules.

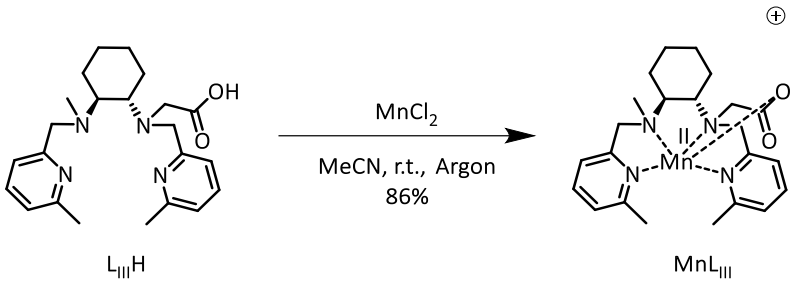

Scheme 20 : *complexation step for MnL_{III}*

The UV-Vis spectrum was conclusive of a Mn^{II} d^5 high spin species, as no d-d transition was observed. The complex was readily engaged in further investigations.

1.1.3. The MnTACNAA as an epoxidation catalyst

MnTACNAA was first described by M. Scarpellini et al. in 2008.[232] The small size of the complex and the rapid preparation process were found quite appealing although the absence of aromatic rings will result of the absence of the π-π stacking with tryptophane residues present in the cavity that might have an effect on the binding to NikA and on the overall ligand/protein stability. Both of these observations will be addressed in the upcoming chapter. The **TACNAA** ligand, 1,4,7-triazacyclononan-1-yl) acetic acid, was prepared in a one-pot fashion according to the literature as illustrated in **scheme 21**.[232]

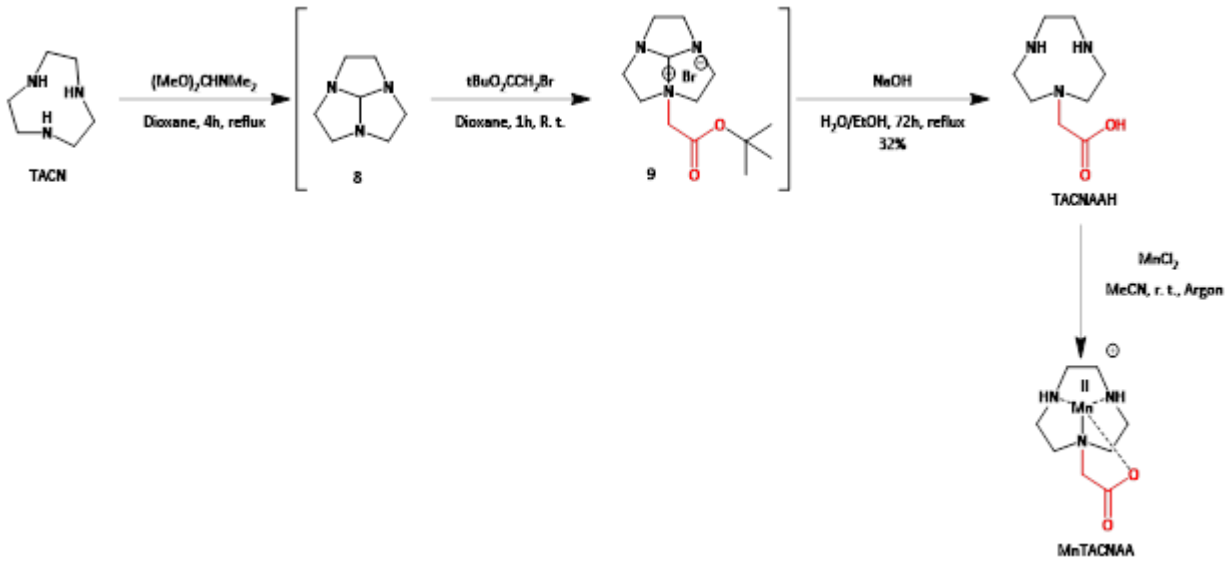

***Scheme 21**: TACNAA synthetic pathway.*

The aminal intermediate **8** was obtained from the commercially available TACN (from Sigma Aldrich) through a reaction with N,N-dimethylformamide dimethyl acetal in dioxane at reflux. It was then monoalkylated by a slow addition of *t*-butylbromoacetate forming the intermediate **9** which was then precipitated and washed using Et_2O. The obtained precipitate was dissolved in a solution of NaOH in 50% aq. EtOH and left under reflux for 72 h before evaporation to dryness. Lastly, the ligand **TACNAAH** was obtained in 32% global yield after purification on an ion exchange column. The obtained ligand was then engaged in a complexation step using $MnCl_2$ as the metal precursor in a method comparable to **MnTACNAA** complexation. The complex was recovered as a white solid after precipitation with diethyl ether with 80% yield and afforded conclusive ESI-MS data, which displaying a sole peak at 241 m/z corresponding to the $[(TACNAA)Mn]^+$ specie.The recovered complex was engaged in catalytic investigations in solution as well as in NikA crystals with no further purification.

1.2.Complexes for anchoring to the *second site*

For the second active site, requiring a cysteine residue, we have decided to work with a maleimide as the Michael acceptor for the covalent modification of the protein. Targeting, in some cases, less hindered and more accessible amino acids such as solvent exposed ones, we took the liberty of working with more geometrically constraint complexes, leading to the selection of metal(salen) complexes. In this part will be described the synthesis and characterization of manganese and iron salen complexes for the epoxidation reaction and a

cobalt salen complex for the CO_2 cycloaddition step. The synthesis will be described in a general pathway and only the complexation and characterization steps will be differentiated, as they are otherwise quite similar.

First approach : the anchoring via a (3S,4S)-pyrrolidine-3,4-diamine.

We sought to prepare chiral and achiral salen complexes. Initially, we wanted to introduce chirality within the coordination sphere of the salen complexes using (3S,4S)-pyrrolidine-3,4-diamine **7** in ***scheme 23***, as the Schiff-base building block. The protected maleimide arm was prepared in two steps depicted in ***scheme 22***. Maleimide **1** was protected with a furan through a Diels alder reaction at 30 °C in diethyl ether. After 18 h, the protected product **2** was isolated with 45 % yield by filtration. Product **3** was obtained in quantitative yield after alkylation of **2** with dibromoethane at 50°C in dichloromethane with satisfactory NMR spectrum.[233]

The synthetic procedure of the ligand core is depicted in ***scheme 23***. The focus of the work was around the construction of the pyrrolidine motif since the desired (3S,4S)-pyrrolidine-3,4-diamine **7** is not commercially available. Starting from L-tartaric acid, product **4** was obtained in quantitative yield in a condensation step with benzylamine following a dean stark setup.[234] Then, product **5** was obtained with 38% yield through the reduction of **4** by $NaBH_4$ and separated through continuous extraction following a previously reported method.[235]

Following a general mesylation procedure with methanesulfonate chloride **5** was obtained with 62% yield and engaged in a SN_2 transformation with sodium azide followed by a reduction step using formic acid and palladium in carbon in a one pot fashion in N,N-dimethylformamide leading to the desired product **7** with 30% yield.[236,237] Direct imination assays involving **7** with *tert*-butyl salicylaldehyde remained unsatisfactory as it leads to the formation of both mono imines and a small quantity of the desired diamine. An analogue pathway was followed with the reduction of the dihydroxypyrrolidine-2,5-dione **4** with similar difficulties encountered at the end of the transformation. Unfortunately, the preparation the salen ligand following the pyrrolidine motif remained unsuccessful and we had decided at this point to change the ligand structure. Although we could separate the final product, it was unstable and efforts on the imination step remained unsatisfactory.

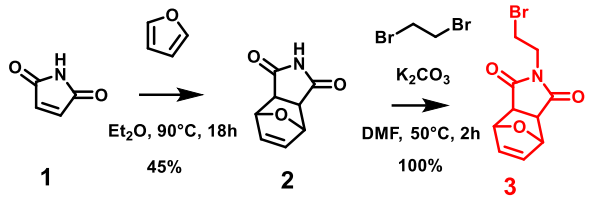

Scheme 22 : *synthetic procedure for 3*

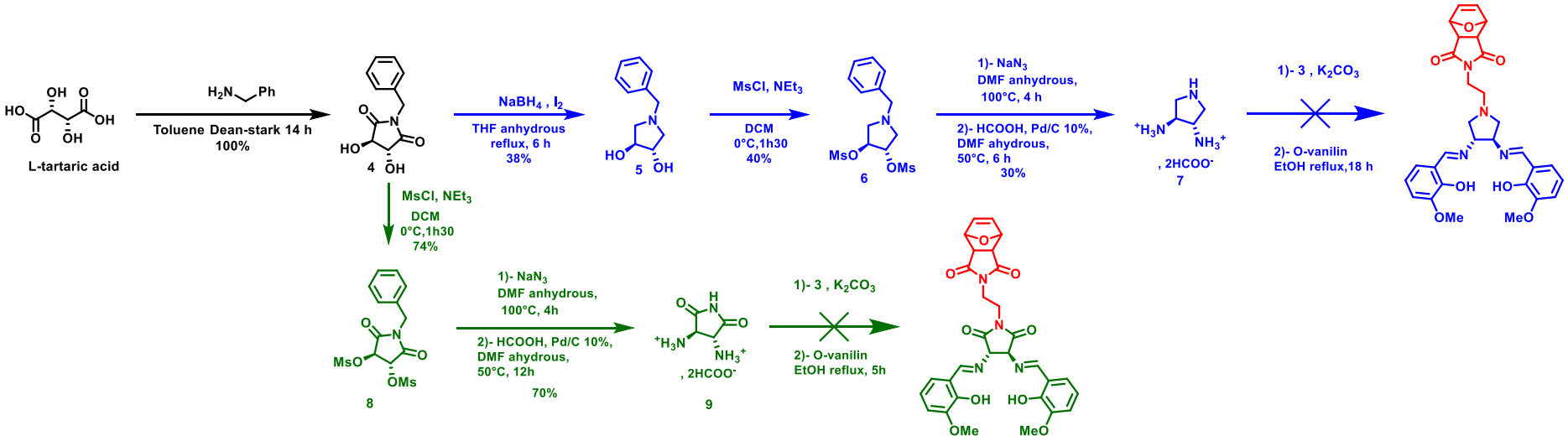

Scheme 23: *general procedure for the synthesis of designed salen ligands*

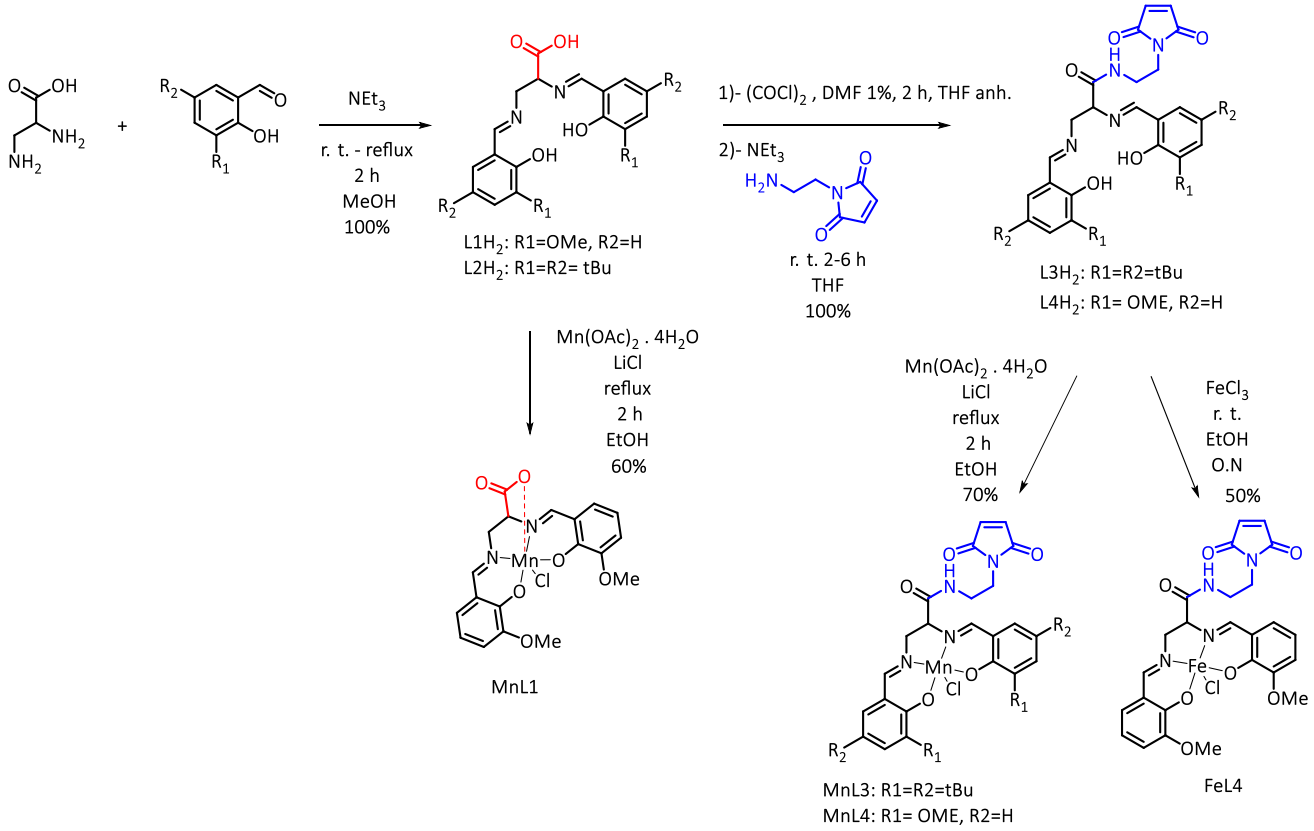

***Scheme 24**: general preparation pathway of the preparation of manganese and iron salen complexes from the diamine 1.*

Racemic (and chiral) 2,3-diaminopropionic acid was then chosen as the building block for the salen ligands. The carboxylic acid function allows the starting diamine to be versatile. It can possibly be engaged in a salt bridge with **Arg137** in the site pocket if geometrically allowed. In addition, it is a great candidate for a straightforward functionalization by the creation of an amide bond for instance. All of this make the starting diamine choice appealing as in theory it allows the creation of a series of complexes with or without a maleimide arm but in any case, a comparable coordination sphere and geometry. This allows the comparison of the catalytic activity according to the position and anchoring mode of analog complexes. Functionalization of the starting material using coupling agents such as the BOP reagent, [BOP= benzotriazol-1-yloxytris(dimethylamino)phosphonium hexafluorophosphate] or N,N'-Dicyclohexylcarbodiimide (DCC) were successful but required further purification steps to afford the final functionalized diamine. Surprisingly, once engaged in an imination step, only the monoimination product was recovered and traces of the diimine, ***scheme 24***. It was then preferable to first prepare the Schiff-base then functionalize the carboxylate moiety. We have investigated a new route as well for this functionalization as an effort to lower purification steps. Therefore, this time, no coupling agent was used.

Following a general procedure,[238] ligands **L1** and **L2** were obtained in quantitative yields from the condensation of **2,3-aminopropionic acid** by the desired salicylaldehyde derivative. The ligands **L3** and **L4** were obtained in quantitative yields as well by the activation of the carboxylate moiety in **L1** and **L2** using oxalyl chloride in THF with a catalytic quantity of DMF (1%) for one hour followed by the addition of a stock solution 2-aminoethlymaleimide and 3 equivalents of triethylamine in THF.[239] Triethylamine chloride, a side product of the reaction precipitates in THF as the reaction progresses. The ligands are recovered by filtration and evaporation of the solvent and engaged in complexation assays with no further purification. Attempts using another base such as potassium carbonates remained unsuccessful leading to the ligand partial hydrolyzation.

Following a general procedure, manganese based complexes **MnL1**, **MnL3** and **MnL4** were prepared by mixing equimolar quantities of $Mn^{II}(OAc)_2 \bullet 4H_2O$, the desired ligand and 3 equivalents of LiCl under reflux at 0.1 M in absolute ethanol, for five hours.[238] Complexes **MnL1** and **MnL4** precipitated out of the solution at room temperature and were recovered by filtration as brown solids.

MnL3 displayed great solubility in ethanol and was precipitated by adding ether and recovered by filtration as a dark brown solid.

FeL4 was prepared in a similar fashion by mixing equimolar quantities of L4 and $FeCl_3$ at 0.1M in EtOH. The complex precipitates in EtOH and is recovered by filtration as a purple solid. ESI-MS analysis of **FeL4** solution in methanol depicts the presence of $L4Fe^{III}(MeOH)^+$ at m/z 580 were the labile chloride ligand is replaced by a solvent molecule.

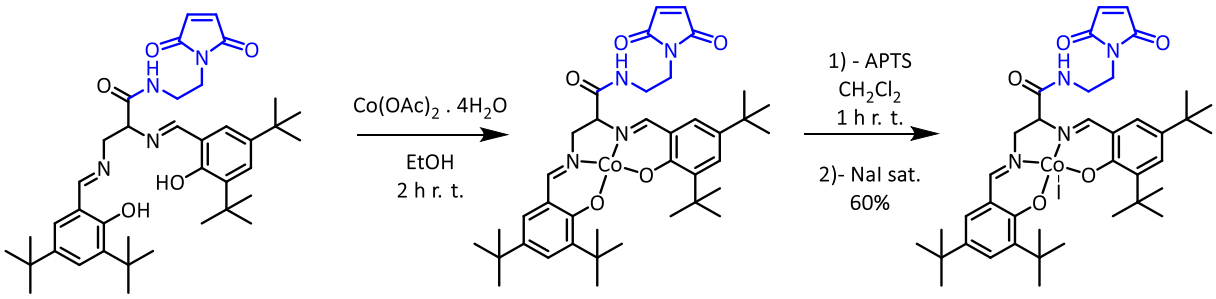

***Scheme 25** : co-complexation pathway of L3 ligand*

Similarly, **L3** was engaged in a complexation step with $Co(OAc)_2$ forming **Co^{II}L3** which was oxidized using 1 equivalent of *p*-toluenesulfonic acid in dichloromethane. The tosylate ligand in the labile position is then substituted by the iodide ion by a simple extraction of the

solution in DCM by saturated sodium iodine as seen in ***scheme 25*** was then replaced by several extraction with saturated sodium iodide to recover **Co^{III}L3** with 60% yield.[240]

The mass spectra of this series of complexes included several fragments. Nevertheless, the molecular ions corresponding to the expected complexes were observed. For example, ESI-Mass analysis of **MnL4** solution in water depicts the presence of the $[L4Mn^{III}Cl\ (H_2O) + H^+]^+$ fragment at m/z 601. ESI-MS analysis of **MnL3** solution in MeOH displayed the presence of several fragments including the complex $[L3Mn^{II}(MeOH) + Na^+]$ at 764 m/z. This could be explained by the instability of the diamine prone to fragmentation under the ESI beam coupled to the replacement of the labile form with solvent molecules such as water, methanol, and acetonitrile. Elemnatl analysis was correct for Mn**L4**Cl•$3H_2O$.

Figure 33 summarizes the UV-Vis spectra of the serie of the salen complexes alongside the ESI-MS spectra described above. **FeL4** UV-Vis profile exhibits characteristic LMCT Oph-Fe^{III} transition at 560 nm (ε=1336 $M^{-1}.cm^{-1}$). **MnL4** spectra display a band at 390 nm (ε=1524 $M^{-1}.cm^{-1}$), which can be attributed to the ligand-to-metal charge transfer (LMCT); comparable data were obtained with **MnL3, attesting the Mn^{III}-Oph system formation**. Finally, **CoL3** UV-Vis absorption profile display two characteristic bands at 400 nm (ε=1639 $M^{-1}.cm^{-1}$) and 550 nm (ε=632 $M^{-1}.cm^{-1}$) (d->d) that can be attributed to an LMCT (d-> Π) and d-d bands respectively of Co^{III}-O_{Ph} systems.

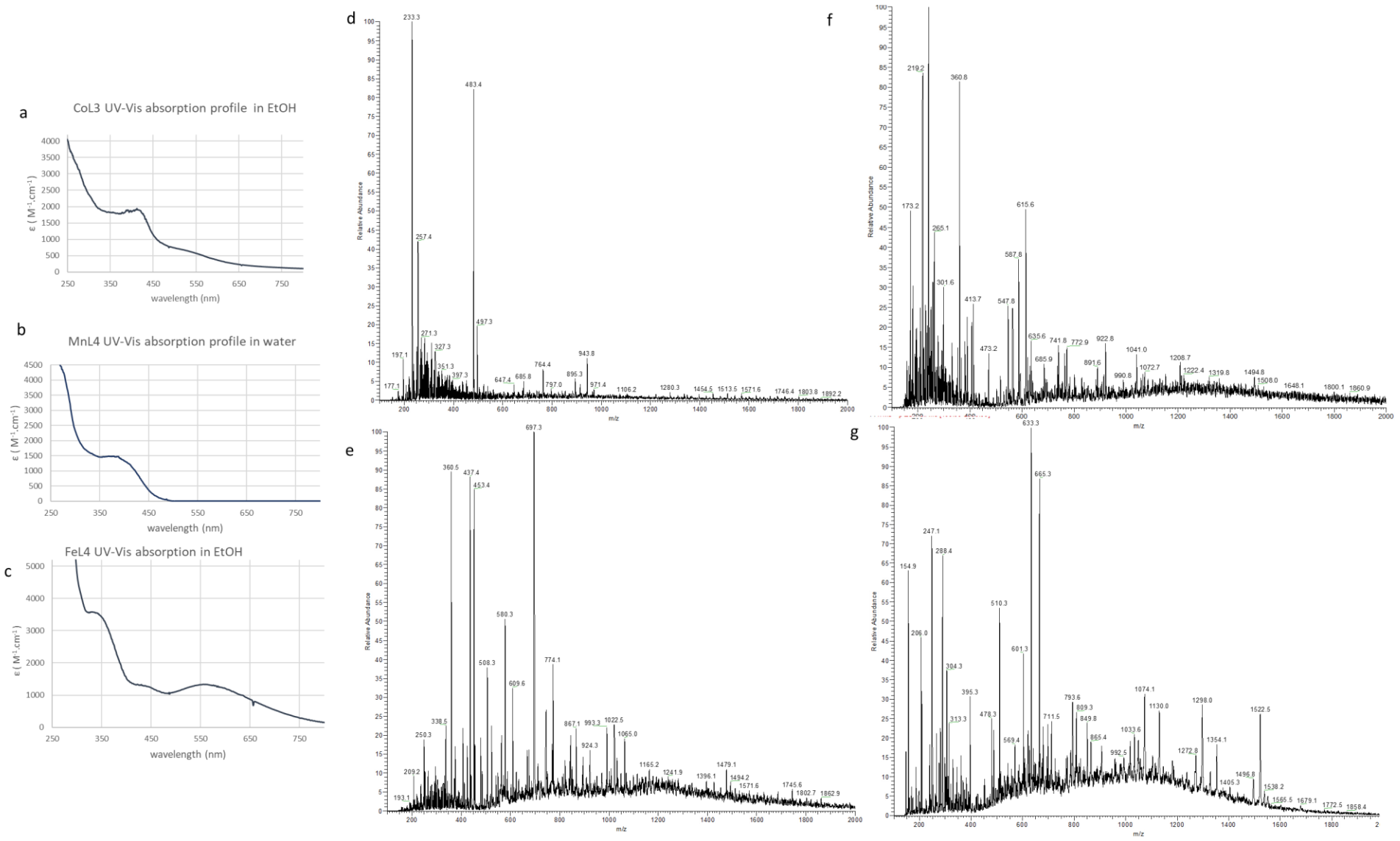

Figure 33 : *UV-Vis and ESI-MS spectra of the salen complexes solution: UV-Vis ; (a)* ***CoL3****, (b)* ***MnL4****, (c) FeL4, ESI-MS : (d)* ***MnL3****, (e)* ***FeL4****, (f)* ***CoL3*** *and g)* ***MnL4***

2. NikA mutant construction and characterization:

This thesis project was conducted in a close collaboration with the BEE team at the LCBM. Expertise of the BioCE team was mainly engaged in the catalyst's choice, preparation and characterization including ArM preparation and catalytic investigations. The expression, purification, and structural characterization of NikA and mutants were taken care of by the BEE team having a better expertise in biochemistry and protein crystallography.

2.1. Mutant production and purification

NikA cysteine mutants were constructed by site-directed mutagenesis by Dr. Patrice Catty from the BEE team at the LCBM. Three mutation sites were selected in the cavity area of the protein, S415, T23 and H416 and two in the solvent channels A1 and D59. All the mutants were produced in *Escherichia Coli*. Mutant purifications were then performed by the protein purification platform PFP3 at the LCBM based on a purification protocol of NikA initially developed by Dr. Christine Cavazza from the BEE team. The novelty in the purification method of the cysteine mutant as compared to the WT protein was the addition of 1 mM of dithiothreitol (DTT) in the purification buffer in order to prevent the formation of intermolecular disulfide bridges and the formation of dimers as it has been observed especially with the D59C mutant.

2.2. Protein crystallization

Protein crystallization assays were adapted from established crystallization method for WT-NikA. In a generic method, protein samples were crystallized using iron-EDTA, since only the closed conformation of NikA, with a ligand bound in the cavity form was able to crystallize up to now. NikA-Fe-EDTA hybrids were formed at 160 µM of protein concentration in 25 mM HEPES at pH 7.6 incubated with two equivalents of Fe^{III}(EDTA) a few minutes prior to the crystallization assay. Crystallization is initiated by mixing 2 µL of NikA WT or mutants/ Fe^{III}(EDTA) with 2 µL of crystallization solution, composed of 0.1 M sodium acetate at pH 4.6 and ammonium sulfate (ranging from 1.5 to 1.9 M). Nextal 15 wells crystallization plates were used and kept at 20°C in a fridge ensuring a constant temperature.

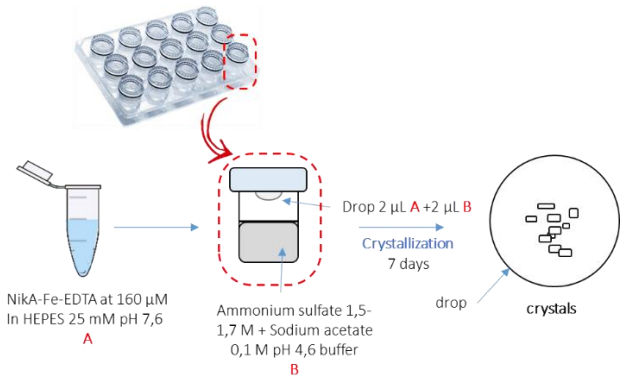

Scheme 26

The crystallization procedure as illustrated in ***scheme 26***, is based on the hanging drop vapor diffusion technique. Production of protein crystals is very sensitive to the environment and the batch of the stock solution used therefore required close and recurrent optimizations of the ammonium sulfate concentration. The aim of our study is to be able to obtain quantitative and reproducible catalytic results. Therefore, it has been crucial for the project to be able to yield crystals with a reproducible size dispersion. Through these investigations, some tendencies have been highlighted as for instance the correlation between the precipitating agent concentration and the number and the size of the produced crystals. ***Figure 34*** displays snapshots of crystallization assays highlighting successful crystallization in case a) and failed crystallization assays in cases b) and c). While D59C (solvent channels, see figure 24) , H416C and T23C (cavity) yielded crystals comparable to WT protein, crystallization assays of A1C and S415C remained unsatisfactory. A1C only yielded precipitates at all tested conditions while S415C yielded very small needle shaped crystals that were hard to handle giving a great source of incertitude if applied in catalytic investigations.

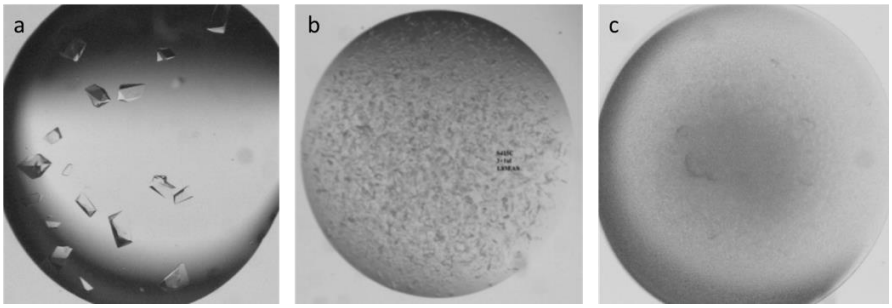

Figure 34: *crystallization results at optimized conditions: (a)- **NikA-WT** at 160 µM with 1.5 M of AS (b)- **NikA-S415C** at 160 µM and 1.8 M of AS (c)-- **NikA-A1C** at 160 µM with 1.5M of AS (Amonium sulfate)*

After these investigations, only mutants T23C (cavity), D59C (solvent channels) and H416C (cavity) were selected for further *in cristallo* investigations while S415C and A1C were benchmarked for further crystallization optimizations. X-ray diffraction analysis of the three

selected mutants, showed that they all crystallized in in the $P2_12_12_1$ space group and led to the determination of the expected structures ***(figure 35)***. Analysis of the structures showed that except the mutated residues, they are similar to the NikA-WT/ Fe^{III}(EDTA). The data will be deposited soon in the PDB databank.

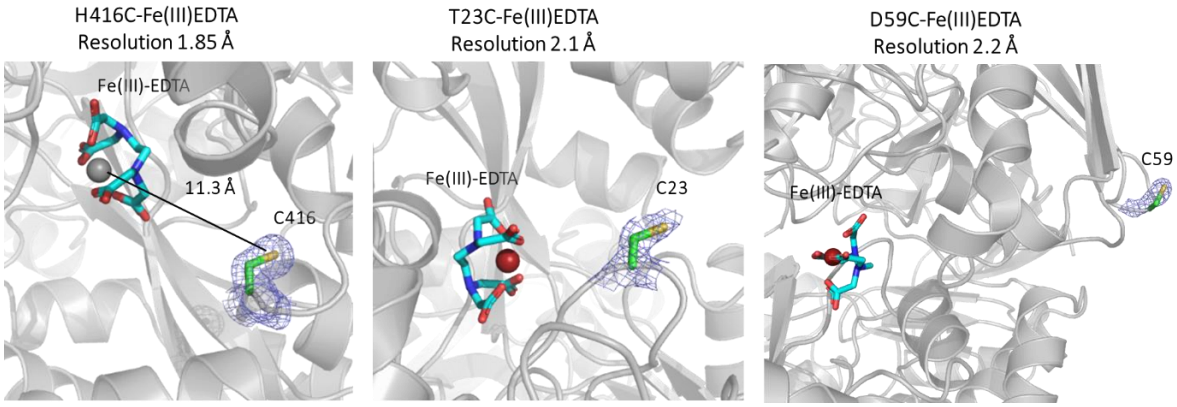

Figure 35: *crystal structures of NiKA-mutants in complex with Fe^{III}(EDTA)*

This step of the investigations was crucial for the continuation of the project, as it has permitted the validation of three differently positioned cysteines in the protein for the creation of the second active site in NikA. Once a small dispersion was reached in terms of crystal number and size, three batches of 20 crystals were selected and solubilized in water for quantification using MALLS (Multi-Angle Laser Light Scattering) technique for the determination of the protein concentration as a first step for the characterization of the newly designed ArM catalysts. ArMs anchoring assays as well as quantification of the complex loading within the protein matrix will be discussed in the upcoming chapter.

2.2.1. Preparation of crossed linked enzyme crystals

Previously, NikA CLEC were prepared by treating the crystals in the crystallization drop with 5% of glutaraldehyde for 5 h at 20°C. The uncolored crystals turn yellow upon stabilization and are recovered from the drop using a crystal loop. This method leads to the formation of glutaraldehyde polymer in which the crystals are embedded. While it is quite easy to retrieve the crystals from the formed polymer, it is quite a hassle to ensure that no leftover polymer is present on the surface of the crystals. In order to see if the presence of the polymer might interfere with the catalytic investigations, a sample of the glutaraldehyde polymer was retrieved and tested with hydrogen peroxide in qualitative assay for the sulfoxidation of thiols. Results showed that indeed the polymer might display oxidation activity when paired with

hydrogen peroxide. At the beginning of the project, we have then investigated optimization routes for the stabilization of the crystals avoiding the formation of the polymer. First, we noticed that the polymerization of glutaraldehyde was enhanced when batched are left under air atmosphere. Working with sealed samples of 25% glutaraldehyde in water under argon and a stabilization assay using 1% of glutaraldehyde in the crystallization buffer for 2h has allowed the yield of stabilized crystals with no apparent formation of glutaraldehyde polymer formation. The NikA-Fe^{III}(EDTA) were found then inactive toward activation of H_2O_2, attesting that the polymer is no longer present.

3. Conclusion

In this chapter was displayed the methodologies followed for the preparation of the two main actors for the design of the ArM, the mutants and the metal cofactors. Out of the mutants series, **H416C**, **T23C** and **D59C** crystallization assays were the most promising and have been selected for covalent anchoring assays. The catalysts candidates for each transformation have been selected as well, especially **MnLIII** and **MnTACNAA** for the first site and **MnL4**, **MnL3**, **FeL4** and **CoL3** for the second.

For Iron picolinates, working with catalysts solution in which the active species is hard to describe is a drawback for such complicated systems. Nevertheless, and as a last resort, we have decided to include this series of complexes in catalytic assays with WT-NikA. Although it is quite a hassle to work with such candidates, we postulated that the tridimensional structure of the protein displays variable affinities towards the different species present in the mixtures.

Metal salen complexes and planar ligands in general have never been able to bind to NikA, due to geometrical constraints. Previous assays using salen complexes in which the carboxylate is directly linked to the aromatic ring remained unsuccessful. Hence, the design of the epoxidase ArM can be considered as a major milestone in the case of this project. Advances in the preparation investigation and validation of such candidates was done with the contribution of Ismail Benhamed who was in a graduate level internship during which he has taken care of the synthesis and study of the complexes **MnL_{III}** and **MnTACNAA**. Although initially for the carbonation step, several candidates were selected, we privileged working on the **CoL3** complex due to lack of time and as the ligand synthesis was previously optimized.

On the side of the protein preparation, the major limiting factor has been the crystallization of the mutants. The preparation and anchoring assays that are to be discussed in the upcoming chapter were investigated simultaneously with concerns of time optimization. Indeed, the catalytic studies are very demanding in terms of number and size of crystals. Consequently, only the mutants allowing the reproducible crystallization of a large number of usable crystals have been prioritized in the upcoming investigations.

Chapter III Preparation of the artificial metalloenzymes

The process of making the dual-site ArM for the intended cascade transformation was segmented into multiple parts: First, the preparation of the metal cofactors and the proteins as described in the previous chapter. Then, the association of the metal complexes with NikA referring to the anchoring step is undertaken. Finally, the activity of the designed mono- and dual-site ArMs is investigated.

This chapter will focus on the description of the anchoring methodology of the different complex-protein couples as well as the characterization of the newly designed entities.

Our investigations led to the preparation of several mono-site ArMs, with either epoxidase or CO_2 cycloaddition activity (***scheme 26, a and b***). Metal cofactors with orthogonal anchoring modes for each transformation were then coupled to a single cysteine mutant to yield the desired bifunctional ArM (***scheme 26c***). The great challenges here are: i) the Michael acceptor to reach the cysteine inside the crystals; ii) the coexistence of both artificial active sites; iii) the full characterization of the C-S bond.

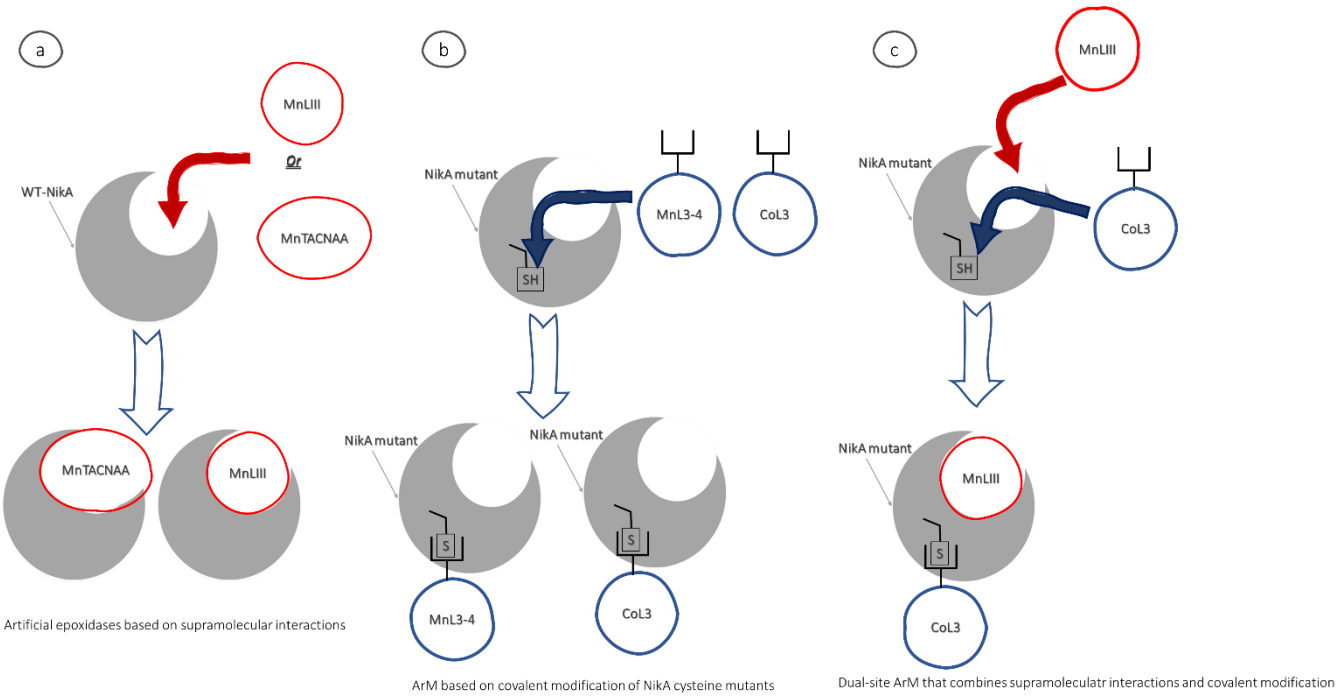

Scheme 26 : strategies for dual active site constructs.

The following discussions will lean on the optimization of the anchoring assays and the characterization efforts for the preparation of the mono-site and dual-site ArMs.

1. Mono-site NikA ArM:

Mono-site ArM refers to the systems produced throughout the optimization of each anchoring mode, supramolecular or covalent, independently. The investigations resulted in the synthesis of several epoxidase ArMs exploiting either of the binding sites involving **MnLx** and **MnTACNAA** : i) the native cavity (***first site***) or ii) the cysteine functionalization in NikA mutants (***second site***). Moreover, we report a mono-site ArM for CO_2 cycloaddition involving the **CoL3** complex associated with NikA cysteine mutants. In the following are discussed the preparation and characterization process in solution and *in cristallo* for said ArMs.

1.1. Anchoring on the *first site*:

The anchoring assays differ whether they are accomplished in solution or *in cristallo*. Indeed, anchoring assays in solution using *apo*-NikA allows to circumvent Fe-EDTA replacement. In addition, the open conformation of *apo*-NikA provides a higher accessibility for metal cofactors to reach the binding pocket. We have designed then a preliminary assay in solution (see below) that proves the feasibility of the ArM preparation when investigating new complexes. Nevertheless, this assay is only restricted to metal complexes soluble in aqueous medium. Conversely, *in cristallo,* Fe^{III}-EDTA needs to be exchanged in WT and mutant NikA-FeEDTA crystals and the diffusion of non-water-soluble complexes are then accessible only once the CLEC are formed. Successful replacement allows the preparation of crystals of NikA-Mn or Co complex hybrids with no further crystallization optimization, a general strategy followed by the BioCE team.[228,241]

Among all the possibilities, we have focused on the design of two NikA-based artificial peroxidases associating epoxidation complexes **MnL_{III}** and **MnTACNAA** with WT-NikA. Regarding the **MnL_{III}** complex, interactions with the binding cavity were expected to be similar to the previously reported iron complex with the major interaction being the salt bridge with the **Arg137** residue.[241] Conversely, the lack of aromatic rings in **MnTACNAA** can possibly have an incidence on the overall protein-complex stabilization due to the absence of π-π stacking with **Trp** residues present in the cavity. Both of these candidates were submitted to anchoring assays in solution and *in cristallo*.

1.1.1. In solution assays: evidence for complex binding

Complexes $Mn^{III}L$ and MnTACNAA have a good solubility in water and polar solvents such as methanol (MeOH) and acetonitrile (MeCN). It offers the ability to reach a complex concentration as high as 100 mM, in buffered solutions. Anchoring assays were performed on *Apo*-NikA samples at 100 µM in 25 mM HEPES buffer at pH 7.6 (protein buffer). The samples were incubated overnight with ten folds excess of either complexes in the same buffer. Samples were desalted to remove the excess of free complex and concentrated using a centrifugal Filter Unit for sample concentration, with a special care to avoid any dilution of the samples, favoring the dissociation of the formed hybrids. Using such concentrators allows discarding any compound with a molecular mass lower than 30 kDaltons, the filter threshold.

The resulting solution remained colorless excluding any characterization by UV-visible spectroscopy, revealed that either the manganese remains in the + 2 oxidation state when bound or was absent in the cavity. Then, precise titration of each component was privileged. The concentration of the protein in the resulting sample was determined using MALLS analysis. Then, the metal content was quantified using ICP-AES, after the mineralization of the aliquots using nitric acid at 50°C overnight. ***Table 1*** summarizes the determined concentrations of the protein and manganese. The metal /protein ratio was calculated and showed that 15% and 4% of NikA-bound $Mn^{III}L$ and MnTACNAA respectively, which might reflect low association and high k_d values. Moreover, the lower anchoring yield for MnTACNAA can be a resultant of the absence of π-π and CH-π stabilizing interactions.

__Table 1__: $Mn^{III}L$ and $Mn^{II}L$ anchoring yields in solution.

Entry	Protein-complex	Protein concentration	Metal concentration	Metal/protein ratio
1	$Mn^{III}L$	245 µM	37 µM	0.15
2	MnTACNAA	582 µM	24 µM	0.04

Although the efficiency of this preparation method remains unsatisfactory, (suggesting a Kd over 100 µM), it does give encouraging insights on the feasibility of the ArM preparation. Accordingly, from this point, characterization efforts were focused on the replacement of Fe^{III}(EDTA) in NikA crystals.

1.1.2. *In cristallo* assays: structural investigations

Preparation of NikA-MnTACNAA and NikA-MnL_{III} crystals was achieved through the crystallization of WT-NikA FeEDTA hybrids. The large crystals are then soaked with a stabilizing solution containing the desired complex to displace FeEDTA present in the protein cavity. To aid the complex solubility, a small percentage of organic solvent were used (1-10% in volume). Following the results obtained in solution, high concentrations of complexes were used. Therefore, five colorless NikA-FeEDTA crystals were transferred in a 5 µL drop of either MnL_{III} or MnTACNAA at 10 mM in 25 mM HEPES and 2.1 M of ammonium sulfate at pH 7.6 for 16 h. Again, the crystals kept their original genuine colors, as observed in solution. The crystals were then fished and washed with the same buffer via their transfer into a drop of stabilizing solution for 15 min. This step is repeated twice before transferring the crystals into the cryoprotecting solution (stabilizing solution containing 25% glycerol) prior to their freezing in liquid nitrogen for X-ray diffraction analysis.

Determination of the crystal structures showed the successful replacement of FeEDTA by both complexes with an occupancy of 100%. As seen in ***figure 36***, both complexes form a salt bridge with the Arg137 residue via their carboxylic function and bear a water molecule coordinated to the metal center. Despite an assumed high K_d in solution, the Fe^{III}(EDTA) has been replaced by the Mn complex in both cases in the crystal. This is due to the high concentration of Mn complex attained in the crystalline buffered media.

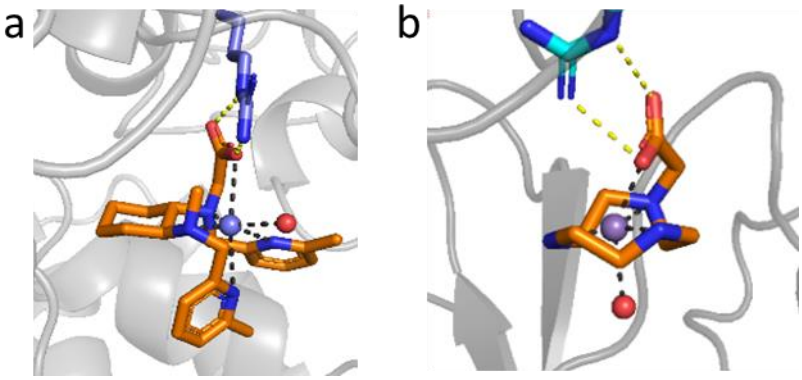

Figure 36: *Crystal structures of the cavity of the ArM* ***NikA-MnLIII*** *(a) and* ***NikA-MnTACNAA*** *(b)*

We are currently refining each structure and all metric parameters will be discussed in the future and deposited in the PDB databank.

1.2.Anchoring on the *second site*

This strategy implicates the presence of a cysteine residue, present in NikA mutants, a novel approach for our ArM preparation methods. Indeed, as an orthogonal anchoring mode to the first site, we opted for a Michael addition on a maleimide moiety, present as a substituent in the **L3** and **L4** ligands out of the different cysteine modification options, covering strategic positions in the crystal lattice. Then, several operating conditions such as temperature and reaction time were considered to optimize the C-S bond formation. Thanks to the generally mild conditions for Michael additions, it is a valuable tool for protein modification.

Starting from reported conditions,[224] preliminary assays were carried out in solution on a first batch of mutants. We then moved on to the direct chemical modification of enzyme crystals as it is going to be discussed in the oncoming paragraphs.

1.2.1. In solution assays

Anchoring on NikA mutants **A1C**, **S415C** were put aside as crystallization assays remained unsatisfactory.

Initial anchoring assays were performed on the **H416C** mutants alongside complex **MnL4** as a model for the metal salen series.

In a general setup, *apo*-NikA **WT** and **H416C** at 100 µM in the protein buffer, were incubated with ten folds excess of the complex **MnL4** in the same buffer with 10% of DMF, overnight at room temperature. The aliquots were then centrifuged at 15000 rpm for 5 min and desalted on a NAP10 resin column, to discard excess of free complex. Recovered samples were concentrated on Centrifugal Filter Unit and analyzed by UV-Vis. Protein concentration was determined using a rose Bengal calibration and **MnL4** quantity was estimated thanks to the LMCT band at 400 nm, a wavelength at which there is no absorption from the apo protein samples.

Figure 37 shows UV-Vis spectra of **WT-NikA-MnL4, H416C-MnL4** and the free complex. All of them are characterized by the presence of absorption bands in the 400-550 nm region.

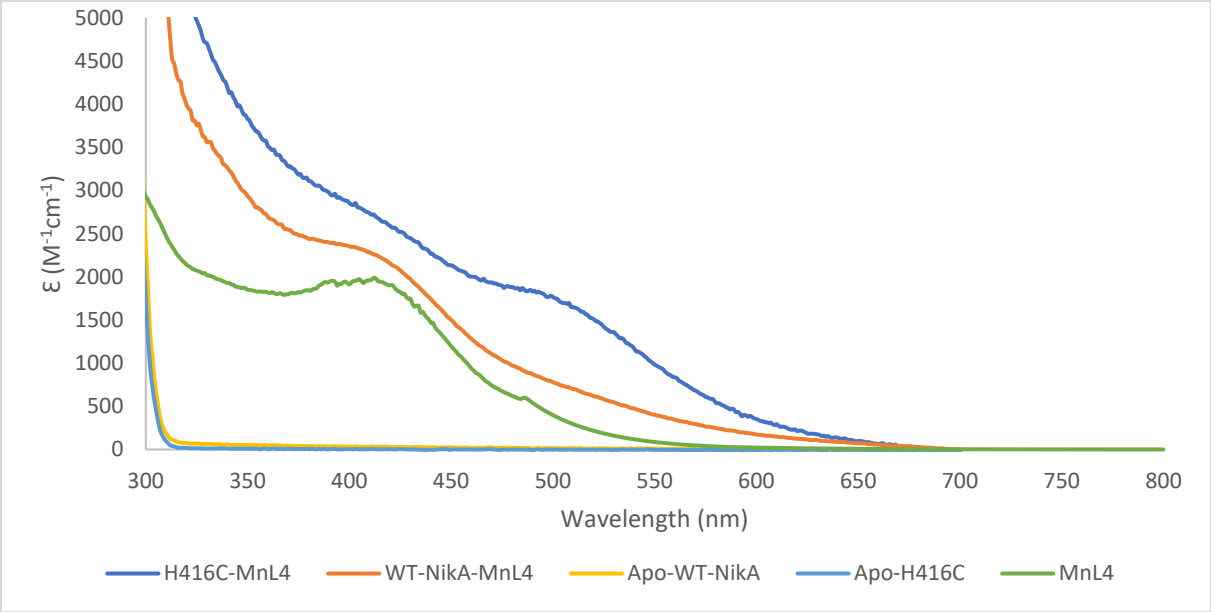

Figure 37: *UV-Vis spectra of* ***MnL4*** *alone or bound to* ***WT-NikA*** *and* ***H416C*** *in the protein buffer*

The presence of this band in the WT-NikA sample strongly indicates the presence of another complex binding site as the native NikA does not contain any cysteine residue. Considering the absorption coefficient of **MnL4** at 420 nm (**ε** = 2000 $M^{-1}.cm^{-1}$, from the **MnL4** sample), complex concentration alongside anchoring yields were estimated as displayed in ***table 2***. This assumption is related to the conservation of the extinction coefficient when the complex is included in NikA.[229]

Table 2 anchoring ratios estimation via UV-Vis analysis of protein samples.

Entry	Protein sample	Complex/protein ratio
1	H416C	0.8 ± 0.2
2	WT-NikA	1.1 ± 0.2

Aside from the fact that some of the free complex might have not been fully separated on the NAP10 column, the yield obtained with **WT NikA** raises few questions concerning the selectivity of the anchoring mode ***(table 2, entry 2).*** Indeed, the 1:1 anchoring ratio obtained with WT-NikA suggests that there is about one complex per protein. Interestingly, the **H416C-MnL4** UV-Vis signature differs from the mutant one. The presence of two binding sites is suggested by the extra band observed at 490 nm additional to the already reported transition band at 420 nm. This can result as well from the modification of the starting complex **MnL4**.

The UV-visible titration does not prove that the Michael addition is effective but strongly suggests the presence of two distinct binding sites in which the metal complex has a different environment.

The amino acids present in NikA as well as many peptides and proteins, offer the possibility of unspecific anchoring modes resulting for a sum of several small interactions. When performing anchoring assays, some unspecific protein-complex interactions might influence the anchoring yield. To determine the nature of theses interactions, due to the high anchoring yields observed for all of the samples, at a comparable magnitude, the samples were analyzed by ESI-MS under denaturing conditions. Deconvoluted mass spectra of the investigated samples should display only the covalent modification of the protein scaffold, discarding any anchoring resulting from and accumulation of small weak protein-complex interactions.

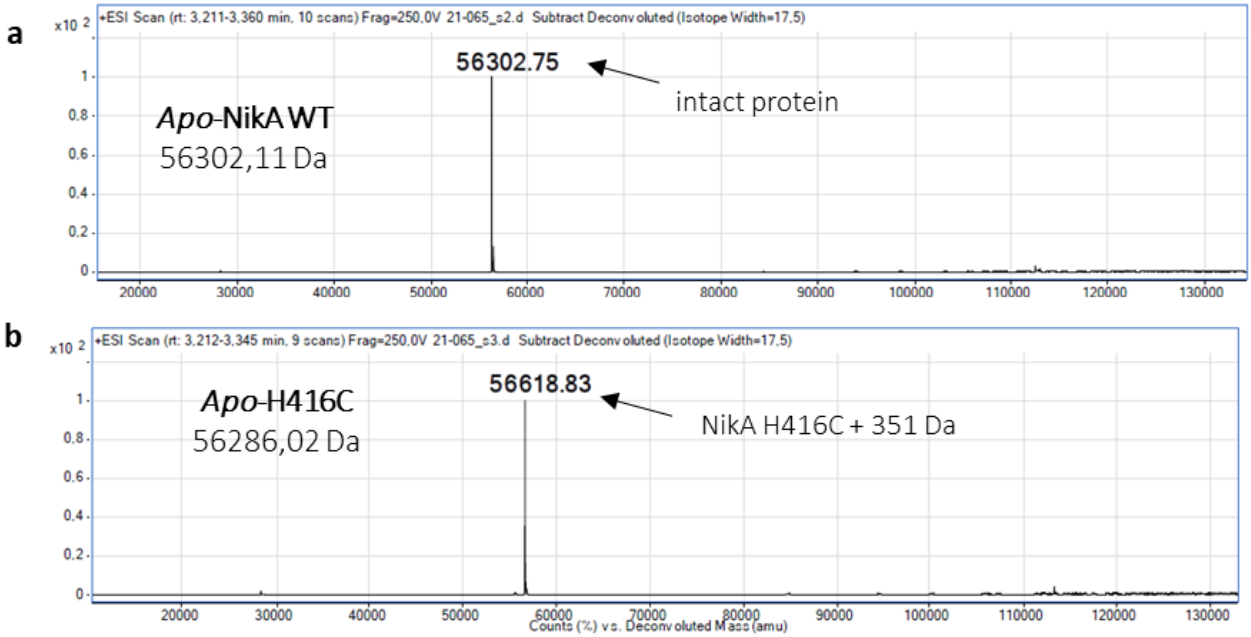

Figure 38: *ESI-Ms spectra of protein samples: (a)* ***WT- NikA-MnL4*** *(b)* ***H416C-MnL4*** *in formic acid buffer.*

H416C-MnL4 ESI-MS data exhibit a sole peak at m/z 56618.83 (compared to the intact protein at 56268 m/z), stating on the total modification of the protein scaffold, ***figure 38b***. The observed mass difference of m/z +351 in the H416C-MnL4 sample does not correspond to the mass of the MnL4 complex (582 m/z) but attest of a covalently attached fragment. The inconclusive mass difference observed can be explained by degradation of the complex under the denaturing conditions of the ESI-MS analysis or prior to the analysis (presence of formic acid). As a matter of fact, this observed mass difference can be attributed to the fragment

$C_9H_{12}Cl_2MnN_4O_3$ (351 m/z) that can result from the hydrolysis of both imine functions of the L4 ligand. We will observe the same behavior on further ESI MS studies.

Conversely, ESI-MS data from the **WT-NikA-MnL4** sample displays a sole peak at 56302.75 m/z, in adequation with the intact WT-NikA protein, ***figure 38a***.This indicates that the observed complex/protein ratio (***entry 2, table 2)*** is due to supramolecular complex- protein interactions.

ESI-MS proof on covalent modification of the **H416C** mutant has encouraged further investigations on the **T23C** and **D59C** mutants. With the concerns of performing a more precise quantification, protein concentration was determined using MALLS analysis and metal content was determined by ICP-AES quantification. This time, the reaction were performed using both **MnL4** and **CoL3** as metal cofactors separately. The incubation was performed as described previously (see above) except that the samples were desalted twice through NAP10 columns.

Table 3: anchoring ratios estimation via ICP-AES and MALLS analyses of protein samples (first attempt)

Entry	Protein	complex	Protein µM	Metal µM	Complex/protein ratio
1	H416C	MnL4	6,2	7.2	1.1
2	D59C	MnL4	14,2	28.3	2
3	T23C	MnL4	14,7	90.0	6
4	H416C	CoL3	15,6	40.0	2,5
5	D59C	CoL3	7,5	38.0	5
6	T23C	CoL3	13,3	46.5	3.5

Results summarized in ***table 3*** depict the same pattern, with excess of complex per protein confirming the presence of interactions other than the covalent one with the cysteine, except for **H416C-MnL4**. The latter case is in accuracy with the UV-visible titration, confirming a quantitative addition and making this hybrid a good candidate for catalysis.

Comparative analysis of the anchoring ratios to identify a correlation with the accessibility of the cysteine residue remained unsatisfactory. Indeed, **MnL4** and **CoL3** complex/protein ratios do not follow the same trend. For instance, this ratio is lower in **D59C-**

MnL4 *(entry 2, table 3)* when compared to T23C-MnL4 *(entry 3, table 3)* whereas this pattern is inverted with the CoL3 complex (*entry 5-6, table 3*).

The reproduction of the same protocol with the CoL3 complex afforded different complex/protein ratios (***table 4)*** attesting on the poor reproducibility of these assays.

***Table 4** : anchoring ratios estimation via ICP-AES and MALLS analyses of protein samples (second attempt)*

Entry	Protein	complex	Protein µM	Metal µM	Complex/protein ratio
1	H416C	CoL3	15.5	11.1	0.7
2	D59C	CoL3	13.9	7.1	0.5
3	T23C	CoL3	6.7	34.3	5.1
4	WT-NikA	CoL3	11.4	11.9	1.0

All together, these results suggest not only the presence of small metal excess due to unspecific interactions but also the randomized aspect of these interactions as yields are not reproducible. Furthermore, the high anchoring yields do not necessarily reflect a successful covalent modification as seen with the WT-NikA controls. It also questions the accuracy of the ICP method, emphasized by the low metal content detected. Then, ESI-MS was expected more reliable for the C-S bond formation.

Then, the depiction of the anchoring mode was verified by ESI-MS analysis under denaturing conditions which highlights covalent modifications exclusively. First, it has to be noted that all the mutant spectra display the expected mass fragment of the free protein. *Figure 39* consists of the ESI-MS data for CoL3-based hybrids.

D59C-CoL3 (*figure 39a)* displays several interesting fragments peaks. The peak corresponding to the intact protein (m/z 56290) attests that the covalent transformation is incomplete. The peak at m/z 56322 displaying a mass difference of m/z +32 may result from the protein oxidation. By taking this into consideration, the peak at m/z 57037 displaying a mass difference of m/z +715, in agreement with a CoL3 mass with a free apical position) , m/z +32 can be attributed to the oxidized D59C-CoL3. Morover, a lower weigth fragments, m/z +305 vs the free protein fragment (56268) could be attributed to the fragment of the covalent CoL3 which have undergone a di hydrolysis of the imine bonds of L3 respectively. It may reveal that

under ESI-MS the ligand is unstable, with the release of the 3,5-di-*tert*-butyl-2-hydroxybenzaldehyde.

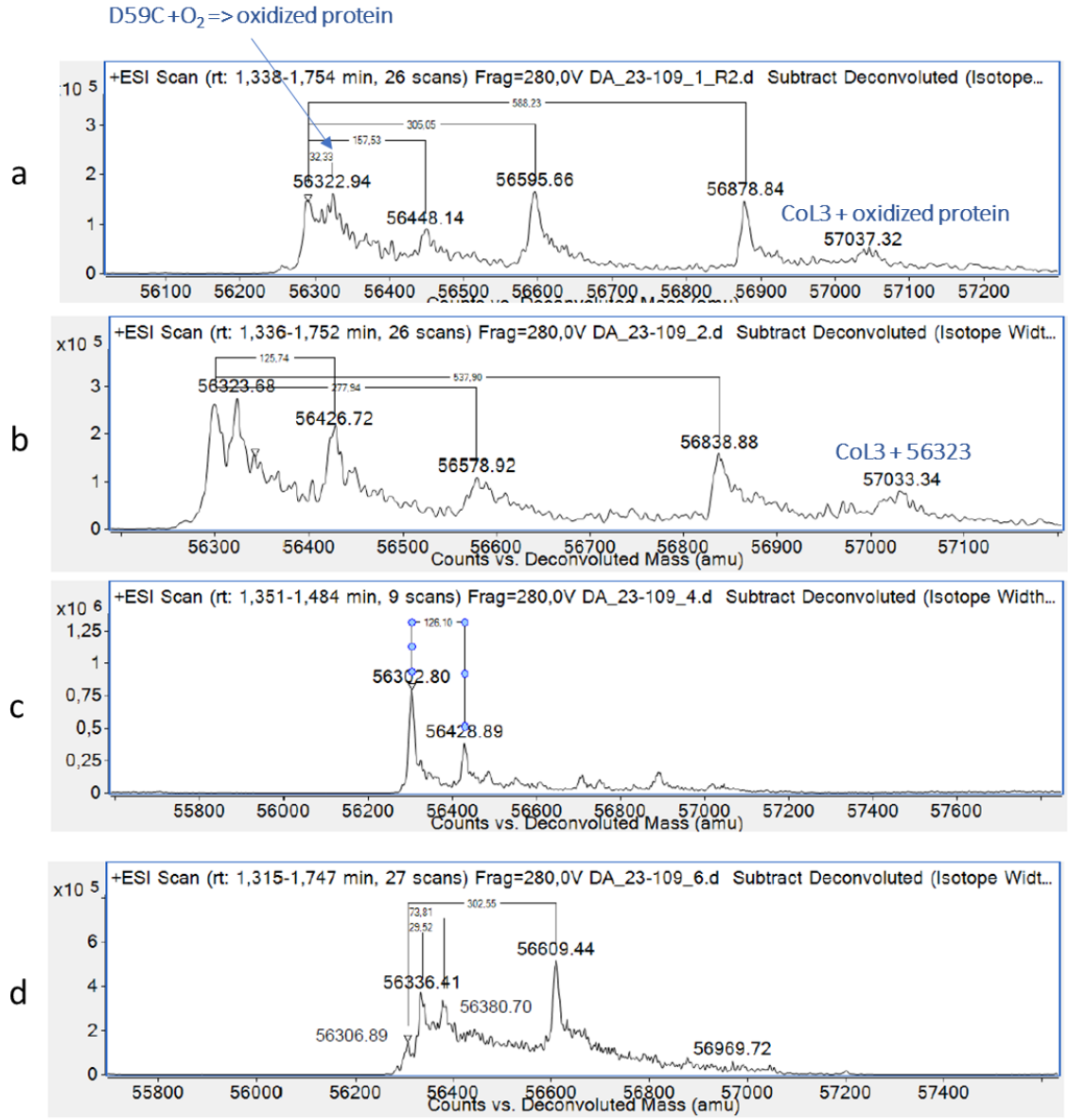

Figure 39: *ESI-MS results for anchoring assays of* ***CoL3*** *on* ***WT-NikA*** *and mutants: a)-* ***D59C****, b)-****H416C****, c)-****WT*** *and d)-****T23C***

In the H416C-CoL3 ESI-MS data (***figure 39b)***, two interesting peaks have been identified at m/z 56323 and m/z 57033. while the first does not correspond to the intact protein, the mass difference between the two peaks corresponds to the mass of the CoL3 complex. Out of this observation, we assumed again that the first peak attests of the protein degradation whereas the second peak confirms the successful covalent modification of the H416C protein with the complex CoL3. The absence of the intact protein, attest that the protein has a quantitative covalent binding.

T23C-CoL3 ESI-MS data were unsatisfactory as no full fragment can be identified (***figure 39d***), except one peak at +307 corresponding to the di hydrolyzed L3 product (56302 m/Z for the free protein) but the free protein was again absent. Moreover, the fact that WT-NikA-CoL3 shows only the minor presence of an unidentified specie at 56428.8 m/z with the mass difference of 126 m/z as compared to the intact protein, in addition to the free protein peak, attests that the cysteine is absolutely required for the attachment but that some very minor unrelated covalent binding with other amino acid is feasible. This same modification was observed with the H416C-CoL3 sample (see ***figure 39b***). Then, both the H416C and D59C displayed strong evidence on CoL3 covalent anchoring.

Surprisingly, ESI-MS data from MnL4 based hybrids were unsatisfactory. The spectra shown in ***figure 41*** attest of covalent modification of the protein, with the absence of the free protein peak but no significant fragment could be identified, except the m/z +300 vs the free protein (m/z 56290) fragment in D59C-NikA-MnL4. The latter is again representing the fragment with the loss of two phenol fragments of the salen backbone. Interestingly, the difference between D59C-NikA-MnL4 and D59C-NikA-CoL3 corresponds to the difference of the metal mass (Co vs Mn = +4), reinforceing the accuracy of the interpretation.

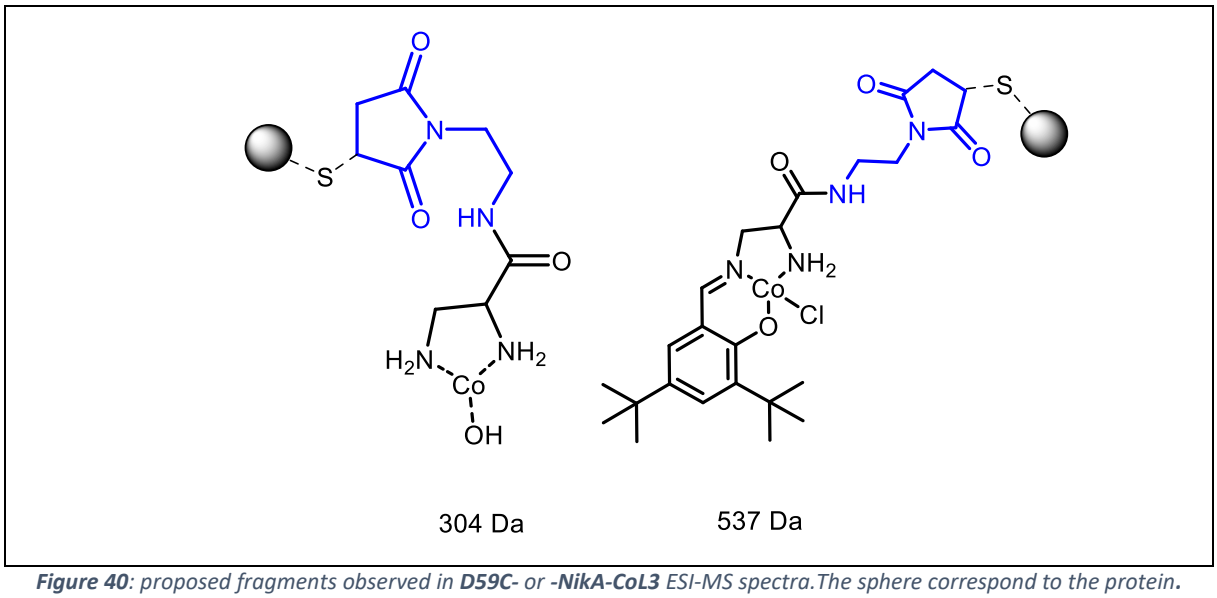

***Figure 40**: proposed fragments observed in **D59C-** or **-NikA-CoL3** ESI-MS spectra.The sphere correspond to the protein.*

Finally, in the case of D59C- and H416C-CoL3, an important fragment is detected that could correspond to the mono hydrolysis of the ligand, as displayed in ***figure 40***, depending upon the mutant, one extra water molecule is added.

As observed to a lesser extent with the WT-NikA-CoL3 sample, a covalent modification of the protein is not necessarily related to the cysteine modification.

This study is still incomplete. The control spectrum of thee MnL4 and CoL3 complexes under denaturing conditions need to be recorded alongside the T23C-MnL4 sample for which previous attempts of mass analysis remained unsatisfactory.

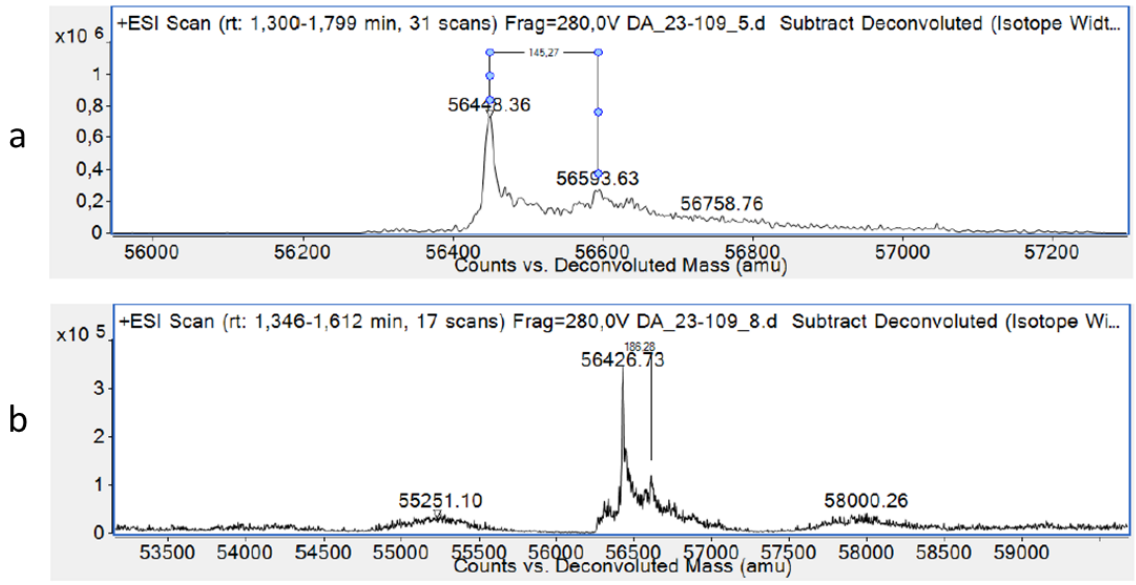

Figure 41: *ESI-MS results for anchoring assays of* ***MnL4*** *on mutants: a)-* ***D59C****, b)-****H416C***

The different titration approaches attest that the MnL4 and CoL3 can be inserted into the NikA protein. First of all, the complexes are bound in solution at least at two distinct binding sites, as demonstrated by the presence of Mn content in WT-NikA. The different ratios may be considered with caution, as the data reproducibility is not reached, probably due to unspecific noncovalent binding of Mn complex. While it is not sure that the covalent binding is complete with all the mutants, the H416C on the other hand seems to possess the expected C-S bond, mostly quantitative based on early ESI-MS studies. On the other hand, the presence of adventitious complex is likely to occur. More work is then needed to prove that the other mutants are relevant to C-S bond formation. The location of the cysteine influences undoubtedly their reactivity toward the maleimide group. Moreover, the hydrolysis of the imine group is likely to occur under the denaturing conditions which explains the observed fragments with this salen series. Overall, several hybrids have been prepared but the C-S bond formation remain to be clarified: X-Ray crystallography experiments should be the perfect approach for this purpose.

1.2.2. In cristallo assays

In cristallo investigations were performed on mutants T23C, D59C, and H416C which yield satisfying crystals in terms of number and size dispersion alongside WT-NikA crystals as the negative control.

The first attempt consisted of soaking the crystals *at room temperature* overnight in a stabilizing buffer solution (25 mM HEPES buffer at pH 7.0, 2.1 M ammonium sulfate) of the complexes MnL3, MnL4 and CoL3 at concentrations ranging from 2 to 10 mM. Complexes CoL3 and MnL3 displayed a very low solubility in the buffered media due to their *tert*-butyl substituents, initially selected to promote stereoselectivity. This low solubility is aggravated by the presence of the precipitating agent (ammonium sulfate), necessary for the preservation of the crystals integrity. Therefore, the exact concentration of both complexes in solution assays remains unknown. Nevertheless, both candidates were included in this investigation.

Qualitative observation of the crystals after soaking at room temperature with either CoL3 or MnL3, at any concentration, displayed no color nor aspect change. Conversely, at 5 mM of complex concentration for both MnL4 and FeL4, mutants and WT-NikA crystals displayed a drastic color change (yellow for MnL4 and purple for FeL4) after 5 min of soaking. The color was persistent in the case of D59C, T23C and H416C as opposed to WT-NikA, as seen in ***figure 42*** *for* ***H416C*** *crystals*.

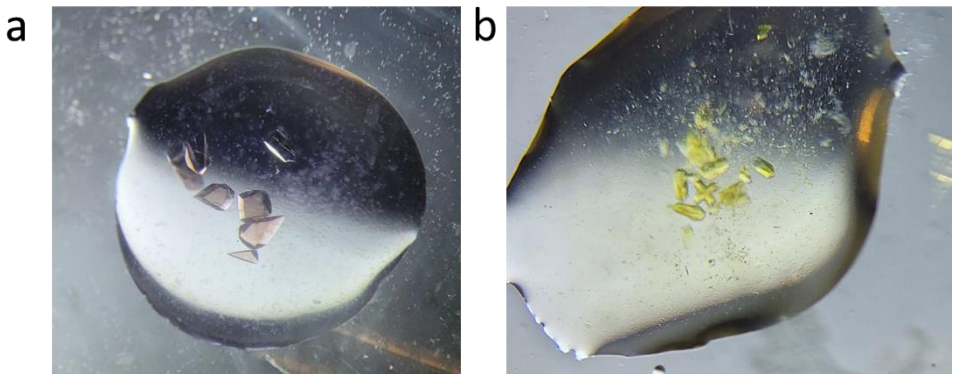

Figure 42: NikA- H416C *crystals after room temperature soaking with: (a)* ***FeL4****, (b)* ***MnL4***

Regardless of these observations, the different crystals of hybrids were analyzed by X-ray diffraction at the ESRF.

As expected, crystals on which no color change was observed had no covalently linked complex. Surprisingly, X-ray data from H416C-MnL4 and FeL4 showed that the cysteine residue remained unmodified as well. This might suggest that the anchoring yield is either too low or

that the color results from the diffusion of the solution inside solvent channel with additional unspecific protein-complex interactions explaining the persistence of the color, even after transfer in the buffer at the washing step. **H416C-MnL4** and **H416C-MnL3** crystals both afforded good X-ray diffraction data quality whereas **H416C-FeL4** displayed no diffraction pattern. It is tempting to correlate the color intensity corresponding to complex concentration to the crystal integrity: In **FeL4**, the amount of **FeL4** might create a large disorder on the protein backbone, leading to the loss of resolution.

An alternative for the determination of the presence of the complex within the crystals is to use X-ray fluorescence (XRF). ***Figure 43*** displays the $K_{\alpha 1}$ and $K_{\beta 1}$ bands for the metals of our interest, iron, manganese and cobalt. In **H416C** and **T23C**, in which the cysteine residue is located near the cavity, the anchored complexes might replace the **FeEDTA**. Conversely, **CoL3** and **MnL4** associated with the **D59C** mutant in which the cysteine is located the farthest from the cavity, XRF data are expected to highlight the presence of two metals, iron and Manganese or cobalt depending on the associated complex.

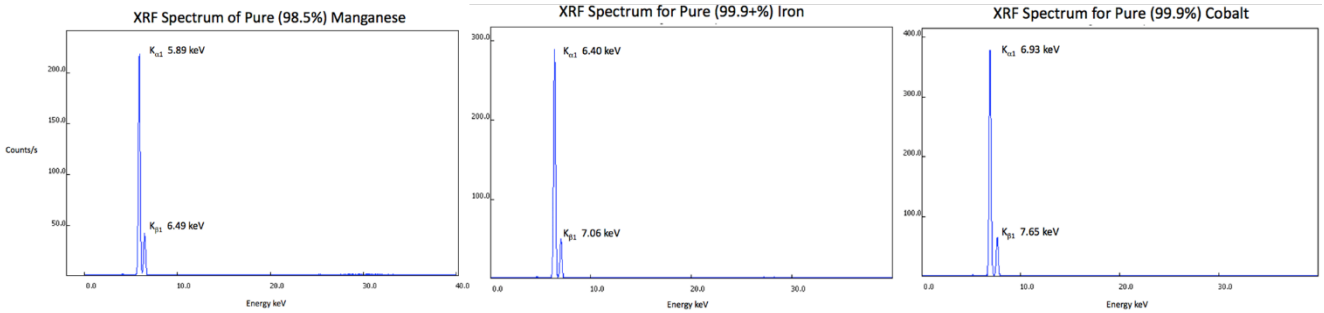

Figure 43: *fluorescence profiles of pure iron, manganese and cobalt* [242]

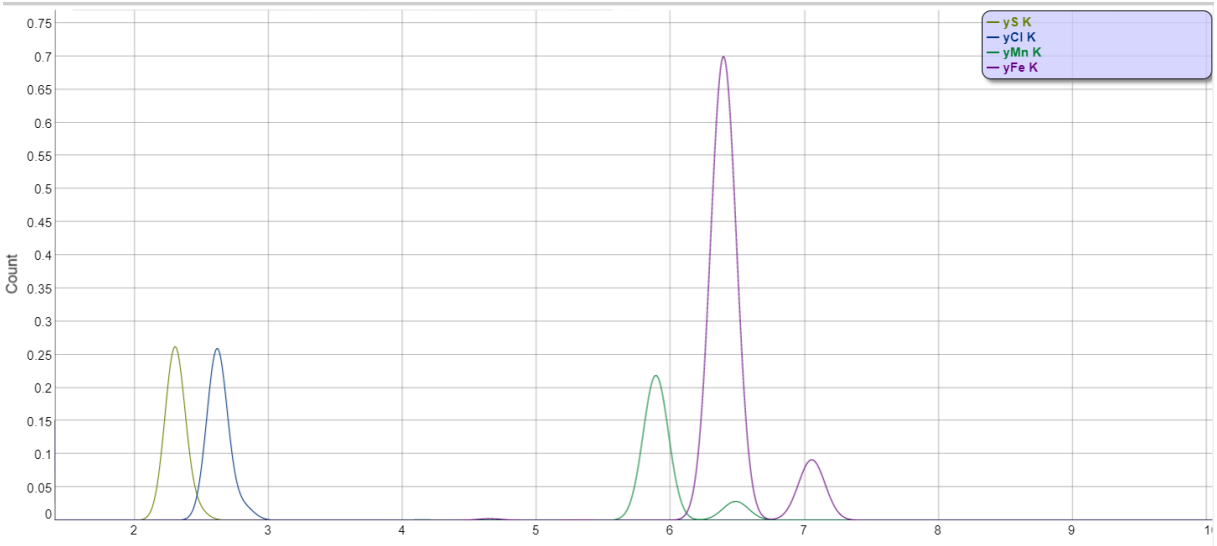

Figure 44*: XRF data of* ***H416C-MnL4*** *crystals after room temperature soaking. Color referred to one metal*

Figure 44 displays the XRF data for the **H416C-MnL4** crystals soaked at room temperature. Although it is unclear if successful anchoring at the C416 position results in the total displacement of Fe^{III}(EDTA), the XRF data show a clear excess of iron as compared to manganese.

As anchoring assays in solution have shown that the Michael addition is feasible at room temperature, the differences observed *in cristallo* can be related to the accessibility of the cysteine mutant within the crysta lattice and the presence of ammonium sulfate in the buffer.

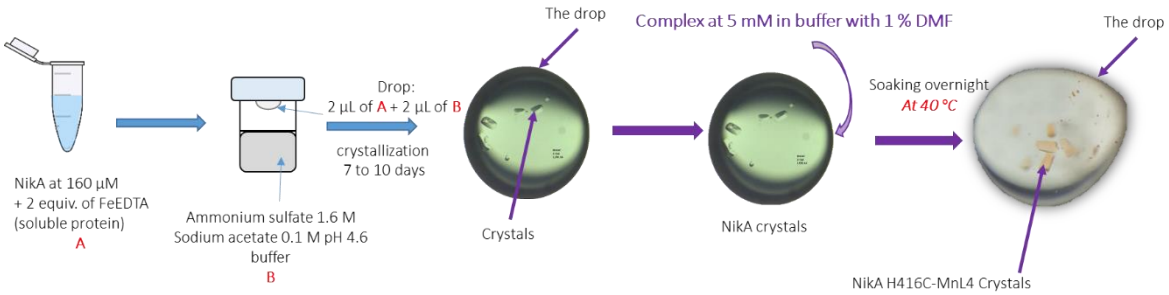

Scheme 27: anchoring methodology for complex soaking

To enhance the chemical transformation, the anchoring methodology was performed *at 40 °C overnight*, under agitation. ***Scheme 27*** highlights the different steps of the procedure. Previous investigations on NikA's thermostability were performed on the stabilized crystals (CLEC); however CLEC are not ideal for structure determination . In fact, the reticulation of the crystals results in a loss of resolution leading to no diffraction at all, if anchoring assays are performed in organic solvent. For the above reasons, a first anchoring assay at 40 °C was performed with the **H416C** mutant alongside the complexes **MnL4**, **FeL4** and **MnL3**. Strikingly, as seen in ***figure 45*** crystals for the three ArMs remained visually intact and displayed a color change compared to the untreated crystals.

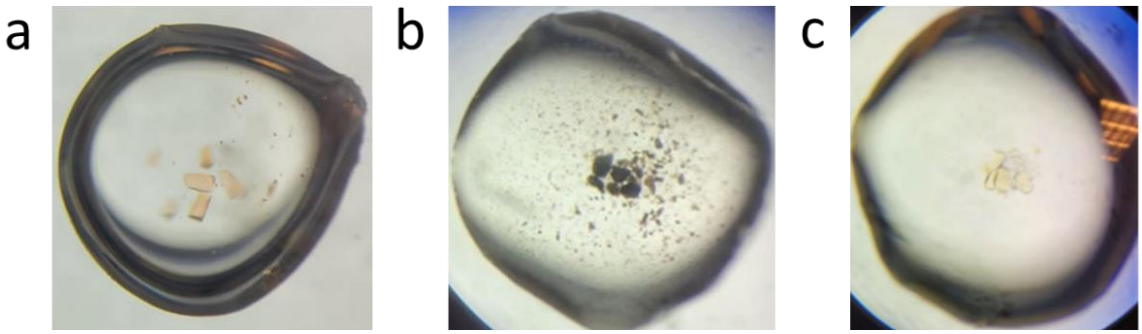

Figure 45** : **NikA-H416C** crystals after 12h of soaking at 40°C with: (a) **MnL3**, (b) **FeL4**, (c) **MnL4

XRF data from this batch of H416C-MnL4, after overnight soaking at 40 °C, with the same concentration of MnL4 as previously investigated, display a much higher manganese content as compared to iron and the manganese content obtained at room temperature. As seen in ***figure 46***, XRF data are characteristic of the presence of manganese with the presence of the $K_{\alpha 1}$ peak at 5,89 KeV. The $K_{\beta 1}$ pic is undistinguished due to the presence of the iron $K_{\alpha 1}$ peak at 6,40 KeV. Although non quantitative, these data state that non total replacement of FeEDTA is observed in the H416C-MnL4 crystals. Nevertheless, the relative intensities of the Fe and Mn band is quite different compared to the ***figure 44***, suggesting a large loss of iron EDTA.

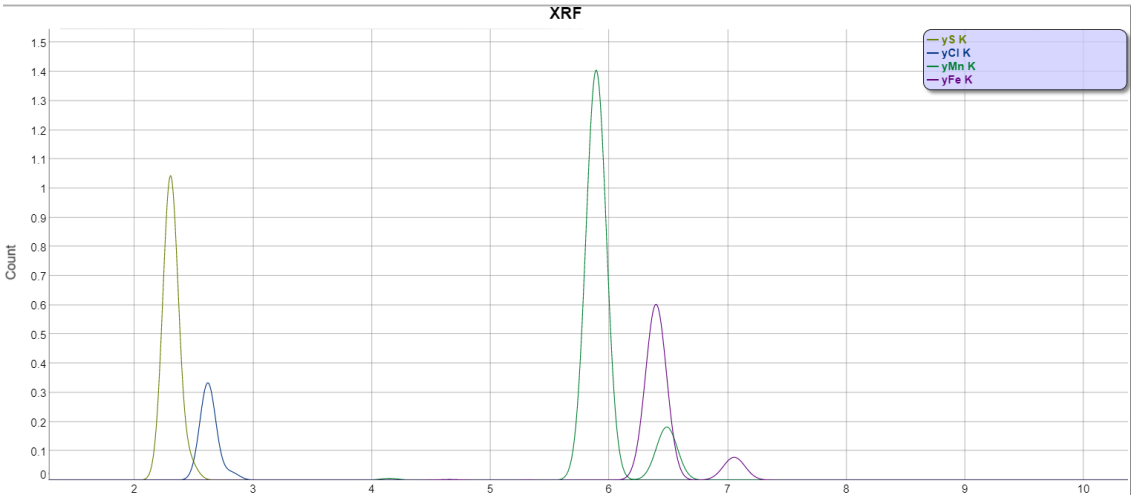

***Figure 46** : XRF data from **H416C-MnL4** crystals soaked at 40 °C*

This anchoring methodology was extended to mutants T23C and D59C alongside complex MnL4. Comparable XRF results were obtained as seen in ***figure 47***. The Kα1 band of both iron and manganese are present. Nevertheless the relative intensity of the iron Kα1 alongside the previous XRF data suggests that the in the T23C mutant covalent anchoring of MnL4 might indeed displace Fe^{III}(EDTA).

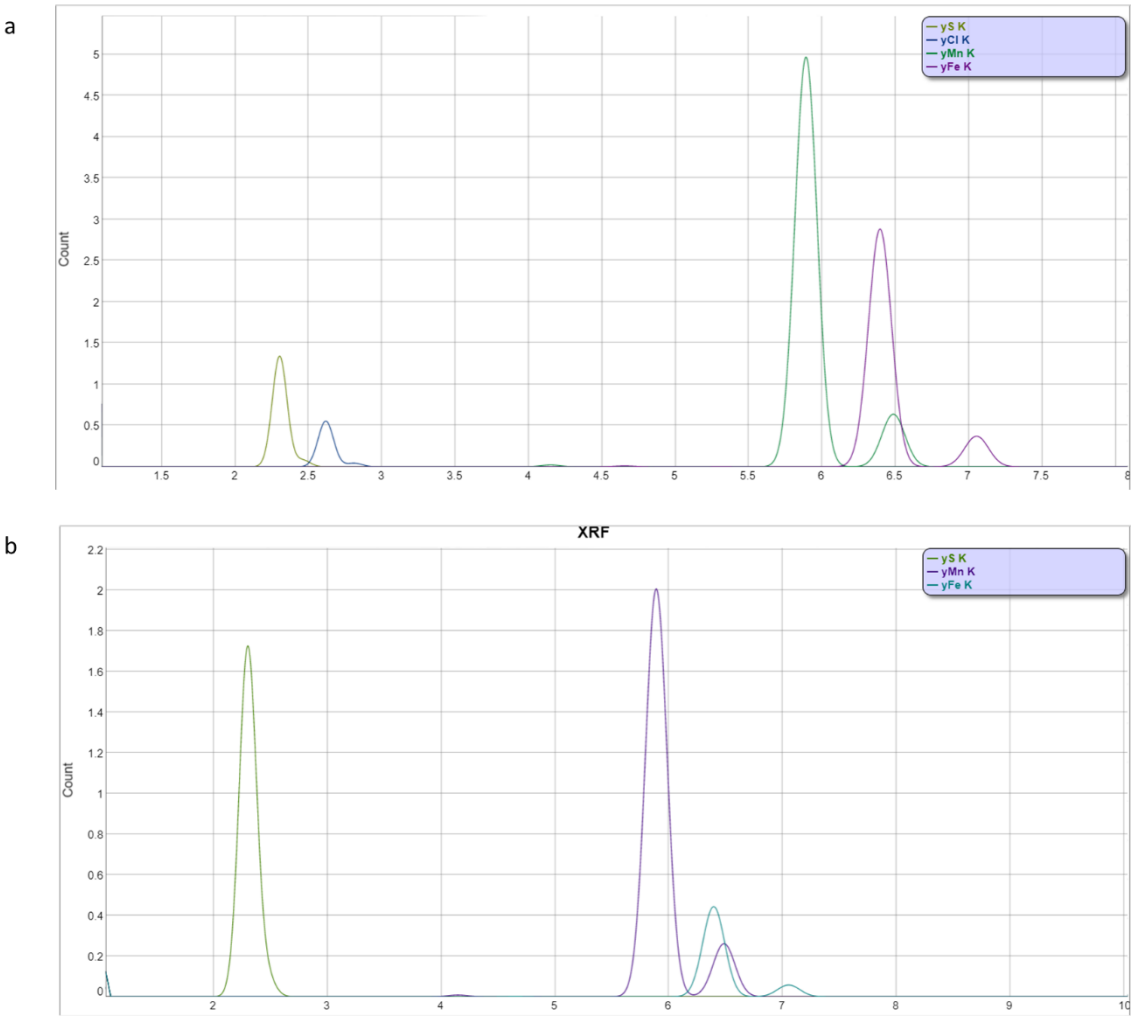

Figure 47: *XRF data from* ***D59C-MnL4*** *(a)* ***T23C-MnL4*** *(b) crystals soaked at 40 °C*

1.2.2.1. X ray structures of Cysteine mutants NikA-MnL

While the crystals were able to withstand high temperature changes, only H416C-MnL4 displayed evidence on covalent modification of the cysteine residue. As seen in ***figure 48,*** a large electron density is visble close to the sulfur atom in molecule B, one of the two NikA molecules that constitute the asymmetric unit. Interestingly, the FeEDTA in both H416C-MnL3 and H416C-MnL4 seems to be displaced judging by the lower electron density observed in the binding pocket. Based on this observation, soaking at 40 °C might be suitable to aid FeEDTA displacement as a new anchoring methodology for the first site.

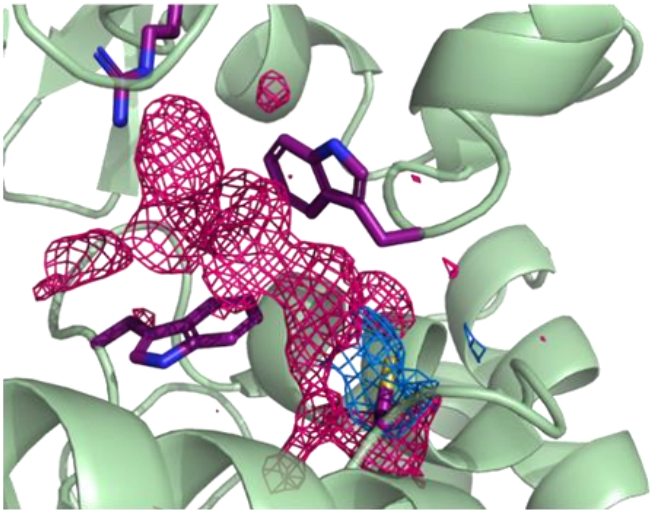

Figure 48: H416C-MnL4 *(resolution 1.6 Å) before refinement showing the electron density (blue and pink) around the sulfur atom at the C416 position (yellow)*

T23C-MnL4 crystals diffract at 1.77 Å after an overnight soaking at 40 °C. As seen in ***figure 49*** the covalently anchored MnL4 complex is positioned towards the backbone on the protein. The displacement of the neighboring Tyr382 and Glu378 attests of the presence of the complex.

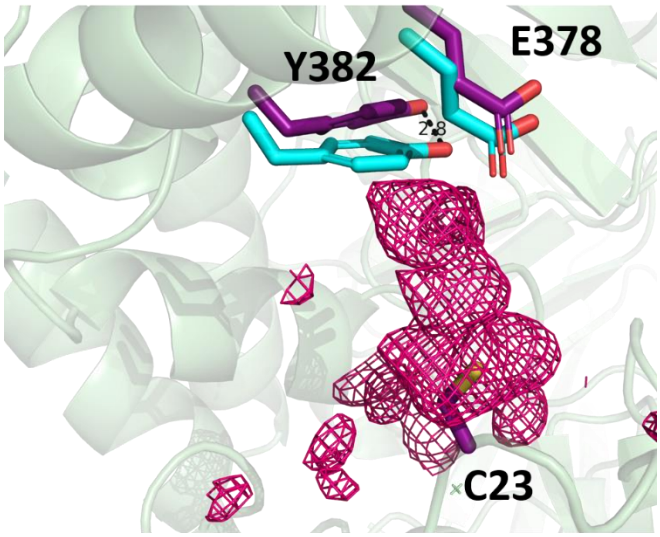

***Figure 49**: **T23C-MnL4** (Resolution : 1.77 Å) The omit map contoured at 2.5 Å (pink) shows the electron density corresponding to the MnL4 complex. A translation of Glu378 and Tyr382 (cyan in the WT and purple in the mutant) gives more room to accommodate the complex*

For the D59C-MnL4 crystals, the cysteine is located in a 5 nm open wide channel allowing thus a great flexibility of the protein backbone as well as the metal complex, if bound. As seen in ***figure 50***, the cysteine C59 is present in an exposed flexible loop, with not very well defined electron density and large B-factors (up to 100 $Å^2$ for C59), responsible for the difficulty to identify MnL4 in this region.

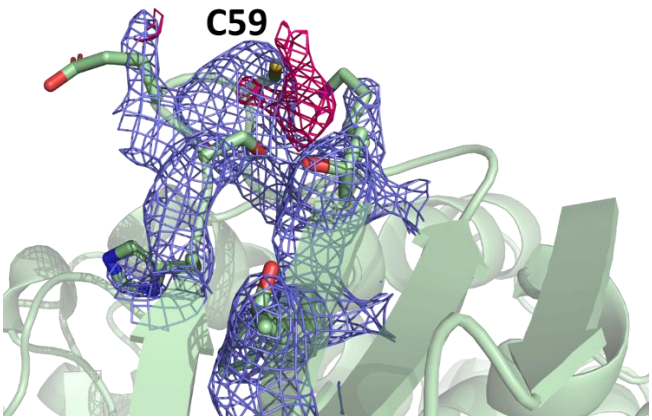

***Figure 50**: **D59C-MnL4** (Resolution : 2.6 Å)*
In blue, 2Fo-Fc map contoured at 1 σ. The omit map contoured at 2.5 σ (pink) shows only residual electron density for MnL4.

The discrepancy between the investigated mutants associated with MnL4 can be relative to the position of the cysteine within the protein scaffold. For instance, in the D59C mutant, the cysteine is located in a less hindered area as compared to H416C and T23C. Occupancy and interaction network will be updated after refinement in the near future.

Anchoring investigations on complexes CoL3 and MnL3 were challenging due to their low solubility in aqueous media. Moreover, the steric hindrance brought by the ligand L3 might prevent access to the cavity area. Due to the challenging conditions, MnL3 was set aside during these investigations in favor of the MnL4 epoxidation catalyst, a choice motivated by their great similarity and the conclusive characterization results obtained with the latter.

Soaking crystals with CoL3 was performed according to the same methodology. Associated with T23C, D59C and H416C crystals, no evidence of a successful modification of the cysteine residue was observed in all of the three cases. Whereas the absence of the CoL3 in the T23C and H416C crystals can be explained by the size of the complex considering the relatively small area in which the cysteine is located, D59C data remain ambiguous. Indeed, localizing and attributing the electron density corresponding to the CoL3 complex depends on the occupancy and the flexibility of the complex. The electron density at the 59 position being blurry in the crystal structure, as seen in ***figure 50,*** combined to a rather low anchoring yield, a partial functionalization cannot be ruled out.

To conclude, we have demonstrated that the C-S bond formation is performed at 40°C *in cristallo* , while not altering significantly the protein crystal integrity. We have definitive evidence of the bond formation in H416C-MnL4 hybrid with the insertion of the complex into

the cavity. In the case of the T23C-MnL4, the flexibility of the region in the proximity of C23 in the X ray structure suggests that partial reaction occurred. Then, for the first time, we have demonstrated the Michael addition directly into a protein crystal. Moreover, while it is not proven that the CoL3 and MnL4 are covalently bound to the D59C mutant protein, The XRF attests of their insertion, at an unknown location.

2. Dual-site artificial metalloenzymes

Out of the available complex candidates, multi-site ArM design options consisted of associating the carbonation catalyst CoL3 with an epoxidation catalyst possessing an orthogonal anchoring mode, either MnTACNAA or MnL_{III}. Due to the low solubility of CoL3 and the discrepancy observed throughout anchoring assays in solution, multi-site ArM preparation was only attempted on protein crystals. Initial anchoring assays were performed on the D59C mutant in which both of the active sites are located the farthest from each other. In this case, interference between MnLIII and CoL3 should be insignificant.

In a typical procedure, D59C-FeEDTA crystals were soaked overnight at 40°C with a solution of CoL3 at 5 mM in the stabilizing solution with 10 % of DMF, under agitation. The crystals are then recovered, rinsed then soaked once more with MnL_{III} solution at 10 mM in the same solution for 16 h. The recovered crystals remained slightly colored as previously observed with both complexes separately.

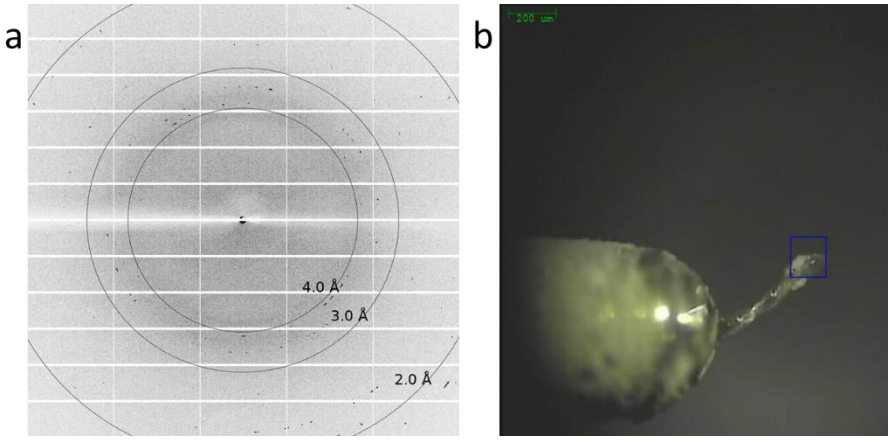

Figure 51: *(a) a diffraction pattern of* ***H416C-CoL3-MnLIII*** *crystal (b) aspect of* ***H416C-CoL3-MnLIII*** *crystal*

Unfortunately, as seen in ***figure 51***, no diffraction pattern was observed with this batch of crystals. The first assumption was that the crystals have been fragilized by the double treatment with the complex solution. Indeed, the non-stabilized crystals tend to be fragile, as they are

typically frozen in the cryoprotectant buffer directly after the first heat treatment. In a second attempt, we have decided to shorten the soaking time for the second complex, **MnL_{III}**, for 6 h instead of roughly 16 h tested previously, but no diffraction was observed in this case either.

Finally, metal content of the crystals, visually intact but very brittle to handle because oddly fragile compared to the untreated crystals or even to the Mono-site ArM crystals, was determined by X-ray fluorescence. XRF data of **D59C-MnL_{III}-CoL3** shown in ***figure 52*** highlight the presence of the predominant cobalt $K_{\alpha 1}$ peak at 6.93 KeV alongside the Mn $K_{\alpha 1}$ at 5.9 KeV and a XRF peak at 6.4 Kev attributed to Fe. Analysis of this spectrum could indicate the successful anchoring of the **CoL3** on the cysteine **59** whereas the second anchoring of **MnL_{III}** remained partial, as the iron brought by **FeEDTA** is still present. Nevertheless, XRF data of the multi-site ArM have been conclusive for the **D59C** mutant as they point to the dual functionalization of the protein scaffold.

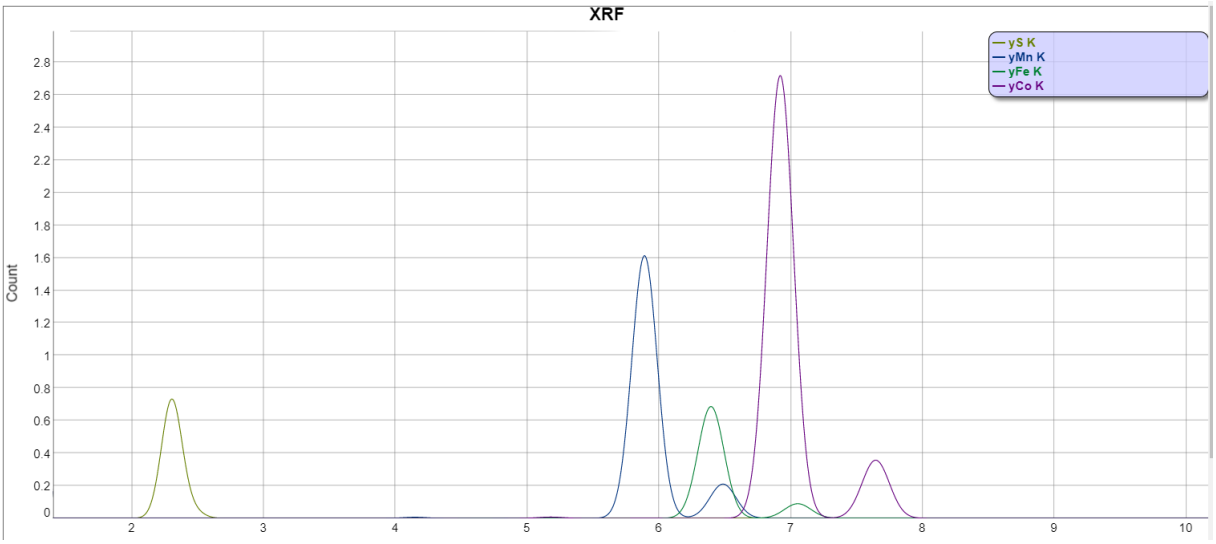

Figure 52: *XRF data of the* ***D59C-CoL3-MnLIII*** *crystal*

3. Conclusion

We have for the first time successfully modified the protein in its crystal form by a Michael addition on a cysteine and define a new route for protein modification. Moreover, one of the greatest challenges in the development of ArM in addition of the stability, is the determination of the complex loading and localization within the protein matrix. Here we have reported five novel epoxidation ArMs, three of which evidence the covalent association of a **MnL4** complex on three different NikA mutants (**H416C**, **D59C** and **T23C**), offering various protein environments. Conclusive X-ray data showing the covalent attachment of **MnL4** on

T23C and H416C mutants were obtained. Interestingly, the insertion of the complex MnL4 into the cavity was not expected but should provide a great impact on selectivity of the catalysis. On the other hand, no tangible X-ray data for D59C-MnL4 ArM was obtained due to lack of resolution. Evidence of the presence of MnL4 on the D59C scaffold was brought by XRF results. Unexpectedly, diffraction data retrieved after the heat treatment under agitation are of of only slightly less quality compared to the untreated crystals. Soaking attempts in the crystallization plates at 37°C in an incubator, under no agitation gave out comparable data quality. This confirms that the overnight heating rather than the agitation affects the crystal quality.

Two other epoxidation ArMs were obtained with the association of MnTACNAA and MnL_{III} with WT-NikA, located in the cavity as determined by conclusive X-ray data.

The preparation of CoL3 complex- based ArMs for carbonation reactions remained challenging due to the low solubility of the complex in buffered media. Nevertheless, XRF data has provided encouraging evidence of the complex presence within the protein crystal.

Mutli-site ArM design options reside in the association of either MnTACNAA or MnLIII and CoL3 in the three available mutants. CO_2 cycloaddition catalyst CoL3 with large bulkiness is less likely to access the narrowest cysteine location in T23C, therefore, the main choice for the development of the multi-site ArM remained D59C. Multi-site ArM using MnTACNAA and the T23C and H416C mutants are still of interest but have not been prioritized. Unfortunately double treatment of the crystals for the soaking step has been found to be damaging. No conclusive diffraction was observed although XRF data afforded promising results for the D59C-MnLII-CoL3 ArM.

The next chapter is going to focus on the reactivity of the prepared ArM, highlighting the influence of the preparation methodologies of the ArM catalysts on the overall catalytic activity.

Chapter IV Catalytic investigations

This chapter is devoted to preliminary results on the exploratory strategy, consisting of generating CLEC before their full characterization. In the previous two chapters, were described the preparation and the partial characterization of a series of ArMs listed in ***table 5***. These hybrid systems will allow us to test the impact of the localization and the nature of the anchored complex on the catalytic activity. Moreover, the mode of interaction will also be challenged during the comparison of the WT and mutant NikA proteins, allowing us to indirectly prove the formation of the C-S bond. Finally, the impact of the anchoring on the activity will be compared to the one of each complex alone, to determine the role of the heterogenization.

Characterization efforts discussed in the previous chapter have put to light the potential presence of an excess of complex in the case of the salen series, regardless of the mutant. This same pattern was observed with **WT-NikA**, quite problematic as no cysteine are present. In order to highlight the catalytic contribution of the unspecifically bound complex as well as the free complex if present, catalytic activity was assessed using different controls including the free complex at a concentration of 40 µM, **CLEC WT-NikA -MnLx** and **CLEC-NikA-Fe^{III}(EDTA).**

It is worthy to note that most initial catalytic investigations were performed before the full characterization of the CLEC. Assessing the activity of the prepared ArM has been then considered as an alternative to characterization results to benchmark the effectiveness of the catalyst preparation methods. In an explorative fashion, this has constituted a first screening of the catalyst preparation methods as well as the catalytic conditions.

This chapter will deal with the preparation of the heterogeneous counterpart of the ArMs described previously, involving the cross-linking step in order to preserve the crystal integrity.[228,243,244] Then, their catalytic properties will be determined considering two reactions: alkene epoxidation and CO_2 cycloaddition, followed by the preliminary cascade transformation assays ending this chapter. As the scope of conditions used in these investigations included oxidants, organic solvents and heating, enzymatic assays were only performed on CLEC. The strategy for the development of each catalyst consists in the variation of several key parameters, influencing the yield and selectivity of the reaction and the catalyst stability as well.

Table 5: summarized ArM investigated in this chapter.

Entry	ArM	Anchoring mode	Active site localization	Activity	Characterization
1	WT-NikA-MnTACNAA	Supramolecular *(Site 1)*	Binding pocket	Epoxidation	X-Ray diffraction
2	WT-NikA-MnLIII	Supramolecular *(Site 1)*	Binding pocket	Epoxidation	X-Ray diffraction
3	H416C-MnL4	Covalent *(Site 2)*	Binding pocket	Epoxidation	X-Ray diffraction ESI-MS XRF
4	T23C- MnL4	Covalent *(Site 2)*	Binding pocket	Epoxidation	X-Ray diffraction XRF
5	D59C- MnL4	Covalent *(Site 2)*	Solvent channels	Epoxidation	ESI-MS XRF
6	H416C- CoL3	Covalent *(Site 2)*	Binding pocket	CO_2 cycloaddition	ESI-MS XRF
7	D59C-CoL3	Covalent *(Site 2)*	Solvent channels	CO_2 cycloaddition	ESI-MS XRF
8	T23C- CoL3	Covalent *(Site 2)*	Binding pocket	CO_2 cycloaddition	ESI-MS XRF
9	D59C- CoL3-MnLIII	Covalent *(Site 2)*	Solvent channels	Cascade transformation	XRF
		Supramolecular *(Site 1)*	Binding pocket		XRF

1. Heterogeneous catalysts preparation

1.1. Mono-site ArM

Previous catalytic investigations using NikA-based ArMs, reported by Lopez *et al.* were accomplished using batches of 100 CLEC each in a 40 µL volume.[95,241] Protein and metal quantification on such system has allowed to determine the catalyst concentration at a range of 31-40 µM. Although quite low, it has been sufficient for outstanding catalytic performance on alkene cleavage, as previously described.[95] These conditions represent the starting point of our investigations.

In a typical procedure, **NikA-Fe^{III}(EDTA)** crystals are soaked overnight in a 10 mM catalyst solution in the stabilizing solution (25 mM HEPES at pH 7.6, 2.1 M ammonium sulfate). The crystals are then washed with the same buffer then stabilized by cross-linking with 1% of glutaraldehyde over 2 h. The CLEC are then recovered in an Eppendorf and washed with water then acetonitrile, the solvent of choice for our catalytic assays.[95]

This two-step procedure (soaking followed by cross linking procedures) is suitable for water soluble catalysts, for which anchoring assays at room temperature were proven effective by X-ray diffraction analysis, mainly the complexes **MnTACNAA** and **MnLIII**.

In the case of the salen series complexes, different preparation methodologies were tested:

Method A: 100 crystals **were soaked overnight at room temperature** in 4 µL drops of the complex at 5 mM in the stabilizing solution with 1% of DMF. Then, they were transferred to clean solution drops and stabilized with 1% of glutaraldehyde in the same buffer for 2 h at room temperature. The crystals were fished out of the drops, added into MeCN and engaged in catalytic assays.

Method B: 100 crystals **were *first* stabilized with 1% of glutaraldehyde** in the stabilizing solution for 2 h at room temperature. *They* were then transferred to 500 µL Eppendorf tubes containing 100 µL of the complex solution at 100 mM in DMF and soaked at room temperature overnight. Complex excess was washed off with DMF; then the crystals were engaged in catalytic assays in MeCN.

Method C: 100 crystals were **stabilized with 1% of glutaraldehyde** in the stabilizing solution for 2 h at room temperature. They were then transferred to 500 µL Eppendorf tubes containing 100 µL of **MnL4** at 100 mM in DMF and soaked at 40 °C overnight.

Method D: 100 crystals were transferred to a 500 µL solution of MnL4 at 5 mM in the stabilizing solution with 1 % of DMF in an Eppendorf tube. Then, they are incubated in thermomixer overnight at 40 °C under agitation. The crystals are retrieved from the solution and transferred back to clean solution drops and stabilized with 1% of glutaraldehyde, in the same buffer, for 2 h at room temperature. The crystals are then transferred to an MeCN solution in 500 µL Eppendorf tubes.

While the integrity of the crystals is maintained, the stabilization related to the formation of random linkers between the lysine residues and the replacement of water with acetonitrile i the crystal solvent channels results in a significant loss of definition in XRD data relative to the percentage of organic solvent in solution. Consequently, CLEC in acetonitrile does not show any diffraction pattern, due to a great disorder inside the crystal. For these reasons, we have been unable to recover XRD data of CLEC functionalized in organic media for the metal salen-based NikA ArMs. Instead, complex content was determined quantitatively by ICP with the approximation that metal present in the structure results from the metal complexes.

The quantification process starts with the determination of the protein concentration in solution after dissolution of the crystals. After optimization of the crystallization process, reaching an acceptable size distribution, three aliquots, in which 20 crystals were dissolved in 20 µL of MiliQ water, were injected into the MALS apparatus. The protein concentration measured is then converted to 100 crystals in a 40 µL. From the same batch of crystals, a sample of 40 crystals were stabilized, the resulting CLEC soaked in a solution of MnL4 at 100 mM in DMF and washed thoroughly with DMF. The three batches were then mineralized overnight in aqua regia at 50 °C. This quantification methodology was tested once on CLEC H415C-MnL4 and evidenced the presence of at most 5 complexes per NikA protein. The protein crystals investigated have different sizes. H416C crystals have been studied extensively and display a crystal size comparable to those of the WT protein, making it the best system for comparison. *Table 6* summarizes the protein concentration of the different mutants expressed for a 100 crystals batch in a 40 µL volume, conditions at which the catalytic assays were pursued.

Table 6: determined protein concentration for 100 crystals in 40 µL

Entry	Protein	Concentration
1	WT-NikA	31 ± 5 µM
2	H416C	21 ± 5 µM
3	T23C	29 ± 5 µM
4	D59C	Estimated at 25 µM*

*average on the calculated concentration of crystals of comparable morphology

1.2. Multi-Site ArM

The multi-site ArM **D59C-MnLIII-CoL3** was prepared in batches of 100 crystals. The first soaking step with **CoL3** requiring high temperatures was performed on the CLEC upon stabilization, in a DMF solution at 100 mM overnight. Next, the crystals were washed with DMF to discard **CoL3** traces then soaked at room temperature with a methanolic solution of **MnLIII** at 100 mM. The **D59C-MnLIII-CoL3** CLEC were engaged in catalysis after a thorough wash with methanol then acetonitrile. Volumes of the soaking and washing solutions engaged were in the range of 40 µL.

2. Catalytic epoxidation of alkenes

Catalytic activity to be discussed in the upcoming paragraphs, will be expressed in TON as compared to the protein concentration. However, effect of the crystals numbers, and by extent the molar quantity of catalysts, on the catalytic efficiency for each mutant was not thoroughly investigated. Epoxidation activity of the prepared ArMs (***entry 1 to 5, table 5***) was assessed using H_2O_2, PAA or O_2 activation system with an aldehyde as the oxygen source.[221,245] A limiting factor has been the choice of the oxidant used. In fact, even though the CLEC are quite robust, their reusability depends greatly on the oxidant used. For these reasons we have avoided the use of harsh oxidants such as sodium hypochlorite and iodosyl benzene usually associated with the Jacobsen catalyst.[246–249]

2.1.Alkene epoxidation using hydrogen peroxide

We have undertaken the design of the alkene epoxidation using H_2O_2 as the oxidant, motivated by the reports of an active iron picolinate catalysts.[230]As reported in the main inspiration paper, the required catalyst concentration needed for an interesting activity is 10 mM concentration compared to our intended concentration range from 20 -100 µM at best, after which the system would be too costly on the protein production and use.

Investigations started with iron picolinates derivatives, as reported for such GoAgg type catalysts.[230] The picolinic acid derived ligands are commercially available and they readily contain the anchoring carboxylate moieties requiring no ligand transformation. The preparation of the catalysts is also straightforward requiring mixing equimolar ratios of Fe $(OAc)_2$, picolinic acid and 6-methylpicolinic in acetonitrile during which the catalytic species Fe(pic)$(Mepic)_2$, **A** is supposedly generated *in situ*.[230,250]

$Fe(Pic)_3$,**B**, $Fe(MePic)_3$ **C**, and Fe(pic)$(Mepic)_2$, **A**, were tested on styrene epoxidation using hydrogen peroxide in the reported conditions conditions, ***scheme 29*** [55].

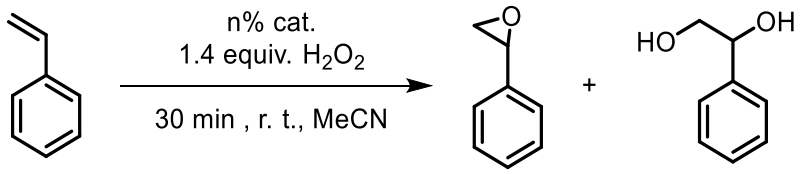

Scheme 28 : catalytic conditions for iron picolinates

At 10 mM of iron complex concentration, and with the ratio catalyst/substrate/oxidant of 1/70/50, styrene oxide was formed with 100 %, 45 % and 46 % respectfully, ***figure 53;***

At 100 µM of catalysts concentration, the efficiency of the catalysts drops significantly. In addition, the conversion of the starting material is high compared to epoxide yield. Although a small amount of benzaldehyde (1-2%) is formed as a byproduct, we suspected that the wrong mass balance was mainly due to styrene evaporation during catalysis. Moreover, catalytic tests performed using a stock solution of either $Fe(pic)_3$, $Fe(Mepic)_3$ crystals or the respective catalysts solution before crystallization provided comparable results. Although Fe(pic)$(Mepic)_2$ **A** is the most efficient compared to $Fe(Pic)_3$ **B** and $Fe(MePic)_3$ **C**, this complex will not be subjected to ArM production due to its content of many species, that will most likely cause reproducibility issues.

In the case of iron picolinates, soaking NikA-FeEDTA crystals before cross-linking was not effective as the complexes are not stable in our usual buffers (Tris-HCl and HEPES). Considering these issues, we have modified the CLEC preparation by inverting the cross-linking and soaking steps. After the cross-linking of NikA-Fe^{III}(EDTA) crystals, the obtained CLEC were engaged in a soaking step in acetonitrile at room temperature at 10 mM of metal concentration. However, no significant activity was observed in crystallo and investigation efforts were put towards the development of other epoxidation routes.

.

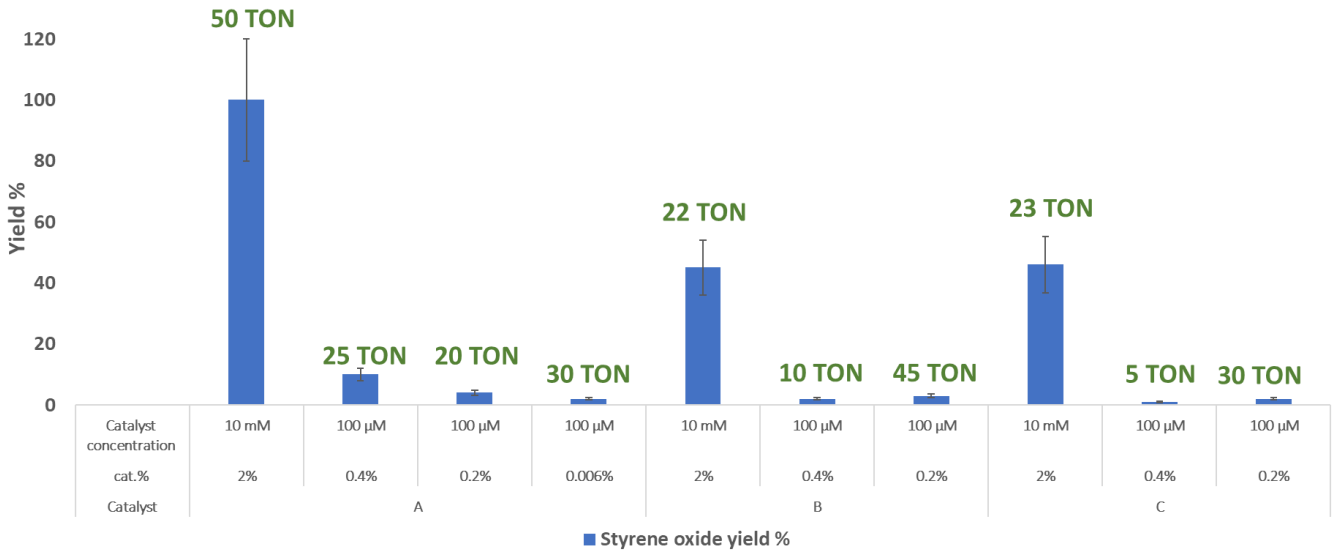

Figure 53: *results on styrene epoxidation catalyzed by iron picolinate derivatives A, B and C.*
Reactions carried out in MeCN using H_2O_2 as the oxidant at room temperature for 30min. Conversion and yield calculated by GC using benzophenone as an internal standard.

Since the *in cristallo* catalytic assay was unsuccessful, we have decided to not pursue further investigations on the iron picolinates series. We have uncovered that these systems are only efficient at high metal concentrations, excluding their use in the NikA catalytic procedures.

2.2.Epoxidation using Peracetic acid

2.2.1. NikA cysteine mutants and the metal salen series

Peracetic acid (PAA) is reported to be selective and efficient for alkene oxidation.[251,252] Initial catalytic assays were performed on the **H416C** mutant alongside the salen complexes **MnL4**, **FeL4** and **MnL3**. Initially, **H416C-MnL4** and -**FeL4** were prepared following the **method A**. On the other hand, for the **H416C-MnL3**, due to the catalyst being completely insoluble in aqueous media, we have decided to perform the covalent anchoring after the cross-linking step, following the **method B**.

The catalytic assays were performed in acetonitrile, at room temperature, using styrene as model substrate, in the presence of 2 equivalents of PAA per substrate for 16 h, ***scheme 30***. Catalyst loading expressed with respect to the protein concentration determined by MALLS analysis was estimated at 21 µM (***entry 2, table 6***). This corresponds to a molar quantity of 0.8 nmole for the catalyst, 1.6 µmole of styrene and 3.2 µmole of PAA and a ratio catalyst/substrate/oxidant of 1/2000/4000.

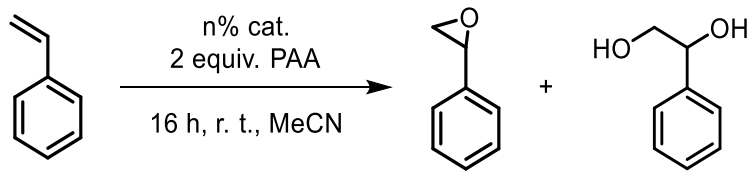

Scheme 29 : *catalytic conditions for styrene oxidation*

as an internal reference.

Throughout this assay, two major oxidation products were observed, styrene oxide and phenyl-ethan-1,2-diol. Benzaldehyde, another oxidation byproduct was observed on the GC as a trace; however, the quantities were negligible (<1 %).

Figure 54 summarizes initial results obtained when investigating the activity of the free complexes versus their **H416C**-based ArM analogues. Homogeneous assays were performed at a metal concentration of 40 µM. These assays as well as the uncatalyzed transformation displayed the same activity with a global yield at 10-11 %, meaning the free complexes are inactive under these conditions.

CLEC **H416C-FeL4** and **H416C-MnL4** displayed comparable activities. Conversely, the CLEC **H416C-MnL3** displayed a much higher yield at 30% with 660 TON. The fact that **H416C-MnL4** and **FeL4** were not as reactive- even though the chimioselectivity was higher-, reflects that either these catalysts are not efficient or that the observed activity difference between **H416C-MnL3** and **H416C-MnL4** and **H416C-FeL4** is related to the different CLEC preparation methodology followed (method A versus B).

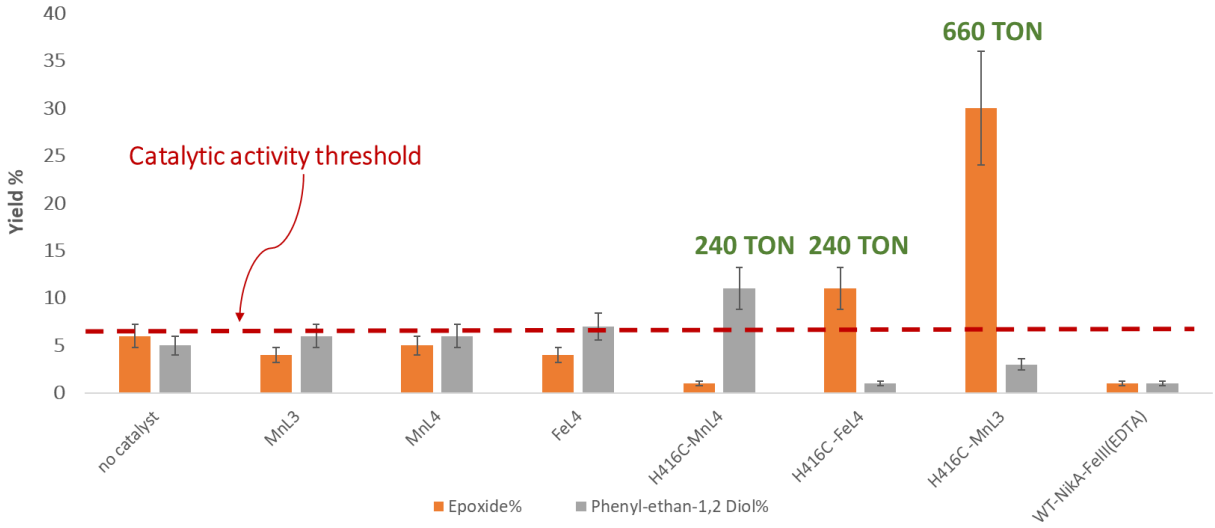

Figure 54 : *catalytic results on styrene epoxidation using CLEC **NikA H416C** with complexes **MnL3**, **MnL**4 and **FeL**4 [cat] = 21 µM catalyst/substrate/oxidant of 1/2000/4000 for 16 h, a for the homogeneous catalytic assays: [cat] = 40 µM catalyst/substrate/oxidant of 1/1000/2000 for 16 h. Yields and conversion were determined by GC-MS analysis using benzophenone*

In order to compare the effect of the metal catalysts on the ArM activity, new batches of CLEC **H416C-MnL3**, **H416C-MnL4** and **H416C-FeL4** were prepared using the effective anchoring method C (40°C, in DMF at a 100 mM of catalyst concentration post stabilization). The heterogeneous catalysts were then washed and tested under the same conditions. The results illustrated in ***figure 55a*** show that the all the manganese CLEC derivatives have comparable activity after six hours at room temperature, while the **H416C-FeL4** is less reactive, which is expected for iron salen derivatives when compared to their manganese analogues.[253] As shown in ***figure 55b***, after 16 h, assuming that the diol derivative is the result of the epoxide ring opening after long reaction times, all the three catalysts display comparable yield neighboring 30% and 580-600 TON but different selectivities for the epoxide formation.

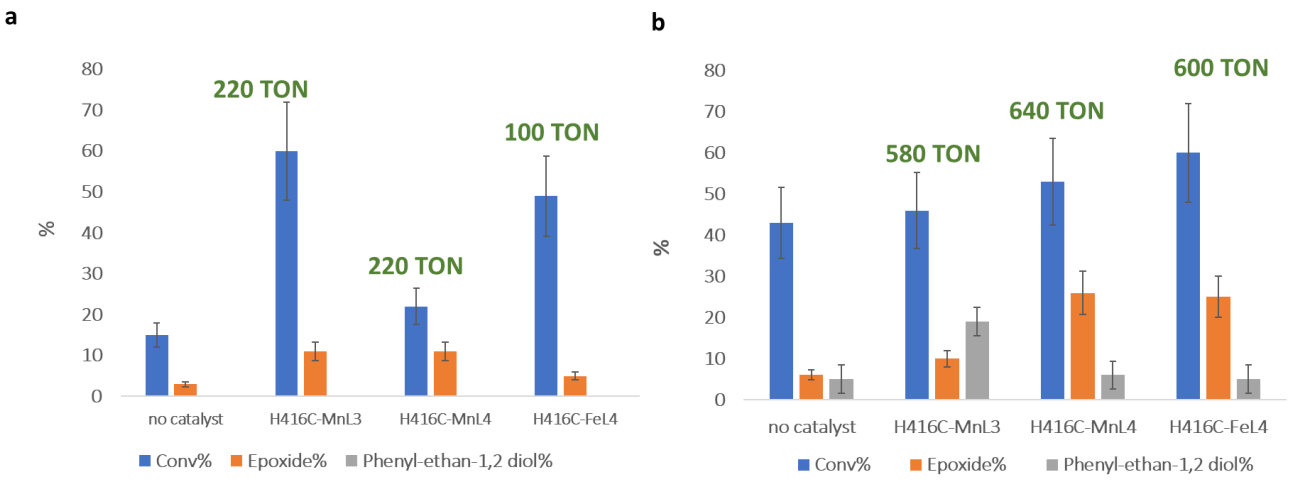

Figure 55: *results on styrene epoxidation using CLEC **NikA H416C** prepared following the method B, [cat] = 21 µM catalyst/substrate/oxidant of 1/2000/4000 reaction for 16 h at r. t. a) 5h; b) 16h*
yields and conversion were determined by GC-MS analysis using benzophenone as an internal reference.

The negligible difference between the three ArMs, alongside characterization results available at the time of the investigations, has led to us to focus on the ArM H416C-MnL4.

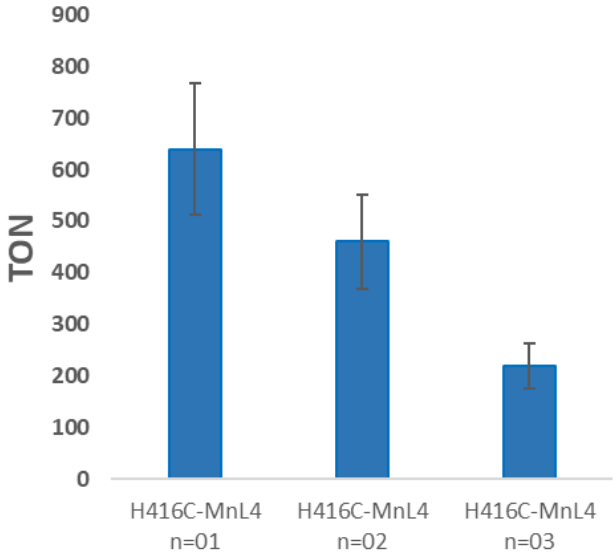

*Figure 56: Evolution of the global TON on styrene epoxidation using CLEC **H416C-MnL4** throughout three consecutive runs at room temperature.*
[cat] = 21 µM, H416C-MnL4/styrene/PAA of 1/2000/4000 for 16 h at r. t.

A good adaptability of this ArM to a cascade transformation requires a high epoxide yield and a good reusability. First, the effect of PAA on the catalyst integrity was assessed through recyclability tests. Three consecutive runs of 16 h each were tested on styrene epoxidation under the investigated conditions, using the same batch of CLEC H416C-MnL4. The results illustrated in ***figure 56*** show a 30 % loss in activity after the first run, the third run displaying 220 TON corresponding to an 11 % yield is in adequation with the uncatalyzed

transformation. Therefore, the system can only be considered reusable for two runs and a cumulated TON of 1100 , a low reusability yield compared to previously reported NikA based ArM.[95]

This low reusability can be attributed to the effect of PAA on the crystals. Strikingly, assays using 1 equiv. of PAA did not highlight any catalytic activity versus the substrate. In an effort to minimize the corrosive effect of PAA on the crystals, the catalytic assays were reproduced using a new batch of CLEC H416C-MnL4 at 15°C. The transformation yielded styrene oxide as a sole product in all cases, including the uncatalyzed reaction with 4 % yield. H416C-MnL4 at the usual catalyst loading 0,05% displayed a yield of 17 % identical to the second batch for which the catalyst loading was twice as high (*figure 57*). Unfortunately, although working at 15 °C allowed the selective formation of styrene oxide, the catalyst did not display any enhanced stability. In fact, at the third run the yields were identical to the uncatalyzed transformation.

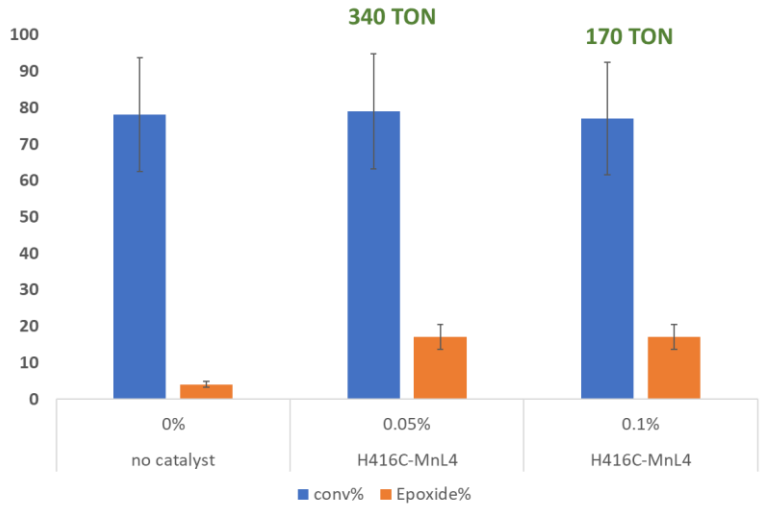

***Figure 57** : impact of catalyst loading at 15°C on styrene epoxidation after one run, [cat] = 21 µM **H416C-MnL4**/styrene/PAA of 1/2000/4000 for 16 h at r. t.*
Yields and conversion were determined by GC-MS analysis using benzophenone as an internal reference

Although no other major side product was observed, the conversion of styrene remained again quite high. This mass discrepancy can be once more attributed to the styrene evaporation or to the formation of a side product unable to be detected by GC-MS. However, ^{1}H NMR analysis of said catalytic solutions (uncatalyzed and complex alone) did not show the presence of any side products. We assume then that this discrepancy is a resultant of combined artifacts form working with low molar quantity over long reaction times favorizing styrene evaporation.

The investigated systems have a poor reusability and specificity for styrene formation. Lowering the reaction temperature has allowed the enhancement of the reaction specificity avoiding the epoxide ring opening but at a cost of a TON and no reusability improvement. Based on the gathered data, this first attempt at the design of an artificial epoxidase based on the NikA protein remains successful displaying interesting activity with up to 600 TON (30 % yield); it remains nevertheless unsatisfying for the requirement of an efficient cascade transformation, as the following carbonation step requires high concentration of the epoxide as a substrate (see below).

Throughout these investigations, working on the chiral complex **MnL4*** or its achiral form associated with **H416C**, no enantiomeric access was observed on the formed styrene oxide. These catalytic results confirm the presence of the complex **MnL4** in the protein, as assays on **WT-NikA-Fe^{III}(EDTA)** did not display evidence on catalytic epoxidation activity (***figure 54***).

Moreover, the instability of the epoxide under the investigated conditions is a certain drawback and a source of unwanted byproducts from the start of the transformation. Adding to these facts, CO_2 cycloadditions promoted with the cobalt salen complex are reactive under room temperature but their efficiency at 15 °C, conditions at which no diol is formed, is unlikely especially coupled to the low styrene oxide formation yields recorded under such temperature. Screening of other complexes were then undertaken.

2.2.2. WT-NikA associated with MnTACNAA and MnLIII

Alkene epoxidation promoted by PAA was also investigated on complexes **MnTACNAA** and **MnLIII** on the styrene substrate model. Epoxidation assays on these candidates started with the use of 1 equivalent of PAA per substrate. The catalytic assays were performed in 500 µL Eppendorf tubes at room temperature. ***Figure 58*** summarizes the results obtained on styrene epoxidation using **MnLIII** and **MnTACNAA** and their ArM counterparts. The efficiency of CLEC **NikA-MnLIII** and CLEC **NikA-MnTACNAA** is significantly higher than their homogeneous counterparts **MnLIII** and **MnTACNAA** with CLEC **NikA-MnLIII** displaying the highest yield at 78% (781 TON) after 6 h.

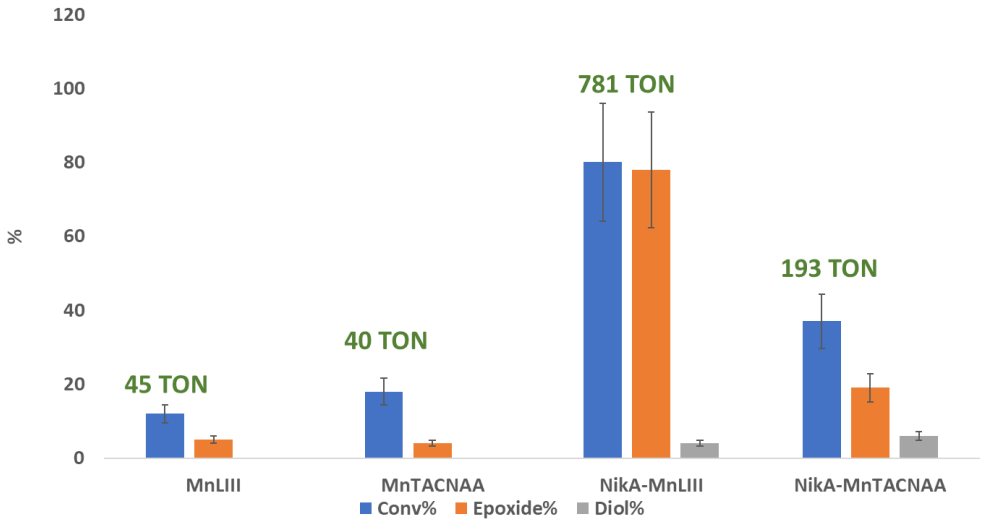

***Figure 58** : catalytic results using CLEC **WT-NikA** with complexes **MnLIII** and **MnTACNAA** [cat] = 31 µM catalyst/substrate/oxidant of 1/1000/2000 for 6 h*
For the homogeneous catalytic assays: [cat] = 40 µM catalyst/styrene/PAA of 1/1000/1000 for 6 h
Yields and conversion were determined by GC-MS analysis using benzophenone as an internal reference

Surprisingly, as seen in ***figure 59***, these yields decreases to 32 %, after 24 h reaction suggesting a loss of epoxide from evaporation as no other product was detected. Furthermore, the CLEC NikA-MnLIII displayed a great stability (compared to the salen series tested under the same conditions), with an accumulated TON of 1794 over a cumulated time of 60 h (five successive catalytic runs).

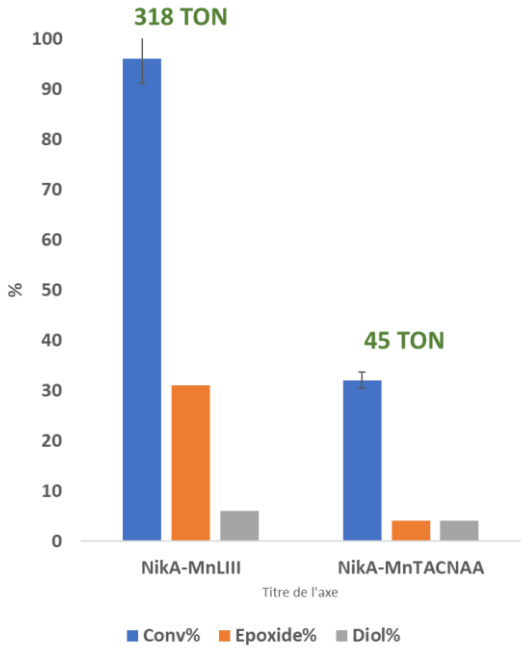

***Figure 59**: catalytic results using CLEC **NikA** with complexes **MnLIII** and **MnTACNAA** [cat] = 31 µM catalyst/substrate/oxidant of 1/1000/2000 for 24 h*

Conversely, CLEC **NikA-MnTACNAA** displayed a complete loss of activity after the third run, reaching nevertheless a cumulated TON of 238. To conclude, we have designed an efficient solid catalyst using these **NikA**-based ArM containing Mn complexes **MnLIII** and **MnTACNAA**. The presence of the complex inthe protein pocket did not alter their activity. On the contrary their activity seems stimulated. A higher efficiency is found with the **MnLIII**-based ArM rather than with the **MnTACNAA** one, allowing us to favor the first one for the cascade reaction.

2.3. Epoxidation with O_2 and isobutyraldehyde

In an effort to define a more suitable procedure for alkene epoxidation, ensuring interesting yields, selectivity and reusability under mild conditions, we opted for the Mukaiyama's procedure. It consists of using molecular oxygen at ambient conditions of pressure and temperature and an aldehyde as a co-catalyst, for instance isobutyraldehyde (IBA). Here, we report our investigations of these procedures on NikA-based ArMs associated with the complex **MnL4**, **MnTACNAA** and **MnLIII**.

2.3.1. NikA cysteine mutants associated with MnL4

Initial investigations were performed using CLEC NikA mutants soaked at 40 °C in a DMF solution of achiral **MnL4** at 100 mM (method C). The recovered dark brown CLEC **NiKA -MnL4** were washed thoroughly then tested using the "man on the moon" © apparatus displayed in ***figure 60***. This interesting small reactor, advertised as a "millireactor" is compatible with steering, heating, and high gas pressure (up to 80 bar). The 2 mL HPLC vials are equipped with a glass insert to facilitate the crystals recovery and recyclability.

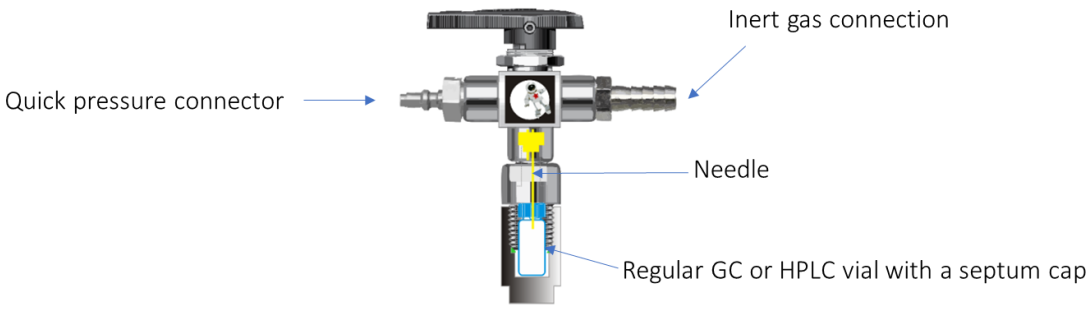

Figure 60: illustration of the "Man On The Moon" © milireactor[254]

Due the small scale investigated, no steering was possible. The catalytic procedures were performed using 5 equivalents of IBA per substrate, as used in earlier procedures,ref in a 40 µL of MeCN.

2.3.1.1. D59C-MnL4 as a first prototype of artificial epoxidase

CLEC **D59C-MnL4** were prepared according to the **method C**. Initially, the purpose was to determine the working oxygen pressure with using mutant **D59C-MnL4** and styrene as a substrate. First, the millireactor was put under 3 bar of continuous oxygen supply for 16 h at room temperature. Unfortunately, only 4 % of styrene oxide was formed alongside benzaldehyde as the major oxidation product as shown in ***figure 61***. At the second run with the same batch of CLEC, working under 1 bar of oxygen for 2 h has allowed to reach a better yield at 14% of styrene oxide.

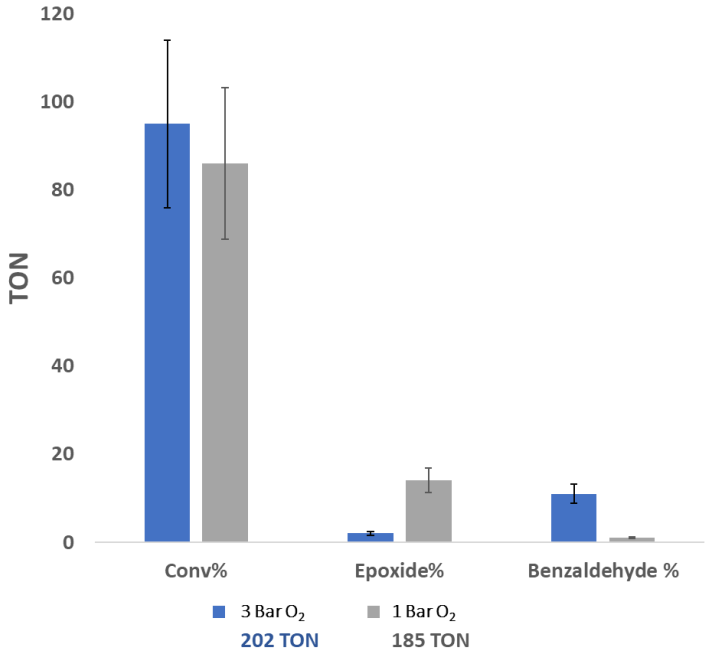

Figure 61: *styrene epoxidation catalyzed by CLEC **D59C-MnL4** [cat] =25 µM, catalyst/substrate/oxidant of 1/1684/8421 Yields and conversion were determined by GC-MS analysis using benzophenone as an internal reference.*

Based on these two assays, we have decided to work under one bar of oxygen and investigate the influence of the reaction time on the epoxide yields. In addition, our efforts were concentrated on the promotion of an enantiomeric and diastereomeric excess. Therefore, investigations were held on *trans* and *cis* β-methylstyrene with hopes to circumvent substrate evaporation as well. ***Figure 62*** shows the conversion and yield percentages obtained on the epoxidation of Cis-β-methylstyrene using a of a new batch of CLEC **D59C-MnL4 for at least 11 runs**. It has to be noted that the same epoxide is formed whatever the configuration of the

alkene was. This has been determined by HPLC traces on pure samples issued of alkene oxidation following an adapted Shi epoxidation protocol (refer to experimental section).

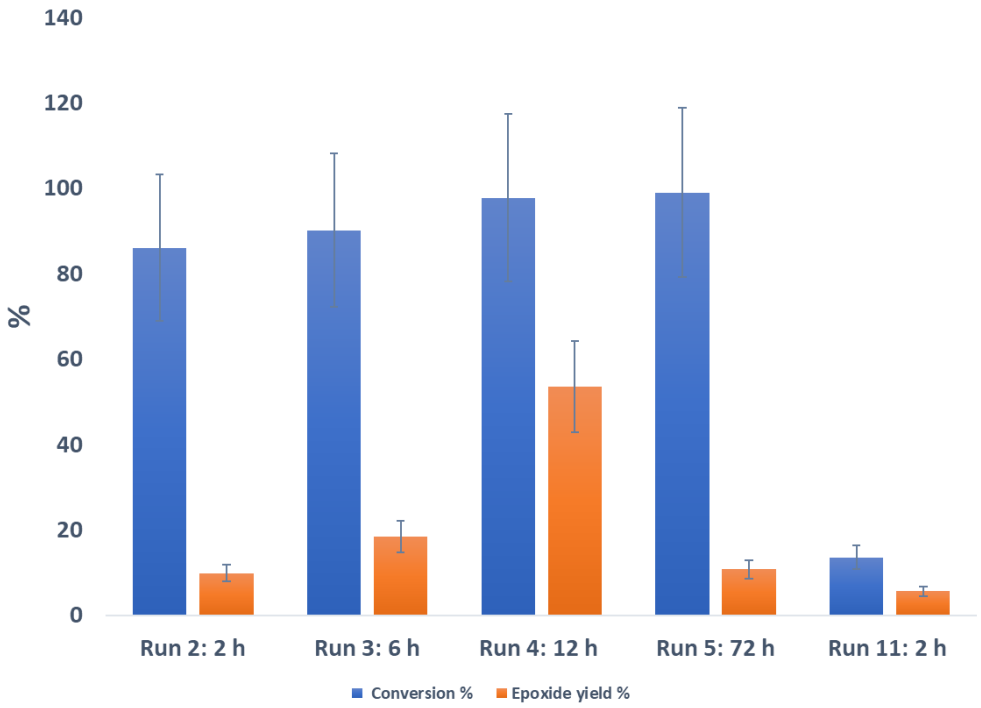

***Figure 62**: results of aerobic epoxidation of Cis-β-methylstyrene catalyzed by CLEC **D59C-MnL4**. [cat] =25 µM, catalyst/substrate/oxidant of 1/1684/8421. A sole sample of CLEC **D59C-MnL4** was used throughout the investigations. Assays are expressed with respect to their trial order.*
Yields and conversion were determined by GC-MS analysis using benzophenone as an internal reference

The highest yield is obtained after 12 h of reaction with a decrease of yield at 72 h. Due to the nature of the setup, a high conversion and its inconsistency were still observed. For example, the same assay reproduced at the eleventh run displayed 14% conversion for a comparable yield, while the other run show over 89% conversion. Based on these data, the presence of a side reaction involving the substrate and the protein matrix is invalidated by the conversion obtained with trans-β–methylstyrene at the seventh and eighth runs as seen in ***figure 63***. Moreover, as can be observed in the same figure, the conversion seems in most cases unrelated to the reaction time. At this point, the loss of substrate seems more related to the set up used that might be unsuitable for such investigations.

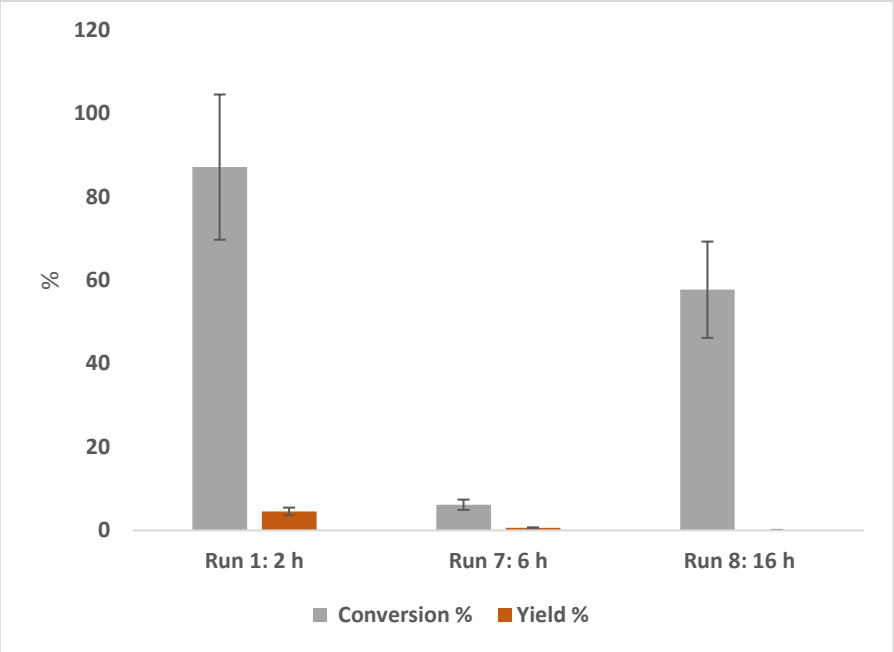

Figure 63: *results of aerobic epoxidation with trans-β-methylstyrene catalyzed by CLEC* ***D59C-MnL4****. [cat] =25 µM, catalyst/substrate/oxidant of 1/1684/8421. Yields and conversion were determined by GC-MS analysis using benzophenone as an internal reference*

Anyway, the first observation is that Mukaiyama's method is efficient for the epoxidation of monosubstituted alkene and disubstituted as well. We have determined that the CLEC D59C-MnL4 is able to catalyse the epoxidation of *cis*-β-methylstyrene efficiently while no catalysis is observed with the *trans*-β-methylstyrene, revealing a selectivity of configuration for this reaction. These properties are not observed in the case of a previous Mn(salen) catalyst, in which a 6:4 cis and trans epoxide ratio was mostly reported.[163] Conversely, this selectivity for the *trans* epoxide was observed in the case of a biomimetic catalyst.[192] The fact that the resulting epoxide is not dependent on the configuration of the epoxide suggests that a long lived radical intermediate or a carbocation intermediate is created before the second C-O epoxide bond is formed.

2.3.1.2. H416C-MnL4 as a stereoselective artificial epoxidase

Chiral and achiral MnL4 associated with the H416C mutant were investigated in the epoxidation of *cis* and *trans*-β-methylstyrene. The choice of the protein scaffold was motivated by the recent advances in its characterization, with expectations of a better reproducibility as compared to T23C and D59C mutants. Moreover, the location on the cysteine residue in the

H416C mutant offers the greater confinement effect around the active site which may favor a stereoselectivity.

Initial catalytic tests were performed using the achiral MnL4. As observed for D59C-MnL4, the major oxidation product observed was the *trans* epoxide, in addition to negligible traces of other oxidation products as the corresponding aldehyde and the terminal ketone. In order to define the reproducibility threshold of the catalytic system, several batches of crystals were tested under identical conditions. As seen in ***figure 64***, the yield and TON vary greatly amongst the set with no evident correlation to the chirality of the complex. Again, no enantioselectivity was observed, while the yield was higher than the one obtained with the complex MnL4 alone. This variability can depend on the crystal size and morphology but most importantly on the catalyst loading. Indeed, as seen previously, anchoring assays tend to yield higher catalyst content than expected. This excess may be attributed to the diffusion of the catalyst in the solvent channels, and an accumulation of weak complex-protein interactions additional to the intended covalent bond. Accordingly, if the covalent interaction is only a minority in the crystals, we can expect similar catalytic properties if the WT protein is concerned. The use of the CLEC WT-MnL4 would then allow to assess the contribution of the adsorbed complexes on the overall activity. As seen in ***figure 64***, it presents a contribution of 4% to the epoxide yield. Although lower than the yields obtained with the CLEC H416C-MnL4, it is of the same order of magnitude of MnL4 alone . These results suggests that this preparation methodlogy does not favor the C-S bond formation against random protein-complex interactions which might influence directly the catalyst loading and the activity of the ArM. Moreover, the total absence of ee with the CLEC H416C-MnL4 bearing the chiral and achiral complexes suggests the presence of several different catalysts bound to the protein, especially because the free chiral complex in solution affords an ee of 60%.

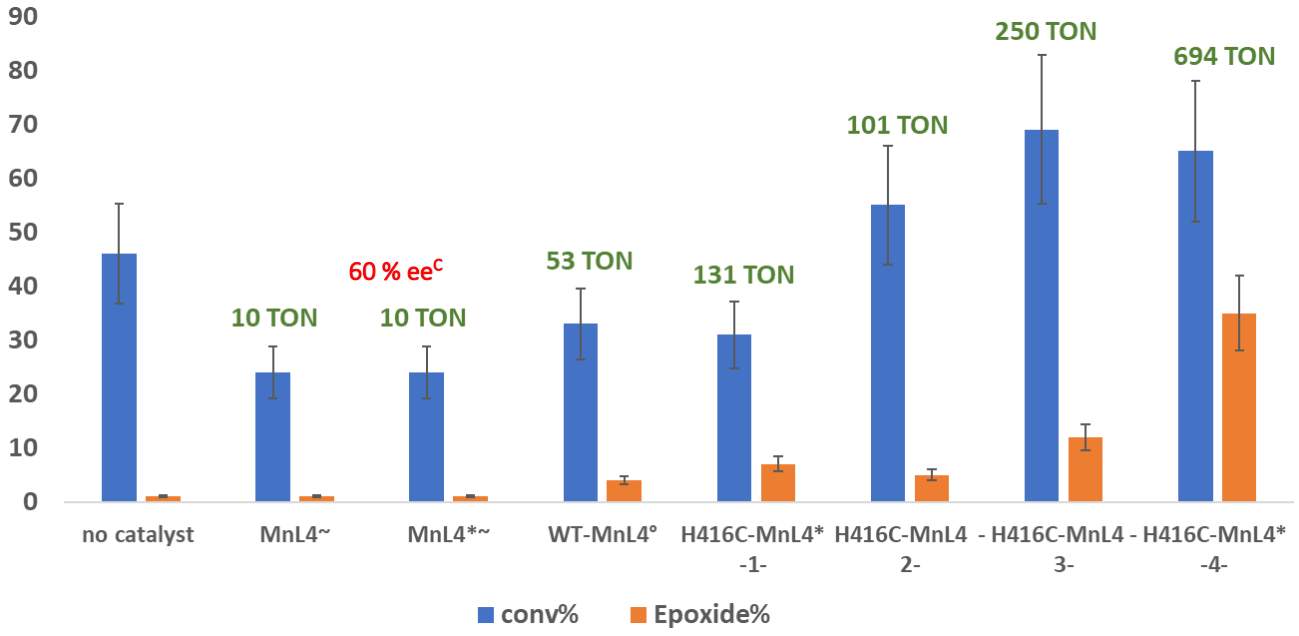

*Figure 64 : catalytic attempts on different batches of CLEC **H416C-MnL4** with achiral **MnL4** on Cis-β-methylstyrene[cat] = 21 µM catalyst/substrate/IBA of 1/2000/10000 for 2 h. Yields and conversions calculated by GC-MS quantification using benzophenone as an internal reference. *Prepared with chiral **MnL4***.Homogeneous catalysis [cat] = 40 µM catalyst/substrate/IBA of 1/1000/5000 for 16 h. °[cat] = 31 µM catalyst/substrate/IBA of 1/1333/6666. [c]Determined by chiral HPLC*

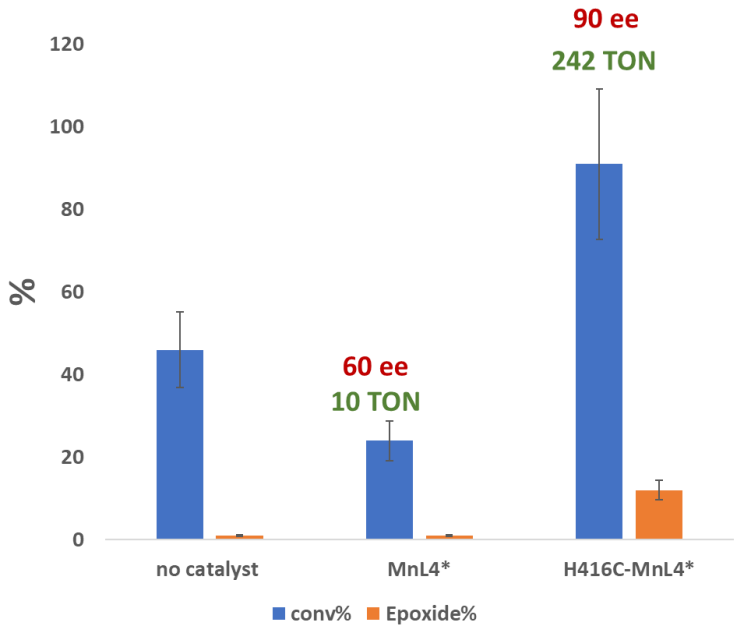

Figure 65:** catalytic results obtained with CLEC **H416C-MnL4 on aerobic epoxidation of Cis-β-methylstyrene. Catalyst prepared with soaking prior to stabilization with chiral **MnL4***. [cat] = 21 µM catalyst/substrate/IBA of 1/2000/10000 for 2 h. Yields and conversions calculated by GC-MS quantification using benzophenone as an internal reference aHomogeneous catalysis [cat] = 40 µM catalyst/substrate/IBA of 1/1000/5000 for 2 h. [cat] = 31 µM catalyst/substrate/IBA of 1/1333/6666. Enantiometric eccess determined by chiral HPLC.*

In order to favor the covalent anchoring to the expense of the supramolecular interaction, a new batch of CLEC **H416C-MnL4** was designed by lowering the catalyst loading and using the cross linking as the second step following the **method D**. This idea was motivated by the evidence of the effective anchoring under these conditions (XRD analysis of a crystal from the same batch and ESI-MS as well discussed in chapter III). Strikingly, as seen in ***figure 65***, the ArM displayed a yield in the same expected range as above obtained with 12% yield but with a 90% ee. This ee compared to the chiral catalyst alone proves the role of the protein scaffold in the promotion of enantioselectivity. This proves as well, that anchoring assays post-stabilization, at much higher concentrations are detrimental to the enantioselective reaction.

2.3.1.3. Influence of the cysteine position on the epoxidation step

The CLEC **T23C** and **D59C** have also been subjected to the same investigation on the cis-β–methylstyrene as a substrate, to highlight the difference of the complex localization on the activity. The heterogeneous catalysts were prepared according to the **method C** (anchoring post stabilization at 40 °C). Yields expressed in TON are shown in ***figure 66***. The highest yield is provided by the **D59C** followed by the **T23C** then the **H416C** CLEC, while no activity is observed for the control and the sole complex displays a modest activity. Moreover, the stereoselectivity between the *cis* and *trans* -β–methylstyrene is also dependent on the mutant, the more specific being the **WT** followed by the **H416C** and the **T23C** CLEC.

One might be tempted to interpret the relative difference of the activity based on the mutant as relative to the accessibility of the mutation site. However, the dependence of the yield on the catalyst loading, an unknown parameter, prevents again any conclusive observation. The only conclusions that can be made is that the prepared ArM regardless of the mutation position do in fact provide more interesting results that the control, the free complex and the WT protein. This difference is most certainly correlated to the presence of the covalently bound complex reinforced by the covalent anchoring evidence obtained throughout the characterization section. Moreover, we will see later that this trend is also observed for the CO_2 cycloaddition.

No ee was recorded under these conditions, as observed for the **H416C** mutant previously when the CLEC were prepared following the **method C**. Upcoming efforts will be consecrated

to the preparation of T23C and D59C CLEC ArM with post anchoring stabilization in order to put to light the influence of the protein environment on the stereoselectivity of the reaction.

To conclude, we have designed an enantioselective epoxidation catalyst based on the H416C mutant associated with the chiral MnL4* complex. The proper ArM preparation methodology for these results suggests that the manganese content has a great impact on the stereoselectivity of the reaction. Moreover, the ee value demonstrates the impact of the complex confinement into the protein.

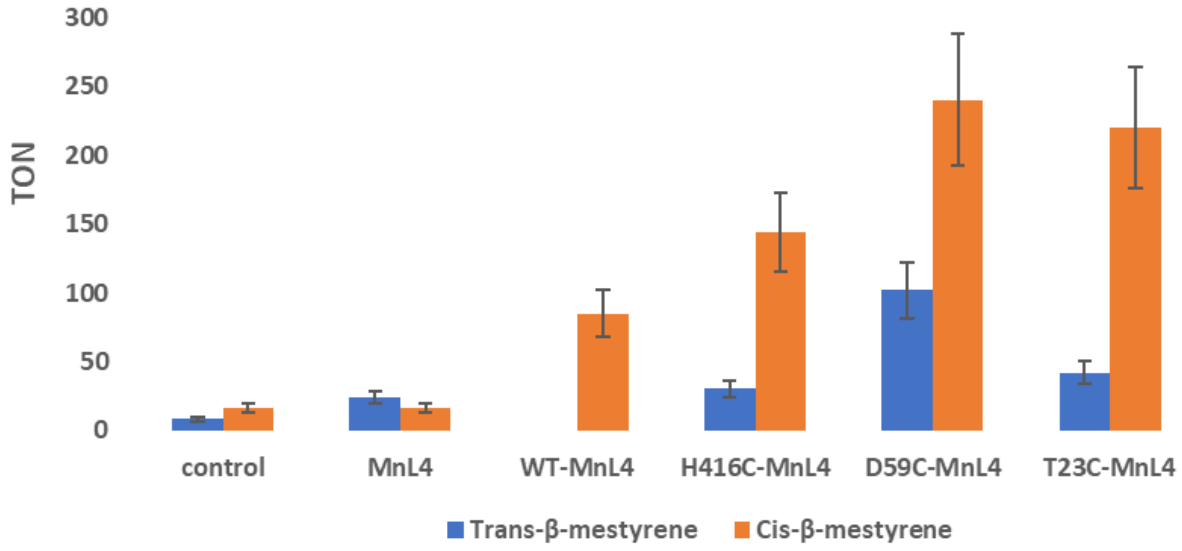

Figure 66**: Catalytic results on the epoxidation of cis- and trans-β-methylstyrene. Catalysts prepared with soaking post stabilization with chiral **MnL4. No ee observed. [cat] = 100 crystals in 40 µL of total volume. catalyst/substrate/IBA of 1/2000/10000 for 2 h. Homogeneous catalysis [cat] = 40 µM catalyst/substrate/IBA of 1/1000/5000 for 2 h. Enantiometric eccess determined by chiral HPLC. Yields and conversions calculated by GC-MS quantification using benzophenone as an internal reference*

2.3.2. MnTACNAA and MnLIII

The preparation of the CLEC with these complexes are rather simple as only the supramolecular binding is present. Accordingly, we have undertaken a more advanced study on the CLEC WT-NikA-MnL, including a selected range of substrates. Substrates were picked to evaluate the efficiency of the CLEC WT-NikA-MnLIII and -MnTACNAA facing steric hindrance and electronic effects.

Before these tests were conducted, experiments were done on *cis-β*-methylstyrene, a less volatile substrate than styrene, in order to optimize the kinetics of the reaction. With the ame batch of CLEC, three reaction times were investigated, as shown in ***figure 67***.

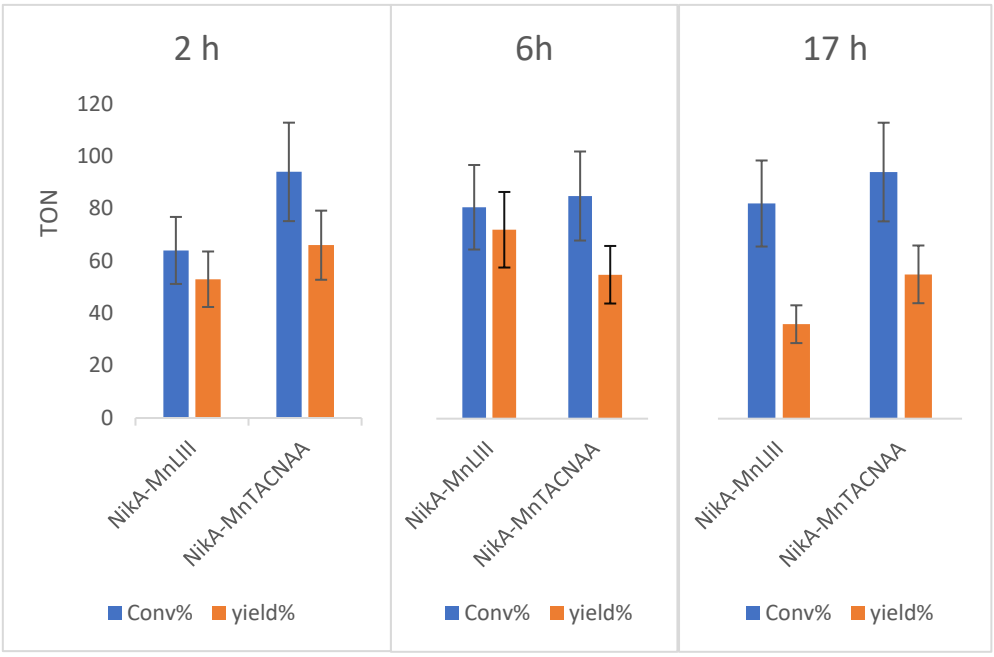

Figure 67: *ascertainment of the optimal reaction time for the catalyzed epoxidation reaction of cis-β-methylstyrene by* ***MnTACNAA*** *and* ***MnLIII****. [cat]= 31 µM cat/substrate/IBA 1/1000/5000. Results quantified using GC-MS analysis.*

The best performance is achieved by CLEC WT-NikA-MnTACNAA after 6 h with an 84 % yield. After 6h, this yield drops to 36% (independent assay), a tendency already observed under peracetic conditions. No products were detected in the absence of IBA or O_2. Moreover, it is to be noted that both CLEC WT-NikA-MnLIII and -MnTACNAA are quite stable, as the activity is retained after the third run.

The yield decrease after 6 h can be attributed to the degradation or the evaporation of the formed epoxide. In contrast, no other product was formed after 6 h of reaction ruling out the degradation hypothesis. Engaging the same batch of CELC in a 6h epoxidation assay, led to comparable yields, attesting of the stability of the catalysts. Regardless, 6 h was taken as duration for the following experiments, considering almost all the substrate was converted in 6 h.

Then, the conformational effects are first studied by testing the activity of the CLEC **WT-NikA-MnL** on the *cis*- and *trans*-β-methylstyrene. Results are depicted in ***figure 68***.

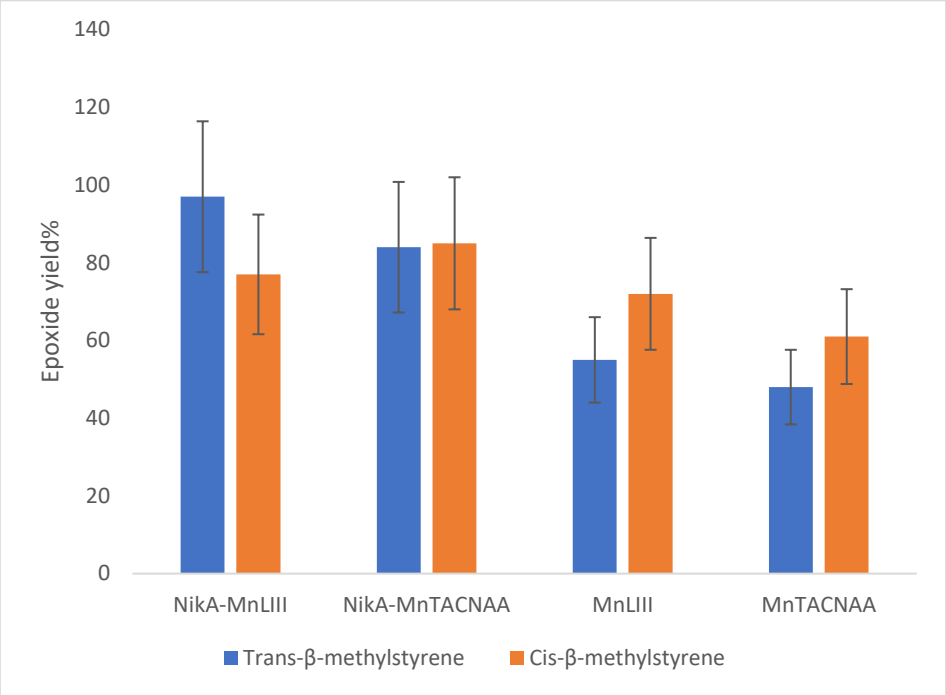

***Figure 68**: study of the effect of the configuration of the β-methylstyrene double bond on the catalytic activity of the CLEC **WT-NikA-MnL** and **MnL** complexes. Representation of the epoxide yield. ([cat]= 31 µM cat/substrate/IBA 1/1000/5000, r. t., MeCN, 6 h).*

The first observation is that the **MnL** complexes are able to catalyze the epoxidation reaction at a same extend both alone or in CLEC **WT-NikA**. Second, we can observe a substantial difference in reactivity between the two regioisomers with, surprisingly, the *trans* isomer yielding around 17 % more epoxide in average, in the case of the CLEC, as steric hindrance is generally in favor of the *cis* isomer. Third, an enhancement in efficiency is seen when the complexes are inside the CLEC **WT-NikA** (10 and 16 points for the **MnLIII** and **MnTACNAA** in average, respectively). Finally, an interesting feature to note is the formation of the *trans*-2-methyl-3-phenyloxirane as the only epoxidation product for both alkenes, leading to the conclusion that the mechanism implies an open intermediate, radical or carbocation, following the trend observed for **MnL4**.

The electronic effects were then studied by testing the activity of the **CLEC NikA-MnL** on the 2- and 4-bromostyrene, in order to test the electronic effects and the position of the substituent. Results on 4-bromostyrene aerobic epoxidation are shown in ***figure 69***.

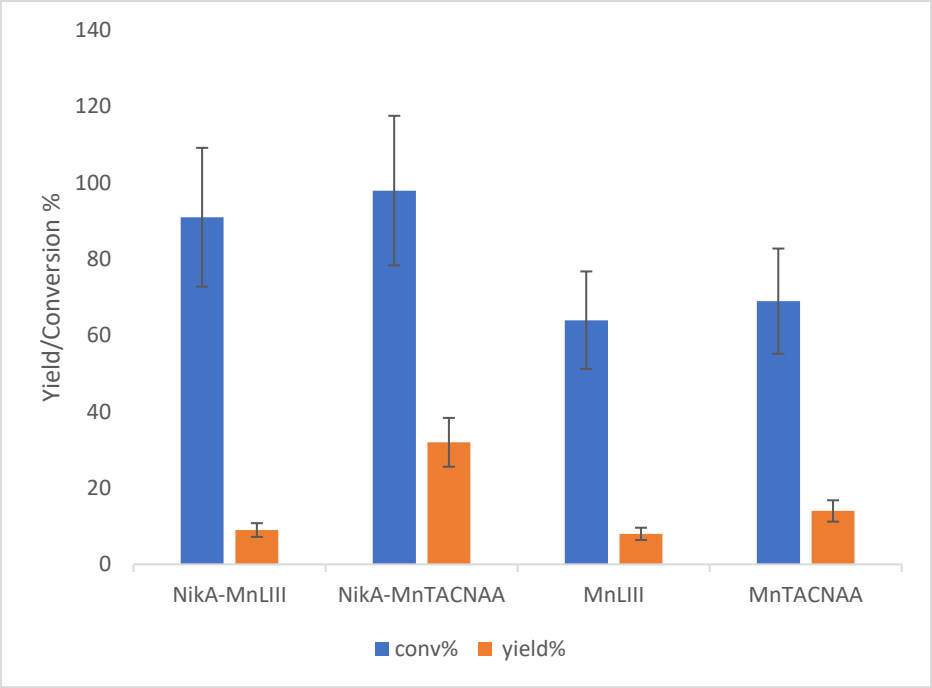

***Figure 69**: study of the effect of the presence and the position of the bromo substituent in the 4-bromostyrene on the catalytic activity of the CLEC **WT-NikA-MnL** and **MnL** complexes. ([cat]= 31 µM cat/substrate/IBA 1/1000/5000, r. t., MeCN, 6 h)*

First of all, a huge discrepancy was observed between conversion and yield for both substrates, making the following conclusions very hypothetic. The only substrate towards which the catalysts exhibited an activity is the 4-bromostyrene whereas no evident activity was observed in the case the 2-bromostyrene (1% of epoxide with MnLIII versus 2% with NikA-MnLIII) Nevertheless, the yields are very far from those observed with styrene and methylstyrene. The trends may also reflect the electrophilic character of the oxidizing species, presumably a Mn=O species. However, the CLEC WT-NikA-MnTACNAA exhibits once again a better activity than its MnLIII counterparts.

Moreover, the position to the electron withdrawing group on the styrene indeed influence the reactivity of the substrate towards the complexes. The further away it is from the alkene the better the reactivity. A phenomenon that could be associated with the richness of the alkene and the steric hindrance by the substituent. This phenomenon is also observed with the MnLIII catalyst in solution, their reactivity being close to the one of CLEC WT-NikA-MnLIII. This agreed with the loss of reactivity due to the substrates nucleophilicity and not with a degradation of theCELC WT-NikA-MnLIII.

An important point concerning the reactivity of the CLEC NikA-MnL hybrids, under O_2/IBA conditions, is that all these reactions assays were conducted with the same set of CLEC for each complex. This means that each set was reused 16 times without any loss of activity, the CLEC attesting of the efficiency of the NikA-MnL system.

2.4.Conclusion on the search for epoxidation catalysts

The above studies taken altogether suggest several remarks:

First, two kinds of Mn-ArMs, differing from their artificial active site insertion mode have been designed and their catalytic activities for the alkene epoxidation have been demonstrated. They all provided a stereoselective epoxidation as only the trans epoxide is formed.

Second, the nature of the oxidant has a great effect on the stability of the catalyst. While H_2O_2 is inert, the degradation of the catalyst is observed gradually in the presence of peracetic acid, the latter affording at least 1200 TONs for a maximum yield of 30%. Moreover, their stereoselectivity is quite good but the enantioselectivity is unsignificant with peroxides and derivatives.

Third, dioxygen as the oxidant in the presence of aldehyde provides a great capacity for alkene catalysis, providing again a stereoselective epoxidation with the formation of the *trans* epoxides. It provides also a more stable system for instance 11 runs were carried out using the CLEC D59C-MnL4. This result is interesting for the design of the cascade as peracid could have interfered with the other required catalysts for CO_2 cycloaddition.

The CLEC with MnL complexes (L = TACNAA or LIII) are more efficient and stable than the Mn salen ones, in agreement with the catalytic capacity of the complex alone, attesting that the complex insertion into NikA crystals has a low impact on their reactivity. Conversely, the enantioselectivity is greatly enhanced when the complex MnL4 is inserted, providing a 90% ee for the trans epoxide of β-methylstyrene.

The comparison for efficiency between the CLEC NikA and the complex alone has to be taken with caution, as the amount of Mn complex per protein remains variable but higher than the expected equimolar ratio (estimated between 1 and 5 depending upon the protein). This is perfectly illustrated for the case of the Mn salen, in which a different soaking treatment has led to the presence of enantioselectivity with dioxygen as the oxidant. Nevertheless, the fact that the efficiency is always lower with the complex alone strongly suggests that the CLEC should be more efficient.

The above fact also prohibits any solid conclusions about the impact of the localization of the covalent bound Mn salen complexes. Nevertheless, we will see in the next section that the trend for reactivity is conserved in the following order: H416C ≤ T23C< D59C. This strongly suggests that the availability of the cysteine for binding and the location in channel favor a greater efficiency but should lower the enantioselectivity.

The catalytic activity may also represent a good marker for the complex insertion. Considering supramolecular anchoring, it seems that the complexes are more prone to bind inside the cavity leading a great activity. Conversely, the covalent anchoring yield may be related to the reactivity as the experiment affording an enantioselective reaction is related to a lower Mn content. We may propose that the lower content favors the covalent binding at the expense of the adventitious supramolecular binding. This fact should be related to a well reported phenomenon on mesoporous phases: the grafting of active molecules is often occurring at the entrance of the pores or channels, preventing a uniform dispersion in the channels. Now, if the grafting reaction is rather slow, several complexes are inserted into the channels before its completion, leading to the confinement of these Mn salen complexes, prior to their release. This phenomenon is complex concentration dependent.

The experiments conditions are subject for a change as we do have a great discrepancy with the mass balance. Different vials and their size have been tested without a better reliability. We have nevertheless observed the presence sometimes of droplets on the cork of the vials that were recover by washing but perhaps only partially.

To conclude, the enantioselectivity, efficiency and selectivity push us to use these two systems for the epoxidation part of the cascade reaction. Due to the time schedule, the search for the substrate scope was not undertaken.

3. Catalytic CO_2 cycloaddition

The above strategy was applied for CO_2 cyclic addition, based on the modification of efficient catalysts from the literature. Again, we chose salen skeleton for practical reasons, as we were already familiar with the synthetic procedures. The catalyst choice for this step of the transformation was greatly inspired by the published work of Zhou *et al.*[255] The reported catalytic procedure was performed in neat styrene oxide. The synthesized analogue of the published complex, **CoL3**, was investigated under homogeneous conditions: at 87 mM, in neat styrene oxide with 1% of catalyst loading and 1% of phosphoranylidene acetaldehyde as a co-catalyst. As reported by Zhou *et al.,* the latter product is expected to activate, as a co-catalyst, the complex **CoL3** promoting the formation of a free halide, the coordinated iodine, which will then promote the epoxide ring opening. The published results were very appealing reaching a quantitative yield overnight, at room temperature, under 1 bar of **CO_2**.[255] For the adaptability to a cascade transformation, several assays were performed were the substrate, styrene oxide, was diluted gradually in acetonitrile. Initial assays were performed in a Hungate tube seen in ***figure 70***. It is a pressure-resistant gas-tight tube usually employed for anaerobic cell cultures in which the catalytic solution was introduced inside an open 200 µL Eppendorf.

Figure 70: Hungate tube[256]

The reported catalytic conditions were reproduced with a 125 µL volume of styrene oxide in the Hungate tube. In order to highlight the influence of the styrene and the catalyst concentrations on the relative quantity of available CO_2 limited by the tube's volume, three kinetic experiments were performed as depicted in ***figure 71*** using GC as analytical tool. The only main observation is that the MeCN diluted solution proceeds with slightly slower kinetics. Moreover, compared to the reported Co(salen) catalyst analogue, **CoL3** reaches total conversion after 144 h only (compared to 24 h for the reported catalyst).

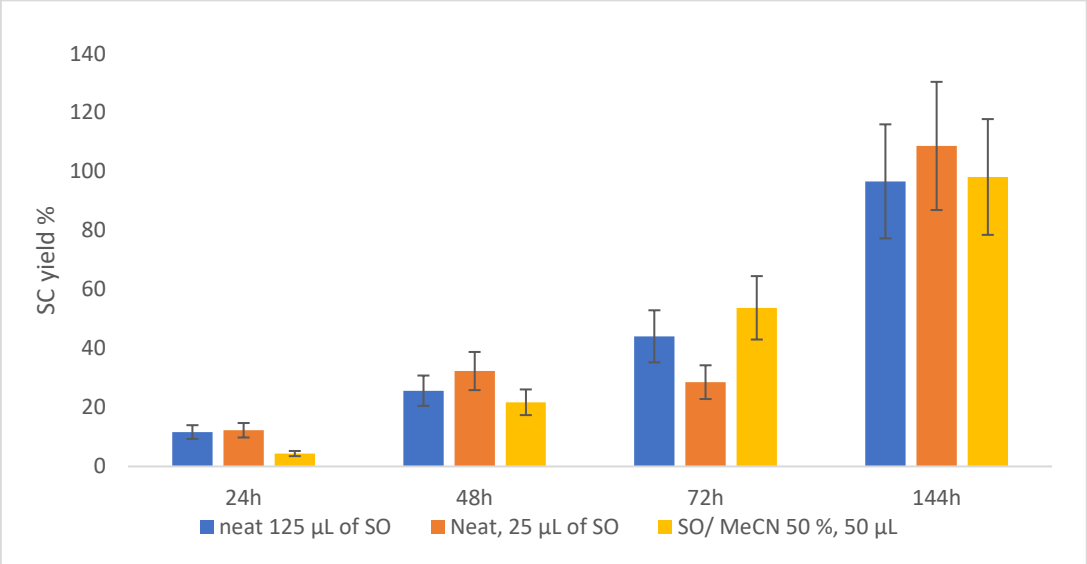

Figure 71: *kinetic study of **CoL3**, reported the SC Yields as function of time (SC: styrene carbonate) under different quantities of substrate. Assays performed using the Hungate tube setup, [cat]=87 mM, in neat styrene oxide with 1% of catalyst loading and 1% of phosphoranylidene acetaldehyde as a co-catalyst. Results quantified using GC-MS analysis.*

This procedure was then adapted to the CLEC catalysts and tested on the **T23C**, **D59C** and **H416C** mutants as well. The resulting CLEC systems remain unsuitable for high catalyst concentrations, here 87 mM, therefore the investigations started from our standard conditions. Neat and diluted conditions using the CLEC **H416C-CoL3** remained unsuccessful. Investigations on higher catalysts concentrations, 100 µM or lowering the solution volume were unfruitful as well. The last investigated attempt on this system was addition of stochiometric amounts of the co-catalyst which did not enhance the reactivity either. Heating the system at 40°C was enough to yield only phosphoranylidene degradation products as observed by GC. However, we did not look for the identification of the byproducts, but their attribution was based on their appearance only when the co-catalyst was present. These same assays were also duplicated using the "man on the moon" © apparatus with up to 3 bar of CO_2 and at 60 °C with no SC formation.

Due to the unsuccessful attempts on the CO_2 cycloaddition using the phosphoranylidene acetaldehyde as the co-catalyst with the CLEC, we have decided to investigate other co-catalysts. Starting with *tert*-butylammonium bromide, TBAB, a well-known carbonation co-catalyst, we designed new catalytic conditions on which 100 CLEC of our desired ArM were introduced in a glass insert vial in 40 µL in an acetonitrile solution of styrene oxide. This time, the catalyst loading is estimated at 0.05% (with regards to the protein concentration) with 2% of TBAB, ***scheme 31.***

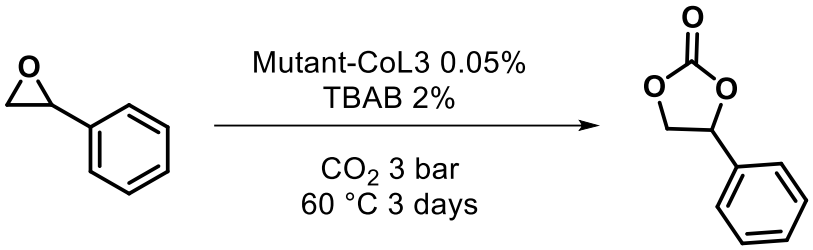

Scheme 30: *Cyclic carbonate preparation from styrene oxide*

Figure 72 shows, the SC yields representation after 96 hours of reaction. The yield of the sole product formed (SC) depends greatly on the accessibility of the cysteine mutation position. Indeed, in the case of CLEC H416C-CoL3 only traces of SC were observed whereas CLEC T23C-CoL3 and D59C-CoL3 display 6 and 10 % yields each. This discrepancy can be induced by the location of the cysteine in H416C, present deeper inside the cavity: it is then reasonable to attribute the activity difference to the anchoring efficiency within the crystal matrix. This trend is also observed in the catalytic epoxidation part (see above), emphasizing that the metal content is not the unique reason of the difference in reactivity but more probably the location of the cysteine.

Based on the gathered preliminary data, we opted for the D59C mutant to investigate the cascade transformation from styrene-to-styrene carbonates. The choice is motivated as well by the fact that this mutation position allows the two active sites to be the farthest from each other thus minimizing the interference between the catalysts from the steric hindrance aspect.

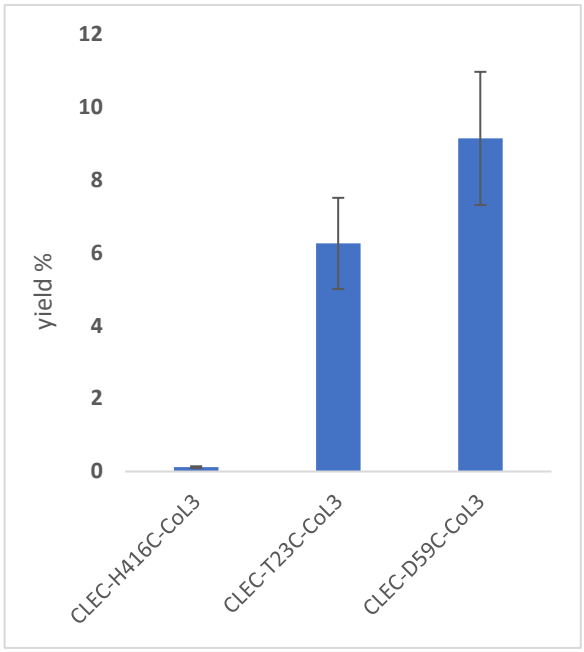

***Figure 72**: CO_2 cycloaddition on styrene oxide yields according to the mutant. Assays performed using the man on the moon apparatus. 100 CLEC used per assay, estimated catalyst concentration at 21 µM. cat/TBAB/substrate at 1/3.2/1600. Results quantified by GC-MS using benzophenone as an innternal reference.*

3.1.D59C as a matrix for a multi-site ArM for styrene carbonate formation:

D59C mutant crystals were investigated as a host for the production a multi-site ArM, CoL3 intended to be covalently anchored on the cysteine residue and associated with either the complex MnLIII or MnTACNAA in the NikA cavity.

Initial investigations were performed using the complex MnLIII for the aerobic epoxidation of styrene alongside CoL3 for the second step of the transformation. The cascade transformation was investigated in a semi sequential mode. The sealed "Man on The Moon"© apparatus containing the catalytic mixture, is first linked to an oxygen tank at 1 bar for 6 h at room temperature. Next, the vial was then degassed and linked to the CO_2 gas tank under gas circulation for up to 96 hours at 60 °C.

Initially the cascade was performed at 25 µM of estimated catalyst concentration with a catalyst/IBA/TBAB/Styrene ratio of 1/8000/3.2/1600, *scheme 32*.

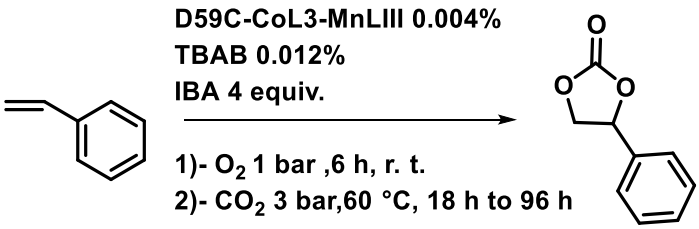

Scheme 31: cascade catalytic conditions

These conditions allowed to reach 33.2 nmoles of SC corresponding to a TON of 33 (*Figure 73*). Although this result was promising, it afforded a significantly low TON compared to the CLEC D59C-CoL3 performance (9%, 144 TON). Moreover, compared to both steps separately, the SC formation was accompanied by the formation of numerous byproducts that seemed a resultant of a degradation. The combination of the possible radical-based epoxidation and heating are most likely the source of this phenomenon as both of the transformations afforded astonishing selectivity when investigated separately.

Therefore, in an attempt to enhance the second step of the transformation, and to lower the possible degradation of the product, higher substrate quantities were engaged in the cascade transformation, and shorter reaction times were investigated as well. Interestingly, the highest TON at 103, is reached after 18 h (after 6 h for the epoxidation step). The SC yield seems to reach a maximum after 18 h of heating, after which the quantity of SC decreases accordingly to the time increase. This observation reinforces the assumption under which the low TON observed can be directly related to the degradation caused by heating under oxidative conditions. It is also tempting to correlate this decrease in the performance with the concentration of IBA present in the mixture when comparing the first assay in which a longer heating period still provides higher TON than the second assay for which the heating is reduced to 24 h but in presence of 3 folds higher IBA concentration. However, the lower TON observed at the fifth assay attests of the degradation of the catalyst. It has to be noted that CLEC D59C-CoL3 had no oxidative activity under aerobic oxidation conditions.

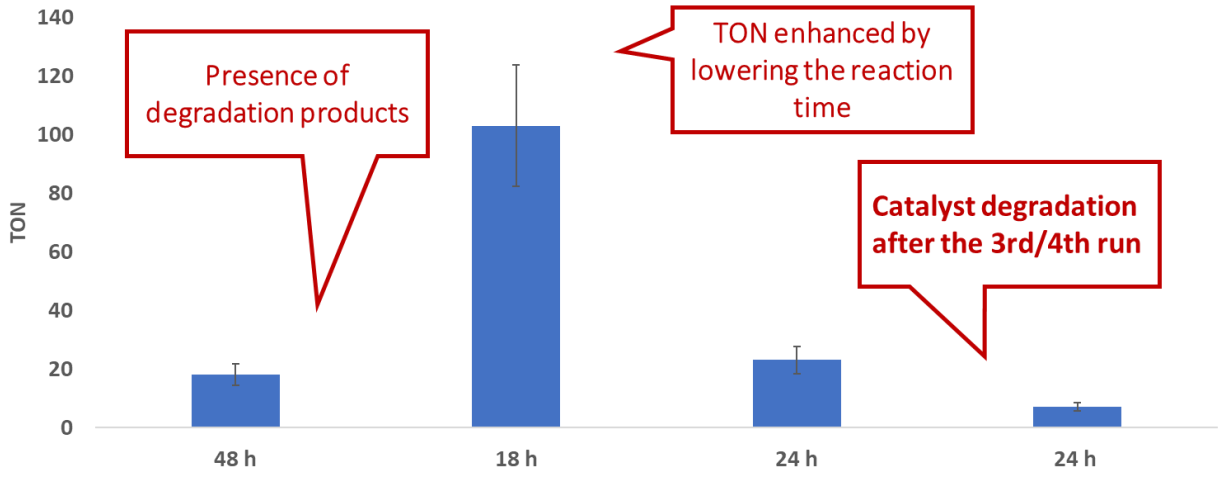

Figure 73: *investigated conditions for the cascade transformation from styrene to styrene carbonates catalyzed by CLEC* ***D59C-MnLIII-CoL3****, [cat]=25 µM, VT=40 µL, cat/IBA/TBAB/Styrene = 1/24000/3.2/96000*
All the above assays are independent, performed using the same batch of CLEC ***D59C-CoL3-MnLIII***

Yields and conversions calculated by GC-MS quantification using benzophenone as an internal reference.

Although no definitive conclusion can be drawn out of theses preliminary assays, the results do depict a successful cascade transformation. Further optimization is required in order to enhance the overall efficiency of the transformation. Nevertheless, we may face efficiency problems as we did not anticipate the difference in kinetics between both catalysts.

4. Conclusion on the cascade transformation investigations

Promising results are available for the test of the cascade reaction. These tests were conducted using the same batch of the dual catalyst CLEC **D59C-CoL3-MnLIII** attesting of a rather good stability of the dual-site ArM catalysts. We plan to design the cascade reaction in a one pot fashion using a O_2/CO_2 mix gas tank in order to highlight if both transformations can occur simultaneously. In addition, the activity will be compared to the mix of the complexes alone under homogeneous conditions as well. Other setups are of interest, such as combining two mono-site ArM, one for each transformation, in order to depict the usefulness of a dual-site ArM compared to the combination of the mono-site counterparts. Another interesting investigation lays in the combination of one mono-site ArM and a homogeneous catalyst.

Conclusions and perspectives

My PhD project aimed to design a multisite catalyst for the transformation of alkenes into their corresponding cyclic organic carbonates, as a new strategy for CO_2 sustainable chemistry. In order to get closer to the requirements of green chemistry, biocatalysis has been privileged, with a special emphasis for abiotic reactions. Then, our strategy dealt with the engineering of proteins based on the insertion of one or several artificial active sites, leading to the creation of artificial metalloenzymes for the two step-transformation of alkenes, in a cascade sequence. The strategy for their design relied on the modifications of well-known inorganic catalysts, preparing them for a facile embedment into the protein. All these aspects were integrated in a very original strategy that relies on the use of protein crystals, considered as a mesoporous phase to generate a heterogeneous catalyst. Indeed, a protein crystal possesses solvent channels, analogous to the pores of silica MCM phases for example, but with a greater homogeneity of the outline of the channels. The physical properties of the protein crystal make it the best solid phase for heterogeneous catalysis, combining purity, structure reliability and the highest density of active sites. As far as I know, there is no example of multi-site crystalline biocatalysts.

Our screening approach, involving the catalytic reactivity as the screening parameter, was perhaps too disruptive, as the full characterization of the selected hybrid solid catalysts was performed gradually. Full characterization was only attempted with the most interesting hybrids. This aspect was dictated by the time schedule of the thesis, largely dedicated to the training for the use of managing small crystals, the design of CLEC or the development of synthetic routes, for example. This led to a delay in our comprehension of the grafting process, the application of the perfect solutions, and probably on the logic of the progress of the manuscript. Finally, it has been discovered that the solution conditions did not translate into the solid ones, mainly due to the presence of structural implication such as the solvent channels and the possible embedment of more than one catalytic system in crystalline proteins. Nevertheless, we do believe that the proof of concept has been validated and that the matters of the PhD results will help for future applications.

Even if crystal properties rely on homogeneity and order, our approach created chaos inside the crystals with the insertion of two external molecules, leading to a great challenge for characterization of our hybrids. To circumvent any complication, each component of the cascade reaction has been first separately characterized. The study on MnLIII- and MnTACNAA-NikA WT has benefited from the team expertise on supramolecular stabilization of an inorganic complex in a protein cavity, mainly centered on the modification of the catalyst by the addition of a carboxylic function. Accordingly, XRD experiments demonstrated unambiguously that the two complexes were localized inside the protein cavity, following an expected coordinated fashion. The electronics of the catalyst are compatible with manganous state under resting state, as proven by UV-visible and indirectly by ESI-MS.

The case of the covalent binding, concerning a Michael addition on a maleimide function and a cysteine as the nucleophile, was far more problematic. The challenge was facing the impact of the crystalline matter as opposed to the solution case. The C-S bond was far easier to ascertain in solution thanks to ESI-MS under denaturating conditions and the metal content measurement by ICP, correlated to the protein concentration determined by MALLS. The bond formation was estimated to be around 100% with Mn salen complexes. In crystal and CLEC samples, the ICP experiments were quite puzzling since a high content of manganese was measured, moreover in a non-reproducible manner. This aspect refers to the difficulty to deal with micrometric crystals but the presence of excess of metal could be detected in all the samples. This aspect was challenged in the catalytic study by adjusting the soaking conditions, allowing us to detect chiral epoxides. Fortunately, XRD studies unambiguously illustrate the existence of the C-S bond in the case of the H416C-MnL4 and T23C-MnL4 and is suspected in the D59C-MnL4. This does not suppress the suspicion of extra Mn in the crystals if the complexes are randomly boun in the solvent channels. Moreover, the ESI MS experiments at the IBS performed on dissolved crystals demonstrated the presence of the C-S formation but to a lesser extent.

There is then still more adjustments to perform in order to gain a large enantioselectivity by adjusting the soaking procedures. Speaking of which, it was quite unexpected to conserve crystalline stability when heating the crystals at 40 °C!

To resume, five artificial metalloenzymes for epoxidation have been designed and used with O_2 or a peracid as the oxidant, all containing a manganese active site while the iron counterparts were quasi-inert. The use of salen ligands was dictated as they are the subject of a multitude of publications for their enantioselectivity capacities but suffer from stability. This has been also the case in the project but the insertion into the crystals allowed a lower degradation.

The major result is the determination of an 90% enantiomeric excess for the *trans* epoxide of the cis-*β*-methylstyrene with the covalent binding assay with MnL4 and H416C NikA mutant, with a reasonable stability up to 240 TON. Another interesting part is that the MnL4 complex is located not outside of the protein but inside its cavity. This leads to a weaker efficiency due to its embedment into the protein but provides a greater influence of the protein environment, leading to an enhancement of the enantiomeric excess observed with the chiral complexes. The absence of any enantioselectivity when the achiral ligand is embedded into the same mutant, attests that a recognition process between the protein and the complex occurs. Conversely, in the case of the WT-NikA -MnL systems (L = TACNAA or LIII), the impact of the protein is questionable as only a slight enhancement of the epoxidation yield is occurring, while the enantioselectivity of the reaction is missing. This result quite disappointing by itself, is still interesting for the cascade reaction, as the yield and kinetics of the reaction and stability of the catalyst are very good. Moreover, a preliminary study on different mutants attests that the protein has still a great effect on both reactivity and selectivity, probably based on the localization and the contact with the protein backbone. As discussed above, the H416C mutant provides less reactive Mn salen due to its confinement while the D59C, located in the crystal solvent channels is more prone for reaction. This aspect is also an indirect proof in favor of the directed catalysis by the C-S bond formation and not the putative "adventitious" MnL complexes.

The Mukaiyama's epoxidation method has never been tested so far with this kind of Mn complexes with poly(aminopyridine) based ligands. Our results then provide a new class of catalysts for O_2 activation. This has been unexpected, at least at this level of efficiency, as the IBA may react with the amine of lysine, quite numerous in NikA (28 lysines per 502 amino acids). The fast kinetics of the reaction combined to the confinement of the lysine residues in the crystal may be responsible for the observed hybrid behavior. A future variation of their

structure may engender a better control by the protein environment to reach enantioselectivity.

Next, preliminary data demonstrate that the inserted complex **CoL3** is capable of CO_2 cycloaddition under mild conditions (temperature, P_{CO2}). It has been found that this reaction is quite slow but better than with the complex alone, emphasizing once again the role of the crystal confinement. This catalytic efficiency was challenged in a sequential cascade reaction using the CLEC **D59C-CoL3-MnLIII**. This artificial enzyme contains both artificial sites, one expected covalently bound to the enzyme and the second in the cavity. Under this condition, 42 catalytic cycles were detected for the cyclic carbonate formation, but the major product remained the epoxide intermediate. Then, it can be learned from this result that our cascade should suffer from a different reaction kinetics, detrimental to the selectivity of the reaction. Anyway, this part of the project is still in its infancy and should be reshaped. Alternatives considering better catalysts such as Zn(II) (TPP) bearing several quaternary ammonium moieties [TPP=tetraphenylporphyrin] will be undertaken.[257]

Our artificial enzymes, still under optimization, can be benchmarked with related systems especially for the epoxidation step. The dioxygen activation process is quite efficient with the **MnLIII** complex and better in terms of selectivity and frequency than the reported Mn salen systems and our **MnL4** systems.[163] The study of the complex alone will be continued further at least to determine the scope of its efficiency. Anyway, the major drawback of this process remains the use of a large excess of IBA to ensure a high efficiency. There is still a need to find a better procedure and we may propose to include into the protein scaffold close to the active site a reactive aldehyde function in order to increase, only at the proximity of the active site, the concentration of co-substrate. It has to be mentioned that only one manganese system was able to avoid the co-substrate use but it was proposed that the oxidant was based on the solvent.[1] In spite of everything, the CLEC **WT-NikA-MnLIII** provides a very high turnover frequency and turnover numbers that are quite rare when comparing with the capacities of iron, ruthenium complexes either with H_2O_2 and O_2 as oxidant. Other epoxidases have been designed from the last 10 years but they all were found with a lower efficiency in terms of TONs

[1] Lee et al. bull Korean Chem Soc 1997, 116, 1259-62

except the Os -Cupin system obtained by metal switch strategy that reaches 9100 TON but for cis -diols,[42] and the $CP450_{LA1}$ monoxygenase from *Rhobacterium*, selected by directed evolution,[258] redirecting an epoxidase into an aldehyde synthase.

The mechanism of the reaction could not be challenged during the thesis. Anyway, in the case of the Mukaiyama's method, the concentration of IBA was found critical for reactivity for **MnLIII** and **MnL4** systems, indicating a radical mechanism. Moreover, addition of a radical trap, tri-*tert*butylphenol, affected drastically the yield of the reaction. All taken together and combined with the observed steroselectivity of the reaction, a radical pathway is proposed. Finally, the similar reactivity between the Mukaiyama's method and the use of peracetic acid suggest the formation of a Mn-OOCO-R (R= tbu or iBu) intermediate. The formation of the peracid from O_2 and IBA remains to be established. Two possibilities are plausible: i) the first step consists of the O_2 autooxidation of IBA (*iso* butyraldehyde) followed by the coordination to the salen complex ; ii) the peracid is formed in the catalytic coordination sphere from a IBA ligand and O_2 binding to the manganese, ***scheme 33.*** Subsequently, the pathway is analoguous to monooxygenase.[259]

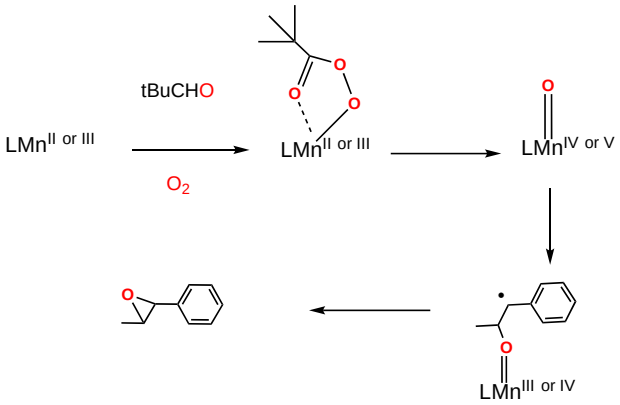

Scheme 32

The content of this thesis will serve as a good foundation for the design of multi-site artificial enzyme for cascade reactions. Even though a confirmation of the cascade reaction has to be achieved, we have the confidence that the heterogeneous strategy is feasible using this type of multi-site artificial biocatalyst. It has been emphasized that the protein crystals can be very robust and can be chemically modified without structural changes. As a new strategy, a lot of challenges have been faced, most of them being successful, in the fields of characterization and catalysis. First, the yield of covalent binding needs an improvement:

several approaches could be followed, from the optimization of the C-S bond formation to the use of new orthogonal reactions involving click chemistry with the help of unnatural amino acids insertion into NikA via Staudinger-Bertozzi Ligation or others. Second, the preliminary catalytic results will have to be optimized and compared to the solution mixture of both catalysts either in the protein scaffold or not. Moreover, the substrate scope needs to be emphasized in particular in the case of the epoxidation process.

Nevertheless, the growth and manipulation of the crystalline catalysts are quite tedious and very time consuming. In order to reach applied research, a gain in automation is required either for screening methods of mutants, - directed evolution is expected- but also for catalytic properties. Solutions already exist in the field of synthetic biology and collaborations should be developed in the future.

Another solution is to go further in biology and let the life generates the crystalline material. Actually, there are living organisms that grow protein crystal in cells.[260] In fact, Baculovirus particles protect themselves from their bacterial host by generating micrometer sized protein crystals called polyhedral. This *in vivo* crystallization process may be used to the benefit of artificial enzyme edifices formation by embedment of our artificial active sites inside these crystalline matters, while promoting some mutations or deletion for a better anchorage and catalytic properties (***figure 74***). So, Uneo *et al.* have developed a self-porous protein materials in insect cells, that fixed a fluorescent molecule *in vitro* and *in vivo* or were modified by a miniprotein fused into the polyhedral.[261]

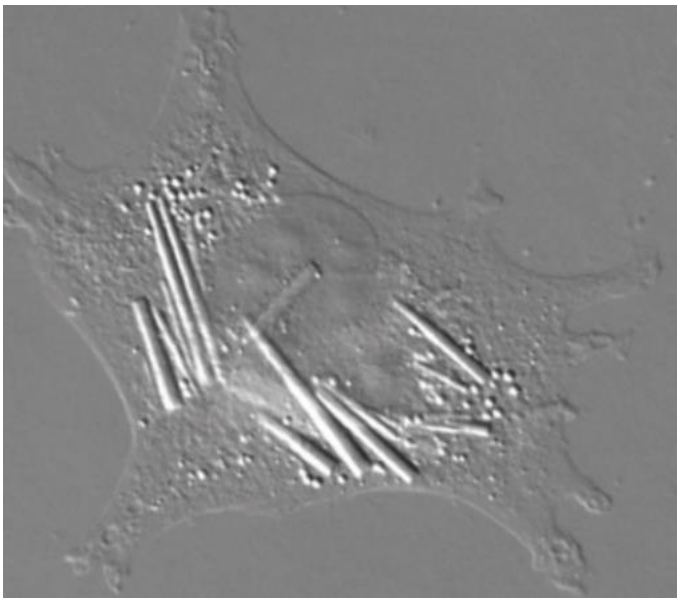

***Figure 74**: example of in-cell crystal growth :) Several needle shaped crystals (up to 20 µm in length) of human IgG2 in CHO hamster cells (Hasegawa et al., 2011; © 2011 The American Society for Biochemistry and Molecular Biology)*

The innovative strategy for heterogeneous catalysis for cascade reaction in the field of synthetic biology is still at its infancy. This interdisciplinary research combining biology and chemistry and physics, represents a very exciting and dynamic area and is a domain very informative for the expression of bio-inspired chemistry. The artificial enzymes, based on the de novo active site reconstitution, will soon be the good alternative to natural enzymes for abiotic enantioselective reactions, as their constructs represent more than the combination of the properties of their components, generating unique properties. Their involvement into the synthesis of drugs should be developed in the near future.[262]

Material and methods

All products and solvents used were purchased at Sigma-Aldrich and were used without any additional purification step.

1. Physical methods

^{1}H and ^{13}C NMR: spectra were performed on a Brüker Avance 300 MHz spectrometer. Chemical shifts (δ) are in ppm (parts per millions). Results are presented under the formalism, δ: (multiplicity, coupling constant, integration, attribution) with d= doublet; dd= doublet of doublet; t= triplet; q= quartet; m= multiplet

UV-visible: spectra were acquired on a Shimadzu UV-1800 spectrometer using 1 cm wide quartz cells.

ICP-AES: analysis were carried on a Shimadzu ICP 9000 apparatus equipped with a mini plasma torch.

Gas chromatography analysis (GC): Analysis were carried on a Perkin-Elmer Clarus 580 spectrometer with an FID detector using an Optima 17 column. The spectrometer is coupled to a mass spectrometer (MS) Perkin Elmer Clarus SQ8S. GC-MS analysis were carried out using the following method: initial temperature at 65°C for 3 min following a 16°C increase per min until reaching 200°C followed by a hold phase at 200 °C for a total run of 26.44 min. Reaction products were identified by confronting GC-FID and GC-MS traces with their pure analogues.

High performance liquid chromatography (HPLC): Analysis were carried on a Perkin Elmer instrument using a UV-Visible detector; product separation was achieved using a chiral Daicel IH-3 column the dimensions: using the following method: Isopropanol / hexane at 10/90 ratio at 1 mL/min for 10 minutes.

Size Exclusion Chromatography coupled to Multi-angle laser light scattering SEC-MALLS: Soluble protein and solubilized crystals were manually injected in 20 µL volume into SEC-MALLS (Wyatt Dawn HELEOS-II) using the SEC column Superdex 200 10/300 (GE Heathcare). The eluant used was 25 mM HEPES pH 7.5, 150 mM NaCl. Data were analyzed using the ASTRA program and protein concentrations were determined by integration of the refractive index.

Mass spectrometry Analysis : Denaturing mass analysis were performed at the IBS mass platform under the supervision of Agneta Kriss. MS data were acquired on a 6545XT AdvanceBio Q-TOF interfaced with LC-Pump system form Agilent technologies. ESI MS spectra on inorganic complexes and ligands were obtained from a Thermoquest Finnigan LCQ apparatus at the platform managed by SYMMES laboratory.

Single crystal X-Ray crystallography data were acquired and analyzed at the Laboratory SYMMES on a X RigaKu Xcalibur S diffractomer with a 2D detector.

2. Ligand synthesis

2.1.Synthesis of (3S,4S)-pyrrolidine-3,4-diaminium

2.1.1. Synthesis of 3a,4,7,7a-tetrahydro-1H-4,7-epoxyisoindole-1,3(2H)-dione (2)

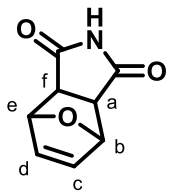

2

In a pressure compatible Schlenk, 10 mmole (1 equiv.) of maleimide were dissolved in 35 mL of diethyl ether. 50 mmoles (5 equiv.) of furan were added. The reaction was stirred at 90 °C for 18 h. The white precipitate formed was filtrated and washed with cold Et_2O. Molecule **2** was recovered with 45 % yield.

^{1}H NMR (300 MHz, MeOD), δ: 4.99 (s,1H, Hc/Hd); 4.95 (s, 1H, Hc/Hd); 3.70 (s, 1H, Hb/He); 3.62 (s, 1H, Hb/He); 2.01 (m, 1H, Ha/Hf); 1.38 (m, 1H, Ha/Hf).

2.1.2. Synthesis of 2-(2-bromoethyl)-3a,4,7,7a-tetrahydro-1H-4,7-epoxyisoindole-1,3(2H)-dione (3)

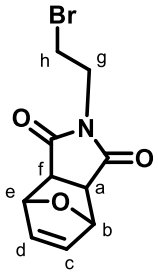

3

In a round bottom flask, 4.5 mmole (1 equiv.) of **2** were solubilized in 35 mL of DMF, 22.5 mmoles (5 equiv.) of K_2CO_3 and 9 mmoles (2 equiv.) of 1,2-dibromoethane were added. The reaction was stirred under argon, at 50 °C, for 2 h. the reaction was treated by the addition of 150 mL of water at room temperature followed by 3 extractions with ethyl acetate. The organic phases were dried with sodium sulfate Na_2SO_4 and the solvent removed under reduced pressure. The product was recovered as light brown crystals with quantitative yield.

^{1}H NMR (300 MHz, $CDCl_3$), δ: 5.77 (m,1H, Hc/Hd); 5.69 (m, 1H, Hc/Hd); 4.57 (m, 1H, Hb/He); 4.52 (s, 1H, Hb/He); 3.23-2.52 (m, 6H, Hg, Hh, Ha, Hf).

2.1.3. Synthesis of (3R,4R)-1-benzyl-3,4-dihydroxypyrrolidine-2,5-dione (4)

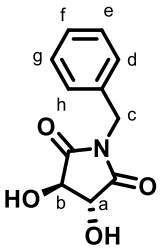

4

In a Dean Stark setup, 1.3 mmole (1 equiv.) of D-(+)-tartaric acid were dissolved in 100 mL of toluene. 1,3 mmole(1 equiv.) of benzylamine were added. The reaction was kept under reflux for 24 h. After the reaction time, the round bottom flask was cooled over an ice bath then filtrated. Molecule **4** was recovered in quantitative yield after recrystallization in water.

^{1}H NMR (300 MHz, MeOD), δ: 7.35-7.51 (m,5H, Hd, He, Hf, Hg, Hh); 4.46 (s, 2H, Ha, Hb); 4.13 (s, 2H, Hc).

2.1.4. Synthesis (3S,4S)-1-benzylpyrrolidine-3,4-diol (5)

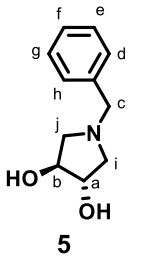

5

20 mmoles (1 equiv.) of molecule **4** dissolved in 60 mL of anhydrous THF. Were slowly added to a round bottom flask containing a suspension of 100 mmoles (5 equiv.) of $NaBH_4$ in 60 mL of anhydrous THF as well. 50 mmoles, (2.5 equiv.) of I_2 in 30 mL of anhydrous THF were slowly added under argon at 0 °C. The reaction was then stirred under reflux for 6 h. After the reflux, the mixture was cooled on an ice bath then and treated with 20 mM of HCL 3N then neutralized with NaOH 3N. The solution was extracted 3 times with 60 mL of Et_2O. the organic phased was washed with brine then dried over Na_2SO_4. The crude product was dissolved in MeOH, 70 g of K_2CO_3 were added before solvent evaporation. The molecule **5** was isolated in 38% yield by continuous extraction from the K_2CO_3 palette using a Soxlet setup.

^{1}H NMR (300 MHz, MeOD), δ: 7.19-7.38 (m,5H, Hd, He, Hf, Hg, Hh); 4.00-4.05 (dd, 2H, Ha, Hb); 3.53-3.71 (dd, 2H, Hc), 2.91-2.96 (dd, 2H, Hi/HJ), 2.42-2.51 (dd, 2H, Hi/HJ).

2.1.5. Synthesis of (3S,4S)-1-benzylpyrrolidine-3,4-diyl dimethanesulfonate (6)

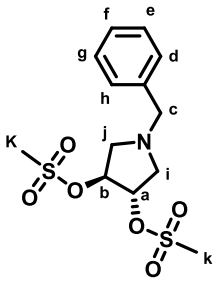

6

in a round bottom flask, 7.7 mmoles (1 equiv.) of molecule **5** were dissolved in 30 mL of CH_2Cl_2 and cooled on an ice bath. 23 mmoles (3 equiv.) of NEt_3 were added followed by 23 mmoles (3 equiv.) of methanesulfonyl chloride (MsCl). The reaction was stirred for 5 h at room temperature under argon. The organic phase was washed three times with 20 mL of water then extracted with HCL 1 N. the acidic phase was neutralized with K_2CO_3 and the product was extracted three times with 20 mL of CH_2Cl_2. The organic phases were washed with brine then dried over Na_2SO4. The product was recovered in 40 % yield as a yellow oil.

^{1}H NMR (300 MHz, $CDCl_3$), δ: 7.23-7.32 (m,5H, Hd, He, Hf, Hg, Hh); 5.06-5.15 (dd, 2H, Ha, Hb); 3.65-6.68 (dd, 2H, Hc), 3.04-3.17 (m, 8H, Hk, Hi/HJ); 2.75-2.80 (dd, 2H, Hi/HJ).

2.1.6. Synthesis of (3S,4S)-pyrrolidine-3,4-diaminium (7)

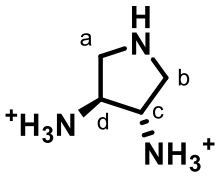

7

In a round bottom flask, 2.7 mmoles (1 equiv.) of molecule **6** were dissolved in 100 mL of DMF. 13,5 mmoles (5 equiv.) of NaN_3 were added under argon an the reaction was stirred overnight at 100 °C. The reaction was filtrated to discard the NaOMs byproduct and 19 mmoles, (7 equiv.) Pd/C 10% and 17 mmoles (10 equiv.) of formic acid were added. The reaction was stirred at 50 °C for 6 h. The Pd/C was filtrated on a celite pad and solvent were removed under reduced pressure. Product **7** was recovered as a brown solid with 38% yield.

^{1}H NMR (300 MHz, MeOD), δ: 2.86 (s, 2H, Hc, Hd); 3 (s, 2H, Ha, Hb).

2.1.7. Synthesis of (3S,4S)-1-benzyl-2,5-dimethylenepyrrolidine-3,4-diyl dimethanesulfonate (8)

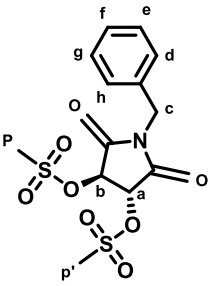

8

In a round bottom flask, 9mmoles (1 equiv.) of molecule **5** were dissolved in 50 mL of dichloroethane. 22.5 mmoles (2.5 equiv.) of NEt_3 and the mixture was cooled on and ice bath and put under argon. 19.8 mmoles (2.2 equiv.) of MsCl were slowly added under vigorous stirring. The reaction was stirred at room temperature for 1 h30. The organic phase was washed with HCl 1N solution to recover the starting material. The organic phase was washed with brine then dried on Na_2SO_4. The molecule **8** was recovered as a red oil with 74 % yield. ^{1}H NMR (300 MHz, $CDCl_3$), δ: 7.24-7.35 (m,5H, Hd, He, Hf, Hg, Hh); 4.67 (s, 2H, Ha, Hb); 3.63-(s, 1H, Hc), 3.63 (s, 3H, Hp/Hp'), 3.37 (s, 3H, Hp/Hp').

2.1.8. Synthesis of (3R,4R)-2,5-dioxopyrrolidine-3,4-diaminium (9)

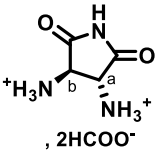

9

in a round bottom flask, 6 mmoles (1 equiv.) of molecule 8 were dissolved in 25 mL of DMF. 30 mmoles (5 equiv.) of NaN_3 were added. The reaction was stirred for 4 h at 100 °C under argon. The reaction was filtrated to discard the NaOMs byproduct and 42 mmoles (7 equiv.) Pd/C 10% and 60 mmoles (10 equiv.) of formic acid were added. The reaction was stirred at 50 °C for 12 h. The Pd/C was filtrated on a celite pad and solvent were removed under reduced pressure. Product **9** was recovered as a brown solid with 70% yield.

^{1}H NMR (300 MHz, D_2O), δ: 3.00 (s, 1H, Ha/Hb), 2.86 (s, 1H, Ha/Hb)

2.2.Synthesis of L1-4

2.2.1. General procedure for L1-L2 synthesis

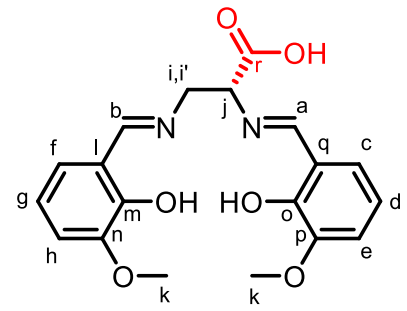

L1

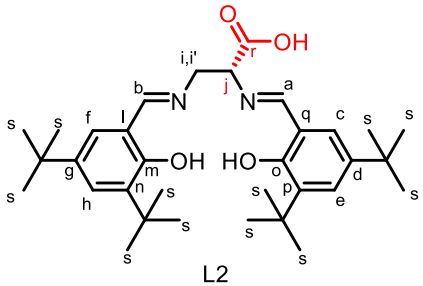

L2

In a round bottom flask, 0.7 mmole (1 equiv.) of commercial diaminopropionic acid were suspended in 5 mL of methanol. 1,4 mmole (2 equiv.) of NEt_3 were added followed by 1,4 mmol (2 equiv.) of the desired salicylaldehyde derivative. The solution was stirred at room temperature for 2 h. The solvent was removed under reduced pressure and the crude is recovered as a yellow wax. The ligands **L1/L2** were recovered in quantitative yields and engaged in the next step with no further treatments. **L1:** ^{1}H NMR (300 MHz, $CDCl_3$), δ: 8.3 (s, 2H, Ha, Hb); 6.65-7.01 (m, 6H, He, Hf, Hg, Hh, Hd,Hc); 4.25 (dd, 1H, Hi), (dd, 1H, Hi'), (dd, 1H, Hj), 3.9 (S, 6H, Hk). **L2:** ^{1}H NMR (300 MHz, CD_3CN), δ: 8.42 (s, 1H, Ha/Hb); 8.39 (s, 1H, Ha/Hb); 7.37 (t, 2H, Hc, Hf); 7.16 (t, 2H, Hh, He),; 4.10-4.22 (m, 2H, Hi, Hi'); 3.94-4.06 (m, 1H, Hj); 1.22-1.4 (m, 36H, Hs).

2.2.2. General procedure for L3-L4 synthesis

In a round bottom flask, 0.4 mmole (1 equiv.) of **L1/2** were dissolved in 3 mL of anhydrous THF un put under nitrogen. A stock solution containing 0.4 mmole (1 equiv.) of oxalyl chloride and 0.004 mmole (0.01 equiv.) of DMF in 2 mL of anhydrous THF was slowly added to the reaction. The reaction was stirred for one hour at room temperature under nitrogen before a slow addition of a stock solution of 0.4 mmole (1 equiv.) of aminoethyl maleimide hydrochloride and 1.2 mmole (3 equiv.) of NEt_3 in 3 mL of acetonitrile. The reaction was stirred under nitrogen at room temperature overnight. the solution is filtered to discard NEt_3.HCl and the solvent is removed under reduced pressure. The ligands **L3/L4** are recovered in quantitative yields as yellow solids and engaged in the complexation step with no further purification.

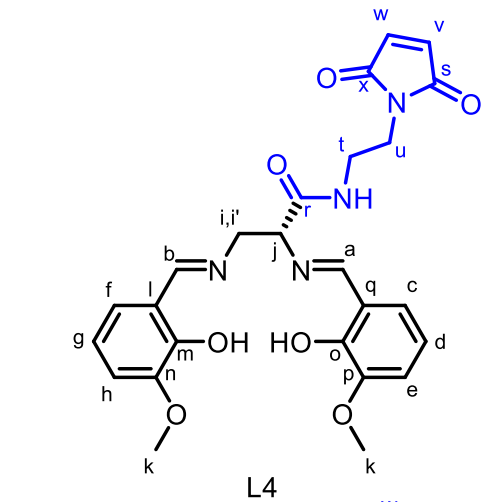

L4

^{1}H NMR (300 MHz, CD_3CN), δ: 8.37 (s, 2H, Ha, Hb); 7.03 -6.99 (dd, 2H, Hf, Hc); 6.91 - 6.95 (dd, 2H, Hh,He); 6.80-6.86 (t, 2H, Hg, Hd), 6.75 (s, 2H, Hv, Hw), 3.76-3.88 (m, 13H, Hu, Ht, Hj, Hi,i', Hk).

^{13}C NMR (300 MHz, CD_3CN), δ: δ 171.5 (Cs, Cx); 168.0 (Cr); 151.8 (Ca); 148.9 (Cb); 134.8 (Co, Cm); 123.8 (Cp, Cn); 119.3 (Cv, Cw); 118.7 (Cq, Ci, Cc, Cf); 115.3 5(Cd, Cg, Ce, Ch), 67.9 (Cj); 57.2 (Ck); 56.2(Ck); 53.7 (Ci,i'); 46.0(Cu) , 38.7(Ct).

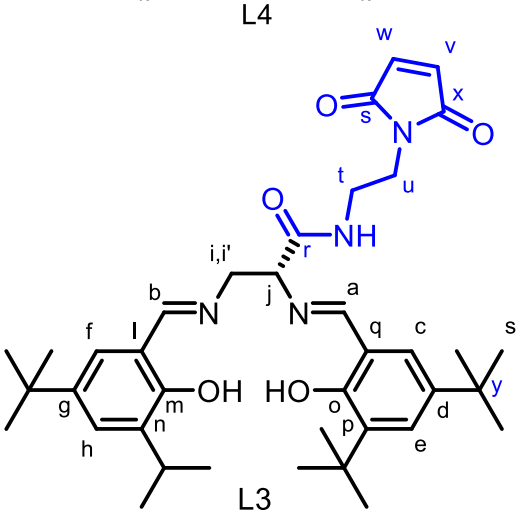

L3

^{1}H NMR (300 MHz, CD_3CN), δ: 8.40 (s, 1H, Ha/Hb); 8.38 (s, 1H, Ha/Hb); 7.34-7.38 (m, 2H, Hc, Hf); 7.15-7.19 (m, 2H, Hh, He), 6.72 (s, 2H, Hv, Hw); 4.08-4.20 (dd, 2H, Hi, Hi'); 3.94-4.03 (dd, 1H, Hj); 3.72-3.80 (m, 4H, Hu, Ht), 1.35-1.4 (m, 36H, Hs).

^{13}C NMR (300 MHz, CD_3CN), δ: 171.5 (Cs, Cx); 168.9 (Cr); 158.3 (Ca); 140.9 (Cb); 136.8 (Co, Cm); 134.8 (Cd, Cp, Cn, Cg); 127.6 (Cv, Cw), 127.1 (Ce, Ch); 118.6 (Cq, Cc, Ci, Cf); 57.3 (Cj); 46.1 (Ci,l'); 38.7 (Cu); 35.3 (Ct); 34.4 5(Cy); 31.3 (Cs).

2.2.3. One pot synthesis of (1,4,7-triazacyclononan-1-yl) acetic acid

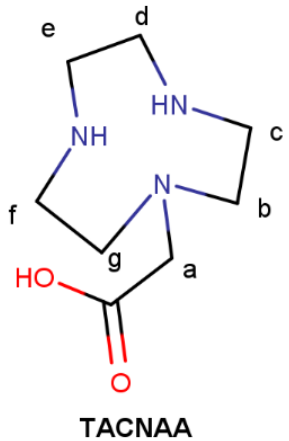

TACNAA

1 g of **TACN** (7.74 mmol; 1 equiv.) is dissolved in 7.5 mL of dioxane before addition of 1.1 mg of *N,N*-dimethylformamide dimethyl acetal (9.3 mmol; 1.2 equiv.). The solution is left under stirring at reflux for 4 h. 1.84 g of 2-bromo-*tert*-butyl acetate (9.3 mmol; 1.2 equiv.) are slowly added at 0°C. The formed suspension is diluted with the addition of 5 mL of dioxane and the mixture left under stirring at room temperature for 1 h. 5 mL of Et_2O is added and the formed yellow solid is filtered and washed with Et_2O before hydrolysis in a solution of 1.25 g of NaOH (30.96 mmol; 4 equiv.) in 50% aq. EtOH (10 mL).

The yellow solution is left under stirring at reflux for 72 h before evaporation of the solvent under reduced pressure. The oily residue is purified on a DOWEX X50 (H^+) ion exchange chromatography with 5% NH_4OH as eluent. The retrieved fraction is evaporated under reduced pressure. The oily residue is diluted in water and the solvent evaporated under reduced pressure; the procedure is done twice. The pure product **TACNAA** is obtained as a yellow oil in an 32 % yield.

^{1}H NMR (300 MHz, $CDCl_3$), δ: 3.27 (s, 2H, Ha); 3.11 (s, 4H, Hb, Hg); 2.96-2.92 (m, 4H, Hd, He); 2.82-2.78 (m, 4H, Hc, Hf).

2.2.4. Synthesis of (1E,1'E)-N,N'-((1S,2S)-cyclohexane-1,2-diyl)bis(1-(6-methylpyridin-2-yl)methanamine)

2.2.4.1. Synthesis of (1S,2S)-N1,N2-bis((6-methylpyridin-2-yl)methyl)cyclohexane-1,2-diamine

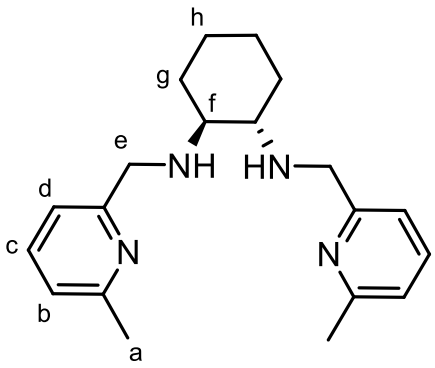

1.5 g of 6-methylpicolinaldehyde (12.4 mmol; 2 equiv.) are dissolved in 20 mL of cooled MeOH. 2.64 g of Na_2SO_4 is added to the solution. 708 mg of cyclohexanediamine (6.2 mmol; 1 equiv.) is dissolved in 20 mL of cooled MeOH and slowly added to the solution followed by a filtration to remove the Na_2SO_4. 961 mg of $NaBH_4$ (25.4 mmol; 4.1 equiv.) is slowly added at 0°C to the filtrate before leaving the solution under stirring for 30 minutes under reflux. After cooling down to room temperature, 10 mL of H_2O are added and the solution is extracted with DCM (3x25 mL). The organic phases are combined, washed with brine (3x25 mL) and dried on Na_2SO_4. After filtration and evaporation of the solvent under reduced pressure, product **A** is obtained as a deep orange oil in an 85 % yield.

^{1}H NMR (300 MHz, $CDCl_3$), δ : 7.5 (t, J= 7.5 Hz, 2H, Hc); 7.23 (d, J= 7.5 Hz, 2H, Hb); 6.99 (d, J=7.5 Hz, 2H, Hd); 4.03 (AB, J= 14.1, 2H, He1); 3.82 (AB, J= 14.1 Hz, 2H, He2); 2.5 (s, 6H, Ha); 2.35-2.32 (m, 2H, Hf); 2.17-2.13 (m, 2H, Hg1); 1.73-1.70 (m, 2H, Hh1); 1.27-1.23 (m, 2H, Hg2); 1.09-1.08 (m, 2H, Hh2)

2.2.4.2. Step 2: Synthesis of (1S,2S)-N1-methyl-N1,N2-bis((6-methylpyridin-2-yl)methyl)cyclohexane-1,2-diamine

1.71 g of **A** (5.27 mmol; 1 equiv.) are diluted in 50 mL of formic acid before slow addition of 3.95 g of paraformaldehyde (131.75 mmol; 25 equiv.) and left under stirring in inert atmosphere for 24 h under reflux. 10 mL of H_2O are added followed by the addition of 40 mg of NaOH pasties at 0°C. An extraction with DCM is done (2x 30 mL). The combined organic phases are washed with brine and dried on Na_2SO_4. After filtration and evaporation of the solvent under reduced pressure the crude product is obtained as an orange oil. After purification on a basic alumina column (Cyclohexane: EtOAc; 8:2), the pure product **B** is obtained as a yellow oil in a 15 % yield.

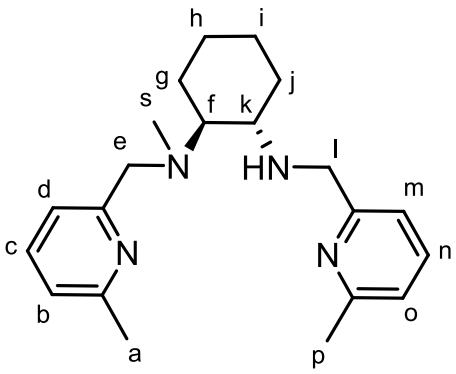

^{1}H NMR (300 MHz, $CDCl_3$), δ: 7.56-6.96 (m, 6H, Hb, Hc, Hd, Hm, Hn, Ho); 4.00-3.1 (m, 6H, He, Hf, Hk, Hl); 2.51-2.48 (6H, Ha, Hp); 2.19-1.69 (m, 12H, Hg, Hh, Hi, Hj, Hs).

2.2.4.3. Step 3: Synthesis of tert-butyl 2-{[(1S,2S)-2-{methyl[(6-methylpyridin-2-yl)methyl]amino}cyclohexyl][(6-methylpyridin-2-yl)methyl]amino}acetate

294 mg of **B** (0.87 mmol; 1 equiv.) are diluted in 15 mL of MeCN before addition of 181 µL of DIPEA (1.04 mmol; 1.2 equiv.) at 0°C. 154 µL (1.04 mmol; 1.2 equiv.) of 2-bromo-*tert*-butyl acetate diluted in 10 mL of MeCN are slowly added at 0°C to the solution and left under stirring under reflux for 24 h. 10 mL of H_2O are added before extraction in DCM (2x 30 mL). The combined organic phases are washed with brine and dried on Na_2SO_4. Filtration and evaporation of the solvent under reduced pressure afford the crude product as a yellow oil. After purification on a basic alumina column (Cyclohexane: EtOAc; 8:2), the pure product **C** is obtained as a clear oil in a 61 % yield.

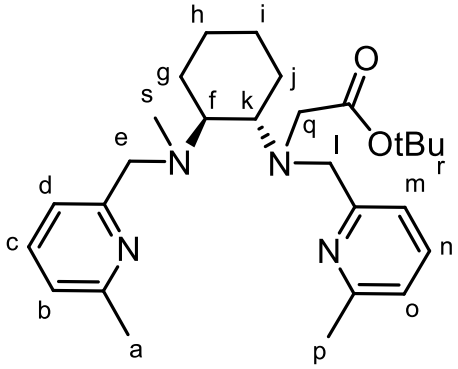

^{1}H NMR (300 MHz, $CDCl_3$), δ: 7.4- 6.93 (m, 6H, Hb, Hc, Hd, Hm, Hn, Ho) 4.12-3.31 (m, 8H, He, Hf, Hk, Hl, Hq); 2.51-2.50 (m, 6H, Ha, Hp) 2.19 (s, 3H, Hs); 1.94 (m, 8H, Hh, Hi, Hj, Hg), 1.41 (s, 18H, Hr).

2.2.4.4. Step 4: Synthesis of 2-{[(1S,2S)-2-{methyl[(6-methylpyridin-2-yl)methyl]amino}cyclohexyl][(6-methylpyridin-2-yl)methyl]amino}acetic acid LIII

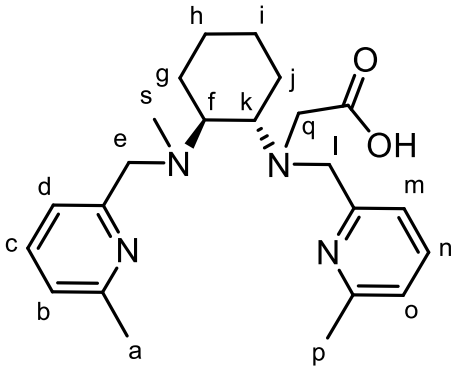

272 mg of **C** (0.60 mmol; 1 equiv.) are diluted in 918 µL of DCM before slow addition of 918 µL of trifluoroacetic acid (12 mmol; 20 equiv.) at 0°C. The mixture is left under stirring at room temperature for 24 h before evaporation of 4/5 of the solvent under reduced pressure. The oily residue is slowly added to 50 mL of cooled Et_2O under vigorous stirring. The supernatant is discarded and the oily residue washed again with Et_2O and the solvent evaporated under reduced pressure. The operation was repeated 5 times to afford the pure product LIII as a clear oil in a 98 % yield.

^{1}H NMR (300 MHz, $CDCl_3$), δ: 8.12-7.30 (m, 6H, Hb, Hc, Hd, Hm, Hn, Ho); 4.66-3.63 (m, 8H, He, Hf, Hk, Hl, Hq); 3.3 (m, 3H, Hs), 2.79 (m, 3H, Hx); 2.81-2.61 (m, 6H, Ha, Hp), 1.4-1.3 (m, 8H, Hg, Hh, Hi, Hj).

3. Synthesis of Complexes

3.1.Complexes MnL4 and MnL3

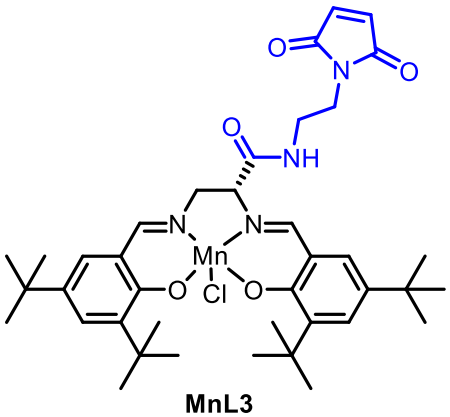

MnL3

In a round bottom flask, 0.2 mmole (1 equiv.) of the ligand is dissolved in 2 mL of absolute ethanol. 0.2 mmole (1 equiv.) of manganese II acetate tetrahydrate and 3 equiv. of lithium iodide were added. The solution was refluxed for 5 h. **MnL3-4** complex started precipitating as a brown powder after 1 h of reflux. Complex is recovered in ethanol with 60 -70 % yield depending on the ligand engaged as a hygrospic brown solid.

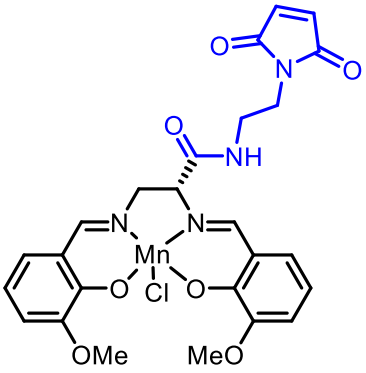

MnL4

MnL4: ESI-MS (ESI+, MeOH): [L4MnCl(H_2O) + H^+]= 601 m/z. EA measured: N% 8.06%, C% 43.63%, H% 4.68%; theoretical for MnL4.6H_2O: $MnC_{25}H_{36}N_4ClO_{13}$ N% 8.11 %, C% 43.46%, H% 5.25%). **MnL3**: ESI-MS (ESI+, MeOH): [L3Mn^{II}(H2O) + Na^+]= 764 m/z

3.2.Complex CoL3

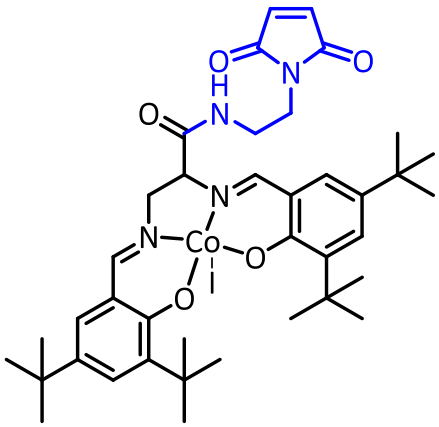

In a round bottom flask 0.25 mmole(1 equiv.) of **L3** were dissolved in 2.5 mL of absolute ethanol and 0.25 mmole (1 equiv.) of cobalt II acetate tetrahydrate were added. The solution was stirred under reflux for 1 h. The solvent was then removed under reduced pressure. The dark green crude was then dissolved in 3 mL dichloromethane, 0.25 mmole (1 equiv.) of p-Toluenesulfonic acid were added and the solution is stirred for one hour at room temperature. The organic solution was the washed three times with a sodium iodide saturated solution then dried over sodium sulfate. Solvents were removed under reduces pressure and the crude was then triturated in pentane, then filtrated. The **CoL3** complex was recovered as a dark brown/red powder with 60 % yield.

ESI-Ms (ESI+, MeOH): [L3Co^{III}I+ H^+]= 842 m/z

EA: measured (N% 6.81%, C% 51.08%, H% 6.25%), theoretical for CoL3.4H_2O (N% 6.13%, C% 51.26%,* H% 6.51%) * may indicate the partial loss of the maleimide substituent.

3.3.Synthesis of FeL4

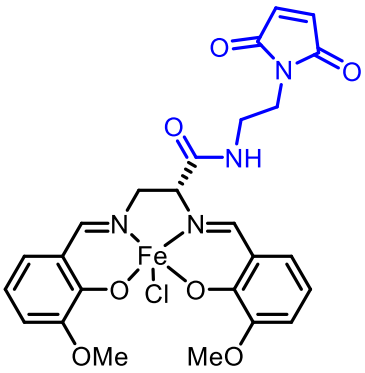

FeL4

0.2 mmole (1 equiv.) of $FeCl_3$ in 500 µL of EtOH were added dropwise to the ligand L4 solution (0.2 mmole, 1 equiv.) at 0.1 M in EtOH. The yellow coloration of the ligand solution turns purple with an immediate start of precipitation of a dark purple solid. The solid was recovered by filtration after 3 h of stirring at room temperature,

ESI-MS (ESI+, MeOH): $[L4Fe^{III} . MeOH]^+$= 580 m/z

3.4.Synthesis of the MnTACNAA complex

50 mg of **TACNAA** (0.27mmol; 1 equiv.) are diluted in 10 mL of H_2O before slow addition of 34 mg of $MnCl_2$ (0.27 mmol; 1 equiv.). The solution is left under stirring for 1 h under reflux under an inert atmosphere. The solvent is evaporated under reduced pressure and the oily residue added to 50 mL of cooled Et_2O. Evaporation under reduced pressure afford [MnTACNAA]Cl as a white precipitate in an 80 % yield.

ESI-MS (ESI+, H_2O) m/z= 241 [Mn(TACNAA)-H]

3.5.Synthesis of MnLIII complex

50 mg of **LIII** (0.12 mmol; 1 equiv.) are diluted in 10 mL of MeCN before slow addition of 15 mg of $MnCl_2$ (0.12 mmol; 1 equiv.). The solution is left under stirring for 2 h at room temperature under inert atmosphere. 2 mL of pentane are added to the solution before evaporation under reduced pressure of 4/5 of the solvent. The oily residue is added to 50 mL of cooled Et_2O and the solvent evaporated under reduced pressure. The mixture of DCM/Pentane/Et_2O allows the complex to precipitate during the evaporation step. **[MnLIII]Cl** is obtained as a white precipitate in an 86 % yield.

ESI-MS (ESI+, MeCN) m/z= 451 [MnLIII-H]

4. Artificial metalloenzymes preparation

NikA cysteine mutants were constructed via site-directed mutagenesis by Dr. Patrice Catty from the BEE team at the LCBM. Mutants A1C, D59C, S415C and H416C were produced in *Escherichia Coli*. Mutants' purification was then transferred to the protein purification platform PFP3 at the LCBM based on a purification protocol of NikA initially developed by Dr. Christine Cavazza from the BEE team. The novelty in the purification method of the cysteine mutant as compared to the WT protein was the addition of 1 mM of DTT in the purification buffer in order to minimize protein-protein intermolecular interaction and avoid the formation of disulfur bridges.

25 mM HEPES (pH 7.0 or 7.6) ammonium sulfate (3.5 M, pH 7.0) and sodium acetate (1 M, pH 4.6) were prepared according to general procedures in MiliQ water and filtrated on 0.22-µm filters. The stabilizing solution corresponds to a solution of 2.1 M of ammonium sulfate in 25 mM HEPES buffer, pH 7.0 and is used for crystal handling post crystallization: functionalization, saoking and stabilization.

4.1.Protein crystallization procedure

WT and NikA mutants were crystallized using the vapor diffusion technique in Nextal 15 well plates, using the drop technique illustrated in ***figure 75***.

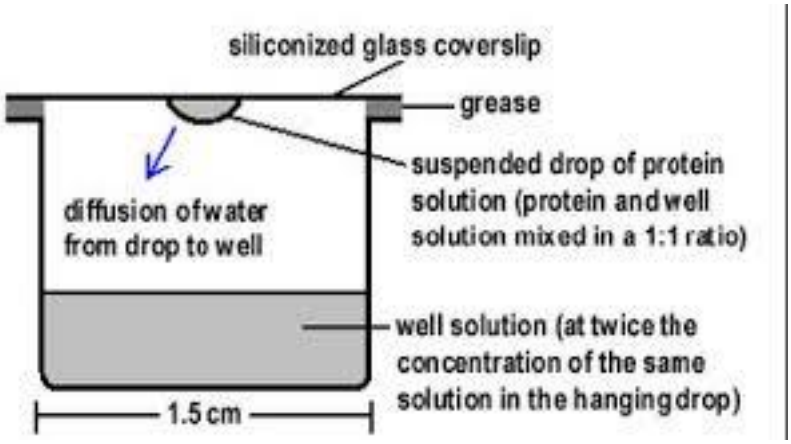

Figure 75: *representation of the hanging drop vapor diffusion technique*

Apo-NikA samples were first incubated with 2 equivalents of Fe(III)-EDTA for 10 min at room temperature. On the siliconized glass coverslip, 2 µL of NikA- Fe(III)-EDTA at 9 $mg.mL^{-1}$ in 25 mM HEPES , pH 7.6 was mixed with 2 µL with the crystallization buffer consisting of 100 mM sodium acetate, pH 4.7 and ammonium sulfate at 1.6 -1.8 M (the adequate concentration is determined by performing screening tests on new protein batches). The greaseless screw-in lamella fit on the crystallization reservoir containing the 500 µL of the same crystallization solution. After a week, the vapor equilibrium leading to the concentration of the protein within the drop leads to the nucleation phenomenon. The orthorhombic NikA-Fe(III) EDTA crystals will then grow in the span of ten days, according to the phase diagram, *figure 76.*

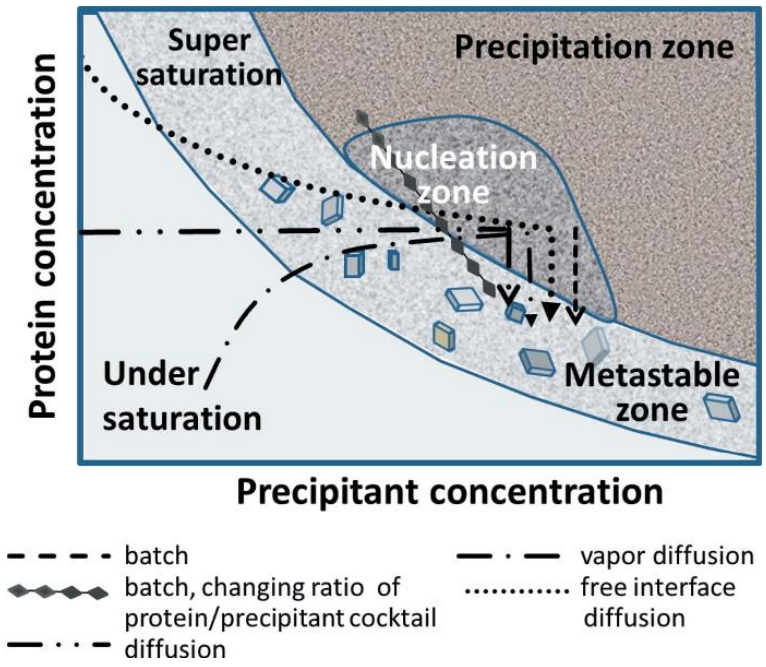

***Figure 76**: phase diagram for protein crystallization*

X-ray data collections and X-ray fluorescence emission spectra were recorded on the ID29, BM-30A and BM-07 beamlines at the European Synchrotron Radiation Facility (ESRF) in Grenoble. The raw data were processed using the XDS program. Crystal structures were resolved using the molecular replacement method (Phaser) on the phenix program confronted with the X-ray atomic model of NikA-Fe-EDTA(H_2O)- (PDB ID code 1zlq). Refinements were performed on phenix and refmac and the 3D models were built and inspected using the COOT program.

4.2.General procedure for anchoring assays in solution

Apo-protein samples at 100 µM in 25 mM HEPES pH 7.6 were incubated with 10 equiv. of the desired complex. The total volume was 500 µL with 10 % of MeCN. The samples were incubated at 25 °C in a thermomixer© and agitated at 1000 rpm overnight. After the incubation time, the samples were centrifuged for 5 min at 4°C, 15000 rpm.

For the salen series, the supernatant was purified twice on a NAP10 desalting column using 25 mM HEPES pH 7.6 as an eluant. The purified samples were then centrifuged again for 5 min at 4°C, 15000 rpm. Out of the supernatant, 25 µL were injected into the SEC-MALLS apparatus for the protein quantification, 100 µL were sent to the IBS platform for the denaturing mass analysis and 100 µL were analyzed by ICP-AES.

For MnTACNAA and MnLIII, the supernatant was washed four times on centricon using 25 mM HEPES pH 7.6. After the washing steps, 25 µL were injected into the SEC-MALLS apparatus for the protein quantification and 100 µL were analyzed by ICP.

*4.3.*Anchoring assays *in cristallo*

Method 1 (at RT): NikA crystals of comparable size were transferred to a 4 µL drop of the desired complex at 5 mM (for the Salen series and 10 mM for MnLIII and MnTACNAA) in the stabilizing solution with 1% of DMF. The crystals are incubated overnight at 20°C then washed with a stabilizing solution (100 mM Na acetate pH 4.6, 2.3 M ammonium sulfate) before their transfer in a cryoprotecting solution (stabilizing solution + 25 % glycerol) and freezing in liquid nitrogen for XRD and XRF analyses.

Method 2 (covalent anchoring at 40 °C): NikA crystals of comparable size were transferred to a 500 µL solution of MnL4 at 5 mM in the stabilizing solution with 1 % of DMF in an Eppendorf tube. The crystals are soaked in the thermomixer overnight at 40 °C and under 1000 rpm agitation. The crystals are retrieved from the solution then washed with the stabilising solution and the cryoprotecting solution before freezing for XRD analysis.

4.4.NikA quantification using rose Bengal test

First, a calibration curve is determined using a BSA sample at 2 $mg.mL^{-1}$. Different aliquots were prepared by sampling (0, 5, 10, 20, 40 et 60 µL) from the BSA solution, the total volume is brought to 2 mL by adding KH_2PO_4 buffer at 10 mM pH 6.8. Then, 100 µL of rose bengal at 1 $mg.mL^{-1}$ are added to each sample. The samples are then incubated at room temperature for 5 min before adding 100 µL acetic acid at 50%. The samples are then vortexed, and the absorbance is read at 560 nm. The NikA protein concentration can be determined following the same calorimetric assay with rose bengal then referring to the calibration curve.

4.5.ICP quantification

Calibration is performed using a multi-element solution. Starting from a solution at 1000 $\mu g.L^{-1}$ 9 reference samples are prepared by ½ fold serial dilution. The reference samples are acquired before the analysis in order to validate the equilibration.

For the quantification assays, 100 µL of the protein samples were mineralized in 1.5 mL of nitric acid 60% at 50°C overnight. the samples are then diluted to 8 mL using a nitric acid solution at 10% in MiliQ water. The samples are then injected into the ICP apparatus in automatic mode.

5. Catalytic investigations

5.1.General procedure for the heterogeneous catalysts' preparation

5.1.1. NikA-MnLIII and NikA-MnTACNAA

100 WT-NikA crystals were stabilized with 1% glutaraldehyde in the soaking buffer for two hours. The crystals are then transferred in an Eppendorf containing 100 µL of the complex solution at 10 mM in MeCN. the crystals are soaked at room temperature overnight then rinsed with MeCN.

5.1.2. Metal salen complexes in complex with NikA mutants

Method A: 100 crystals were soaked overnight at room temperature in 4 µL drops of the complex at 5mM in the stabilizing solution with 1% of DMF. They are then transferred to clean solution drops and stabilized with 1% of glutaraldehyde in the same buffer for 2 h at room temperature. The crystals were then transferred to an MeCN solution in 500 µL Eppendorf tubes.

Method B: 100 crystals were stabilized with 1% of glutaraldehyde in the stabilizing solution for 2 h at room temperature. They were then transferred to 500 µL Eppendorf tubes containing 100 µL of MnL4 at 100 mM in DMF and soaked at room temperature overnight.

Method C: 100 crystals were stabilized with 1% of glutaraldehyde in the stabilizing solution for 2 h at room temperature. They were then transferred to 500 µL Eppendorf tubes containing 100 µL of MnL4 at 100 mM in DMF and soaked at 40 °C overnight.

Method D: 100 crystals were transferred to a 500 µL solution of MnL4 at 5 mM in the stabilizing solution with 1 % of DMF in an Eppendorf tube. The crystals were soaked in the thermomixer overnight at 40 °C and under 1000 rpm agitation. The crystals are retrieved from the solution and transferred back to clean soaking drops and stabilized with 1% of glutaraldehyde in the same buffer for 2 h at room temperature. The crystals are then transferred to an MeCN solution in 500 µL Eppendorf tubes.

5.2.General procedures for epoxidation with hydrogen peroxide

5.2.1. Adaptation of the reported conditions for the catalysts preparation

$Fe(Pic)(MePic)_2$ was prepared using (0.2 mmole, 1 equiv) of $Fe^{II}(OAc)_2$, (0.2 mmole, 1 equiv) of picolinic acid and (0.2 mmole, 1 equiv) of methyl picolinic acid were suspended in 16 mL of MeCN. The solution was stirred at 40°C for 30min during which the solution becomes light green. The solution is then filtered and the concentration adjusted to 10 mM.[230]

This same procedure was followed in the preparation of $Fe(MePic)_3$ using 6 equivalent of Methyl picolinic acid and $Fe(Pic)_3$ using 2 equivalents of picolinic acid.

Crystals were obtained through the slow evaporation of MeCN overnight.

Catalytic solution of the recovered crystals were prepared at 10 mM by the dissolution of the adequate amount of catalyst in acetonitrile at 40°C to aid the solubility.

5.2.2. General preparation of the catalytic solutions

For a ratio of catalyst/substrate/oxidant of 1/50/70, a stock solution of the catalytic mixture was prepared according to the reported conditions: (1 mmole, 50 equiv.) of styrene were directly added to the catalytic solution at room temperature followed by (14 mmole, 70 equiv.) of aqueous H_2O_2 35%. The reaction was stirred at room temperature. 1 µL of the catalytic solution were diluted in 100 µL of MeCN, 3 µL of a benzophenone solution at 0.1 M dichloroethane were added before GC quantification.

For a ratio of catalyst/substrate/oxidant of 1/1500/2100: To 85.5 µL of MeCN were added; 7.5 µL of styrene at 2 M in MeCN, 6 µL of H_2O_2 solution at 3.5 M and 1 µl of the catalyst solution at 10 mM.

For a ratio of catalyst/substrate/oxidant of 1/500/700: To 95 µL of MeCN were added; 2 µL of styrene at 2.5 M in MeCN, 2 µL of H_2O_2 solution at 3.5 M in MeCN and 1 µl of the catalyst solution at 10 mM.

5.2.3. Catalytic assays using the CLEC NikA

100 CLEC of NikA were soaked at room temperature with the catalytic solution of $Fe(Pic)_3$ at 10 mM MeCN, overnight. The recovered CLEC were washed in acetonitrile and engaged in catalytic assays with a ratio of catalyst/substrate/oxidant of 1/500/700 and 1/1500/2100. In both cases the reaction was stirred at room temperature for up to 18 hours. No product was formed.

5.3.General procedure for epoxidation with PAA

Catalytic assays were performed in 500 µL eppendorf tubes. 100 CLEC-ArM were suspended in 30 µL of acetonitrile. 5 µL of a stock solution of the desired substrate at 320 mM were added following 5 µL PAA at 640 mM in acetonitrile as well. The aliquots were stirred in the thermomixer for the desired reaction time. 3 µL of benzophenone at 0.1 M in DCE were added before the GC-Ms analysis.

Catalytic assays in solution were performed in a similar fashion replacing the CLEC crystals in the addition of 10 µL of the complex stock solution at 160 µM in acetonitrile then completing the volume to 40 µL total.

5.4.General procedure for aerobic epoxidation

5.4.1. MnLIII and MnTACNAA and the artificial metalloenzyme analogues

Catalysis using these candidates were performed under ambient atmosphere in 500 µL eppendorfs. In the tubes, 100 CLEC NikA-MnTACNAA or MnLIII were suspended in 10 µL of acetonitrile. 5 µL of a stock solution of the desired substrate at 320 mM were added following 25 µL of IBA at 128 mM as well. The aliquots were stirred in the thermomixer© for the desired reaction time. 5 µL of the catalytic solution were diluted in 100 µL of MeCN and analyzed by HPLC. In the remaining 35 µL, 3 µL of benzophenone (the internal reference) in dichloroethane were added before the GC-Ms analysis.

Catalytic assays in solution were performed in a similar fashion replacing the CLEC crystals in 10 µL of acetonitrile by the addition of 10 µL of the complex stock solution at 160 µM in acetonitrile.

5.4.2. MnL4 and the artificial metalloenzyme analogues

Catalysis using these candidates were performed in the Man on the Moon© apparatus under 1 bar of pure oxygen. In an HPLC glass vial equipped with a glass insert, 100 CLEC NikA-MnL4 (WT and mutants) were suspended in 10 µL of acetonitrile. 5 µL of a stock solution of the desired substrate at 320 mM were added following 25 µL of IBA at 128 mM as well. The vial was then introduced in the mini reactor, the atmosphere was purged 5 times and the system was left on continuous supply of oxygen for 2 h. 5 µL of the catalytic solution were diluted in 100 µL of MeCN and analyzed by HPLC. In the remaining 35 µL, 3 µL of benzophenone (the internal reference) in dichloroethane were added before the GC-Ms analysis.

Catalytic assays in solution were performed in a similar fashion replacing the CLEC crystals in 10 µL of acetonitrile by the addition of 10 µL of the complex stock solution at 160 µM in acetonitrile.

5.5.General procedure for CO_2 cycloaddition

5.5.1. Homogeneous assays in the Hungate tube

In a 200 µL Eppendorf tube, 0.01 mmole of **CoL3** and 0.01 mmole of phosphoranylidene acetaldehyde were mixed in 142 µL of 1.25 mmole of styrene oxide. The tube was introduced in a hungate tube. The system was purged with a CO_2 balloon for 5 min then closed under a CO_2 atmosphere. The reaction evolution was monitored by GC-MS by sampling 1 µL of the catalytic solution that were then diluted in 100 µL of MeCN with 3 µL of benzophenone at 0.1 M in dichloromethane. The same procedure was followed for homogeneous assays performed under diluted conditions.

5.5.2. ArMs catalyzed CO_2 cycloaddition with phosphoranylidene acetaldehyde

These assays were performed in the mini reactor, in a glass HPLC vial. 100 CLEC of the desired mutant-**CoL3** ArM were suspended in 35 µL of acetonitrile. 2.5 µL of a stock solution of styrene oxide at 640 mM in acetonitrile and 2.5 µL of the co-catalyst at 640 µM (or 640 mM for stochiometric reaction) were added. The reactor was purged 5 times at the desired CO_2 pressure. the temperature was set using a heating plate equipped with a small sand bath. The results were quantified by GC-MS after adding 3 µL of benzophenone at 0.1 M in DCE.

5.5.3. ArMs catalyzed CO_2 cycloaddition with TBAB

Catalytic procedure was performed in the mini reactor. In a glass HPLC vial equipped with an insert, 100 CLEC of the studied mutant-CoL3 were suspended in 32.5 µL acetonitrile. 5 µL of s styrene oxide solution at 640 mM in acetonitrile were added followed by 2.5 µL of a solution of TBAB at 1.28 mM in acetonitrile as well. The system was purged five times under CO_2 then put under 3 bars of CO_2 at 60 °C for 96 h. Results were quantified by GC-MS after the addition of the internal reference (3 µL of benzophenone at 0.1 M in DCE).

5.5.4. General procedure for the tandem reaction

Using the mini reactor, 100 CLEC of the multi-site ArM were suspended in 5 µL of acetonitrile. 5µL of styrene oxide at 1.9 M, 5 µL of TBAB at 1.28 M and 25 µL of IBA at 1.9 M, in acetonitrile, were added subsequently. The reactor was connected to an oxygen tank with continuous supply of O_2 at 1 bar for 6 h at room temperature. The oxygen was then purged and replaced by CO_2 at 3 bar. The system was heated over a heating plate at 60 °C over 24 to 96 h. The results were quantified by GC-MS using benzophenone as and internal reference (3 µL of stock solution at 0.1 M in DCE).

6. Reference synthesis

6.1. Adapted Shi Epoxidation for the preparation of *cis* and *trans*-2-methyl-3-phenyloxirane

1 mmol (1 equiv.) of alkene was diluted in 7.5 mL od MeCN before addition of 5 mL of a solution of Na_2EDTA at 4.10^{-4} M. 1 mL of trifluroacetone (11.2 mmol; 11,2 equiv.) is slowly added at 0°C to the solution. A mixture of 3.07 g of oxone (20.17 mmol ; 20.17 equiv.) and 651 mg of potassium carbonate (7.7 mmol ; 7.7 equiv.) is slowly added over 1h45 at 0°C under stirring. The mixture is left under stirring at 0°C for 10'' before addition of 50 mL of H_2O and extraction with DCM (2x50 mL). The combined organic phases were washed with brine and dried on Na_2SO_4. Filtration and Evaporation under reduced pressure of the solvent afford the pure products **1A** and **3A** as yellow oils in a 60 % and 82 % yield respectively. For **2A** a purification on a silica column (Cyclohexane: EtOAc; 9:1) afford the pure product as a clear oil in a 36 % yield.

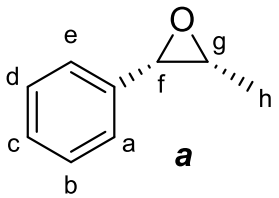

a

a : ^{1}H NMR (300 MHz, $CDCl_3$), δ: 7.34-7.24 (m, 5H, Ha, Hb, Hc, Hd, He); 3.64-3.56 (m, 1H, Hf); 3.06-3.00 (m, 1H, Hg); 1.46 (s,3H, Hh).

HPLC retention time: 4.3 min (not separated)

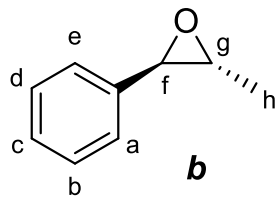

b

b : ^{1}H NMR (300 MHz, $CDCl_3$), δ: 7.35-7.23) (m, 5H, Ha, Hb, Hc, Hd, He); 3.56 (m, 1H, Hf); 3.04-3.02 (m, 1H, Hg); 1.42 (s, 3H, Hh).

HPLC retention time: 4.6 min , 5.1 min

6.2.Synthesis of 4-phenyl-1,3-dioxolan-2-one

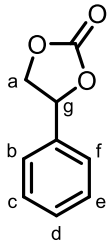

CO_2 cycloadditions performed in the Hungate tube (see i. Homogeneous assays in the Hungate tube) were grouped then purified on a silica column using CH_2Cl_2 as the eluant. Styrene carbonate was isolated in 80% yield.

^1H NMR (300 MHz, $CDCl_3$), δ: 7.14-7.56 (m, 5H, Hf, Hb, Hc, Hd, He); 4.15 (dd, 1H, Hg); 3.18 (dd, 1H, Ha); 2.65 (dd,1H, Ha).GC-MS: RT: 18.60 min, m/z= 164

7. GC-MS and HPLC analysis

Catalytic results were quantified using GC-MS analysis and benzophenone as an internal reference. The response factor for each substrate/ product was determined using a calibration curve. The calibration was done by injecting product samples at different concentrations using the same internal reference, benzophenone. This reference samples were prepared in accordance to the catalytic procedure followed (substrate concentration, solvent type etc).

7.1.General example for GC-MS response factor determination

In a typically procedure, from a solution S_0 at 320 mM of the desired substrate in MeCN were prepared four samples at 256 mM, 192 mM, 128 mM and 64 mM in the same solvent. 5 µL of these solutions were added to 35 µL of acetonitrile and vortexed. 3 µL of benzophenone solution in dichloroethane at 0.1 M were added before the GC acquisition. The response factor was determined as the curve slope of the plot of the molar (n sample/ n reference) ratio as a function of the area ratio (A sample/ A reference). Retention times and calculated response factors are displayed in ***table 16***.

Table 7*: Summary of the response factor and retention time for investigated compounds*

Compound	*Response Factor*	*Retention Time (min)*
Styrene	0.78	7.15
cis-β-Methylstyrene	0.85	8.02
trans-β-Methylstyrene	0.92	8.54
2-Bromostyrene	2.62	10.61
4-Bromostyrene	0.89	10.54
Styrene Oxide	0.63	9.82
Benzaldehyde	0.62	8.50
1,2-phenylethanediol	0.86	13.41
Cis-2-methyl-3-phenyloxirane	0.95	9.97
Trans-2-methyl-3-phenyloxirane	1.2	10.07
4-phenyl-1,3-dioxolan-2-one	1.02	18.30

Bibliographical references

(1) Cornish-Bawden, A. *New Beer in an Old Bottle. Eduard Buchner and the Growth of Biochemical Knowledge*; Universitat de València, 1997.

(2) New and Future Developments in Catalysis. In *New and Future Developments in Catalysis*; Suib, S. L., Ed.; Elsevier: Amsterdam, 2013; p i. https://doi.org/10.1016/B978-0-444-53870-3.00022-8.

(3) Anastas, P. T.; Warner, J. C. *Green Chemistry: Theory and Practice*; Oxford University Press, 1998.

(4) Green Chemistry By Paul T. Anastas and John C. Warner. Oxford University Press: Oxford. 2000. Paperback. 135 Pp. £14.99. ISBN 0-19-850698-9. *Org. Process Res. Dev.* **2000**, *4* (5), 437–438. https://doi.org/10.1021/op000054t.

(5) Armor, J. N. Environmental Catalysis. *Appl. Catal. B Environ.* **1992**, *1* (4), 221–256. https://doi.org/10.1016/0926-3373(92)80051-Z.

(6) Anastas, P. T.; Bartlett, L. B.; Kirchhoff, M. M.; Williamson, T. C. The Role of Catalysis in the Design, Development, and Implementation of Green Chemistry. *Catal. Today* **2000**, *55* (1), 11–22. https://doi.org/10.1016/S0920-5861(99)00222-9.

(7) Berndt, M.; Landri, P. An Overview about Engelhard Approach to Non-Standard Environmental Catalysis. *Catal. Today* **2002**, *75* (1), 17–22. https://doi.org/10.1016/S0920-5861(02)00038-X.

(8) Yu, F.; Cangelosi, V. M.; Zastrow, M. L.; Tegoni, M.; Plegaria, J. S.; Tebo, A. G.; Mocny, C. S.; Ruckthong, L.; Qayyum, H.; Pecoraro, V. L. Protein Design: Toward Functional Metalloenzymes. *Chem. Rev.* **2014**, *114* (7), 3495–3578. https://doi.org/10.1021/cr400458x.

(9) Akabori, S.; Sakurai, S.; Izumi, Y.; Fujii, Y. An Asymmetric Catalyst. *Nature* **1956**, *178* (4528), 323–324. https://doi.org/10.1038/178323b0.

(10) Liu, B.; Song, Y.; Jin, L.; Wang, Z.; Pu, D.; Lin, S.; Zhou, C.; You, H.; Ma, Y.; Li, J.; Yang, L.; Sung, K. L. P.; Zhang, Y. Silk Structure and Degradation. *Colloids Surf. B Biointerfaces* **2015**, *131*, 122–128. https://doi.org/10.1016/j.colsurfb.2015.04.040.

(11) Ma, L.; Liu, Q.; Wu, R.; Meng, Z.; Patil, A.; Yu, R.; Yang, Y.; Zhu, S.; Fan, X.; Hou, C.; Li, Y.; Qiu, W.; Huang, L.; Wang, J.; Lin, N.; Wan, Y.; Hu, J.; Liu, X. Y. From Molecular Reconstruction of Mesoscopic Functional Conductive Silk Fibrous Materials to Remote Respiration Monitoring. *Small* **2020**, *16* (26), 2000203. https://doi.org/10.1002/smll.202000203.

(12) Wu, R.; Ma, L.; Liu, X. Y. From Mesoscopic Functionalization of Silk Fibroin to Smart Fiber Devices for Textile Electronics and Photonics. *Adv. Sci.* **2022**, *9* (4), 2103981. https://doi.org/10.1002/advs.202103981.

(13) Shoji, O.; Fujishiro, T.; Nakajima, H.; Kim, M.; Nagano, S.; Shiro, Y.; Watanabe, Y. Hydrogen Peroxide Dependent Monooxygenations by Tricking the Substrate Recognition of Cytochrome P450BSβ. *Angew. Chem. Int. Ed.* 2007, *46* (20), 3656–3659. https://doi.org/10.1002/anie.200700068.

(14) Shoji, O.; Fujishiro, T.; Nakajima, H.; Kim, M.; Nagano, S.; Shiro, Y.; Watanabe, Y. Inside Cover: Hydrogen Peroxide Dependent Monooxygenations by Tricking the Substrate Recognition of Cytochrome P450BSβ (Angew. Chem. Int. Ed. 20/2007). *Angew. Chem. Int. Ed.* 2007, *46* (20), 3592–3592. https://doi.org/10.1002/anie.200790087.

(15) Fujishiro, T.; Shoji, O.; Kawakami, N.; Watanabe, T.; Sugimoto, H.; Shiro, Y.; Watanabe, Y. Chiral-Substrate-Assisted Stereoselective Epoxidation Catalyzed by H2O2-Dependent Cytochrome P450SPα. *Chem. – Asian J.* 2012, *7* (10), 2286–2293. https://doi.org/10.1002/asia.201200250.

(16) Okamoto, Y.; Kojima, R.; Schwizer, F.; Bartolami, E.; Heinisch, T.; Matile, S.; Fussenegger, M.; Ward, T. R. A Cell-Penetrating Artificial Metalloenzyme Regulates a Gene Switch in a Designer Mammalian Cell. *Nat. Commun.* 2018, *9* (1), 1943. https://doi.org/10.1038/s41467-018-04440-0.

(17) Vong, K.; Eda, S.; Kadota, Y.; Nasibullin, I.; Wakatake, T.; Yokoshima, S.; Shirasu, K.; Tanaka, K. An Artificial Metalloenzyme Biosensor Can Detect Ethylene Gas in Fruits and Arabidopsis Leaves. *Nat. Commun.* 2019, *10* (1), 5746. https://doi.org/10.1038/s41467-019-13758-2.

(18) Chen, X.; Ren, X.; Gao, X. Peptide or Protein-Protected Metal Nanoclusters for Therapeutic Application. *Chin. J. Chem.* 2022, *40* (2), 267–274. https://doi.org/10.1002/cjoc.202100523.

(19) Gao, L.; Zhang, Y.; Zhao, L.; Niu, W.; Tang, Y.; Gao, F.; Cai, P.; Yuan, Q.; Wang, X.; Jiang, H.; Gao, X. An Artificial Metalloenzyme for Catalytic Cancer-Specific DNA Cleavage and Operando Imaging. *Sci. Adv.* 2020, *6* (29), eabb1421. https://doi.org/10.1126/sciadv.abb1421.

(20) Wilson, M. E.; Whitesides, G. M. Conversion of a Protein to a Homogeneous Asymmetric Hydrogenation Catalyst by Site-Specific Modification with a Diphosphinerhodium(I) Moiety. *J. Am. Chem. Soc.* 1978, *100* (1), 306–307. https://doi.org/10.1021/ja00469a064.

(21) Livnah, O.; Bayer, E. A.; Wilchek, M.; Sussman, J. L. Three-Dimensional Structures of Avidin and the Avidin-Biotin Complex. *Proc. Natl. Acad. Sci.* 1993, *90* (11), 5076–5080. https://doi.org/10.1073/pnas.90.11.5076.

(22) Jain, A.; Barve, A.; Zhao, Z.; Jin, W.; Cheng, K. Comparison of Avidin, Neutravidin, and Streptavidin as Nanocarriers for Efficient SiRNA Delivery. *Mol. Pharm.* 2017, *14* (5), 1517–1527. https://doi.org/10.1021/acs.molpharmaceut.6b00933.

(23) Eisenberg-Domovich, Y.; Hytönen, V. P.; Wilchek, M.; Bayer, E. A.; Kulomaa, M. S.; Livnah, O. High-Resolution Crystal Structure of an Avidin-Related Protein: Insight into High-

Affinity Biotin Binding and Protein Stability. *Acta Crystallogr. D Biol. Crystallogr.* 2005, *61* (5), 528–538. https://doi.org/10.1107/S0907444905003914.

(24) Eisenberg-Domovich, Y.; Pazy, Y.; Nir, O.; Raboy, B.; Bayer, E. A.; Wilchek, M.; Livnah, O. Structural Elements Responsible for Conversion of Streptavidin to a Pseudoenzyme. *Proc. Natl. Acad. Sci.* 2004, *101* (16), 5916–5921. https://doi.org/10.1073/pnas.0308541101.

(25) Lesch, H. P.; Kaikkonen, M. U.; Pikkarainen, J. T.; Ylä-Herttuala, S. Avidin-Biotin Technology in Targeted Therapy. *Expert Opin. Drug Deliv.* 2010, *7* (5), 551–564. https://doi.org/10.1517/17425241003677749.

(26) Collot, J.; Gradinaru, J.; Humbert, N.; Skander, M.; Zocchi, A.; Ward, T. R. Artificial Metalloenzymes for Enantioselective Catalysis Based on Biotin−Avidin. *J. Am. Chem. Soc.* 2003, *125* (30), 9030–9031. https://doi.org/10.1021/ja035545i.

(27) Skander, M.; Humbert, N.; Collot, J.; Gradinaru, J.; Klein, G.; Loosli, A.; Sauser, J.; Zocchi, A.; Gilardoni, F.; Ward, T. R. Artificial Metalloenzymes: (Strept)Avidin as Host for Enantioselective Hydrogenation by Achiral Biotinylated Rhodium−Diphosphine Complexes. *J. Am. Chem. Soc.* 2004, *126* (44), 14411–14418. https://doi.org/10.1021/ja0476718.

(28) Ward, T. R. Artificial Metalloenzymes Based on the Biotin−Avidin Technology: Enantioselective Catalysis and Beyond. *Acc. Chem. Res.* 2011, *44* (1), 47–57. https://doi.org/10.1021/ar100099u.

(29) Lee, P.; Wu, X. Review: Modifications of Human Serum Albumin and Their Binding Effect. *Curr. Pharm. Des. 21* (14), 1862–1865.

(30) Sudlow, G.; Birkett, D. J.; Wade, D. N. The Characterization of Two Specific Drug Binding Sites on Human Serum Albumin. *Mol. Pharmacol.* 1975, *11* (6), 824–832.

(31) Mishra, V.; Heath, R. J. Structural and Biochemical Features of Human Serum Albumin Essential for Eukaryotic Cell Culture. *Int. J. Mol. Sci.* 2021, *22* (16), 8411. https://doi.org/10.3390/ijms22168411.

(32) Rondot, L.; Girgenti, E.; Oddon, F.; Marchi-Delapierre, C.; Jorge-Robin, A.; Ménage, S. Catalysis without a Headache: Modification of Ibuprofen for the Design of Artificial Metalloenzyme for Sulfide Oxidation. *J. Mol. Catal. Chem.* 2016, *416*, 20–28. https://doi.org/10.1016/j.molcata.2016.02.015.

(33) Sleep, D.; Cameron, J.; Evans, L. R. Albumin as a Versatile Platform for Drug Half-Life Extension. *Biochim. Biophys. Acta BBA - Gen. Subj.* 2013, *1830* (12), 5526–5534. https://doi.org/10.1016/j.bbagen.2013.04.023.

(34) Mahy, J.-P.; Avenier, F.; Ghattas, W.; Ricoux, R.; Salmain, M. Current Applications of Artificial Metalloenzymes and Future Developments. In *Enzymes for Solving Humankind's Problems: Natural and Artificial Systems in Health, Agriculture, Environment and Energy*;

Moura, J. J. G., Moura, I., Maia, L. B., Eds.; Springer International Publishing: Cham, 2021; pp 363–411. https://doi.org/10.1007/978-3-030-58315-6_12.

(35) Ghattas, W.; Cotchico-Alonso, L.; Maréchal, J.-D.; Urvoas, A.; Rousseau, M.; Mahy, J.-P.; Ricoux, R. Artificial Metalloenzymes with the Neocarzinostatin Scaffold: Toward a Biocatalyst for the Diels–Alder Reaction. *ChemBioChem* 2016, *17* (5), 433–440. https://doi.org/10.1002/cbic.201500445.

(36) Raffy, Q.; Ricoux, R.; Mahy, J.-P. Synthesis of a New Estradiol–Iron Metalloporphyrin Conjugate Used to Build up a New Hybrid Biocatalyst for Selective Oxidations by the 'Trojan Horse' Strategy. *Tetrahedron Lett.* 2008, *49* (11), 1865–1869. https://doi.org/10.1016/j.tetlet.2008.01.022.

(37) Avenier, F.; Ghattas, W.; Ricoux, R.; Mahy, J.-P. Recent Progress in the Development of New Artificial Metalloenzymes as Biocatalysts for Selective Oxidations and Diels-Alder Reaction - Mini-Review. *Vietnam J. Chem.* 2020, *58* (4), 423–433. https://doi.org/10.1002/vjch.202000033.

(38) Raffy, Q.; Ricoux, R.; Sansiaume, E.; Pethe, S.; Mahy, J.-P. Coordination Chemistry Studies and Peroxidase Activity of a New Artificial Metalloenzyme Built by the "Trojan Horse" Strategy. *J. Mol. Catal. Chem.* 2010, *317* (1), 19–26. https://doi.org/10.1016/j.molcata.2009.10.016.

(39) Drevelle, A.; Graille, M.; Heyd, B.; Sorel, I.; Ulryck, N.; Pecorari, F.; Desmadril, M.; van Tilbeurgh, H.; Minard, P. Structures of in Vitro Evolved Binding Sites on Neocarzinostatin Scaffold Reveal Unanticipated Evolutionary Pathways. *J. Mol. Biol.* 2006, *358* (2), 455–471. https://doi.org/10.1016/j.jmb.2006.02.002.

(40) Heyd, B.; Pecorari, F.; Collinet, B.; Adjadj, E.; Desmadril, M.; Minard, P. In Vitro Evolution of the Binding Specificity of Neocarzinostatin, an Enediyne-Binding Chromoprotein. *Biochemistry* 2003, *42* (19), 5674–5683. https://doi.org/10.1021/bi0273664.

(41) Sansiaume-Dagousset, E.; Urvoas, A.; Chelly, K.; Ghattas, W.; Maréchal, J.-D.; Mahy, J.-P.; Ricoux, R. Neocarzinostatin-Based Hybrid Biocatalysts for Oxidation Reactions. *Dalton Trans.* 2014, *43* (22), 8344–8354. https://doi.org/10.1039/C4DT00151F.

(42) Fujieda, N.; Nakano, T.; Taniguchi, Y.; Ichihashi, H.; Sugimoto, H.; Morimoto, Y.; Nishikawa, Y.; Kurisu, G.; Itoh, S. A Well-Defined Osmium–Cupin Complex: Hyperstable Artificial Osmium Peroxygenase. *J. Am. Chem. Soc.* 2017, *139* (14), 5149–5155. https://doi.org/10.1021/jacs.7b00675.

(43) Cuatrecasas, P.; Fuchs, S.; Anfinsen, C. B. Catalytic Properties and Specificity of the Extracellular Nuclease of Staphylococcus Aureus. *J. Biol. Chem.* 1967, *242* (7), 1541–1547.

(44) Fernández-Gacio, A.; Codina, A.; Fastrez, J.; Riant, O.; Soumillion, P. Transforming Carbonic Anhydrase into Epoxide Synthase by Metal Exchange. *ChemBioChem* 2006, *7* (7), 1013–1016. https://doi.org/10.1002/cbic.200600127.

(45) Natoli, S. N.; Hartwig, J. F. Noble–Metal Substitution in Hemoproteins: An Emerging Strategy for Abiological Catalysis. *Acc. Chem. Res.* **2019**, *52* (2), 326–335. https://doi.org/10.1021/acs.accounts.8b00586.

(46) Dydio, P.; Key, H. M.; Nazarenko, A.; Rha, J. Y.-E.; Seyedkazemi, V.; Clark, D. S.; Hartwig, J. F. An Artificial Metalloenzyme with the Kinetics of Native Enzymes. *Science* **2016**, *354* (6308), 102–106. https://doi.org/10.1126/science.aah4427.

(47) Key, H. M.; Dydio, P.; Liu, Z.; Rha, J. Y.-E.; Nazarenko, A.; Seyedkazemi, V.; Clark, D. S.; Hartwig, J. F. Beyond Iron: Iridium-Containing P450 Enzymes for Selective Cyclopropanations of Structurally Diverse Alkenes. *ACS Cent. Sci.* **2017**, *3* (4), 302–308. https://doi.org/10.1021/acscentsci.6b00391.

(48) Dydio, P.; Key, H. M.; Hayashi, H.; Clark, D. S.; Hartwig, J. F. Chemoselective, Enzymatic C–H Bond Amination Catalyzed by a Cytochrome P450 Containing an Ir(Me)-PIX Cofactor. *J. Am. Chem. Soc.* **2017**, *139* (5), 1750–1753. https://doi.org/10.1021/jacs.6b11410.

(49) Sugimoto, H.; Kitayama, K.; Mori, S.; Itoh, S. An Osmium(III)/Osmium(V) Redox Couple Generating OsV(O)(OH) Center for Cis-1,2-Dihydroxylation of Alkenes with H2O2: Os Complex with a Nitrogen-Based Tetradentate Ligand. *J. Am. Chem. Soc.* **2012**, *134* (46), 19270–19280. https://doi.org/10.1021/ja309566c.

(50) Qi, D.; Tann, C.-M.; Haring, D.; Distefano, M. D. Generation of New Enzymes via Covalent Modification of Existing Proteins. *Chem. Rev.* **2001**, *101* (10), 3081–3112. https://doi.org/10.1021/cr000059o.

(51) Davies, R. R.; Distefano, M. D. A Semisynthetic Metalloenzyme Based on a Protein Cavity That Catalyzes the Enantioselective Hydrolysis of Ester and Amide Substrates. *J. Am. Chem. Soc.* **1997**, *119* (48), 11643–11652. https://doi.org/10.1021/ja970820k.

(52) Kruithof, C. A.; Casado, M. A.; Guillena, G.; Egmond, M. R.; van der Kerk-van Hoof, A.; Heck, A. J. R.; Klein Gebbink, R. J. M.; van Koten, G. Lipase Active-Site-Directed Anchoring of Organometallics: Metallopincer/Protein Hybrids. *Chem. – Eur. J.* **2005**, *11* (23), 6869–6877. https://doi.org/10.1002/chem.200500671.

(53) Panella, L.; Broos, J.; Jin, J.; Fraaije, M. W.; Janssen, D. B.; Jeronimus-Stratingh, M.; Feringa, B. L.; Minnaard, A. J.; Vries, J. G. de. Merging Homogeneous Catalysis with Biocatalysis; Papain as Hydrogenation Catalyst. *Chem. Commun.* **2005**, No. 45, 5656–5658. https://doi.org/10.1039/B512138H.

(54) Bertozzi, C. R. A Decade of Bioorthogonal Chemistry. *Acc. Chem. Res.* **2011**, *44* (9), 651–653. https://doi.org/10.1021/ar200193f.

(55) Carey, J. R.; Ma, S. K.; Pfister, T. D.; Garner, D. K.; Kim, H. K.; Abramite, J. A.; Wang, Z.; Guo, Z.; Lu, Y. A Site-Selective Dual Anchoring Strategy for Artificial Metalloprotein Design. *J. Am. Chem. Soc.* **2004**, *126* (35), 10812–10813. https://doi.org/10.1021/ja046908x.

(56) Talbi, B.; Haquette, P.; Martel, A.; Montigny, F. de; Fosse, C.; Cordier, S.; Roisnel, T.; Jaouen, G.; Salmain, M. (H6-Arene) Ruthenium(II) Complexes and Metallo-Papain Hybrid as Lewis Acid Catalysts of Diels–Alder Reaction in Water. *Dalton Trans.* 2010, *39* (24), 5605–5607. https://doi.org/10.1039/C001630F.

(57) Roelfes, G. LmrR: A Privileged Scaffold for Artificial Metalloenzymes. *Acc. Chem. Res.* 2019, *52* (3), 545–556. https://doi.org/10.1021/acs.accounts.9b00004.

(58) Laureanti, J. A.; Buchko, G. W.; Katipamula, S.; Su, Q.; Linehan, J. C.; Zadvornyy, O. A.; Peters, J. W.; O'Hagan, M. Protein Scaffold Activates Catalytic CO2 Hydrogenation by a Rhodium Bis(Diphosphine) Complex. *ACS Catal.* 2019, *9* (1), 620–625. https://doi.org/10.1021/acscatal.8b02615.

(59) Proceedings of the Chemical Society. October 1961. *Proc. Chem. Soc.* 1961, No. October, 357–396. https://doi.org/10.1039/PS9610000357.

(60) Kolb, H. C.; Finn, M. G.; Sharpless, K. B. Click Chemistry: Diverse Chemical Function from a Few Good Reactions. *Angew. Chem. Int. Ed.* 2001, *40* (11), 2004–2021. https://doi.org/10.1002/1521-3773(20010601)40:11<2004::AID-ANIE2004>3.0.CO;2-5.

(61) Zhang, L.; Chen, X.; Xue, P.; Sun, H. H. Y.; Williams, I. D.; Sharpless, K. B.; Fokin, V. V.; Jia, G. Ruthenium-Catalyzed Cycloaddition of Alkynes and Organic Azides. *J. Am. Chem. Soc.* 2005, *127* (46), 15998–15999. https://doi.org/10.1021/ja054114s.

(62) McNulty, J.; Keskar, K.; Vemula, R. The First Well-Defined Silver(I)-Complex-Catalyzed Cycloaddition of Azides onto Terminal Alkynes at Room Temperature. *Chem. – Eur. J.* 2011, *17* (52), 14727–14730. https://doi.org/10.1002/chem.201103244.

(63) M. Palomo, J. Click Reactions in Protein Chemistry: From the Preparation of Semisynthetic Enzymes to New Click Enzymes. *Org. Biomol. Chem.* 2012, *10* (47), 9309–9318. https://doi.org/10.1039/C2OB26409A.

(64) Milles, S.; Tyagi, S.; Banterle, N.; Koehler, C.; VanDelinder, V.; Plass, T.; Neal, A. P.; Lemke, E. A. Click Strategies for Single-Molecule Protein Fluorescence. *J. Am. Chem. Soc.* 2012, *134* (11), 5187–5195. https://doi.org/10.1021/ja210587q.

(65) Lewis, J. C. Artificial Metalloenzymes and Metallopeptide Catalysts for Organic Synthesis. *ACS Catal.* 2013, *3* (12), 2954–2975. https://doi.org/10.1021/cs400806a.

(66) Haquette, P.; Dumat, B.; Talbi, B.; Arbabi, S.; Renaud, J.-L.; Jaouen, G.; Salmain, M. Synthesis of N-Functionalized 2,2′-Dipyridylamine Ligands, Complexation to Ruthenium (II) and Anchoring of Complexes to Papain from Papaya Latex. *J. Organomet. Chem.* 2009, *694* (6), 937–941. https://doi.org/10.1016/j.jorganchem.2008.11.052.

(67) Doble, M. V.; Jarvis, A. G.; Ward, A. C. C.; Colburn, J. D.; Götze, J. P.; Bühl, M.; Kamer, P. C. J. Artificial Metalloenzymes as Catalysts for Oxidative Lignin Degradation. *ACS Sustain. Chem. Eng.* 2018, *6* (11), 15100–15107. https://doi.org/10.1021/acssuschemeng.8b03568.

(68) Faiella, M.; Maglio, O.; Nastri, F.; Lombardi, A.; Lista, L.; Hagen, W. R.; Pavone, V. De Novo Design, Synthesis and Characterisation of MP3, A New Catalytic Four-Helix Bundle Hemeprotein. *Chem. – Eur. J.* 2012, *18* (50), 15960–15971. https://doi.org/10.1002/chem.201201404.

(69) Berwick, M. R.; Lewis, D. J.; Jones, A. W.; Parslow, R. A.; Dafforn, T. R.; Cooper, H. J.; Wilkie, J.; Pikramenou, Z.; Britton, M. M.; Peacock, A. F. A. De Novo Design of Ln(III) Coiled Coils for Imaging Applications. *J. Am. Chem. Soc.* 2014, *136* (4), 1166–1169. https://doi.org/10.1021/ja408741h.

(70) Ln, S.; Oj, D.; H, C.; Sa, W.; Afa, P. Location-Dependent Lanthanide Selectivity Engineered into Structurally Characterized Designed Coiled Coils. *Angew. Chem. Int. Ed Engl.* 2021, *60* (46). https://doi.org/10.1002/anie.202110500.

(71) Lombardi, A.; Pirro, F.; Maglio, O.; Chino, M.; DeGrado, W. F. De Novo Design of Four-Helix Bundle Metalloproteins: One Scaffold, Diverse Reactivities. *Acc. Chem. Res.* 2019, *52* (5), 1148–1159. https://doi.org/10.1021/acs.accounts.8b00674.

(72) Lee, K.-H.; Cabello, C.; Hemmingsen, L.; Marsh, E. N. G.; Pecoraro, V. L. Using Nonnatural Amino Acids to Control Metal-Coordination Number in Three-Stranded Coiled Coils. *Angew. Chem.* 2006, *118* (18), 2930–2934. https://doi.org/10.1002/ange.200504548.

(73) Tegoni, M.; Yu, F.; Bersellini, M.; Penner-Hahn, J. E.; Pecoraro, V. L. Designing a Functional Type 2 Copper Center That Has Nitrite Reductase Activity within α-Helical Coiled Coils. *Proc. Natl. Acad. Sci.* 2012, *109* (52), 21234–21239. https://doi.org/10.1073/pnas.1212893110.

(74) Leone, L.; D'Alonzo, D.; Maglio, O.; Pavone, V.; Nastri, F.; Lombardi, A. Highly Selective Indole Oxidation Catalyzed by a Mn-Containing Artificial Mini-Enzyme. *ACS Catal.* 2021, *11* (15), 9407–9417. https://doi.org/10.1021/acscatal.1c01985.

(75) Bos, J.; Browne, W. R.; Driessen, A. J. M.; Roelfes, G. Supramolecular Assembly of Artificial Metalloenzymes Based on the Dimeric Protein LmrR as Promiscuous Scaffold. *J. Am. Chem. Soc.* 2015, *137* (31), 9796–9799. https://doi.org/10.1021/jacs.5b05790.

(76) Villarino, L.; Splan, K. E.; Reddem, E.; Alonso-Cotchico, L.; Gutiérrez de Souza, C.; Lledós, A.; Maréchal, J.-D.; Thunnissen, A.-M. W. H.; Roelfes, G. An Artificial Heme Enzyme for Cyclopropanation Reactions. *Angew. Chem. Int. Ed.* 2018, *57* (26), 7785–7789. https://doi.org/10.1002/anie.201802946.

(77) Rousselot-Pailley, P.; Bochot, C.; Marchi-Delapierre, C.; Jorge-Robin, A.; Martin, L.; Fontecilla-Camps, J. C.; Cavazza, C.; Ménage, S. The Protein Environment Drives Selectivity for Sulfide Oxidation by an Artificial Metalloenzyme. *ChemBioChem* 2009, *10* (3), 545–552. https://doi.org/10.1002/cbic.200800595.

(78) Ueno, T.; Koshiyama, T.; Ohashi, M.; Kondo, K.; Kono, M.; Suzuki, A.; Yamane, T.; Watanabe, Y. Coordinated Design of Cofactor and Active Site Structures in Development of New Protein Catalysts. *J. Am. Chem. Soc.* 2005, *127* (18), 6556–6562. https://doi.org/10.1021/ja045995q.

(79) *The structure of the periplasmic nickel-binding protein NikA provides insights for artificial metalloenzyme design | SpringerLink*. https://link.springer.com/article/10.1007/s00775-012-0899-7 (accessed 2020-09-07).

(80) Kokubo, T.; Sugimoto, T.; Uchida, T.; Tanimoto, S.; Okano, M. The Bovine Serum Albumin–2-Phenylpropane-1,2-Diolatodioxo-Somium(VI) Complex as an Enantioselective Catalyst for Cis-Hydroxylation of Alkenes. *J. Chem. Soc. Chem. Commun.* 1983, No. 14, 769–770. https://doi.org/10.1039/C39830000769.

(81) Oliveri, V.; Vecchio, G. A Novel Artificial Superoxide Dismutase: Non-Covalent Conjugation of Albumin with a MnIII Salophen Type Complex. *Eur. J. Med. Chem.* 2011, *46* (3), 961–965. https://doi.org/10.1016/j.ejmech.2010.12.023.

(82) Tang, J.; Huang, F.; Wei, Y.; Bian, H.; Zhang, W.; Liang, H. Bovine Serum Albumin–Cobalt(II) Schiff Base Complex Hybrid: An Efficient Artificial Metalloenzyme for Enantioselective Sulfoxidation Using Hydrogen Peroxide. *Dalton Trans.* 2016, *45* (19), 8061–8072. https://doi.org/10.1039/C5DT04507J.

(83) Zhang, J.-L.; Garner, D. K.; Liang, L.; Chen, Q.; Lu, Y. Protein Scaffold of a Designed Metalloenzyme Enhances the Chemoselectivity in Sulfoxidation of Thioanisole. *Chem. Commun.* 2008, No. 14, 1665–1667. https://doi.org/10.1039/B718915J.

(84) Eitinger, T.; Wolfram, L.; Degen, O.; Anthon, C. A Ni2+ Binding Motif Is the Basis of High Affinity Transport of the Alcaligenes Eutrophus Nickel Permease *. *J. Biol. Chem.* 1997, *272* (27), 17139–17144. https://doi.org/10.1074/jbc.272.27.17139.

(85) Wolfram, L.; Friedrich, B.; Eitinger, T. The Alcaligenes Eutrophus Protein HoxN Mediates Nickel Transport in Escherichia Coli. *J. Bacteriol.* 1995, *177* (7), 1840–1843. https://doi.org/10.1128/jb.177.7.1840-1843.1995.

(86) Heddle, J.; Scott, D. J.; Unzai, S.; Park, S.-Y.; Tame, J. R. H. Crystal Structures of the Liganded and Unliganded Nickel-Binding Protein NikA from Escherichia Coli*. *J. Biol. Chem.* 2003, *278* (50), 50322–50329. https://doi.org/10.1074/jbc.M307941200.

(87) De Pina, K.; Navarro, C.; Mcwalter, L.; Boxer, D. H.; Price, N. C.; Kelly, S. M.; Mandrand-Berthelot, M.-A.; Wu, L.-F. Purification and Characterization of the Periplasmic Nickel-Binding Protein NikA of Escherichia Coli K12. *Eur. J. Biochem.* 1995, *227* (3), 857–865. https://doi.org/10.1111/j.1432-1033.1995.0857p.x.

(88) Cherrier, M. V.; Girgenti, E.; Amara, P.; Iannello, M.; Marchi-Delapierre, C.; Fontecilla-Camps, J. C.; Ménage, S.; Cavazza, C. The Structure of the Periplasmic Nickel-Binding Protein NikA Provides Insights for Artificial Metalloenzyme Design. *JBIC J. Biol. Inorg. Chem.* 2012, *17* (5), 817–829. https://doi.org/10.1007/s00775-012-0899-7.

(89) Cherrier, M. V.; Cavazza, C.; Bochot, C.; Lemaire, D.; Fontecilla-Camps, J. C. Structural Characterization of a Putative Endogenous Metal Chelator in the Periplasmic Nickel Transporter NikA. *Biochemistry* 2008, *47* (38), 9937–9943. https://doi.org/10.1021/bi801051y.

(90) Lebrette, H.; Iannello, M.; Fontecilla-Camps, J. C.; Cavazza, C. The Binding Mode of Ni-(L-His)2 in NikA Revealed by X-Ray Crystallography. *J. Inorg. Biochem.* 2013, *121*, 16–18. https://doi.org/10.1016/j.jinorgbio.2012.12.010.

(91) Chivers, P. T.; Benanti, E. L.; Heil-Chapdelaine, V.; Iwig, J. S.; Rowe, J. L. Identification of Ni-(l-His)2 as a Substrate for NikABCDE-Dependent Nickel Uptake in Escherichia Coli†. *Metallomics* 2012, *4* (10), 1043–1050. https://doi.org/10.1039/c2mt20139a.

(92) Cavazza, C.; Martin, L.; Laffly, E.; Lebrette, H.; Cherrier, M. V.; Zeppieri, L.; Richaud, P.; Carrière, M.; Fontecilla-Camps, J. C. Histidine 416 of the Periplasmic Binding Protein NikA Is Essential for Nickel Uptake in Escherichia Coli. *FEBS Lett.* 2011, *585* (4), 711–715. https://doi.org/10.1016/j.febslet.2011.01.038.

(93) Lopez, S.; Rondot, L.; Cavazza, C.; Iannello, M.; Boeri-Erba, E.; Burzlaff, N.; Strinitz, F.; Jorge-Robin, A.; Marchi-Delapierre, C.; Ménage, S. Efficient Conversion of Alkenes to Chlorohydrins by a Ru-Based Artificial Enzyme. *Chem. Commun.* 2017, *53* (25), 3579–3582. https://doi.org/10.1039/C6CC08873B.

(94) Cavazza, C.; Bochot, C.; Rousselot-Pailley, P.; Carpentier, P.; Cherrier, M. V.; Martin, L.; Marchi-Delapierre, C.; Fontecilla-Camps, J. C.; Ménage, S. Crystallographic Snapshots of the Reaction of Aromatic C–H with O2 Catalysed by a Protein-Bound Iron Complex. *Nat. Chem.* 2010, *2* (12), 1069–1076. https://doi.org/10.1038/nchem.841.

(95) Lopez, S.; Rondot, L.; Leprêtre, C.; Marchi-Delapierre, C.; Ménage, S.; Cavazza, C. Cross-Linked Artificial Enzyme Crystals as Heterogeneous Catalysts for Oxidation Reactions. *J. Am. Chem. Soc.* 2017, *139* (49), 17994–18002. https://doi.org/10.1021/jacs.7b09343.

(96) Lopez, S.; Marchi-Delapierre, C.; Cavazza, C.; Ménage, S. A Selective Sulfide Oxidation Catalyzed by Heterogeneous Artificial Metalloenzymes Iron@NikA. *Chem. – Eur. J.* 2020, *26* (70), 16633–16638. https://doi.org/10.1002/chem.202003746.

(97) Kawakami, N.; Shoji, O.; Watanabe, Y. Use of Perfluorocarboxylic Acids To Trick Cytochrome P450BM3 into Initiating the Hydroxylation of Gaseous Alkanes. *Angew. Chem. Int. Ed.* 2011, *50* (23), 5315–5318. https://doi.org/10.1002/anie.201007975.

(98) Zilly, F. E.; Acevedo, J. P.; Augustyniak, W.; Deege, A.; Häusig, U. W.; Reetz, M. T. Corrigendum: Tuning a P450 Enzyme for Methane Oxidation. *Angew. Chem. Int. Ed.* 2013, *52* (51), 13503–13503. https://doi.org/10.1002/anie.201309655.

(99) Zilly, F. E.; Acevedo, J. P.; Augustyniak, W.; Deege, A.; Häusig, U. W.; Reetz, M. T. Tuning a P450 Enzyme for Methane Oxidation. *Angew. Chem. Int. Ed.* 2011, *50* (12), 2720–2724. https://doi.org/10.1002/anie.201006587.

(100) Karasawa, M.; Yonemura, K.; Stanfield, J. K.; Suzuki, K.; Shoji, O. Designer Outer Membrane Protein Facilitates Uptake of Decoy Molecules into a Cytochrome P450BM3-Based Whole-Cell Biocatalyst. *Angew. Chem. Int. Ed.* 2022, *61* (7), e202111612. https://doi.org/10.1002/anie.202111612.

(101) Kariyawasam, K.; Di Meo, T.; Hammerer, F.; Valerio-Lepiniec, M.; Sciortino, G.; Maréchal, J.-D.; Minard, P.; Mahy, J.-P.; Urvoas, A.; Ricoux, R. An Artificial Hemoprotein with Inducible Peroxidase- and Monooxygenase-Like Activities. *Chem. – Eur. J.* 2020, *26* (65), 14929–14937. https://doi.org/10.1002/chem.202002434.

(102) A. Sheldon, R.; Pelt, S. van. Enzyme Immobilisation in Biocatalysis: Why, What and How. *Chem. Soc. Rev.* 2013, *42* (15), 6223–6235. https://doi.org/10.1039/C3CS60075K.

(103) Guisan, J. M.; López-Gallego, F.; Bolivar, J. M.; Rocha-Martín, J.; Fernandez-Lorente, G. The Science of Enzyme Immobilization. In *Immobilization of Enzymes and Cells: Methods and Protocols*; Guisan, J. M., Bolivar, J. M., López-Gallego, F., Rocha-Martín, J., Eds.; Methods in Molecular Biology; Springer US: New York, NY, 2020; pp 1–26. https://doi.org/10.1007/978-1-0716-0215-7_1.

(104) Cao, L.; Langen, L. van; Sheldon, R. A. Immobilised Enzymes: Carrier-Bound or Carrier-Free? *Curr. Opin. Biotechnol.* 2003, *14* (4), 387–394. https://doi.org/10.1016/S0958-1669(03)00096-X.

(105) *Carrier-bound Immobilized Enzymes: Principles, Application and Design | Wiley*. Wiley.com. https://www.wiley.com/en-fr/Carrier+bound+Immobilized+Enzymes%3A+Principles%2C+Application+and+Design-p-9783527312320 (accessed 2020-09-09).

(106) Mosbach, K.; Mattiasson, B. Immobilized Model Systems of Enzyme Sequences. In *Current Topics in Cellular Regulation*; Horecker, B. L., Stadtman, E. R., Eds.; Academic Press, 1978; Vol. 14, pp 197–241. https://doi.org/10.1016/B978-0-12-152814-0.50009-5.

(107) Brady, D.; Jordaan, J. Advances in Enzyme Immobilisation. *Biotechnol. Lett.* 2009, *31* (11), 1639. https://doi.org/10.1007/s10529-009-0076-4.

(108) Gill, I.; Ballesteros, A. Encapsulation of Biologicals within Silicate, Siloxane, and Hybrid Sol- Gel Polymers: An Efficient and Generic Approach. *J. Am. Chem. Soc.* 1998, *120* (34), 8587–8598. https://doi.org/10.1021/ja9814568.

(109) Li, P.; Moon, S.-Y.; Guelta, M. A.; Harvey, S. P.; Hupp, J. T.; Farha, O. K. Encapsulation of a Nerve Agent Detoxifying Enzyme by a Mesoporous Zirconium Metal–Organic Framework Engenders Thermal and Long-Term Stability. *J. Am. Chem. Soc.* 2016, *138* (26), 8052–8055. https://doi.org/10.1021/jacs.6b03673.

(110) Drout, R. J.; Robison, L.; Farha, O. K. Catalytic Applications of Enzymes Encapsulated in Metal–Organic Frameworks. *Coord. Chem. Rev.* 2019, *381*, 151–160. https://doi.org/10.1016/j.ccr.2018.11.009.

(111) Jegan Roy, J.; Emilia Abraham, T. Strategies in Making Cross-Linked Enzyme Crystals. *Chem. Rev.* 2004, *104* (9), 3705–3722. https://doi.org/10.1021/cr0204707.

(112) *Stabilized soluble enzymes | SpringerLink*. https://link.springer.com/chapter/10.1007/3540092625_7 (accessed 2022-11-22).

(113) Broun, G.; Selegny, E.; Avrameas, S.; Thomas, D. Enzymatically Active Membranes: Some Properties of Cellophane Membranes Supporting Cross-Linked Enzymes. *Biochim. Biophys. Acta BBA - Enzymol.* 1969, *185* (1), 260–262. https://doi.org/10.1016/0005-2744(69)90305-2.

(114) Erarslan, A.; Ertan, H. Thermostabilization of Penicillin G Acylase Obtained from a Mutant of Escherichia Coli ATCC 11105 by Bisimidoesters as Homobifunctional Cross-Linking Agents. *Enzyme Microb. Technol.* 1995, *17* (7), 629–635. https://doi.org/10.1016/0141-0229(94)00100-6.

(115) Kazan, D.; Ertan, H.; Erarslan, A. Stabilization of Escherichia Coli Penicillin G Acylase against Thermal Inactivation by Cross-Linking with Dextran Dialdehyde Polymers. *Appl. Microbiol. Biotechnol.* 1997, *48* (2), 191–197. https://doi.org/10.1007/s002530051037.

(116) Quiocho, F. A.; Richards, F. M. Intermolecular Cross Linking of a Protein in the Crystalline State: Carboxypeptidase-A*. *Proc. Natl. Acad. Sci.* 1964, *52* (3), 833–839. https://doi.org/10.1073/pnas.52.3.833.

(117) Richards, F. M.; Knowles, J. R. Glutaraldehyde as a Protein Cross-Linking Reagent. *J. Mol. Biol.* 1968, *37* (1), 231–233. https://doi.org/10.1016/0022-2836(68)90086-7.

(118) Sasvári, Z.; Asbóth, B. Crosslinking of Glucoamylases via Carbohydrates Hardly Affects Catalysis but Impairs Stability. *Biotechnol. Bioeng.* 1999, *63* (4), 459–463. https://doi.org/10.1002/(SICI)1097-0290(19990520)63:4<459::AID-BIT9>3.0.CO;2-I.

(119) Gupta, M. N. Cross-Linking Techniques. In *Biocatalyst Design for Stability and Specificity*; ACS Symposium Series; American Chemical Society, 1993; Vol. 516, pp 307–324. https://doi.org/10.1021/bk-1993-0516.ch025.

(120) Margolin, A. L.; Navia, M. A. Protein Crystals as Novel Catalytic Materials. *Angew. Chem. Int. Ed.* 2001, *40* (12), 2204–2222. https://doi.org/10.1002/1521-3773(20010618)40:12<2204::AID-ANIE2204>3.0.CO;2-J.

(121) Lee, K. M.; Blaghen, M.; Samama, J.-P.; Biellmann, J.-F. Crosslinked Crystalline Horse Liver Alcohol Dehydrogenase as a Redox Catalyst: Activity and Stability toward Organic Solvent. *Bioorganic Chem.* 1986, *14* (2), 202–210. https://doi.org/10.1016/0045-2068(86)90031-3.

(122) Tabe, H.; Abe, S.; Hikage, T.; Kitagawa, S.; Ueno, T. Porous Protein Crystals as Catalytic Vessels for Organometallic Complexes. *Chem. – Asian J.* 2014, *9* (5), 1373–1378. https://doi.org/10.1002/asia.201301347.

(123) Cao, L.; van Rantwijk, F.; Sheldon, R. A. Cross-Linked Enzyme Aggregates: A Simple and Effective Method for the Immobilization of Penicillin Acylase. *Org. Lett.* 2000, *2* (10), 1361–1364. https://doi.org/10.1021/ol005593x.

(124) Cao, L.; van Langen, L. M.; van Rantwijk, F.; Sheldon, R. A. Cross-Linked Aggregates of Penicillin Acylase: Robust Catalysts for the Synthesis of β-Lactam Antibiotics. *J. Mol.*

Catal. B Enzym. 2001, *11* (4), 665–670. https://doi.org/10.1016/S1381-1177(00)00078-3.

(125) López-Serrano, P.; Cao, L.; van Rantwijk, F.; Sheldon, R. A. Cross-Linked Enzyme Aggregates with Enhanced Activity: Application to Lipases. *Biotechnol. Lett.* 2002, *24* (16), 1379–1383. https://doi.org/10.1023/A:1019863314646.

(126) Sheldon, R. A.; Schoevaart, R.; Langen, L. M. V. Cross-Linked Enzyme Aggregates (CLEAs): A Novel and Versatile Method for Enzyme Immobilization (a Review). *Biocatal. Biotransformation* 2005, *23* (3–4), 141–147. https://doi.org/10.1080/10242420500183378.

(127) Schrittwieser, J. H.; Velikogne, S.; Hall, M.; Kroutil, W. Artificial Biocatalytic Linear Cascades for Preparation of Organic Molecules. *Chem. Rev.* 2018, *118* (1), 270–348. https://doi.org/10.1021/acs.chemrev.7b00033.

(128) Ueberbacher, B. T.; Hall, M.; Faber, K. Electrophilic and Nucleophilic Enzymatic Cascade Reactions in Biosynthesis. *Nat. Prod. Rep.* 2012, *29* (3), 337–350. https://doi.org/10.1039/C2NP00078D.

(129) Hammer, S. C.; Marjanovic, A.; Dominicus, J. M.; Nestl, B. M.; Hauer, B. Squalene Hopene Cyclases Are Protonases for Stereoselective Brønsted Acid Catalysis. *Nat. Chem. Biol.* 2015, *11* (2), 121–126. https://doi.org/10.1038/nchembio.1719.

(130) Gavezzotti, P.; Bertacchi, F.; Fronza, G.; Křen, V.; Monti, D.; Riva, S. Laccase-Catalyzed Dimerization of Piceid, a Resveratrol Glucoside, and Its Further Enzymatic Elaboration. *Adv. Synth. Catal.* 2015, *357* (8), 1831–1839. https://doi.org/10.1002/adsc.201500185.

(131) Navarra, C.; Goodwin, C.; Burton, S.; Danieli, B.; Riva, S. Laccase-Mediated Oxidation of Phenolic Derivatives. *J. Mol. Catal. B Enzym.* 2010, *65* (1), 52–57. https://doi.org/10.1016/j.molcatb.2009.12.016.

(132) Ponzoni, C.; Beneventi, E.; Cramarossa, M. R.; Raimondi, S.; Trevisi, G.; Pagnoni, U. M.; Riva, S.; Forti, L. Laccase-Catalyzed Dimerization of Hydroxystilbenes. *Adv. Synth. Catal.* 2007, *349* (8–9), 1497–1506. https://doi.org/10.1002/adsc.200700043.

(133) Díaz-Rodríguez, A.; Borzęcka, W.; Lavandera, I.; Gotor, V. Stereodivergent Preparation of Valuable γ- or δ-Hydroxy Esters and Lactones through One-Pot Cascade or Tandem Chemoenzymatic Protocols. *ACS Catal.* 2014, *4* (2), 386–393. https://doi.org/10.1021/cs4010024.

(134) Bornadel, A.; Hatti-Kaul, R.; Hollmann, F.; Kara, S. A Bi-Enzymatic Convergent Cascade for ε-Caprolactone Synthesis Employing 1,6-Hexanediol as a 'Double-Smart Cosubstrate.' *ChemCatChem* 2015, *7* (16), 2442–2445. https://doi.org/10.1002/cctc.201500511.

(135) Knaus, T.; Mutti, F. G.; Humphreys, L. D.; Turner, N. J.; Scrutton, N. S. Systematic Methodology for the Development of Biocatalytic Hydrogen-Borrowing Cascades: Application to the Synthesis of Chiral α-Substituted Carboxylic Acids from α-Substituted

α,β-Unsaturated Aldehydes. *Org. Biomol. Chem.* **2014**, *13* (1), 223–233. https://doi.org/10.1039/C4OB02282C.

(136) Paul, C. E.; Lavandera, I.; Gotor-Fernández, V.; Kroutil, W.; Gotor, V. Escherichia Coli/ADH-A: An All-Inclusive Catalyst for the Selective Biooxidation and Deracemisation of Secondary Alcohols. *ChemCatChem* **2013**, *5* (12), 3875–3881. https://doi.org/10.1002/cctc.201300409.

(137) Parmeggiani, F.; Ahmed, S. T.; Thompson, M. P.; Weise, N. J.; Galman, J. L.; Gahloth, D.; Dunstan, M. S.; Leys, D.; Turner, N. J. Single-Biocatalyst Synthesis of Enantiopure d-Arylalanines Exploiting an Engineered d-Amino Acid Dehydrogenase. *Adv. Synth. Catal.* **2016**, *358* (20), 3298–3306. https://doi.org/10.1002/adsc.201600682.

(138) Seisser, B.; Lavandera, I.; Faber, K.; Spelberg, J. H. L.; Kroutil, W. Stereo-Complementary Two-Step Cascades Using a Two-Enzyme System Leading to Enantiopure Epoxides. *Adv. Synth. Catal.* **2007**, *349* (8–9), 1399–1404. https://doi.org/10.1002/adsc.200700027.

(139) Schallmey, A.; Schallmey, M. Recent Advances on Halohydrin Dehalogenases—from Enzyme Identification to Novel Biocatalytic Applications. *Appl. Microbiol. Biotechnol.* **2016**, *100* (18), 7827–7839. https://doi.org/10.1007/s00253-016-7750-y.

(140) You, Z.-Y.; Liu, Z.-Q.; Zheng, Y.-G. Properties and Biotechnological Applications of Halohydrin Dehalogenases: Current State and Future Perspectives. *Appl. Microbiol. Biotechnol.* **2013**, *97* (1), 9–21. https://doi.org/10.1007/s00253-012-4523-0.

(141) Bechi, B.; Herter, S.; McKenna, S.; Riley, C.; Leimkühler, S.; Turner, N. J.; Carnell, A. J. Catalytic Bio–Chemo and Bio–Bio Tandem Oxidation Reactions for Amide and Carboxylic Acid Synthesis. *Green Chem.* **2014**, *16* (10), 4524–4529. https://doi.org/10.1039/C4GC01321B.

(142) McKenna, S. M.; Leimkühler, S.; Herter, S.; Turner, N. J.; Carnell, A. J. Enzyme Cascade Reactions: Synthesis of Furandicarboxylic Acid (FDCA) and Carboxylic Acids Using Oxidases in Tandem. *Green Chem.* **2015**, *17* (6), 3271–3275. https://doi.org/10.1039/C5GC00707K.

(143) Pérez-Sánchez, M.; Müller, C. R.; Domínguez de María, P. Multistep Oxidase–Lyase Reactions: Synthesis of Optically Active 2-Hydroxyketones by Using Biobased Aliphatic Alcohols. *ChemCatChem* **2013**, *5* (8), 2512–2516. https://doi.org/10.1002/cctc.201300093.

(144) Guterl, J.-K.; Garbe, D.; Carsten, J.; Steffler, F.; Sommer, B.; Reiße, S.; Philipp, A.; Haack, M.; Rühmann, B.; Koltermann, A.; Kettling, U.; Brück, T.; Sieber, V. Cell-Free Metabolic Engineering: Production of Chemicals by Minimized Reaction Cascades. *ChemSusChem* **2012**, *5* (11), 2165–2172. https://doi.org/10.1002/cssc.201200365.

(145) Qi, P.; You, C.; Zhang, Y.-H. P. One-Pot Enzymatic Conversion of Sucrose to Synthetic Amylose by Using Enzyme Cascades. *ACS Catal.* **2014**, *4* (5), 1311–1317. https://doi.org/10.1021/cs400961a.

(146) France, S. P.; Hussain, S.; Hill, A. M.; Hepworth, L. J.; Howard, R. M.; Mulholland, K. R.; Flitsch, S. L.; Turner, N. J. One-Pot Cascade Synthesis of Mono- and Disubstituted Piperidines and Pyrrolidines Using Carboxylic Acid Reductase (CAR), ω-Transaminase (ω-TA), and Imine Reductase (IRED) Biocatalysts. *ACS Catal.* 2016, *6* (6), 3753–3759. https://doi.org/10.1021/acscatal.6b00855.

(147) Agudo, R.; Reetz, M. T. Designer Cells for Stereocomplementary de Novo Enzymatic Cascade Reactions Based on Laboratory Evolution. *Chem. Commun.* 2013, *49* (93), 10914–10916. https://doi.org/10.1039/C3CC46229C.

(148) Tenbrink, K.; Seßler, M.; Schatz, J.; Gröger, H. Combination of Olefin Metathesis and Enzymatic Ester Hydrolysis in Aqueous Media in a One-Pot Synthesis. *Adv. Synth. Catal.* 2011, *353* (13), 2363–2367. https://doi.org/10.1002/adsc.201100403.

(149) Wang, Z. J.; Clary, K. N.; Bergman, R. G.; Raymond, K. N.; Toste, F. D. A Supramolecular Approach to Combining Enzymatic and Transition Metal Catalysis. *Nat. Chem.* 2013, *5* (2), 100–103. https://doi.org/10.1038/nchem.1531.

(150) Ahmed, S. T.; Parmeggiani, F.; Weise, N. J.; Flitsch, S. L.; Turner, N. J. Synthesis of Enantiomerically Pure Ring-Substituted l-Pyridylalanines by Biocatalytic Hydroamination. *Org. Lett.* 2016, *18* (21), 5468–5471. https://doi.org/10.1021/acs.orglett.6b02559.

(151) Okamoto, Y.; Köhler, V.; Ward, T. R. An NAD(P)H-Dependent Artificial Transfer Hydrogenase for Multienzymatic Cascades. *J. Am. Chem. Soc.* 2016, *138* (18), 5781–5784. https://doi.org/10.1021/jacs.6b02470.

(152) Köhler, V.; Wilson, Y. M.; Dürrenberger, M.; Ghislieri, D.; Churakova, E.; Quinto, T.; Knörr, L.; Häussinger, D.; Hollmann, F.; Turner, N. J.; Ward, T. R. Synthetic Cascades Are Enabled by Combining Biocatalysts with Artificial Metalloenzymes. *Nat. Chem.* 2013, *5* (2), 93–99. https://doi.org/10.1038/nchem.1498.

(153) Lopes, E. J. C.; Ribeiro, A. P. C.; Martins, L. M. D. R. S. New Trends in the Conversion of CO2 to Cyclic Carbonates. *Catalysts* 2020, *10* (5), 479. https://doi.org/10.3390/catal10050479.

(154) Monie, F.; Grignard, B.; Thomassin, J.-M.; Mereau, R.; Tassaing, T.; Jerome, C.; Detrembleur, C. Chemo- and Regioselective Additions of Nucleophiles to Cyclic Carbonates for the Preparation of Self-Blowing Non-Isocyanate Polyurethane Foams. *Angew. Chem.* 2020, *132* (39), 17181–17189. https://doi.org/10.1002/ange.202006267.

(155) Clements, J. H. Reactive Applications of Cyclic Alkylene Carbonates. *Ind. Eng. Chem. Res.* 2003, *42* (4), 663–674. https://doi.org/10.1021/ie020678i.

(156) Balas, M.; Villanneau, R.; Launay, F. Bibliographic Survey of the Strategies Implemented for the One-Pot Synthesis of Cyclic Carbonates from Styrene and Other Alkenes Using CO2 and Green Oxidants. *J. CO2 Util.* 2022, *65*, 102215. https://doi.org/10.1016/j.jcou.2022.102215.

(157) Deng, L.; Sun, W.; Shi, Z.; Qian, W.; Su, Q.; Dong, L.; He, H.; Li, Z.; Cheng, W. Highly Synergistic Effect of Ionic Liquids and Zn-Based Catalysts for Synthesis of Cyclic Carbonates from Urea and Diols. *J. Mol. Liq.* 2020, *316*, 113883. https://doi.org/10.1016/j.molliq.2020.113883.

(158) Deng, L.; Su, Q.; Tan, X.; Wang, Y.; Dong, L.; He, H.; Li, Z.; Cheng, W. Tunable Imidazolium Ionic Liquids as Efficient Catalysts for Conversion of Urea into Cyclic Carbonates. *Mol. Catal.* 2022, *519*, 112153. https://doi.org/10.1016/j.mcat.2022.112153.

(159) Joergensen, K. A. Transition-Metal-Catalyzed Epoxidations. *Chem. Rev.* 1989, *89* (3), 431–458. https://doi.org/10.1021/cr00093a001.

(160) Xia, Q.-H.; Ge, H.-Q.; Ye, C.-P.; Liu, Z.-M.; Su, K.-X. Advances in Homogeneous and Heterogeneous Catalytic Asymmetric Epoxidation. *Chem. Rev.* 2005, *105* (5), 1603–1662. https://doi.org/10.1021/cr0406458.

(161) McGarrigle, E. M.; Gilheany, D. G. Chromium− and Manganese−salen Promoted Epoxidation of Alkenes. *Chem. Rev.* 2005, *105* (5), 1563–1602. https://doi.org/10.1021/cr0306945.

(162) Lane, B. S.; Burgess, K. Metal-Catalyzed Epoxidations of Alkenes with Hydrogen Peroxide. *Chem. Rev.* 2003, *103* (7), 2457–2474. https://doi.org/10.1021/cr020471z.

(163) Bryliakov, K. P. Catalytic Asymmetric Oxygenations with the Environmentally Benign Oxidants H2O2 and O2. *Chem. Rev.* 2017, *117* (17), 11406–11459. https://doi.org/10.1021/acs.chemrev.7b00167.

(164) Yuan, Y.-C.; Mellah, M.; Schulz, E.; David, O. R. P. Making Chiral Salen Complexes Work with Organocatalysts. *Chem. Rev.* 2022, *122* (9), 8841–8883. https://doi.org/10.1021/acs.chemrev.1c00912.

(165) Breuer, M.; Ditrich, K.; Habicher, T.; Hauer, B.; Keßeler, M.; Stürmer, R.; Zelinski, T. Industrial Methods for the Production of Optically Active Intermediates. *Angew. Chem. Int. Ed.* 2004, *43* (7), 788–824. https://doi.org/10.1002/anie.200300599.

(166) Fukusaki, E.-I.; Satoda, S.; Senda, S.; Omata, T. Lipase-Catalyzed Kinetic Resolution of 2,3-Epoxy-1-Tridecanol and Its Application to Facile Synthesis of (+)-Disparlure. *J. Biosci. Bioeng.* 1999, *87* (1), 103–104. https://doi.org/10.1016/S1389-1723(99)80016-4.

(167) Chartrain, M. M.; Senanayake, C. H.; Rosazza, J. P. N.; Zhang, J. Biological Resolution of Racemic Indene Oxide to (1s,2r)-Indene Oxide. WO1996012818A1, May 2, 1996. https://patents.google.com/patent/WO1996012818A1/en (accessed 2023-01-20).

(168) Lutje Spelberg, J. H.; van Hylckama Vlieg, J. E. T.; Tang, L.; Janssen, D. B.; Kellogg, R. M. Highly Enantioselective and Regioselective Biocatalytic Azidolysis of Aromatic Epoxides. *Org. Lett.* 2001, *3* (1), 41–43. https://doi.org/10.1021/ol0067540.

(169) Katsuki, T.; Sharpless, K. B. Method for Asymmetric Epoxidation. US4471130A, September 11, 1984. https://patents.google.com/patent/US4471130A/en (accessed 2023-01-20).

(170) Jr, J. C. J.; Zajacek, J. G.; Crocco, G. L. Integrated Process for Epoxidation. EP0720984B1, April 22, 1998. https://patents.google.com/patent/EP0720984B1/en (accessed 2023-01-20).

(171) Ford, D. D.; Nielsen, L. P. C.; Zuend, S. J.; Jacobsen, E. N. Mechanistic Basis for High Stereoselectivity and Broad Substrate Scope in the (Salen)Co(III)-Catalyzed Hydrolytic Kinetic Resolution. *J. Am. Chem. Soc.* 2013, *135* (41), 15595–15608. https://doi.org/10.1021/ja408027p.

(172) Nielsen, L. P. C.; Stevenson, C. P.; Blackmond, D. G.; Jacobsen, E. N. Mechanistic Investigation Leads to a Synthetic Improvement in the Hydrolytic Kinetic Resolution of Terminal Epoxides. *J. Am. Chem. Soc.* 2004, *126* (5), 1360–1362. https://doi.org/10.1021/ja038590z.

(173) Park, H.; Lee, D. Ligand Taxonomy for Bioinorganic Modeling of Dioxygen-Activating Non-Heme Iron Enzymes. *Chem. – Eur. J.* 2020, *26* (27), 5916–5926. https://doi.org/10.1002/chem.201904975.

(174) Baglia, R. A.; Zaragoza, J. P. T.; Goldberg, D. P. Biomimetic Reactivity of Oxygen-Derived Manganese and Iron Porphyrinoid Complexes. *Chem. Rev.* 2017, *117* (21), 13320–13352. https://doi.org/10.1021/acs.chemrev.7b00180.

(175) Costas, M.; Mehn, M. P.; Jensen, M. P.; Que, L. Dioxygen Activation at Mononuclear Nonheme Iron Active Sites: Enzymes, Models, and Intermediates. *Chem. Rev.* 2004, *104* (2), 939–986. https://doi.org/10.1021/cr020628n.

(176) Vicens, L.; Olivo, G.; Costas, M. Rational Design of Bioinspired Catalysts for Selective Oxidations. *ACS Catal.* 2020, *10* (15), 8611–8631. https://doi.org/10.1021/acscatal.0c02073.

(177) Oloo, W. N.; Que, L. Jr. Bioinspired Nonheme Iron Catalysts for C–H and C═C Bond Oxidation: Insights into the Nature of the Metal-Based Oxidants. *Acc. Chem. Res.* 2015, *48* (9), 2612–2621. https://doi.org/10.1021/acs.accounts.5b00053.

(178) Lyakin, O. Y.; Bryliakov, K. P.; Talsi, E. P. Non-Heme Oxoiron(V) Intermediates in Chemo-, Regio- and Stereoselective Oxidation of Organic Substrates. *Coord. Chem. Rev.* 2019, *384*, 126–139. https://doi.org/10.1016/j.ccr.2019.01.010.

(179) Chen, J.; Yoon, H.; Lee, Y.-M.; Seo, M. S.; Sarangi, R.; Fukuzumi, S.; Nam, W. Tuning the Reactivity of Mononuclear Nonheme Manganese(IV)-Oxo Complexes by Triflic Acid. *Chem. Sci.* 2015, *6* (6), 3624–3632. https://doi.org/10.1039/C5SC00535C.

(180) Hong, S.; Pfaff, F. F.; Kwon, E.; Wang, Y.; Seo, M.-S.; Bill, E.; Ray, K.; Nam, W. Spectroscopic Capture and Reactivity of a Low-Spin Cobalt(IV)-Oxo Complex Stabilized by Binding

Redox-Inactive Metal Ions. *Angew. Chem. Int. Ed.* 2014, *53* (39), 10403–10407. https://doi.org/10.1002/anie.201405874.

(181) Nam, W.; Kim, H. J.; Kim, S. H.; Ho, R. Y. N.; Valentine, J. S. Metal Complex-Catalyzed Epoxidation of Olefins by Dioxygen with Co-Oxidation of Aldehydes. A Mechanistic Study. *Inorg. Chem.* 1996, *35* (4), 1045–1049. https://doi.org/10.1021/ic950782a.

(182) Suh, Y.; Seo, M. S.; Kim, K. M.; Kim, Y. S.; Jang, H. G.; Tosha, T.; Kitagawa, T.; Kim, J.; Nam, W. Nonheme Iron(II) Complexes of Macrocyclic Ligands in the Generation of Oxoiron(IV) Complexes and the Catalytic Epoxidation of Olefins. *J. Inorg. Biochem.* 2006, *100* (4), 627–633. https://doi.org/10.1016/j.jinorgbio.2005.12.013.

(183) Lyons, C. T.; Stack, T. D. P. Recent Advances in Phenoxyl Radical Complexes of Salen-Type Ligands as Mixed-Valent Galactose Oxidase Models. *Coord. Chem. Rev.* 2013, *257* (2), 528–540. https://doi.org/10.1016/j.ccr.2012.06.003.

(184) Bernd, M. A.; Dyckhoff, F.; Hofmann, B. J.; Böth, A. D.; Schlagintweit, J. F.; Oberkofler, J.; Reich, R. M.; Kühn, F. E. Tuning the Electronic Properties of Tetradentate Iron-NHC Complexes: Towards Stable and Selective Epoxidation Catalysts. *J. Catal.* 2020. https://doi.org/10.1016/j.jcat.2020.08.037.

(185) Ahmad, I.; Shagufta; Rehman, S. Metal-Porphyrin in Epoxidation of Olefins: Recent Advances. *Tetrahedron* 2022, *104*, 132604. https://doi.org/10.1016/j.tet.2021.132604.

(186) Marchi-Delapierre, C.; Jorge-Robin, A.; Thibon, A.; Ménage, S. A New Chiral Diiron Catalyst for Enantioselective Epoxidation. *Chem. Commun.* 2007, No. 11, 1166–1168. https://doi.org/10.1039/B616172C.

(187) Chishiro, T.; Kon, Y.; Nakashima, T.; Goto, M.; Sato, K. Practical Iron-Catalyzed Hydrogen Peroxide Epoxidation of Aromatic Olefins Using a Combination of Two Kinds of Simple Picolinate Ligands under Halide-Free Reaction Conditions. *Adv. Synth. Catal.* 2014, *356* (2–3), 623–627. https://doi.org/10.1002/adsc.201300774.

(188) Kiani, S.; Tapper, A.; Staples, R. J.; Stavropoulos, P. Functional Aspects of Gif-Type Oxidation of Hydrocarbons Mediated by Iron Picolinate H2O2-Dependent Systems: Evidence for the Generation of Carbon- and Oxygen-Centered Radicals. *J. Am. Chem. Soc.* 2000, *122* (31), 7503–7517. https://doi.org/10.1021/ja000063h.

(189) Yamada, T.; Imagawa, K.; Nagata, T.; Mukaiyama, T. Enantioselective Epoxidation of Unfunctionalized Olefins with Molecular Oxygen and Aldehyde Catalyzed by Optically Active Manganese(III) Complexes. *Chem. Lett.* 1992, *21* (11), 2231–2234. https://doi.org/10.1246/cl.1992.2231.

(190) Qi, J.-Y.; Li, Y.-M.; Zhou, Z.-Y.; Che, C.-M.; Yeung, C.-H.; Chan, A. S. C. Novel Manganese Complex as an Efficient Catalyst for the Isobutyraldehyde-Mediated Epoxidation of Cyclic Alkenes with Dioxygen. *Adv. Synth. Catal.* 2005, *347* (1), 45–49. https://doi.org/10.1002/adsc.200404224.

(191) Khavasi, H. R.; Sasan, K.; Pirouzmand, M.; Ebrahimi, S. N. Highly Efficient Isobutyraldehyde-Mediated Epoxidation of Cyclic Alkenes with Dioxygen Catalyzed by a Novel Dimeric Manganese(II) Complex Containing an Easy-to-Prepare Flexible Carboxamide Ligand. *Inorg. Chem.* 2009, *48* (13), 5593–5595. https://doi.org/10.1021/ic900334w.

(192) Schröder, K.; Join, B.; Amali, A. J.; Junge, K.; Ribas, X.; Costas, M.; Beller, M. A Biomimetic Iron Catalyst for the Epoxidation of Olefins with Molecular Oxygen at Room Temperature. *Angew. Chem. Int. Ed.* 2011, *50* (6), 1425–1429. https://doi.org/10.1002/anie.201004623.

(193) Singh, K. K.; Gupta, S. S. Reductive Activation of O2 by a Bioinspired Fe Complex for Catalytic Epoxidation Reactions. *Chem. Commun.* 2017, *53* (43), 5914–5917. https://doi.org/10.1039/C7CC00933J.

(194) Koya, S.; Nishioka, Y.; Mizoguchi, H.; Uchida, T.; Katsuki, T. Asymmetric Epoxidation of Conjugated Olefins with Dioxygen. *Angew. Chem. Int. Ed.* 2012, *51* (33), 8243–8246. https://doi.org/10.1002/anie.201201848.

(195) Lai, T.-S.; Zhang, R.; Cheung, K.-K.; Che, C.-M.; Lai, T.-S.; Kwong, H.-L. Aerobic Enantioselective Alkene Epoxidation by a Chiral Trans-Dioxo(D4-Porphyrinato)Ruthenium(VI) Complex. *Chem. Commun.* 1998, No. 15, 1583–1584. https://doi.org/10.1039/A802009D.

(196) Corrado, M. L.; Knaus, T.; Mutti, F. G. A Chimeric Styrene Monooxygenase with Increased Efficiency in Asymmetric Biocatalytic Epoxidation. *ChemBioChem* 2018, *19* (7), 679–686. https://doi.org/10.1002/cbic.201700653.

(197) Wu, S.; Zhou, Y.; Wang, T.; Too, H.-P.; Wang, D. I. C.; Li, Z. Highly Regio- and Enantioselective Multiple Oxy- and Amino-Functionalizations of Alkenes by Modular Cascade Biocatalysis. *Nat. Commun.* 2016, *7* (1), 11917. https://doi.org/10.1038/ncomms11917.

(198) Sigmund, M.-C.; Poelarends, G. J. Current State and Future Perspectives of Engineered and Artificial Peroxygenases for the Oxyfunctionalization of Organic Molecules. *Nat. Catal.* 2020, *3* (9), 690–702. https://doi.org/10.1038/s41929-020-00507-8.

(199) Farokhi, A.; Hosseini-Monfared, H. A Recyclable Mn–Porphyrin Catalyst for Enantioselective Epoxidation of Unfunctionalized Olefins Using Molecular Dioxygen. *New J. Chem.* 2016, *40* (6), 5032–5043. https://doi.org/10.1039/C6NJ00808A.

(200) Xu, Y.; Zhao, L.; Bai, H.; Hong, W.; Li, C.; Shi, G. Chemically Converted Graphene Induced Molecular Flattening of 5,10,15,20-Tetrakis(1-Methyl-4-Pyridinio)Porphyrin and Its Application for Optical Detection of Cadmium(II) Ions. *J. Am. Chem. Soc.* 2009, *131* (37), 13490–13497. https://doi.org/10.1021/ja905032g.

(201) McDonald, A. R.; Franssen, N.; van Klink, G. P. M.; van Koten, G. 'Click' Silica Immobilisation of Metallo-Porphyrin Complexes and Their Application in Epoxidation

Catalysis. *J. Organomet. Chem.* 2009, *694* (14), 2153–2162. https://doi.org/10.1016/j.jorganchem.2009.02.020.

(202) Hwang, E. T.; Lee, S. Multienzymatic Cascade Reactions via Enzyme Complex by Immobilization. *ACS Catal.* 2019, *9* (5), 4402–4425. https://doi.org/10.1021/acscatal.8b04921.

(203) North, M. Chapter 13 - Synthesis of Cyclic Carbonates from Carbon Dioxide and Epoxides. In *New and Future Developments in Catalysis*; Suib, S. L., Ed.; Elsevier: Amsterdam, 2013; pp 379–413. https://doi.org/10.1016/B978-0-444-53882-6.00014-0.

(204) Sachs, H. M. Preparation of Alkylene Carbonates. US4786741A, November 22, 1988. https://patents.google.com/patent/US4786741A/en (accessed 2022-12-29).

(205) Yoshida, M.; Ihara, M. Novel Methodologies for the Synthesis of Cyclic Carbonates. *Chem. – Eur. J.* 2004, *10* (12), 2886–2893. https://doi.org/10.1002/chem.200305583.

(206) Han, Q.; Qi, B.; Ren, W.; He, C.; Niu, J.; Duan, C. Polyoxometalate-Based Homochiral Metal-Organic Frameworks for Tandem Asymmetric Transformation of Cyclic Carbonates from Olefins. *Nat. Commun.* 2015, *6* (1), 10007. https://doi.org/10.1038/ncomms10007.

(207) Pizarro, A.; Abarca, G.; Gutiérrez-Cerón, C.; Cortés-Arriagada, D.; Bernardi, F.; Berrios, C.; Silva, J. F.; Rezende, M. C.; Zagal, J. H.; Oñate, R.; Ponce, I. Building Pyridinium Molecular Wires as Axial Ligands for Tuning the Electrocatalytic Activity of Iron Phthalocyanines for the Oxygen Reduction Reaction. *ACS Catal.* 2018, *8* (9), 8406–8419. https://doi.org/10.1021/acscatal.8b01479.

(208) Han, Z.; Rong, L.; Wu, J.; Zhang, L.; Wang, Z.; Ding, K. Catalytic Hydrogenation of Cyclic Carbonates: A Practical Approach from CO2 and Epoxides to Methanol and Diols. *Angew. Chem. Int. Ed.* 2012, *51* (52), 13041–13045. https://doi.org/10.1002/anie.201207781.

(209) Fukuoka, S.; Kawamura, M.; Komiya, K.; Tojo, M.; Hachiya, H.; Hasegawa, K.; Aminaka, M.; Okamoto, H.; Fukawa, I.; Konno, S. A Novel Non-Phosgene Polycarbonate Production Process Using by-Product CO2 as Starting Material. *Green Chem.* 2003, *5* (5), 497–507. https://doi.org/10.1039/B304963A.

(210) Paddock, R. L.; Nguyen, S. T. Chemical CO2 Fixation: Cr(III) Salen Complexes as Highly Efficient Catalysts for the Coupling of CO2 and Epoxides. *J. Am. Chem. Soc.* 2001, *123* (46), 11498–11499. https://doi.org/10.1021/ja0164677.

(211) Meléndez, J.; North, M.; Pasquale, R. Synthesis of Cyclic Carbonates from Atmospheric Pressure Carbon Dioxide Using Exceptionally Active Aluminium(Salen) Complexes as Catalysts. *Eur. J. Inorg. Chem.* 2007, *2007* (21), 3323–3326. https://doi.org/10.1002/ejic.200700521.

(212) Decortes, A.; Castilla, A. M.; Kleij, A. W. Salen-Complex-Mediated Formation of Cyclic Carbonates by Cycloaddition of CO2 to Epoxides. *Angew. Chem. Int. Ed.* 2010, *49* (51), 9822–9837. https://doi.org/10.1002/anie.201002087.

(213) Meléndez, J.; North, M.; Villuendas, P. One-Component Catalysts for Cyclic Carbonate Synthesis. *Chem. Commun.* 2009, No. 18, 2577–2579. https://doi.org/10.1039/B900180H.

(214) Xie, Y.; Wang, T.-T.; Liu, X.-H.; Zou, K.; Deng, W.-Q. Capture and Conversion of CO2 at Ambient Conditions by a Conjugated Microporous Polymer. *Nat. Commun.* 2013, *4* (1), 1960. https://doi.org/10.1038/ncomms2960.

(215) Wang, S.; Song, K.; Zhang, C.; Shu, Y.; Li, T.; Tan, B. A Novel Metalporphyrin-Based Microporous Organic Polymer with High CO2 Uptake and Efficient Chemical Conversion of CO2 under Ambient Conditions. *J. Mater. Chem. A* 2017, *5* (4), 1509–1515. https://doi.org/10.1039/C6TA08556C.

(216) Chen, Y.; Luo, R.; Xu, Q.; Zhang, W.; Zhou, X.; Ji, H. State-of-the-Art Aluminum Porphyrin-Based Heterogeneous Catalysts for the Chemical Fixation of CO2 into Cyclic Carbonates at Ambient Conditions. *ChemCatChem* 2017, *9* (5), 767–773. https://doi.org/10.1002/cctc.201601578.

(217) Shaikh, R. R.; Pornpraprom, S.; D'Elia, V. Catalytic Strategies for the Cycloaddition of Pure, Diluted, and Waste CO2 to Epoxides under Ambient Conditions. *ACS Catal.* 2018, *8* (1), 419–450. https://doi.org/10.1021/acscatal.7b03580.

(218) Aresta, M.; Quaranta, E.; Ciccarese, A. Direct Synthesis of 1,3-Benzodioxol-2-One from Styrene, Dioxygen and Carbon Dioxide Promoted by Rh(I). *J. Mol. Catal.* 1987, *41* (3), 355–359. https://doi.org/10.1016/0304-5102(87)80112-8.

(219) Bai, D.; Jing, H. Aerobic Oxidative Carboxylation of Olefins with Metalloporphyrin Catalysts. *Green Chem.* 2010, *12* (1), 39–41. https://doi.org/10.1039/B916042F.

(220) Carvalho Rocha, C.; Onfroy, T.; Launay, F. Towards a Combined Use of Mn(Salen) and Quaternary Ammonium Salts as Catalysts for the Direct Conversion of Styrene to Styrene Carbonate in the Presence of Dioxygen and Carbon Dioxide. *Comptes Rendus Chim.* 2015, *18* (3), 270–276. https://doi.org/10.1016/j.crci.2014.12.003.

(221) Balas, M.; Mayoufi, A.; Villanneau, R.; Launay, F. Revisiting the Mukaiyama-Type Epoxidation for the Conversion of Styrene into Styrene Carbonate in the Presence of O2 and CO2. *React. Chem. Eng.* 2022. https://doi.org/10.1039/D2RE00330A.

(222) Girard, A.-L.; Simon, N.; Zanatta, M.; Marmitt, S.; Gonçalves, P.; Dupont, J. Insights on Recyclable Catalytic System Composed of Task-Specific Ionic Liquids for the Chemical Fixation of Carbon Dioxide. *Green Chem.* 2014, *16* (5), 2815–2825. https://doi.org/10.1039/C4GC00127C.

(223) Sun, J.; Fujita, S.; Zhao, F.; Hasegawa, M.; Arai, M. A Direct Synthesis of Styrene Carbonate from Styrene with the Au/SiO2–ZnBr2/Bu4NBr Catalyst System. *J. Catal.* 2005, *230* (2), 398–405. https://doi.org/10.1016/j.jcat.2004.12.015.

(224) Haquette, P.; Salmain, M.; Svedlung, K.; Martel, A.; Rudolf, B.; Zakrzewski, J.; Cordier, S.; Roisnel, T.; Fosse, C.; Jaouen, G. Cysteine-Specific, Covalent Anchoring of Transition

Organometallic Complexes to the Protein Papain from Carica Papaya. *ChemBioChem* 2007, *8* (2), 224–231. https://doi.org/10.1002/cbic.200600387.

(225) Levine, H. L.; Nakagawa, Y.; Kaiser, E. T. Flavopapain: Synthesis and Properties of Semi-Synthetic Enzymes. *Biochem. Biophys. Res. Commun.* 1977, *76* (1), 64–70. https://doi.org/10.1016/0006-291X(77)91668-0.

(226) Crankshaw, M. W.; Grant, G. A. Modification of Cysteine. *Curr. Protoc. Protein Sci.* 1996, *3* (1), 15.1.1-15.1.18. https://doi.org/10.1002/0471140864.ps1501s03.

(227) Tanaka, S.; Kon, Y.; Nakashima, T.; Sato, K. Chemoselective Hydrogen Peroxide Oxidation of Allylic and Benzylic Alcohols under Mild Reaction Conditions Catalyzed by Simple Iron-Picolinate Complexes. *RSC Adv.* 2014, *4* (71), 37674–37678. https://doi.org/10.1039/C4RA05819D.

(228) Lopez, S.; Rondot, L.; Leprêtre, C.; Marchi-Delapierre, C.; Ménage, S.; Cavazza, C. Cross-Linked Artificial Enzyme Crystals as Heterogeneous Catalysts for Oxidation Reactions. *J. Am. Chem. Soc.* 2017, *139* (49), 17994–18002. https://doi.org/10.1021/jacs.7b09343.

(229) Cavazza, C.; Bochot, C.; Rousselot-Pailley, P.; Carpentier, P.; Cherrier, M. V.; Martin, L.; Marchi-Delapierre, C.; Fontecilla-Camps, J. C.; Ménage, S. Crystallographic Snapshots of the Reaction of Aromatic C–H with O2 Catalysed by a Protein-Bound Iron Complex. *Nat. Chem.* 2010, *2* (12), 1069–1076. https://doi.org/10.1038/nchem.841.

(230) Chishiro, T.; Kon, Y.; Nakashima, T.; Goto, M.; Sato, K. Practical Iron-Catalyzed Hydrogen Peroxide Epoxidation of Aromatic Olefins Using a Combination of Two Kinds of Simple Picolinate Ligands under Halide-Free Reaction Conditions. *Adv. Synth. Catal.* 2014, *356* (2–3), 623–627. https://doi.org/10.1002/adsc.201300774.

(231) Sun, W.; Sun, Q. Bioinspired Manganese and Iron Complexes for Enantioselective Oxidation Reactions: Ligand Design, Catalytic Activity, and Beyond. *Acc. Chem. Res.* 2019, *52* (8), 2370–2381. https://doi.org/10.1021/acs.accounts.9b00285.

(232) Scarpellini, M.; Gätjens, J.; Martin, O. J.; Kampf, J. W.; Sherman, S. E.; Pecoraro, V. L. Modeling the Resting State of Oxalate Oxidase and Oxalate Decarboxylase Enzymes. *Inorg. Chem.* 2008, *47* (9), 3584–3593. https://doi.org/10.1021/ic701953g.

(233) Intagliata, S.; Agha, H.; Kopajtic, T. A.; Katz, J. L.; Kamble, S. H.; Sharma, A.; Avery, B. A.; McCurdy, C. R. Exploring 1-Adamantanamine as an Alternative Amine Moiety for Metabolically Labile Azepane Ring in Newly Synthesized Benzo[d]Thiazol-2(3H)One σ Receptor Ligands. *Med. Chem. Res.* 2020, *29* (9), 1697–1706. https://doi.org/10.1007/s00044-020-02597-2.

(234) Zheng, J.-L.; Liu, H.; Zhang, Y.-F.; Zhao, W.; Tong, J.-S.; Ruan, Y.-P.; Huang, P.-Q. A Study on the Racemization Step in the Synthesis of Pyrrolidinols via Cyclic α-Hydroxyimides. *Tetrahedron Asymmetry* 2011, *22* (3), 257–263. https://doi.org/10.1016/j.tetasy.2011.01.012.

(235) Skarżewski, J.; Gupta, A. Synthesis of C2 Symmetric Primary Vicinal Diamines. Double Stereospecific Mitsunobu Reaction on the Heterocyclic Diols Derived from Tartaric Acid. *Tetrahedron Asymmetry* 1997, *8* (11), 1861–1867. https://doi.org/10.1016/S0957-4166(97)00173-0.

(236) Gowda, D. C.; Gowda, S. ChemInform Abstract: Formic Acid with 10% Palladium on Carbon: A Reagent for Selective Reduction of Aromatic Nitro Compounds. *ChemInform* 2001, *32* (19). https://doi.org/10.1002/chin.200119091.

(237) O'Donnel, C. J.; Burke, S. D. Selective Mesylation of Vicinal Diols: A Systematic Case Study. *J. Org. Chem.* 1998, *63* (23), 8614–8616. https://doi.org/10.1021/jo981532p.

(238) Jacobsen, E. N.; Zhang, W.; Muci, A. R.; Ecker, J. R.; Deng, L. Highly Enantioselective Epoxidation Catalysts Derived from 1,2-Diaminocyclohexane. *J. Am. Chem. Soc.* 1991, *113* (18), 7063–7064. https://doi.org/10.1021/ja00018a068.

(239) SYNTHESIS OF 2-ARYLINDOLE-4-CARBOXYLIC AMIDES: [2-(4-FLUOROPHENYL)-1H-INDOL-4-YL]-1-PYRROLIDINYLMETHANONE. *Org. Synth.* 2009, *86*, 92. https://doi.org/10.15227/orgsyn.086.0092.

(240) Jain, S.; Zheng, X.; Jones, C. W.; Weck, M.; Davis, R. J. Importance of Counterion Reactivity on the Deactivation of Co−Salen Catalysts in the Hydrolytic Kinetic Resolution of Epichlorohydrin. *Inorg. Chem.* 2007, *46* (21), 8887–8896. https://doi.org/10.1021/ic700782f.

(241) Lopez, S.; Marchi-Delapierre, C.; Cavazza, C.; Ménage, S. A Selective Sulfide Oxidation Catalyzed by Heterogeneous Artificial Metalloenzymes Iron@NikA. *Chem. – Eur. J.* 2020, *26* (70), 16633–16638. https://doi.org/10.1002/chem.202003746.

(242) *XRF Research – Composition Analysis by X-Ray Fluorescence*. http://www.xrfresearch.com/ (accessed 2023-04-09).

(243) Lee, K. M.; Blaghen, M.; Samama, J.-P.; Biellmann, J.-F. Crosslinked Crystalline Horse Liver Alcohol Dehydrogenase as a Redox Catalyst: Activity and Stability toward Organic Solvent. *Bioorganic Chem.* 1986, *14* (2), 202–210. https://doi.org/10.1016/0045-2068(86)90031-3.

(244) *Cross-Linked Artificial Enzyme Crystals as Heterogeneous Catalysts for Oxidation Reactions | Journal of the American Chemical Society*. https://pubs.acs.org/doi/10.1021/jacs.7b09343 (accessed 2020-09-02).

(245) Yamada, T.; Imagawa, K.; Nagata, T.; Mukaiyama, T. Enantioselective Epoxidation of Unfunctionalized Olefins with Molecular Oxygen and Aldehyde Catalyzed by Optically Active Manganese(III) Complexes. *Chem. Lett.* 1992, *21* (11), 2231–2234. https://doi.org/10.1246/cl.1992.2231.

(246) Katsuki, T. Chiral Metallosalen Complexes: Structures and Catalyst Tuning for Asymmetric Epoxidation and Cyclopropanation. *Adv. Synth. Catal.* 2002, *344* (2), 131–147. https://doi.org/10.1002/1615-4169(200202)344:2<131::AID-ADSC131>3.0.CO;2-T.

(247) Katsuki, T. Mn-Salen Catalyst, Competitor of Enzymes, for Asymmetric Epoxidation. *J. Mol. Catal. Chem.* 1996, *113* (1), 87–107. https://doi.org/10.1016/S1381-1169(96)00106-9.

(248) Jacobsen, E. N. Asymmetric Catalysis of Epoxide Ring-Opening Reactions. *Acc. Chem. Res.* 2000, *33* (6), 421–431. https://doi.org/10.1021/ar960061v.

(249) Konsler, R. G.; Karl, J.; Jacobsen, E. N. Cooperative Asymmetric Catalysis with Dimeric Salen Complexes. *J. Am. Chem. Soc.* 1998, *120* (41), 10780–10781. https://doi.org/10.1021/ja982683c.

(250) Kiani, S.; Tapper, A.; Staples, R. J.; Stavropoulos, P. Functional Aspects of Gif-Type Oxidation of Hydrocarbons Mediated by Iron Picolinate H2O2-Dependent Systems: Evidence for the Generation of Carbon- and Oxygen-Centered Radicals. *J. Am. Chem. Soc.* 2000, *122* (31), 7503–7517. https://doi.org/10.1021/ja000063h.

(251) Dubois, G.; Murphy, A.; Stack, T. D. P. Simple Iron Catalyst for Terminal Alkene Epoxidation. *Org. Lett.* 2003, *5* (14), 2469–2472. https://doi.org/10.1021/ol0347085.

(252) *Ligand and pH Influence on Manganese-Mediated Peracetic Acid Epoxidation of Terminal Olefins | Organic Letters*. https://pubs.acs.org/doi/abs/10.1021/ol048846l (accessed 2021-08-05).

(253) Chaube, V. D.; Shylesh, S.; Singh, A. P. Synthesis, Characterization and Catalytic Activity of Mn(III)- and Co(II)-Salen Complexes Immobilized Mesoporous Alumina. *J. Mol. Catal. Chem.* 2005, *241* (1), 79–87. https://doi.org/10.1016/j.molcata.2005.07.005.

(254) *Man on the moon tech - Lab solutions*. https://www.manonthemoontech.com/index.html (accessed 2023-04-09).

(255) Zhou, F.; Xie, S.-L.; Gao, X.-T.; Zhang, R.; Wang, C.-H.; Yin, G.-Q.; Zhou, J. Activation of (Salen)CoI Complex by Phosphorane for Carbon Dioxide Transformation at Ambient Temperature and Pressure. *Green Chem.* 2017, *19* (16), 3908–3915. https://doi.org/10.1039/C7GC01458A.

(256) Choo, J. M.; Rogers, G. B. Gut Microbiota Transplantation for Colonization of Germ-Free Mice. *STAR Protoc.* 2021, *2* (3), 100610. https://doi.org/10.1016/j.xpro.2021.100610.

(257) Maeda, C.; Shimonishi, J.; Miyazaki, R.; Hasegawa, J.; Ema, T. Frontispiece: Highly Active and Robust Metalloporphyrin Catalysts for the Synthesis of Cyclic Carbonates from a Broad Range of Epoxides and Carbon Dioxide. *Chem. – Eur. J.* 2016, *22* (19). https://doi.org/10.1002/chem.201681962.

(258) Hammer, S. C.; Kubik, G.; Watkins, E.; Huang, S.; Minges, H.; Arnold, F. H. Anti-Markovnikov Alkene Oxidation by Metal-Oxo–Mediated Enzyme Catalysis. *Science* 2017, *358* (6360), 215–218. https://doi.org/10.1126/science.aao1482.

(259) Que, L.; Tolman, W. B. Biologically Inspired Oxidation Catalysis. *Nature* 2008, *455* (7211), 333–340. https://doi.org/10.1038/nature07371.

(260) Abe, S.; Tabe, H.; Ijiri, H.; Yamashita, K.; Hirata, K.; Atsumi, K.; Shimoi, T.; Akai, M.; Mori, H.; Kitagawa, S.; Ueno, T. Crystal Engineering of Self-Assembled Porous Protein Materials in Living Cells. *ACS Nano* **2017**, *11* (3), 2410–2419. https://doi.org/10.1021/acsnano.6b06099.

(261) Kojima, M.; Abe, S.; Furuta, T.; Tran, D. P.; Hirata, K.; Yamashita, K.; Hishikawa, Y.; Kitao, A.; Ueno, T. Engineering of an In-Cell Protein Crystal for Fastening a Metastable Conformation of a Target Miniprotein. *Biomater. Sci.* **2023**, *11* (4), 1350–1357. https://doi.org/10.1039/D2BM01759H.

(262) Ye, R.; Zhao, J.; Wickemeyer, B. B.; Toste, F. D.; Somorjai, G. A. Foundations and Strategies of the Construction of Hybrid Catalysts for Optimized Performances. *Nat. Catal.* **2018**, *1* (5), 318–325. https://doi.org/10.1038/s41929-018-0052-2.

Catalyse hétérogène des oxydations en cascade par des enzymes artificielles mésoporeuse

Le projet NikAGARA s'est articulé autour de la mise au point de métalloenzymes artificielles et de la catalyse hétérogène. Dans le but de contribuer au développement des réactions abiotiques catalysées par des metalloenzymes, nous nous sommes intéressés aux réactions d'époxydation d'alcène et de cycloaddition du CO_2, dans le cadre d'un réaction cascade. Pour y parvenir, La stratégie a consisté à introduire dans des cristaux de protéine NikA deux sites actifs artificiels, chacun associé à une de ces deux réactions. Le challenge était de construire ces deux sites par des méthodologies d'ancrage orthogonales : nous avons alors dans un premier temps testé une nouvelle série d'époxydases produites selon deux modes de préparation distincts à partir de la protéine NikA. Le premier, maitrisé par le consortium, repose sur des interactions supramoléculaires entre les résidus présents dans la cavité de la protéine NikA et des complexes complexe de Mn, jouant le rôle de site actif. Le second est basé sur la modification covalente d'une cystéine introduite dans NikA par mutagenèse dirigée. Une réaction de Michael d'un substituant d'un ligand salen avec la seule cystéine de la protéine NiKA a alors été démontrée pour la première fois dans des cristaux de NiKA. Cinq nouvelles époxydases artificielles ont démontré des activités intéressantes avec l'acide peracétique ou le dioxygène comme oxydant. Un des principaux acquis de cette partie est la démonstration du mode d'insertion covalente, démontré par un faisceau de spectroscopies dont la diffraction X et la spectrométrie de masse. Egalement, l'optimisation des essais d'ancrage covalent d'un complexe Mn(salen) modifié sur le mutant NikA-H416C autorise un excès énantiomérique de 90% sur l'époxydation aérobie du cis-β-méthylstyrène. La localisation des cystéines au sein de la protéine influence fortement le rendement de la réaction, soulignant l'importance de l'accès au site lors de la construction du site actif et sans doute de l'approche des substrats. Dans un second temps, le mutants cystéine de NikA associés à un complexe Co(salen) lié de manière covalente, ont conduit à la production d'enzymes pour la cycloaddition du CO_2 qui se sont avérées efficaces dans des conditions assez douces. Enfin, la preuve de concept de catalyse duale à partir de deux sites artificiels dans des cristaux de protéine a été démontrée. L'association du complexe Co(salen) avec un complexe d'époxydation portant un mode d'ancrage orthogonal (interaction supramoléculaire) sur un échafaudage mutant NikA unique, a permis la création d'une enzyme duale capable de catalyser une transformation d'époxydation-cycloaddition du CO_2 en cascade. S'il reste encore un travail conséquent d'optimisation dans chaque approche citée, ces résultats permettent d'ouvrir de nouveaux champs d'applications pour les enzymes artificielles en biologie de synthèse. Elle démontre aussi une nouvelle approche de la catalyse cascade hétérogène bioinspirée.

Heterogeneous Cascade Oxidations Catalyzed by Mesoporous Artificial Enzymes

This thesis project was built around the principles of artificial metalloenzymes and heterogeneous catalysis. In an attempt to fill the gap in the development of abiotic reactions catalysed by artificial metalloenzymes, we aimed at the design of a series of artificial metalloenzymes with distinct and interesting catalytic activities: alkene epoxidation, CO_2 cycloaddition leading to the design of a dual-site artificial metalloenzyme for cascade transformations. Moreover, we ambitioned to exploit the protein environment in order to induce chirality throughout our investigations on alkene epoxidation. Working on the protein NikA, we have successfully reported a series of artificial epoxidases based on two distinct preparation modes. The first one relied on the supramolecular interactions with the native cavity of NikA. The second was based on covalent modification of a cysteine inserted in NikA through a Michael addition. This led to the development of five artificial epoxidases that displayed interesting activities with peracetic acid and Mukayama aerobic epoxidation. Interestingly, our investigations have put to light the influence of the artificial metalloenzymes preparation methodology on the stereoselectivity of the reaction. Indeed, optimization of anchoring assays led to an enantiomeric excess of 90% on the aerobic epoxidation of *cis*-β-methylstyrene with the NikA mutant H416C associated to a modified Mn(salen) ligand. Working on the same protein scaffold, associated with a covalently linked Co(salen) complex have led to the production of a new ArM for CO_2 cycloaddition that was efficient under quite mild conditions. Associating this complex with an epoxidation complex on a single NikA mutant has allowed the creation of a dual-site ArM able to perform a cascade transformation to form cyclic carbonates from styrene through and epoxidation-CO_2 cycloaddition reaction. This dual-site ArM was proven to be active and stable for up to five runs. Although further optimization is needed, this project has paved the way of ArM design from the NikA protein through a novel anchoring methodology, via covalent modification, orthogonal to the characteristic supramolecular anchoring mode of NikA's binding cavity.